PAGES 117–220

ISSN 0003-2654

The Analyst

A monthly international journal dealing with all branches of the theory and practice of analytical chemistry, including instrumentation and sensors, and physical, biochemical, clinical, pharmaceutical, biological, environmental, automatic and computer-based methods

Vol.116 No.2 February 1991

The Analyst

The Analytical Journal of The Royal Society of Chemistry

Editorial Manager, Analytical Journals: Judith Egan

Editor, *The Analyst*
Harpal S. Minhas
The Royal Society of Chemistry,
Thomas Graham House, Science Park,
Milton Road, Cambridge CB4 4WF, UK
Telephone 0223 420066.
Fax 0223 423623. Telex No. 818293 ROYAL.

US Associate Editor, *The Analyst*
Dr J. F. Tyson
Department of Chemistry,
University of Massachusetts,
Amherst MA 01003, USA
Telephone 413 545 0195
Fax 413 545 4490

Senior Assistant Editor
Paul Delaney

Assistant Editors
Brenda Holliday, Paula O'Riordan, Sheryl Whitewood

Editorial Secretary: Claire Harris

Advertisements: Advertisement Department, The Royal Society of Chemistry, Burlington House, Piccadilly, London, W1V 0BN. Telephone 071-437 8656. Telex No. 268001. Fax 071-437 8883.

The Analyst (ISSN 0003–2654) is published monthly by The Royal Society of Chemistry. Thomas Graham House, Science Park, Milton Road, Cambridge CB4 4WF, UK. All orders, accompanied with payment by cheque in sterling, payable on a UK clearing bank or in US dollars payable on a US clearing bank, should be sent directly to The Royal Society of Chemistry, Turpin Transactions Ltd., Blackhorse Road, Letchworth, Herts SG6 1HN, United Kingdom. Turpin Transactions Ltd., distributors, is wholly owned by the Royal Society of Chemistry. 1991 Annual subscription rate EC £246.00, USA $580, Rest of World £283.00. Purchased with *Analytical Abstracts* EC £551.00, USA $1299.00, Rest of World £634.00. Purchased with *Analytical Abstracts* plus *Analytical Proceedings* EC £648.00, USA $1527.00, Rest of World £745.00. Purchased with *Analytical Proceedings* EC £313.00, USA $738.00, Rest of World £360.00. Air freight and mailing in the USA by Publications Expediting Inc., 200 Meacham Avenue, Elmont, NY 11003.

USA Postmaster: Send address changes to: *The Analyst,* Publications Expediting Inc., 200 Meacham Avenue, Elmont, NY 11003. Second class postage paid at Jamaica, NY 11431. All other despatches outside the UK by Bulk Airmail within Europe, Accelerated Surface Post outside Europe. PRINTED IN THE UK.

Information for Authors

Full details of how to submit material for publication in *The Analyst* are given in the Instructions to Authors in the January issue. Separate copies are available on request.

The Analyst publishes papers on all aspects of the theory and practice of analytical chemistry, fundamental and applied, inorganic and organic, including chemical, physical, biochemical, clinical, pharmaceutical, biological, environmental, automatic and computer-based methods. Papers on new approaches to existing methods, new techniques and instrumentation, detectors and sensors, and new areas of application with due attention to overcoming limitations and to underlying principles are all equally welcome. There is no page charge.

The following types of papers will be considered:

Full research papers.

Communications, which must be on an urgent matter and be of obvious scientific importance. Rapidity of publication is enhanced if diagrams are omitted, but tables and formulae can be included. Communications receive priority and are usually published within 5–8 weeks of receipt. They are intended for brief descriptions of work that has progressed to a stage at which it is likely to be valuable to workers faced with similar problems. A fuller paper may be offered subsequently, if justified by later work. Although publication is at the discretion of the Editor, communications will be examined by at least one referee.

Reviews, which must be a critical evaluation of the existing state of knowledge on a particular facet of analytical chemistry.

Every paper (except Communications) will be submitted to at least two referees, by whose advice the Editorial Board of *The Analyst* will be guided as to its acceptance or rejection. Papers that are accepted must not be published elsewhere except by permission. Submission of a manuscript will be regarded as an undertaking that the same material is not being considered for publication by another journal.

Regional Advisory Editors. For the benefit of potential contributors outside the United Kingdom and North America, a Group of Regional Advisory Editors exists. Requests for help or advice on any matter related to the preparation of papers and their submission for publication in *The Analyst* can be sent to the nearest member of the Group. Currently serving Regional Advisory Editors are listed in each issue of *The Analyst.*

Manuscripts (four copies typed in double spacing) should be addressed to:

Harpal S. Minhas, Editor, *The Analyst,*
Royal Society of Chemistry,
Thomas Graham House,
Science Park, Milton Road,
CAMBRIDGE CB4 4WF, UK *or*:

Dr. J. F. Tyson
US Associate Editor, *The Analyst*
Department of Chemistry
University of Massachusetts
Amherst MA 01003, USA

Particular attention should be paid to the use of standard methods of literature citation, including the journal abbreviations defined in Chemical Abstracts Service Source Index. Wherever possible, the nomenclature employed should follow IUPAC recommendations, and units and symbols should be those associated with SI.

All queries relating to the presentation and submission of papers, and any correspondence regarding accepted papers and proofs, should be directed either to the Editor, or Associate Editor, *The Analyst* (addresses as above). Members of the Analytical Editorial Board (who may be contacted directly or via the Editorial Office) would welcome comments, suggestions and advice on general policy matters concerning *The Analyst.*

Fifty reprints are supplied free of charge.

PUBLISH IN THE ANALYST

Cambridge, 1991.

Dear Subscriber,

As a regular reader of *The Analyst* you probably know a fair amount about the journal. But did you know that *The Analyst*

- is the oldest English-language analytical science journal
- has the largest circulation of any European analytical science journal
- is truly international, going to over 90 countries worldwide, with US and Canadian sales equalling those in the UK
- accepts papers on all aspects of analytical chemistry
- is produced using full-time qualified professional editors, with a high standard of error detection (top in a recent independent survey of analytical chemistry journals)
- has no page or other charges, and provides authors with 50 free reprints
- uses peer review of submissions by two independent referees, and is backed by an internationally known editorial board
- now has a US Associate Editor, enabling North American submissions to be reviewed in their country of origin
- achieves rapid publication (5 months from acceptance to publication of papers, or 6–8 weeks for communications)?

If you did, you're probably already submitting your primary papers to *The Analyst*. If not, don't you think you should be? We welcome submissions in the areas stated below, and look forward to hearing from you.

Yours sincerely,

Harpal S. Minhas,
Editor

THE ANALYST
WELCOMES PAPERS ON:

- **Biochemical analysis**
- **Chemometrics**
- **Mass spectrometry**
- **Vibrational spectroscopy**
- **EPR and ESR**
- **Atomic & molecular absorption spectroscopy**
- **Chromatography**
- **Electrochemistry**

Editor, *The Analyst*, Harpal S. Minhas,
The Royal Society of Chemistry,
Thomas Graham House, Science Park,
Milton Road, Cambridge CB4 4WF, UK
Tel: 0223 420066. Fax: 0223 423623.
Tlx: 818293 ROYAL

US Associate Editor, Dr. J. F. Tyson,
Department of Chemistry,
University of Massachusetts, Amherst,
MA 01003, USA
Tel: 413 545 0195. Fax: 413 545 4490

ROYAL SOCIETY OF CHEMISTRY
Information Services

Editorial Manager, Analytical Journals: Judith Egan

Construction and Evaluation of a Regenerable Fluoroimmunochemical-based Fibre Optic Biosensor

James R. Bowyer, Jean Pierre Alarie and Michael J. Sepaniak*
The University of Tennessee, Department of Chemistry, Knoxville, TN 37996-1600, USA
Tuan Vo-Dinh
Health and Safety Research Division, Oak Ridge National Laboratory, Oak Ridge, TN 37831-6101, USA
Robert Q. Thompson
Department of Chemistry, Oberlin College, Oberlin, OH 44074, USA

A microscale fibre optic biosensor that is capable of *in situ* regeneration is described and characterized. By combining recently developed fibre optic sensing technology with a capillary column reagent delivery system, it is possible to perform a variety of bench-top affinity assay procedures both repetitively and remotely. The configuration of the sensing chamber at the terminus of the fibre is an important design feature. The construction and operation of the sensor is described and the results of evaluations of the sensor using an antibody–antigen system are presented. Affinity assay steps such as the delivery of solid phase affinity reagents, secondary reagents and rinse solutions are demonstrated. Sampling is accomplished by mild aspiration. Relative standard deviations (RSDs) for these steps are all less than 10%. The capability of selectively measuring fluorescently labelled anti-rabbit immunoglobulin G (IgG), in the presence of a similar protein, by utilizing its immunospecific interaction with rabbit IgG immobilized on silica beads is demonstrated, and exhibits an RSD of 6.2%. A near linear calibration graph is presented over a concentration range of between 0.011 (approximately the limit of detection) and 0.11 mg ml^{-1}.

Keywords: *Fibre optic; biosensor; fluoroimmunoassay; laser; immunoglobulin G*

The ability to monitor chemical concentrations spectrally both at a distance and *in situ* has been enhanced with the advent of small diameter optical fibres that transmit light efficiently over long distances and wide spectral regions. Such measurements offer advantages over traditional approaches that involve sampling, then transporting the sample to the laboratory for subsequent analysis. In particular, chemical concentrations can be measured directly in hostile or not easily accessible environments without the chemical or physical alterations of sample composition commonly associated with traditional approaches. Ideally, the measurements are performed continuously without removing the fibre optic 'sensor' from the remotely located sample. Unfortunately, *in situ* measurements can be complicated and generally do not exhibit the analytical sensitivity and selectivity associated with conventional laboratory techniques.

These problems have been addressed with the development of fibre optic chemical sensors (FOCSs).[1–3] The FOCS signals are a result of the interaction of an analyte with a reagent phase. The chemical and physical specificity afforded by the interaction contributes to the selectivity of the measurement, and high sensitivity is achieved if the interaction results in a signal that can be detected by laser excited fluorimetry. The reagent phase is immobilized at the sensing terminus of the optical fibre in a variety of ways including direct covalent attachment,[4] entrapment in a gel[5] and containment in an analyte permeable chamber.[6] Traditionally, FOCSs have been used to measure small molecules or ions.[7–11] The application of FOCSs to the measurement of large molecules has been accomplished recently by using bioaffinity reagent phases.[3] Among the analyte–reagent phase combinations that have been employed are lectin–carbohydrate,[12,13] enzyme–substrate,[14–16] and antibody–antigen or –hapten.[17–23] Recent work has focused on the use of immunochemical reagent phases to perform remote measurements by competitive-binding[17] and direct[4,6] assay procedures. The specificity of the immunochemical recognition (antibody–antigen association constant, K_a, typically in the range 10^8–10^{12}) resulted in excellent sensitivity and selectivity in the previous work.

In order for a sensor to be used in a continuous fashion one of the following criteria must be met: one, the interaction of the analyte and reagent phase must be rapid and reversible, thereby permitting a competitive equilibrium binding operation;[24] two, the reagent phase reservoir must not be appreciably depleted during the measurement period; or three, the sensor must be capable of *in situ* regeneration. Many of the sensors that have been described in the literature do not adequately satisfy any of these criteria and are more correctly termed probes. In general, our previous immunochemical-based FOCSs fall into this category. Two approaches to continuous monitoring with immunochemical-based FOCSs have been reported. Anderson and Miller[21] utilized a competitive equilibrium binding approach to monitor continuously the drug phenytoin with an antibody-based FOCS. Sensor operation was based on homogeneous fluoroimmunoassay (FIA) principles and involved competition between labelled and unlabelled drug for the antibody. We have demonstrated the feasibility of using a microscale regenerable biosensor (MRB) to perform rapid, repetitive (*i.e.*, pseudo-continuous) measurements of a benzo[*a*]pyrene metabolite.[25,26] Operation of this sensor is based on heterogeneous FIA procedures. Each approach has its advantages and disadvantages. The competitive equilibrium binding approach requires a compromise in K_a value, as rapid response favours small values, whereas sensitivity and selectivity are enhanced with large values.[3] The MRB is versatile and can exploit the advantages of antibodies with large values of K_a, but its operation can be relatively complicated.

The MRB combines typical FOCS instrumentation with a reagent delivery system that employs capillary columns. In principle, the many FIAs that are used extensively in clinical laboratories[27] can be performed remotely, *in situ*, and in very small samples with the MRB. The appropriate FIA protocol for a given analysis depends largely on the nature of the analyte. Natural fluorophores can be measured using a direct assay procedure that does not involve the complication of labelling reagents with fluorophores. The determination of non-fluorescent analytes can be accomplished by either competitive binding or sandwich assay techniques.[3] The former is used for small analytes and involves competition

* To whom correspondence should be addressed.

between labelled and unlabelled analyte for a limited amount of antibody. The antibody is usually immobilized on a support to facilitate the removal of any unbound reagents. Dose–response graphs have a negative slope and exhibit short dynamic ranges. Labelled and unlabelled materials are generally mixed simultaneously, a process that does not easily lend itself to *in situ* analysis. Nevertheless, we used an immunochemical-based FOCS to perform remote, single-measurement, competitive-binding assays.[17] Sandwich assays are generally performed using a solid-phase antibody (immobilized on a support) that binds the analyte, and a second antibody that is fluorescently labelled and which 'tags' the analyte for measurement. Dose–response graphs have a positive slope and a moderate dynamic range. However, the analyte must be fairly large (relative molecular mass $>10^3$) so that the two antibodies can recognize different epitopes on the analyte.[3] As the labelled reagent can be added subsequent to the initial incubation, the sandwich assay procedure is more easily adapted to continuous sensing. We are currently exploring the use of the MRB for performing sandwich-type FIAs.

As described above, assay protocols can vary greatly, but generally employ affinity reagents immobilized on solid supports (immunobeads in this work) and involve the addition of secondary reagents and rinse solutions. The analytical significance of the MRB can be seen by comparing its operation and characteristics with that of one of the most popular instruments for performing FIAs. In the early 1980s, Pandex developed a versatile method of using immunobeads to perform FIAs.[28] With the Pandex method, the immunobeads are mixed with the sample and various reagents and placed in funnel-shaped microtitre plate wells that contain a frit at the bottom. The reagents and rinse solutions are drawn through the frit and the signal emanating from the trapped immunobeads is measured by front-surface fluorimetry. The microtitre wells are arranged on a plate that permits many samples to be analysed in a short period of time. It is very significant that the operational protocols for the MRB resemble those of the instrument used with the Pandex method. Immunobeads, secondary reagents, and rinse solutions can be added in different orders with the MRB in order to perform a variety of FIAs. Although large numbers of samples cannot be analysed, repetitive measurements can be performed remotely in very small volume samples.

The principal aim of the work presented herein is to demonstrate the feasibility and to evaluate the repeatability of performing isolated and combined affinity assay operations with the MRB. The general design of the MRB is also described. Calibration graphs were obtained for a rabbit immunoglobulin G–anti-rabbit immunoglobulin G (rab IgG–anti-rab IgG) immunological system. These graphs were used to evaluate the response range and sensitivity of the MRB. By rinsing to expel non-specific interferents (compounds that do not bind to the immobilized affinity reagent), the specificity of the affinity–analyte interaction is exploited in order to measure the analyte selectively. Another advantage of the MRB is that reproducible sampling of the analyte can be accomplished by an aspiration procedure. Previously described sensors[3] sampled the analyte by passive diffusion, a procedure that has limited applicability as many analytes exhibit low diffusivities either because of their large size or a lack of sensor permeability. Future prospects for the MRB are also briefly discussed in this paper.

Experimental

Materials

Capillary columns used in the MRB were of various sizes ranging from 200 to 520 μm i.d. and were purchased from Polymicro Technologies, Phoenix, AZ, USA. The fibre optics used in this work were of 400 μm core diameter, plastic-clad fused silica fibres (QSF-400), supplied by General Fiber Optics, Cedar Grove, NJ, USA. The epoxy used was a 5 minute Epoxy manufactured by Devcon, Danvers, MA, USA. Syringe needles were of a standard size 16-gauge Luer lock variety. A fibre optic column bundle template was constructed in-house from Lexan. Stainless-steel frits (5 μm porosity) were obtained from Newmet Krebsoge, Terryville, CN, USA. A Model 7010 Rheodyne high-performance liquid chromatography (HPLC) injection valve and Luer lock syringe valves (Mininert syringe valves, Catalogue No. 654051) were purchased from Alltech, Deerfield, IL, USA. The injection valve, fitted with a 50 μl injection loop, was used for bead injection. Plexiglas T-connectors were fashioned in-house. The syringe pump, for sample and reagent introduction, was obtained from Sage Instruments, Cambridge, MA, USA (Model 341A). Phosphate buffered saline (PBS), pH 7.4; fluorescein isothiocyanate (FITC); anti-rabbit immunoglobulin G–fluorescein isothiocyanate (anti-rab IgG–FITC), of fluorophore to protein (F : P) ratio of approximately 3; rabbit immunoglobulin G–fluorescein isothiocyanate (rab IgG–FITC), F : P ratio of approximately 4; rabbit immunoglobulin G (rab IgG) (lyophilized); and human immunoglobulin G–fluorescein isothiocyanate (human IgG–FITC), F : P ratio of approximately 4, were obtained from Sigma, St. Louis, MO, USA. Human blood serum was donated by a single subject. Immunobeads were prepared by immobilizing the immunospecific reagent rab IgG on silica beads (5 μm diameter) using a previously reported procedure.[29] Fluorescently labelled latex beads used in the bead delivery studies were Fluoresbrite plain microspheres (6.29 μm diameter; excitation wavelength, 488 nm; emission wavelength, 525 nm) and were obtained from Polysciences, Warrington, PA, USA.

Instrumentation

The instrumentation consisted of an argon ion laser operated at 488 nm (Model 2001SL, Cyonics/Uniphase, San Jose, CA, USA), a photomultiplier tube (PMT) (R943-02, Hamamatsu, Middlesex, NJ, USA) and housing (Thorn EMI, Fairfield, NJ, USA), a chopper (Model 9479, EG&G Ortec, Oak Ridge, TN, USA), various lenses and optical filters (Corion, Holliston, MA, USA), a 25 mm diameter mirror with a 2 mm hole bored through the centre (prepared in-house), a monochromator (Model H-10, Instrument SA, Metuchen, NJ, USA), a strip-chart recorder (Cole-Parmer Instruments, Chicago, IL, USA), PMT-HV power supply (Model 556, EG&G Ortec, Oak Ridge, TN, USA), and a picoammeter (Model 485, Keithley, Cleveland, OH, USA). The arrangement of these components is shown in Fig. 1 and is similar to a previously described arrangement.[6]

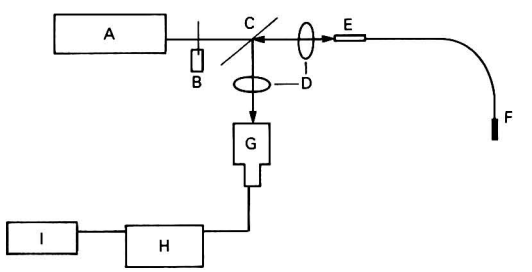

Fig. 1 Schematic diagram of the optical configuration used with an MRB. A, Argon ion laser (488 nm); B, chopper; C, mirror with hole; D, focusing optics; E, fibre positioner; F, MRB; G, monochromator and PMT; H, picoammeter; and I, strip-chart recorder

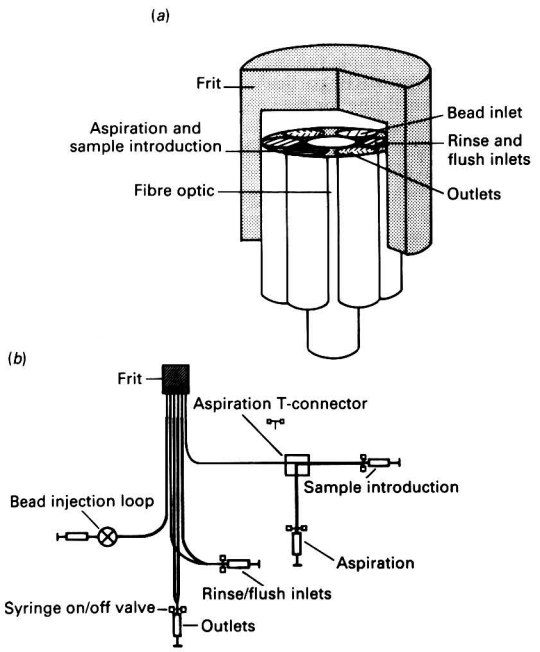

Fig. 2 Diagram of (*a*) frit and column configuration at MRB sensing chamber and (*b*) reagent delivery system

Construction

Construction of the MRB (see Fig. 2) is begun by affixing six short sections of a 200 μm i.d. capillary column and the fibre optic into a template such that they protrude through the template by approximately $\frac{1}{2}$ to $\frac{3}{4}$ in. A reasonably symmetrical tip is formed by smoothing the applied epoxy along the columns, thereby forming a bundle with the periphery defined by the columns (see Fig. 2). As the epoxy hardens, the bundle is drawn out of the template slightly and more epoxy is added in the same manner. After carrying out this procedure, the tip is sufficiently long to allow grinding and polishing without losing the symmetrical arrangement. In order to ensure that the bundle fits tightly in the stainless-steel frit (shown in Fig. 2), the template is constructed with the hole arrangement slightly smaller than the frit opening. Once the epoxy has set, the bundle is removed from the template and ground to a flat polished surface using a grinding wheel with fine lapping film; during this process, the tip is sized using the frit. In order to keep the columns from becoming plugged with debris during the grinding, water is pumped through the columns.

In order to facilitate the operation of the MRB, different diameter capillary columns are connected to the 200 μm i.d. columns just beyond the epoxy; two 520 μm i.d. columns are used as outlets, three 320 μm i.d. columns are used as inlets (two are used as rinsing inlets and one is used for introduction of beads), and one of the original 200 μm i.d. columns is used to aspirate a given volume of sample (see below). Outlet and inlet columns are secured in 16-gauge needles with epoxy and terminated with a syringe on/off valve. The capillary column for bead injection is secured in a short length of tubing and, by use of a suitable ferrule and fitting, is attached to the HPLC injection valve. Column lengths are arbitrary except for the aspiration column, which has a length dictated by the desired aspiration volume and is attached to an aspiration T-connector. Construction of the MRB is completed by affixing the hollowed frit on the polished capillary column–fibre optic bundle such that a small volume (approximately 1 μl) sensing chamber is formed (see Fig. 2). The operation of the MRB for each of the main evaluation steps is described below.

Sensor Conditioning Procedure

Before using the MRB, all tubes were connected to their respective reservoirs and filled with water to remove any trapped air. It is important that air be removed to avoid problems with 'signal altering voids' in the system. Water was also forced through the frit to remove air trapped in the pores. In order to ensure there were no leaks, water was aspirated through the frit and any air bubbles observed in the capillaries were an indication of a leak in the system. Throughout this procedure reagent delivery and rinsing steps are performed with the outlet columns sealed using the syringe on/off valves, thereby restricting flow through the frit; flushing steps are performed with the outlets opened.

Reagent Phase Delivery

The first evaluation of the MRB involved determining the repeatability of reagent delivery to the sensing chamber. The ability to rinse and then flush the chamber was also evaluated. In this study, bead slurry and liquid reagent solutions are individually placed in the sensing chamber *via* their respective delivery capillaries. The Fluoresbrite beads (50 μl, 8 mg ml^{-1}) are introduced from the HPLC injection valve into the chamber. Once a stable fluorescence signal is obtained and recorded the chamber is rinsed with approximately 25 μl of solvent. When performing actual assays, rinsing is necessary to remove unreacted material and possible interferents. After the rinse is completed, a second signal is recorded; the tip is then cleared by flushing, and the process repeated. The repeatability of delivering liquid reagents was similarly evaluated. The FITC solution (1×10^{-4} mol dm^{-3}), used in the evaluation, is introduced from a reservoir and not as an aspirated sample. This operation mimics the introduction, and subsequent removal, of an excess of secondary reagents, such as a labelled second antibody in an MRB-implemented sandwich assay.

Sampling by Aspiration

Samples are collected by connecting a 30 cm length of one of the 200 μm capillary columns (volume, approximately 10 μl) to the T-connector configuration shown in Fig. 2, and then aspirating with a 5 ml syringe while the sensing tip is in the sample. Once the sample has been drawn past the junction in the T-connector, the tip is rinsed and a background signal recorded. The sample is then delivered *via* the aspiration tube from the junction in the T-connector. This operation reduces variations in the sample volume resulting from experimental variables such as frit permeability. The sample and rinse (approximately 50 μl) are collected in 1 ml calibrated vials and diluted to the mark prior to spectrophotometric measurement using an ultraviolet/visible diode array spectrophotometer (Hewlett-Packard, Model HP 8452, Palo Alto, CA, USA). By comparing the absorbances with a calibration graph, sampled volumes are determined.

Combined Affinity Steps

After demonstrating the feasibility and determining the repeatability of performing isolated affinity steps, the steps were combined to measure fluorescently labelled anti-rab IgG and a possible interferent, human IgG–FITC. In this study, the injection loop is filled with immunobeads (10 mg ml^{-1}), the sample is collected, any excess of sample is rinsed from the sensing chamber and the immunobeads are delivered to the sensing chamber. Once the beads are in place, a syringe pump is used to deliver slowly (flow-rate approximately 10 μl min^{-1}) the aspirated sample, followed by the rinse solution, to the immunobeads in the sensing chamber. At several points during the rinsing step, the flow is stopped and the signal from the immunobead-bound anti-rab IgG–FITC is recorded. The

beads are then flushed from the chamber and the background signal is recorded. This procedure is also used to obtain a dose–response graph for anti-rab IgG–FITC. In this and other studies, the incident radiation is chopped (duty cycle about 6%) in order to avoid any photo-decomposition of the reagents.

Results and Discussion

The analytical attributes afforded by fluoroimmunoassays (*e.g.*, high sensitivity and selectivity) are all potentially available with the MRB. The purpose of this work is to demonstrate that the steps common to FIAs can be performed individually and in combination in a repeatable fashion with the MRB, thereby illustrating its versatility as an analytical tool. Detectability, calibration capability, and the selectivity afforded by the specificity of immune reactions, are also demonstrated. Future reports will emphasize the utilization of the MRB for specific assays.

Isolated Affinity Assay Steps

The performance of FIAs with the MRB requires that: (*i*) controlled and adjustable amounts of immunobeads can be delivered to the sensing chamber; (*ii*) secondary reagents can be reproducibly delivered to the chamber; (*iii*) the chamber can be rinsed to remove excess of liquid-phase reagents and impurities that do not bind to the immunobeads; (*iv*) sample solutions can be accurately and precisely aspirated, then delivered to the immunobeads; and (*v*) the contents of the chamber can be flushed completely so that the process can be repeated.

The results of an evaluation of these isolated affinity assay steps are presented in Table 1. Fluorescently labelled beads (Fluoresbrite) were delivered to the chamber five times with a relative standard deviation (RSD) of 7.7% (first column in the table). Following each delivery, the beads were rinsed without being removed from the chamber (third column), and were then flushed from the sensor. The complete flushing of the beads sometimes required mild aspiration to remove beads lodged in the sensing chamber. Delivery of solutions to the beads without removing them from the field of view of the fibre optic was critical to the operation of the MRB. In order to improve precision in an actual assay, the beads can be labelled with a spectrally distinct fluorophore to provide some normalization for the amount of beads introduced. The second column in the table illustrates the result of delivering an FITC solution to the chamber five times. The precision of this operation was very good (RSD = 0.6%) and, as the fourth column indicates, the FITC solution was efficiently removed from the chamber by rinsing.

Reproducible sample volume collection is also critical to the operation of the MRB, particularly as there is no convenient means of normalizing for the volume of sample taken *in situ*. Whereas previous sensors have collected the analyte *via* slow passive diffusion through permeable materials, the MRB has a unique analyte aspiration function which is rapid, and independent of analyte diffusivity and permeability variations. In fact, the capability of 'cleaning-out' the MRB frit *in situ*, by rinsing, represents a significant advantage of this sensor.

The last three columns of Table 1 illustrate the precision of aspirating small and large volumes of analytes in water (series 1 and 2) and in blood serum (series 3). The RSDs for five aspirations were always less than 8.0% with the biological matrix exhibiting the lowest RSD. The differences in sampled volumes and the RSD are probably due to the size and adhesion characteristics of the IgG, as compared with the FITC, and the viscosity of the matrix in series 3.

Combined Assay Steps (Measurement of Anti-rab IgG–FITC)

Having verified that the MRB can accomplish commonly encountered steps in FIA protocols, experiments were conducted to demonstrate that the operations can be combined to conduct an actual assay. In this experiment, rab IgG was covalently bound to silica beads, using a 1,1′-carbonyldiimidazole linkage that has been shown to bind about 12 mg of IgG per gram of beads,[29] and anti-rab IgG was measured. Although not studied in this work, proteins are normally measured by using either a competitive-binding or a sandwich assay procedure. Alternatively, IgG can be measured using the native fluorescence of the protein; however, the quantum efficiency is low and the maximum excitation wavelength (approximately 280 nm) is not convenient. Thus, FITC-labelled antibody was chosen as the analyte (anti-rab IgG–FITC, at approximately 0.1 mg ml^{-1}) in this measurement, which represents the direct assay of a large molecule. A similar protein (human IgG–FITC, at approximately 0.1 mg ml^{-1}) was chosen as an interferent. The advantages of employing this system include: the availability and low cost; the compatibility with the argon ion laser source; the established immobilization procedure;[29] and the availability of structurally similar potential interferents (see below). Moreover, the sensing of IgG is clinically significant[30] and the measurement of a large protein with an FOCS is novel and demonstrates the aforementioned advantages of sampling by aspiration.

Table 1 Signal and reproducibility data for performing isolated affinity assay steps with the MRB (for details see under Experimental)

	Delivery of reagents (signal/nA)		Rinsing of reagents (signal/nA)*		Aspiration volume/μl†		
Measurement	Solid phase‡	Liquid phase§	Solid phase	Liquid phase	Series 1	Series 2	Series 3
0	—	—	—	3.78	—	—	—
1	510	25.2	510	3.70	12.3	10.5	13.4
2	560	25.2	560	3.83	13.4	12.9	13.4
3	470	25.3	470	3.78	11.7	11.5	13.9
4	550	25.2	550	3.73	11.9	11.4	13.2
5	470	25.3	470	3.78	12.1	11.4	13.0
$\bar{x}$	510	25.3	510	3.77	12.0	11.9	13.0
RSD	7.7	0.6	7.7	1.2	5.4	7.5	2.5

* A 20–30 μl volume of water delivered to sensing chamber *via* inlet capillary columns (bead signal unchanged, FITC expelled). Between measurements, a 50–60 μl volume of water delivered to sensing chamber with outlet capillaries open to flush the sensor.

† Aspiration of 1×10^{-4} mol dm^{-3} FITC (series 1); 5 mg ml^{-1} rab IgG–FITC, FITC concentration = 1.4×10^{-4} mol dm^{-3} (series 2); and 5 mg ml^{-1} rab IgG–FITC in human blood serum (series 3).

‡ A 50 μl volume of 8 mg ml^{-1}, 6 μm, Fluoresbrite beads delivered to sensing chamber.

§ A 20 μl volume of 1×10^{-4} mol dm^{-3} FITC delivered to sensing chamber *via* inlet capillary columns with unlabelled beads in chamber.

Table 2 Demonstration of combined affinity assay steps with the MRB (for details see under Experimental)

	Rabbit IgG affinity beads						Non-affinity beads		
	Anti-rab IgG–FITC			Human IgG–FITC			Anti-rab IgG–FITC		
Measurement	A*	B†	C‡	A	B	C	A	B	C
1	13	90	21	16	140	16	15	100	16
2	14	91	23	15	138	16	14	98	15
3	13	92	20	15	138	15	14	100	14
4	13	96	20	15	136	15	14	98	14
5	12	100	22	16	138	17	14	96	14
$\bar{x}$	13	94	22	15	138	16	14	98	15
RSD§	5.4	4.3	6.2	3.6	1.0	5.3	3.1	1.7	6.1

* A, Background signal.

† B, Aspiration signal, measured using MRB following aspiration (approximately 10 μl) and before delivering beads to the sensing chamber.

‡ C, Post delivery signal, measured after delivering beads, aspirated sample and rinse solution to the sensing chamber.

§ Values for RSD are given as percentages.

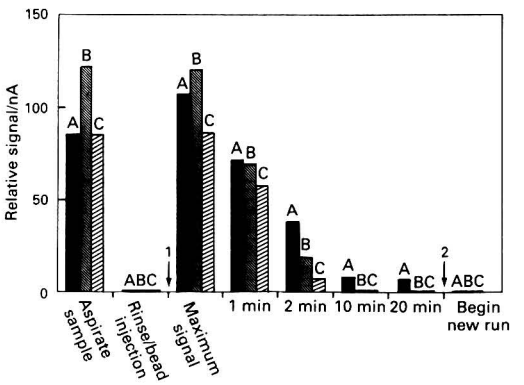

Fig. 3 Temporal representation of the signals obtained in the assay of anti-rab IgG–FITC (see Table 2 for further details). A, Anti-rab IgG–FITC reacted with immunobeads; B, human IgG–FITC reacted with immunobeads; and C, anti-rab IgG–FITC reacted with silica beads. Arrows indicate: 1, sample introduction followed by rinse; and 2, tip flush

The procedure described in the Experimental section was used to obtain the data in Table 2. The signal levels shown in the table represent three points in the analysis and are recorded for the test system and two immunologically non-specific systems. The three measurements are: the background level; the signal after the aspiration step; and the signal after immunobeads, sample and rinse solution are delivered to the chamber. Recall that the aspiration first fills (or partly fills depending on flow patterns) the sensing chamber, then fills the aspiration capillary. As the immunobeads are delivered, the sample that occupies the sensing chamber is expelled and the signal drops to the background level. When the aspirated sample is delivered to the chamber, the signal increases dramatically then drops during rinsing as the excess of sample analyte is removed from the chamber. The change in signal during operation is described later with reference to Fig. 3. Table 2 provides encouraging data, and an indication that refinements in the sensor chamber configuration and optimization of the operating procedures are necessary.

An important point illustrated in Table 2 is that the precision is actually better for the combined affinity steps than for the isolated aspiration step (the RSD for immune specific assay is 6.2%). This indicates that the combined variance in a particular assay is not necessarily an additive function of those for the isolated steps. This is not surprising as the evaluation of the isolated steps does not perfectly mimic the steps in every assay. In particular, the effects of differences in the amount of anti-rab IgG–FITC solution aspirated in the present study are reduced, because, as the sampled volume passes through the immunobeads, the most readily observed beads are saturated with the analyte and, subsequently, beads that are less easily viewed by the fibre optic are involved in the immune reaction. Nevertheless, the wide variety of available assay protocols validates the previous evaluation of precision of the isolated assay steps, as it can provide some insight into the expected assay precision.

A second notable advantage of the MRB in this assay is the selectivity afforded by the specificity of the immune reaction. After rinsing, the anti-rab IgG–FITC signal is appreciable, while the assay of the similar protein, human IgG–FITC, is statistically negligible. This indicates that the immunobeads can be rinsed to remove non-specific interferents while retaining the analyte. The blank signal for anti-rab IgG–FITC, obtained using non-affinity beads, is also negligible. This excellent selectivity is particularly important in sensing applications as, unlike conventional analyses, bench-top isolation of analyte *via* extractions, chromatographic separations, *etc.*, is difficult or impossible. Hence, samples are inherently complex and analyses susceptible to interference.

Fig. 3 readily illustrates several points that are not apparent from Table 2. The first is that the signal obtained from the sampled anti-rab IgG–FITC, when initially delivered to the sensing chamber that is filled with immunobeads, is higher than the aspiration signal. This is probably due to the reaction and concentration of the analyte on the beads closest to the fibre before the beads redistribute during the rinse. The non-specific human IgG–FITC and the non-affinity beads do not exhibit this signal pattern. Variation in the initial heights of the aspiration signals for the two types of IgGs is due to the variation in the labelling ratios. The second is the decrease in the signal as the rinsing continues. This occurs despite the amount of immunobead-bound antibody in the sensing chamber being several times the amount of anti-rab IgG–FITC in the 10 μl sample. The decrease is associated with removal of the unbound protein, removal of the specifically bound protein and redistribution of the beads. Having removed the unbound protein in the first 10 min of the rinse (see Fig. 3), removal of specifically bound protein does not seem to be a major contributor to the signal decrease. This can be seen in Fig. 3, where the rinse continues for an additional 10 min with negligible signal reduction. The decrease in signal due to immunobead redistribution is most problematic, and probably occurs when the rinsing mixes the reacted and unreacted beads and pushes the beads to the outside walls of the sensing chamber, out of the fibre optic field of view. Movement out of the field of view is because the side-walls of the frit are thinner than the end-wall (see Fig. 2). This is supported by the observation that during rinsing, the flow is most prominent through the side-walls and not the end of the frit. Studies with a new frit design, having approximately equal thicknesses for the end-wall and the side-walls, are in progress. Currently, work is also progressing on a delivery system consisting of three inlets and three outlets (symmetrically arranged), through which all of the reagents will be introduced and removed. It is hoped that this arrangement will permit more symmetrical flow patterns within the sensing chamber, thereby minimizing the effects of redistribution. Other operational and design parameters which were not optimized in these preliminary experiments are bead concentration, reagent phase flow-rates, chamber geometry and frit permeability.

A dose–response graph was constructed over the range

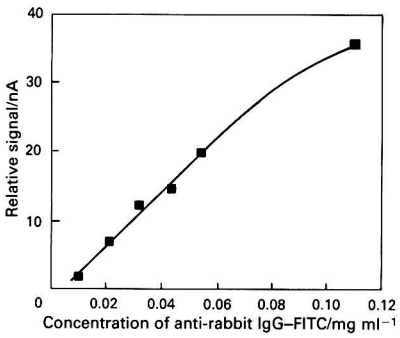

Fig. 4 Dose–response (*i.e.*, calibration) graph for anti-rab IgG–FITC assay

0.011–0.11 mg ml^{-1} of anti-rab IgG–FITC (see Fig. 4). Excluding the highest concentration data point, the correlation coefficient for the linear portion of the graph was 0.9969. The non-linear portion of the graph is possibly due to the saturation of those beads within the field of view, before rinsing removes the sample and redistributes the beads. The limit of detection (LOD) (signal to noise ratio of 2) is approximately 8×10^{-3} mg ml^{-1} (5×10^{-8} mol dm^{-3}) but could possibly be improved by increasing the volume of aspirated sample. By increasing the sample volume, the sample would come into contact with the beads for a longer time before rinsing and redistribution influences the signal. The absolute LOD is approximately 8×10^{-5} mg (5×10^{-13} mol). Although the linear dynamic range was limited for this MRB, it is not believed that this is an inherent difficulty with the design but rather because the operational and design parameters have yet to be fully developed. Both the dynamic range and the LOD are expected to improve when the changes discussed above are implemented. Future work will be necessary in order to realize the full potential of this system for performing long-term FIA sensing in real matrices using sandwich, competitive-binding and enzyme assay protocols.

This research was supported by the National Science Foundation under contract number CHE-8708581 and the Division of Chemical Sciences, Office of Basic Energy Research, US Department of Energy, under contract number DE-FG05-86ER13613 with the University of Tennessee, Knoxville, TN, USA.

References

1 Seitz, W. R., *CRC Crit. Rev. Anal. Chem.*, 1988, **19**, 135.
2 Wolfbeis, O. S., *TrAC, Trends Anal. Chem., Pers. Ed.*, 1985, **4**, 184.
3 Sepaniak, M. J., Tromberg, B. J., and Vo-Dinh, T., *Prog. Anal. At. Spectrosc.*, 1988, **11**, 481.
4 Vo-Dinh, T., Tromberg, B. J., Griffin, G. D., Ambrose, K. R., Sepaniak, M. J., and Gardenhire, E. M., *Appl. Spectrosc.*, 1987, **41**, 735.
5 Kulp, T. J., Camins, I., Angel, S. M., Munkholm, C., and Walt, D. R., *Anal. Chem.*, 1987, **59**, 2849.
6 Tromberg, B. J., Sepaniak, M. J., Alarie, J. P., Vo-Dinh, T., and Santella, R. M., *Anal. Chem.*, 1988, **60**, 1901.
7 Saari, L. A., and Seitz, W. R., *Anal. Chem.*, 1982, **54**, 821.
8 Munkholm, C., Walt, D. R., Milanovich, F. P., and Klainer, S. M., *Anal. Chem.*, 1986, **58**, 1427.
9 Zhujun, Z., Mullin, J. L., and Seitz, W. R., *Anal. Chim. Acta*, 1986, **184**, 251.
10 Wyatt, W. A., Bright, F. V., and Hieftje, G. M., *Anal. Chem.*, 1987, **59**, 2272.
11 Zhujun, Z., and Seitz, W. R., *Anal. Chim. Acta*, 1984, **160**, 305.
12 Schultz, J. S., Mansouri, S., and Goldstein, I. J., *Diabetes Care*, 1982, **5**, 245.
13 Meadows, D., and Schultz, J. S., *Talanta*, 1988, **35**, 145.
14 Arnold, M. A., *Anal. Chem.*, 1985, **57**, 565.
15 Fuh, M. R. S., Burgess, L. W., and Christian, G. D., *Anal. Chem.*, 1988, **60**, 433.
16 Wangsa, J., and Arnold, M. A., *Anal. Chem.*, 1988, **60**, 1080.
17 Tromberg, B. J., Sepaniak, M. J., Vo-Dinh, T., and Griffin, G. D., *Anal. Chem.*, 1987, **59**, 1226.
18 Petrea, R. D., Sepaniak, M. J., and Vo-Dinh, T., *Talanta*, 1988, **35**, 139.
19 Sutherland, R., Dahne, C., Place, J. F., and Ringrose, A. S., *Clin. Chem. (Winston-Salem, NC)*, 1984, **30**, 1533.
20 Andrade, J. D., Vanwagenen, R. A., Gregonis, D. E., Newby, K., and Lin, J. N., *IEEE Trans. Electron Devices*, 1985, **ED-32**, 1175.
21 Anderson, F. P., and Miller, W. G., *Clin. Chem. (Winston-Salem, NC)*, 1988, **34**, 1417.
22 Vo-Dinh, T., Tromberg, B. J., Sepaniak, M. J., Griffin, G. D., Ambrose, K. R., and Santella, R. M., in *Optical Fibers in Medicine III*, ed. Katzir, A., Proceedings of SPIE 910-18, Los Angeles, 1988.
23 Tromberg, B. J., Sepaniak, M. J., and Vo-Dinh, T., in *Optical Fibers in Medicine III*, ed. Katzir, A., Proceedings of SPIE 906-06, Los Angeles, 1988.
24 Liu, B. L., and Schultz, J. S., *IEEE Trans. Biomed. Eng.*, 1986, **BME-33**, 133.
25 Alarie, J. P., Bowyer, J. R., Sepaniak, M. J., Hoyt, A. M., and Vo-Dinh, T., *Anal. Chim. Acta*, 1990, **236**, 237.
26 Sepaniak, M. J., Tromberg, B. J., Alarie, J. P., Bowyer, J. R., Hoyt, A. M., and Vo-Dinh, T., in *196th National Meeting of the American Chemical Society* (Los Angeles, CA), eds. Murray, R. W., Dessy, R. E., Heineman, W. R., Janata, J., and Seitz, W. R., American Chemical Society, Washington, 1989, pp. 318–330.
27 Sepaniak, M. J., *Clin. Chem. (Winston-Salem, NC)*, 1985, **31**, 671.
28 Jolley, M. E., Pandex Research Report, Lit. No. 4001/1.5M, July, 1983.
29 Alarie, J. P., Sepaniak, M. J., and Vo-Dinh, T., *Anal. Chim. Acta*, 1990, **229**, 169.
30 Papadea, C., and Check, I. J., *CRC Crit. Rev. Clin. Lab. Sci.*, 1989, **27**, 27.

Paper 0/03429K
Received July 27th, 1990
Accepted October 4th, 1990

Voltammetric Behaviour of Screen-printed Carbon Electrodes, Chemically Modified With Selected Mediators, and Their Application as Sensors for the Determination of Reduced Glutathione

Stephen A. Wring and John P. Hart*
Science Department, Bristol Polytechnic, Coldharbour Lane, Frenchay, Bristol BS16 1QY, UK
Brian J. Birch
Unilever Research, Sensors Group, Colworth Laboratory, Colworth House, Sharnbrook, Bedford MK44 1LQ, UK

The evaluation of screen-printed carbon electrodes, chemically modified with selected ferrocene, phthalocyanine and hexacyanoferrate(III) derivative mediators for the determination of reduced glutathione (GSH), is described. Cyclic voltammetry was used to investigate the effect of pH on the electrochemical behaviour of these mediators incorporated in the disposable electrodes. Values of the electron-transfer coefficient (αn_a) were calculated for the oxidation of the mediators in phosphate buffer solution and solutions containing 0.48 mmol dm^{-3} GSH. Amperometry in stirred solutions was used to construct hydrodynamic voltammograms for each of the modified electrodes; these voltammograms were used to elucidate their steady-state behaviour. Both electrochemical techniques were used to calculate the reduction in overpotential for the oxidation of GSH; these calculations were performed for all of the chemically modified electrodes. Amperometry in stirred solutions was used as the technique for quantitative measurements, to determine the calibration response factors ($\mu A\ mmol^{-1}\ dm^3$) and limits of detection for selected mediators towards GSH. The appropriate applied potentials were selected by reference to the hydrodynamic waves; a range of values were investigated to find the potential that gave the maximum sensitivity. The most promising mediators were cobalt phthalocyanine, iron phthalocyanine and ferrocenecarbaldehyde.

Keywords: *Screen-printed carbon electrodes; chemically modified ferrocene, phthalocyanine and hexacyanoferrate(III) mediators; reduced glutathione; cyclic voltammetry; amperometry*

Recently, there has been considerable interest in the use of disposable, chemically modified electrodes for the determination of various biomolecules.[1–7] Indeed, careful selection of suitable electron mediators can significantly reduce the overpotential necessary for the determination of some analytes and enhance the selectivity of electroanalytical sensors.[4–7] Frew and co-workers[5,7] described this enhancement in a device for plasma glucose which uses the electrochemically generated ferricinium ion to act as an electron acceptor from the reduced flavoenzyme, glucose oxidase. Batchelor *et al.*[6] also demonstrated that 4-methyl-*o*-benzoquinone could be incorporated in a disposable device for the determination of the ketone body 3-hydroxybutyrate.

In a recent investigation,[8] we described a method of producing screen-printed graphite electrodes chemically modified with the important electrocatalyst cobalt phthalocyanine (CoPC); these devices successfully reduced the overpotential necessary for the determination of reduced glutathione (GSH), ascorbic acid and coenzyme A at plain graphite electrodes. This electrocatalyst has also been incorporated in carbon-paste[9,10] and re-usable carbon–epoxy resin electrodes,[10] which were used for the determination of GSH in human whole blood[9] and plasma[11] by high-performance liquid chromatography with electrochemical detection.

Our chemically modified screen-printed electrodes (SPEs) previously described[8] were easily and reliably fabricated and could be employed, using differential-pulse voltammetry or in the amperometric mode with stirred solutions, for quantitative determinations in simple sample matrices. However, before analyses could be performed on complex biological samples their selectivity would need to be further enhanced.[10]

Therefore, it was considered that the study of other mediators that could permit improved selectivity, through application of even lower applied potentials,[12] was worthy of investigation. We set out to examine the possibility of using a variety of organometallic compounds as mediators for the determination of GSH. To our knowledge, apart from CoPC, none of these compounds has previously been used for this application with SPEs.

This investigation involved three studies. The purpose of the first was to use cyclic voltammetry to examine the electrochemical behaviour of the selected mediators in plain phosphate buffer solutions, and those containing GSH, over a range of pH values. In the second part, hydrodynamic voltammograms were obtained by using simple amperometry in stirred solutions for each of the modified SPEs. Finally, amperometry in stirred solutions was used to compare the selectivity and sensitivity of the most promising electrodes for the determination of GSH.

In these studies, GSH was used as the analyte of choice, because it is a very important cofactor in many physiological processes and also plays a key role in the detoxification of some common drugs;[13,14] in addition, changes in its circulating concentration can be used as a marker for certain disorders.[15–17]

Experimental

Chemicals and Reagents

The CoPC was purchased from Kodak, all other mediators studied were obtained from Aldrich. Graphite (Ultra Carbon Ultra 'F' grade UCP-1M) and GSH were supplied by Johnson Matthey and Sigma, respectively.

All the materials used for the production and cleaning of the screen-printing template were obtained from Sericol. The inert support used for the electrodes was semi-rigid, white poly(vinyl chloride) (PVC) marketed under the trade name Pentawhite and was obtained from ADP. The cellulose acetate and solvents used to prepare the graphite suspension for printing on to the Pentawhite were obtained from Aldrich.

* To whom correspondence should be addressed.

The supporting electrolyte used throughout all the investigations was phosphate buffer solution, prepared from 0.5 mol dm^{-3} stock solutions of sodium dihydrogen orthophosphate, disodium hydrogen orthophosphate and orthophosphoric acid. These were mixed to yield buffer solutions of the required pH values (a pH meter was used). These were subsequently diluted to provide working solutions of 0.05 mol dm^{-3}. All solutions were prepared with purified water (> 18 MΩ cm) obtained using a Millipore Milli-Q purification system. All GSH solutions were prepared in the appropriate working buffer immediately prior to use and were protected from light during all investigations. Purified nitrogen was obtained from BOC.

Apparatus

Cyclic voltammetric and amperometric measurements were obtained using a Metrohm E612 VA-scanner in conjunction with a Metrohm E611-detector; these were used with a JJ Instruments PN4 *x–y* plotter to record voltammograms and amperograms. A three-electrode cell was used, incorporating the SPEs with a saturated calomel reference electrode (Russell Electrodes) and a laboratory-constructed platinum-wire counter electrode. Electrical contact to the SPEs was facilitated with a spade connector glued into a piece of glass tubing (15 × 0.3 cm i.d.) to form an electrode holder.

For amperometric measurements in stirred solutions, a small circular stirring disc of 14 mm diameter (BDH) was placed in the bottom of the cell and rotated at a fixed rate by a Whatman Mini-MR stirrer.

Electrode Construction

The SPEs consisted of a circular 3 mm working area with a 25 × 1 mm connecting strip. These were printed in parallel groups of six electrodes separated by a 7 mm space.[8]

The SPEs were prepared by the method and template described previously.[8] In brief, for the unmodified electrode this involved preparing a 1.5% m/m solution of cellulose acetate in a 1 + 1 (v/v) mixture of cyclohexanone and acetone; this solvent system permits the graphite film to adhere to the PVC support. Immediately prior to use, 1.1 g of this solution were added to 0.5 g of graphite in a small glass vial. These components were mixed to form an even suspension, which could then be printed through the screen on to the PVC support, which had previously been cleaned with ethanol. After use, the screen template was cleaned in a commercial thinner solution (Sericol XG).

For the modified electrodes, 5% m/m of the required mediator was added to the graphite. Once printed, the electrodes were left in the fume cupboard overnight to allow the solvents to evaporate.

Immediately prior to use individual electrodes were cut from the piece of PVC, and the connecting strip was trimmed to 15 mm and covered with insulating tape (RS Components), leaving the 3 mm circular working area exposed, in addition to a 6 mm length at the opposite end to allow electrical contact with the spade connector in the electrode holder.

Voltammetric Procedures Using SPEs

Cyclic voltammetry

Cyclic voltammetric measurements were obtained for blank solutions of 0.05 mol dm^{-3} phosphate buffer (pH 3, 5 and 7) and then for the same solutions containing 0.48 mmol dm^{-3} GSH, using both the unmodified and 5% m/m modified SPEs in order to investigate the effects of pH. Higher pH values were not studied because GSH is particularly unstable in alkaline media.[18] The mediators used for this study were split into two groups; the first group consisted of molecules based on ferrocene, namely, ferrocene itself, dimethylferrocene, ferrocenedicarboxylic acid, ferrocenecarboxylic acid, ferrocenecarbaldehyde and dimethylferrocenedicarboxylic acid. The second group consisted of CoPC, iron phthalocyanine (FePC), Prussian Blue and potassium hexacyanoferrate(III).

The voltammetric conditions were as follows: initial potential, −0.5 V; scan rate, 20 mV s^{-1}; and final potential, 1.2 V. All experiments were performed in triplicate, using a fresh electrode for each run; all the results quoted in later sections are the mean values for each of the parameters studied. Prior to each experiment the supporting electrolyte solution was de-aerated with purified nitrogen to eliminate the oxygen reduction waves.

Hydrodynamic voltammetry

Hydrodynamic voltammograms were obtained for both modified and unmodified SPEs by amperometry in stirred solutions of 0.05 mol dm^{-3} phosphate buffer (20 ml) and in similar buffer solutions containing 0.48 mmol dm^{-3} GSH. The applied potentials of the working electrodes were increased in steps; the resulting steady-state anodic-current responses were measured for each plateau and plotted *versus* applied potential. Each experiment was performed in triplicate with fresh electrodes and the results quoted represent the mean current values.

Calibration, Sensitivity and Selectivity

By use of amperometry, in stirred solutions of 0.05 mol dm^{-3} phosphate buffer (pH 7), the magnitude of the anodic current responses following additions of small volumes of stock GSH solutions was recorded over the final concentration range 1.48×10^{-7}–2×10^{-3} mol dm^{-3} GSH (*i.e.*, for solutions containing 1.48×10^{-7}, 8.67×10^{-7}, 4.76×10^{-6}, 4.97×10^{-5}, 4.76×10^{-4} and 2×10^{-3} mol dm^{-3} GSH). In each instance, the stock GSH solution was added to 20 ml of plain buffer solution in the voltammetric cell, and the difference in the recorded current was measured; a fresh electrode was used for each individual determination.[8] The applied potential values selected for these investigations were taken, where possible, at different points along the hydrodynamic wave for each mediator studied. The sensitivity of the calibration response (calculated from the slope of the calibration graph) was then determined at every applied potential for each of the selected mediators; these results were plotted *versus* applied potential and could be used to establish the relationship between sensitivity and selectivity for each electrode type.

Results and Discussion

The voltammetric evaluation of the different mediators for the electrocatalytic determination of GSH at the modified screen-printed electrodes is described below.

Cyclic Voltammetry

Cyclic voltammograms were recorded, for both groups of the modified SPEs, in 0.05 mol dm^{-3} phosphate buffer (pH 3, 5 and 7) and in similar solutions containing 0.48 mmol dm^{-3} GSH.

Cyclic voltammetric studies on the ferrocene group of mediators

For all but one mediator, the cyclic voltammograms obtained in plain buffer solutions, at the SPEs modified with the ferrocene compounds, showed a single quasi-reversible redox couple; the anodic (E_{pa}) and cathodic (E_{pc}) peak potential values, and their separation (δEp), are given in Table 1. The voltammograms obtained at the electrodes modified with dimethylferrocenedicarboxylic acid revealed only a single

Table 1 Values of peak potential recorded, using cyclic voltammetry in plain phosphate buffer solution, at the SPEs modified with the ferrocene group of mediators

Mediator	Buffer pH	E_{pa}/ V	E_{pc}/ V	δE_p/ V
Ferrocene	3	0.330	0.146	0.184
	5	0.347	0.137	0.210
	7	0.372	0.150	0.222
Ferrocene-carbaldehyde	3	0.540	0.250	0.290
	5	0.540	0.240	0.300
	7	0.530	0.200	0.330
Dimethylferrocene	3	0.200	0.063	0.137
	5	0.203	0.063	0.140
	7	0.223	0.070	0.153
Ferrocene-carboxylic acid	3	0.428	0.310	0.118
	5	0.315	0.237	0.078
	7	0.315	0.233	0.082
Ferrocene-dicarboxylic acid	3	0.640	0.490	0.150
	5	0.460	0.370	0.090
	7	0.450	0.360	0.090
Dimethylferrocene-dicarboxylic acid	3	0.810	—	—
	5	0.810	—	—
	7	0.800	—	—

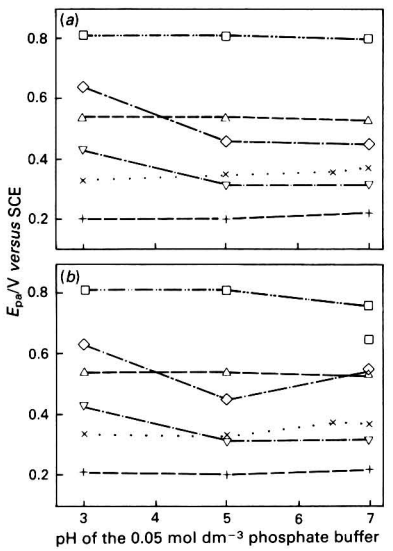

Fig. 1 Effect of pH on E_{pa} for the ferrocene group of mediators using (*a*) 0.05 mol dm^{-3} phosphate buffer and (*b*) solutions of the same buffer containing 0.48 mmol dm^{-3} GSH. ×, Ferrocene; Δ, ferrocene-carbaldehyde; +, dimethylferrocene; ▽, ferrocenecarboxylic acid; ◇, ferrocenedicarboxylic acid; and □, dimethylferrocenedicarboxylic acid

anodic wave; hence, the oxidation appeared to be irreversible over the potential range studied.

For the determination of GSH involving mediated processes, anodic responses are of more importance than the cathodic responses because the magnitude of the former current is expected to increase during electrocatalysis. Bearing this in mind, the behaviour of the oxidation waves was investigated during the remainder of this study.

The graph of E_{pa} *versus* pH for the modified electrodes in plain buffer solution [Fig. 1(*a*)] indicates that the anodic wave

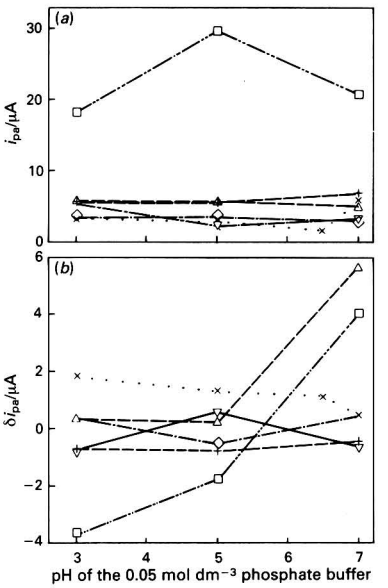

Fig. 2 Effect of pH on i_{pa} for the ferrocene group of mediators using (*a*) 0.05 mol dm^{-3} phosphate buffer and (*b*) solutions of the same buffer containing 0.48 mmol dm^{-3} GSH. Symbols as in Fig. 1

shifts to more negative potentials with increasing pH only for the electrodes modified with ferrocenecarboxylic and ferrocenedicarboxylic acids; for the remainder of the mediators the electrochemical behaviour was independent of pH over the range studied. For the first two SPEs, a break in the graph line occurs at pH 5; this suggests the presence of a pK_a (or pK') for the carboxylic acid groups at this approximate value.

Similar redox behaviour was observed in the presence of 0.48 mmol dm^{-3} GSH [Fig. 1(*b*)]; however, in solutions of pH 7 an extra anodic wave (E_{pa}, 0.65 V) was seen for the dimethylferrocenedicarboxylic acid-modified electrodes, and the peak for ferrocenedicarboxylic acid-modified devices had moved to a more positive potential.

All of the electrodes, except those modified with dimethylferrocene, afforded an enhanced anodic current response in the presence of GSH. Fig. 2(*b*) shows the difference in current measured between the plain buffer solution [Fig. 2(*a*)] and solutions containing GSH; a negative value indicates that the anodic current measured in the presence of GSH was less than that recorded in the plain buffer solution. Interestingly, the i_{pa} *versus* pH graph reveals that the mediators with the most positive E_{pa} values afforded the most enhanced current responses.

Values of the electron-transfer coefficient (αn_a) were calculated,[19] where possible, for the anodic waves obtained with plain buffer solution and with solutions containing 0.48 mmol dm^{-3} GSH (Fig. 3). This graph indicates clearly that the αn_a values determined at the modified SPEs, which demonstrate an electrocatalytic response for GSH, are reduced in the presence of the analyte. This observation is especially apparent for the SPEs modified with ferrocenedicarboxylic acid and ferrocenecarbaldehyde in pH 7 solutions. These electrodes were amongst those that exhibited the largest increase in current response in the presence of GSH. (Unfortunately, the αn_a values could not be determined for GSH at the other promising SPE containing dimethylferrocenedicarboxylic acid, because the resulting new wave at 0.65 V was not sufficiently resolved.) The decrease in the observed αn_a values implies that, in the presence of GSH electrocatalysis, the oxidation of the mediator becomes more irreversible.

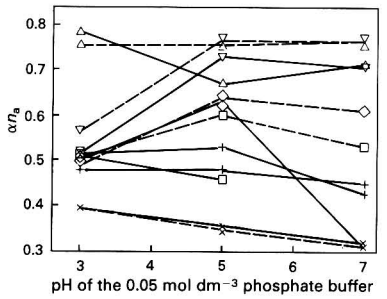

Fig. 3 Effect of pH on the values of the electron transfer coefficient (αn_a), determined for the ferrocene group of mediators, in 0.05 mol dm^{-3} phosphate buffer (broken lines) and solutions of the same buffer containing 0.48 mmol dm^{-3} GSH (solid lines). Symbols as in Fig. 1

However, as enhanced current responses were recorded at these devices, the reduction in the αn_a values could be reflecting the increased time taken during the ECE mechanism[5] involved in the mediated oxidation of GSH compared with the simple E mechanism occurring in the plain buffer solutions. Therefore, the results suggest that the intermediate chemical reaction is the rate-determining step in the over-all oxidation process.

Approximate values for the apparent experimental rate constant (k_s) were calculated from the δE_p values (at scan rates when δE_p was greater than 200 mV), by the method of Laviron,[20,21] for two of the most promising mediators (ferrocenecarbaldehyde and ferrocenedicarboxylic acid) in pH 7 buffer solutions. The mean value of k_s for the ferrocenedicarboxylic acid-modified electrodes, for scan rates between 150 and 250 mV s^{-1}, was 0.357 s^{-1} [n = 3, relative standard deviation (RSD) = 13.9%]. This value agrees well with those determined by Laviron and Roullier[21] for ferrocene-modified polymer electrodes. However, the calculated mean value of k_s for the ferrocenecarbaldehyde-modified electrodes, under the same experimental conditions, was only 0.049 s^{-1} (n = 3, RSD = 8.5%). This suggests that electron-transfer rates for the latter mediator in the present SPE matrix can appear very slow, particularly at high scan rates; this observation is confirmed by the large δE_p values (Table 1) observed with this compound.

Cyclic voltammetry with the phthalocyanine and hexacyanoferrate(III) derivative mediators

CoPC. The electrochemical behaviour of CoPC-modified electrodes has been described previously,[8,10] and the observations from the present study confirm these findings. In plain phosphate buffer solution, two irreversible anodic waves were recorded; *e.g.*, in the pH 3 buffer solution these occurred at 0.48 and 0.80 V, respectively. Using the notation published previously,[10] these were designated waves 2 and 3, respectively. When GSH was added to the supporting electrolyte solution, an additional irreversible anodic wave (wave 1) was observed at less positive potentials than waves 2 and 3 [Fig. 4(*b*)]. As peak 1 has been used successfully for the determination of GSH in biological samples, it was again studied as the peak of interest for the remainder of this investigation.

FePC. The cyclic voltammograms recorded for the FePC-modified SPEs in plain phosphate buffer solution (pH 3) revealed two anodic waves [Fig. 4(*a*)] and one broad cathodic ($E_{pc}1$, −0.15 V) wave; the position of the second anodic wave was found to be dependent on the pH of the supporting electrolyte. In the pH 5 and 7 buffer solutions the broad cathodic wave was resolved into two smaller waves (pH 5: $E_{pc}1$, −0.08V; $E_{pc}2$, −0.23 V, and pH 7: $E_{pc}1$, −0.13 V; $E_{pc}2$, −0.30 V). This suggests that the electrode reactions for FePC are reversible.

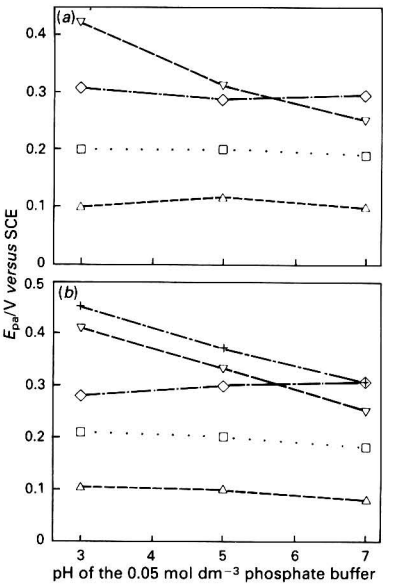

Fig. 4 Effect of pH on E_{pa} for the phthalocyanine and hexacyanoferrate(III) group of mediators using (*a*) 0.05 mol dm^{-3} phosphate buffer and (*b*) solutions of the same buffer containing 0.48 mmol dm^{-3} GSH. □, Prussian blue; △, FePC wave 1; ▽, FePC wave 2; ◇, hexacyanoferrate(III); and +, CoPC wave 1

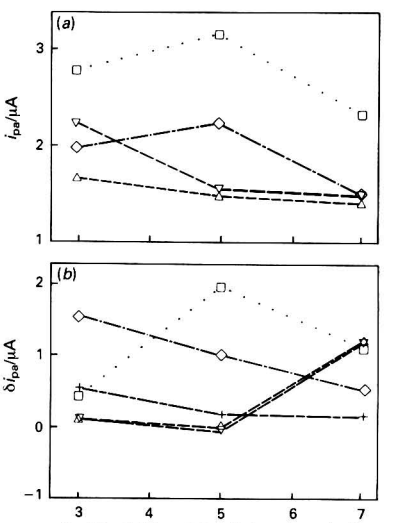

Fig. 5 Effect of pH on i_{pa} for the phthalocyanine and hexacyanoferrate(III) group of mediators using (*a*) 0.05 mol dm^{-3} phosphate buffer and (*b*) solutions of the same buffer containing 0.48 mmol dm^{-3} GSH. Symbols as in Fig. 4

Similar voltammetric behaviour was observed for the electrodes in the buffer solutions containing 0.48 mmol dm^{-3} GSH [Fig. 4(*b*)]; however, an additional, poorly resolved, anodic wave was recorded at about 0.7 V for each of the pH values studied (not shown). The magnitude of the anodic waves 1 and 2 was also found to increase in the presence of GSH in pH 7 phosphate buffer solution [Fig. 5(*a*) and (*b*)]. As the electrocatalytic response of waves 1 and 2 was the most promising in terms of sensor selectivity, their behaviour was

investigated during the remainder of this study, and is summarized in Figs. 4 and 5.

Hexacyanoferrate(III). For each buffer pH studied, two anodic waves ($E_{pa}1$, about 0.30 V; $E_{pa}2$, about 0.45 V) and one cathodic wave were recorded; the behaviour of the first anodic wave is summarized in Fig. 4(*a*) and (*b*). The second anodic wave observed for this usually model redox system probably arises owing to some interaction of the hexacyanoferrate(III) with the electrode matrix or solvent system. This behaviour has been described previously for other modified polymer-based electrodes,[21] and this process is considered probable because only a single, small and tailing cathodic wave was observed; in addition, at applied potentials below 0.0 V the current response became very erratic and noisy.

Fig. 5(*a*) and (*b*) clearly indicates that, despite the presence of these matrix interactions, the magnitude of the first anodic wave increases in the presence of GSH, with the maximum response occurring in pH 3 buffer solutions.

Prussian Blue [*iron*(III) *hexacyanoferrate*(III)]. The cyclic voltammograms of the Prussian Blue-modified electrodes, obtained at each buffer pH studied in the absence of GSH, reveal an ideal quasi-reversible redox couple with single anodic and cathodic waves. As seen in Fig. 4(*a*) and (*b*) the position of the peak potential (E_{pa}) is independent of pH over the range studied. In buffer solutions containing 0.48 mmol dm^{-3} GSH, the anodic current increases to give the maximum mediated response at pH 5 [Fig. 5(*a*) and (*b*)].

The values of αn_a were calculated for the anodic responses shown in Fig. 5(*a*) and (*b*) for each of the second group of modified SPEs (Fig. 6). This graph confirms the observations made by using the ferrocene group of electrodes, where the electron-transfer coefficient is decreased in the presence of a mediated response to GSH. The mechanism for this process is undoubtedly similar to that mentioned previously and involves an ECE mechanism as the Fe^{2+} moiety is electrochemically oxidized to Fe^{3+}, whereupon it is chemically reduced by the GSH and subsequently re-oxidized electrochemically. For the CoPC-modified SPEs, values of αn_a could only be determined in the presence of GSH because wave 1 is absent in plain buffer solution; the mechanistic behaviour of this mediator has been described previously.[10]

Hydrodynamic Voltammetry

For biomedical sensor applications with use of enzymes to enhance selectivity, buffer solutions usually need to be at, or near, physiological pH values. In the second part of our current investigation, we studied the anodic current response of each of the modified SPEs to GSH in pH 7 phosphate buffer solution, using amperometric detection in stirred solutions.

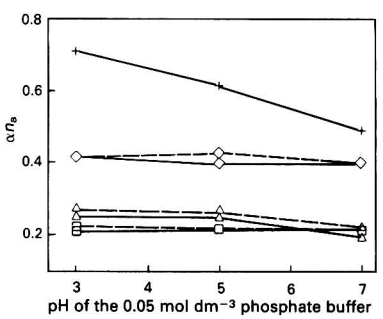

Fig. 6 Effect of pH on the values of the electron transfer coefficient (αn_a), determined for the phthalocyanine and hexacyanoferrate(III) group of mediators, in 0.05 mol dm^{-3} phosphate buffer (broken lines) and solutions of the same buffer containing 0.48 mmol dm^{-3} GSH (solid lines). □, Prussian Blue; △, FePC wave 1; +, CoPC wave 1; and ◇, hexacyanoferrate(III) wave 1

This simple detection technique is particularly important for sensor applications and has been used successfully for the analysis of selected biomolecules in our work and that of other workers.[10,22–24]

Hydrodynamic voltammetry with the ferrocene group of mediators

The hydrodynamic voltammograms [Fig. 7(*a*)] indicate that, for solutions of GSH prepared in phosphate buffer solution (pH 7), enhanced anodic current responses are observed only at the SPEs modified with ferrocenedicarboxylic acid, ferrocenecarbaldehyde and dimethylferrocenedicarboxylic acid. These findings confirm the observations carried out by cyclic voltammetry in the same buffer solutions. These voltammograms were constructed by plotting the difference in current measured between the response in plain phosphate buffer solution (pH 7) and the same solution containing 0.48 mmol dm^{-3} GSH; the current at the initial applied potential, under steady-state conditions, was used as the zero reference point. Hence, the voltammograms illustrate the current arising solely from the mediated oxidation of GSH at the electrode surface.

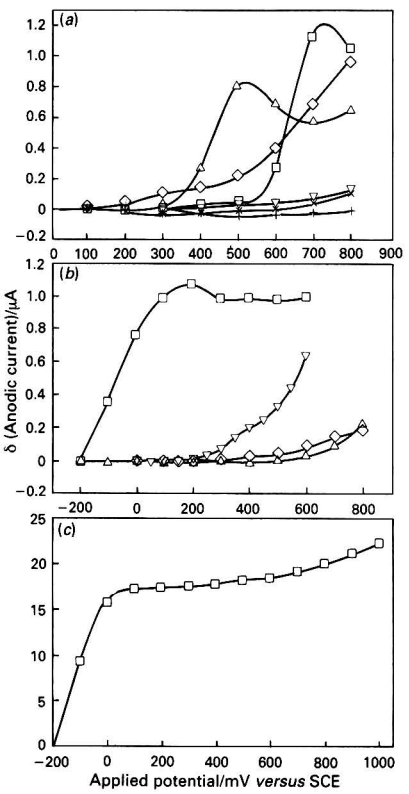

Fig. 7 Hydrodynamic voltammograms for (*a*) the ferrocene group of mediators; (*b*) CoPC and the hexacyanoferrate(III) mediators; and (*c*) FePC. The anodic current values represent the difference in the measured current between 0.05 mol dm^{-3} phosphate buffer (pH 7) solutions and those containing 0.48 mmol dm^{-3} GSH, and hence illustrate the current arising from the mediated oxidation of GSH at the modified electrodes. (*a*): ×, Ferrocene; △, ferrocenecarbaldehyde; +, dimethylferrocene; ▽, ferrocenecarboxylic acid; ◇, ferrocenedicarboxylic acid; and □, dimethylferrocenedicarboxylic acid. (*b*): □, Prussian Blue; ◇, hexacyanoferrate(III); ▽, CoPC; and △, unmodified

Hydrodynamic voltammetry with the phthalocyanine and hexacyanoferrate(III) group of mediators

The hydrodynamic voltammograms for the four mediators confirm their electrocatalytic behaviour in stirred solutions [Fig. 7(*b*) and (*c*)]. The response for the CoPC-modified SPEs clearly reveals a 'shoulder' at 0.4 V on the main voltammogram owing to the first analytical wave (peak 1), which is seen only in the presence of GSH.

Fig. 7(*b*) also shows the current response recorded at the unmodified SPEs; as expected, negligible current values were recorded at the applied potentials, corresponding to the maximum steady-state currents for the mediated electrodes.

Reduction of Overpotential With the Different Mediators

The results from both of the voltammetric studies indicate clearly that the overpotential necessary for the electrochemical detection of GSH can be decreased by using suitable electron mediators. Final selection of the optimum mediator for a particular application will depend on its efficiency at reducing overpotential and its sensitivity, *i.e.*, its current response factor (μA mmol^{-1} dm^3) during calibration. The reductions in overpotential for the electrocatalytic oxidation of GSH are given in Table 2 for each of the modified electrodes that demonstrated a favourable response. The values given are the differences between the E_{pa} values for the oxidation of GSH at the unmodified SPEs, obtained by cyclic voltammetry (E_{pa}, 1.26 V) and hydrodynamic voltammetry (>1.4 V, a plateau was not reached within the usable potential window of the electrodes), and the E_{pa} values at the modified devices. From those data, and the magnitude of the amperometric current responses seen in Fig. 7(*a–c*), the most promising mediators for the selective determination of GSH at pH 7 are: CoPC, FePC, ferrocenedicarboxylic acid, ferrocenecarbaldehyde and Prussian Blue. Large increases in the current response were also recorded for dimethylferrocenedicarboxylic acid; however, for the last mediator the applied potentials necessary for oxidation were deemed to be too positive for practical sensor applications.

Calibration

In the final part of this investigation, amperograms were recorded, by using the method described previously,[8] for the most promising modified electrodes. The concentrations studied covered the range 1.48 × 10^{-7}–2 × 10^{-3} mol dm^{-3} GSH, and the applied potential values were selected from different points on their hydrodynamic waves. The current response factors were calculated from the slope of the calibration graph for each of the mediators by using the different applied potentials; these values were plotted *versus* potential to yield the current response profiles [Fig. 8(*a*) and (*b*)]. Fig. 8(*a*) indicates that FePC-modified electrodes offer the best selectivity during calibration owing to the low applied potentials required. However, for optimum sensitivity, the ferrocenecarbaldehyde-modified SPEs become the devices of choice, although for concentrations of <4.76 × 10^{-6} mol dm^{-3} GSH, high background currents and noise restricted the practical detection limits to this concentration when the applied potential was 400 mV and to 8.67 × 10^{-7} mol dm^{-3} for $E_{applied}$ = 525 mV. By using the most sensitive potential (450 mV) the limit of detection was 1.48 × 10^{-7} mol dm^{-3} GSH as determined for the other devices.

Fig. 8(*a*) also indicates that the optimum sensitivity cannot be obtained on the plateau of the hydrodynamic wave, but at a potential slightly greater than $E_{0.5}$. Fig. 8(*b*) illustrates the current response factors plotted *versus* the position of the applied potential on the hydrodynamic wave. For the ferrocenecarbaldehyde- and CoPC-modified electrodes the optimum response was achieved at approximately the $E_{0.65}$ point. Unfortunately, owing to excessive baseline noise, calibration was not possible for the full range of potentials with the FePC- and ferrocenedicarboxylic acid-modified electrodes; however, the slopes of their response curves do increase towards the mid-point of the hydrodynamic wave. A possible explanation for this observation involves the redox cycling mechanism that was proposed earlier. At lower applied potentials the energy barrier for the chemical reduction of the oxidized electron mediator by the GSH will be at a minimum, allowing this reaction to proceed at a greater rate. This process would in turn replenish the reduced form of the mediator for further electro-oxidation and hence the generation of larger electrocatalytic currents.

Table 2 Comparison of the reduction in measured overpotential for the oxidation of GSH between the modified and unmodified SPEs in 0.05 mol dm^{-3} phosphate buffer (pH 7); where: $\Delta\eta_{CV} = E_{CVunmodified} - E_{CVmodified}$ and $\Delta\eta_{AMP} = E_{AMPunmodified} - E_{AMPmodified}$

Mediator	Cyclic voltammetry ($\Delta\eta_{CV}$)/mV	Amperometry ($\Delta\eta_{AMP}$)/mV
Ferrocene	889	*
Ferrocene-carbaldehyde	730	>880
Dimethylferrocene-dicarboxylic acid	610	>670
Ferrocene-dicarboxylic acid	720	>1000
Prussian Blue	1080	>1200
FePC (wave 1)	1180	>1010
FePC (wave 2)	1010	*
Hexacyanoferrate(III)	960	>950
CoPC (wave 1)	960	>1000

* Indicates no significant response.

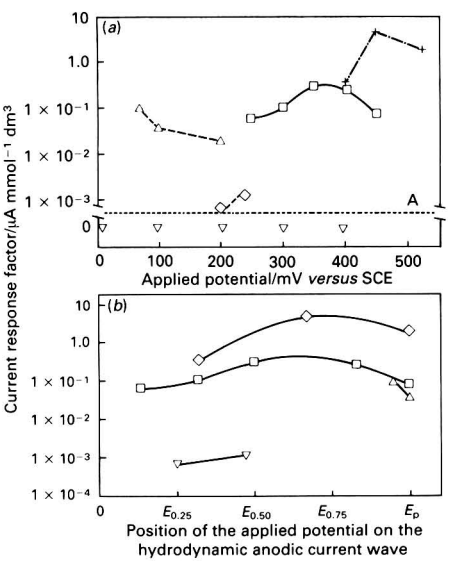

Fig. 8 Amperometric current response factors for the determination of GSH at the SPEs modified with the selected mediators: (*a*) current response factors plotted against applied potential and (*b*) current response factors plotted against the position of the selected applied potential on the hydrodynamic oxidation wave. (*a*): □, CoPC; △, FePC; ◇, ferrocenedicarboxylic acid; +, ferrocenecarbaldehyde; and ▽, Prussian Blue. The line marked A represents no response during calibration. (*b*): □, CoPC; △, FePC; ▽, ferrocenedicarboxylic acid; and ◇, ferrocenecarbaldehyde

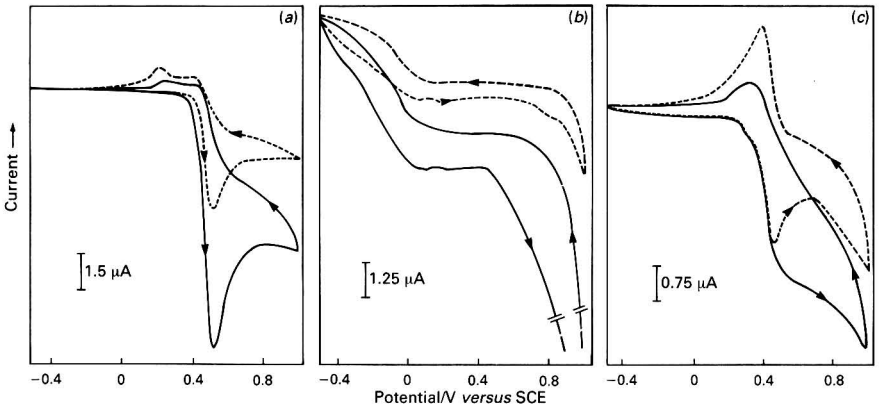

Fig. 9 Cyclic voltammograms recorded in 0.05 mol dm^{-3} phosphate buffer (broken lines) and the same solutions containing 0.48 mmol dm^{-3} GSH (solid lines) using: (*a*) ferrocenecarbaldehyde; (*b*) FePC; and (*c*) ferrocenedicarboxylic acid modified SPEs. Scan rate, 20 mV s^{-1}

For comparison, Fig. 9(*a*)–(*c*) shows the cyclic voltammetric behaviour of these iron-containing mediators in 0.05 mol dm^{-3} phosphate buffer (pH 7) and for the same solutions containing 0.48 mmol dm^{-3} GSH; the cyclic voltammograms for CoPC have been described previously.[8,10]

No response was observed with use of amperometry at constant potential for the Prussian Blue-modified electrodes during calibration. (The experiments were repeated and the results confirmed; at present we are unable to explain this phenomenon.) The highest current responses were obtained with the phthalocyanine-based sensors. This suggests that they should offer better sensitivity and selectivity when compared to other mediators.

Conclusion

The voltammetric data and calibration results reported here suggest that the screen-printed carbon electrodes can be used as a substrate suitable for modification with a variety of electron mediators. The systematic evaluation of these electrocatalysts has shown that, with careful selection of the potential, the oxidation process for GSH can be controlled; therefore, the selectivity and sensitivity can be altered to suit the particular application.

This study has shown that, of the mediators selected initially, the most promising for the determination of GSH are: CoPC, FePC and ferrocenecarbaldehyde. The most selective mediator, requiring the least positive applied potential, was FePC, while the most sensitive was ferrocenecarbaldehyde. However, both of these responses were superimposed on anodic background currents arising from an initial electrochemical oxidation of the Fe^{2+} moieties. Conversely, the anodic current measured at the CoPC devices arises solely from the presence of the GSH in solution, which could permit faster response times for some applications.

It is envisaged that the screen-printed carbon electrodes chemically modified with these mediators, and used in conjunction with selective enzymes, could form the basis of selective biosensors for the determination of GSH in biological matrices.

The authors thank the National Advisory Board for financial support. They are also grateful to Apple Litho (Bristol) for their help and advice regarding the screen-printing of the carbon electrodes.

References

1 Turner, A. P. F., *Sens. Actuat.*, 1989, **17**, 433.
2 Scheller, F., Schubert, F., Pfeiffer, D., Hintsche, R., Dransfeld, I., Renneberg, R., Wollenberger, U., Riedel, K., Pavlova, M., Kühn, M., Müller, H.-G., Tan, P. M., Hoffmann, W., and Moritz, W., *Analyst*, 1989, **114**, 653.
3 Frew, J. E., Bayliff, S. W., Gibbs, P. N. B., and Green, M. J., *Anal. Chim. Acta*, 1989, **224**, 39.
4 Patriarche, G. J., Kauffmann, J.-M., and Viré, J.-C., *Redox Chem. Interfacial Behav. Biol. Mol.*, 1987, **3**, 479.
5 Frew, J. E., and Hill, H. A. O., *Anal. Chem.*, 1987, **59**, 933A.
6 Batchelor, M. J., Green, M. J., and Sketch, C. L., *Anal. Chim. Acta*, 1989, **221**, 289.
7 Frew, J. E., and Green, M. J., *Anal. Proc.*, 1988, **25**, 276.
8 Wring, S. A., Hart, J. P., Bracey, L., and Birch, B. J., *Anal. Chim. Acta*, 1990, **231**, 203.
9 Halbert, M. K., and Baldwin, R. P., *J. Chromatogr., Biomed. Appl.*, 1985, **345**, 43.
10 Wring, S. A., Hart, J. P., and Birch, B. J., *Analyst*, 1989, **114**, 1563.
11 Wring, S. A., Hart, J. P., and Birch, B. J., *Analyst*, 1989, **114**, 1571.
12 Imisides, M. D., Wallace, G. G., and Wilke, E. A., *TrAC, Trends Anal. Chem., Pers. Ed.*, 1988, **7**, 143.
13 Meister, A., *J. Biol. Chem.*, 1988, **263**, 17205.
14 Black, M., *Ann. Rev. Med.*, 1984, **35**, 577.
15 Curello, S., Ceconi, C., Cargnoni, A., Cornacchiari, A., Ferrari, R., and Albertinia, A., *Clin. Chem.*, 1987, **33**, 1448.
16 Hall, R., and Malia, R. G., *Medical Laboratory Haematology*, Butterworths, London, p. 294.
17 Eastman, R. D., *Clinical Haematology*, Wright, Bristol, 6th edn., 1984, p. 126.
18 Perrett, D., and Rudge, S. R., *J. Pharm. Biomed. Anal.*, 1985, **3**, 3.
19 Galus, Z., *Fundamentals of Electrochemical Analysis*, Ellis Horwood, Chichester, 1976, p. 237.
20 Laviron, E., *J. Electroanal. Chem.*, 1979, **101**, 19.
21 Laviron, E., and Roullier, L., *J. Electroanal. Chem.*, 1980, **115**, 65.
22 Swain, A., *Int. Ind. Biotechnol.*, 1988, **8**, 11.
23 Bennetto, H. P., Dekeyzer, D. R., Delaney, G. M., Koshy, A., Mason, J. R., Razack, L. A., Stirling, J. L., and Thurston, C. F., *Int. Analyst*, 1987, **8**, 22.
24 Wring, S. A., Hart, J. P., and Birch, B. J., *Anal. Chim. Acta*, 1990, **229**, 63.

Paper 0/03295F
Received July 23rd, 1990
Accepted September 27th, 1990

Accumulation Voltammetry of Copper(II) Using a Carbon Paste Electrode Modified With Di-8-quinolyl Disulphide

Kazuharu Sugawara, Shunitz Tanaka and Mitsuhiko Taga*
Department of Chemistry, Faculty of Science, Hokkaido University, Nishi-8, Kita-10, Kita-ku, Sapporo-shi, Hokkaido 060, Japan

The accumulation voltammetry of copper(II) was investigated with a carbon paste electrode modified with di-8-quinolyl disulphide (DQDS). The DQDS was reduced to quinoline-8-thiol by applying a suitable potential. Copper(II) was accumulated on the electrode as the copper(II)–quinoline-8-thiol complex at a constant potential in 0.1 mol dm^{-3} acetate buffer. The reduction peak of the copper(II) complex was then observed at −0.30 V by scanning the potential in a negative direction using the differential-pulse mode. The calibration graph for copper(II) was linear over the range 3×10^{-9}–2×10^{-6} mol dm^{-3} with accumulation for 5 min at −0.05 V. As copper(II) was selectively accumulated on the electrode, the influence of concomitant ions was negligible. The method was applied to the determination of copper(II) in Geological Survey of Japan rock reference materials.

Keywords: *Accumulation voltammetry; copper(II) determination; di-8-quinolyl disulphide; quinoline-8-thiol*

Voltammetric methods involving an accumulation process, such as stripping voltammetry and adsorptive voltammetry, are generally very sensitive for the determination of trace metal ions. However, their application to practical samples is limited by the interferences from the sample matrix. In order to solve this problem, it is necessary to accumulate the analyte on an electrode selectively. For this purpose, chemically modified electrodes (CMEs) have been used; for example, a glassy carbon electrode the surface of which was modified by a ligand[1,2] and a carbon paste electrode (CPE) prepared by mixing a ligand and graphite powder. The CPE is easily prepared and gives a stable electrode response. The CPEs modified with dimethylglyoxime[3] and diethylenetriamine[4] were applied to the selective accumulation of nickel(II) and silver(I), respectively, and the determination of trace metal ions in natural water was achieved. In addition, the CPE modified with the iron(II)–pyridine-4-carbaldehyde complex was able to accumulate organic compounds such as primary amines by the formation of a Schiff's base.[5] We have also reported on the accumulation behaviour and stripping voltammetry of silver(I) with a CPE modified with thia-crown compounds.[6]

In this paper, the accumulation and voltammetric behaviour of copper(II) using a CPE modified with di-8-quinolyl disulphide (DQDS) is described. For the accumulation of copper(II) on an electrode, CMEs modified with 2,9-dimethyl-1,10-phenanthroline[7] and diethyldithiocarbamate[8] have been reported. However, the pre-treatment of the electrode modified with 2,9-dimethyl-1,10-phenanthroline is troublesome and the electrode modified with diethyldithiocarbamate lacks selectivity.

On the other hand, DQDS has been used for the selective solvent extraction of copper(II) from acidic medium.[9] The reagent is stable and insoluble in water, and forms quinoline-8-thiol on reduction. The voltammetric behaviour of metal–quinoline-8-thiol complexes has also been studied.[10–12] Hence it should be possible to develop a highly sensitive and selective method for the determination of copper(II) by using a CPE modified with DQDS. The influence of concomitant ions on the method was found to be negligible. The method was applied to the determination of copper(II) in Geological Survey of Japan rock reference materials.

* To whom correspondence should be addressed.

Experimental

Apparatus

A polarographic analyser [Princeton Applied Research (PAR) 174A] coupled to a PAR 315 electroanalytical controller and an Omnigraphic Model 2000H *x–y* recorder were used. A glassy carbon rod was used as the counter electrode, and a saturated calomel electrode (SCE) with a diaphragm tube containing 1 mol dm^{-3} potassium nitrate was used as the reference electrode. All potentials were measured against the SCE. The measurements were carried out at 25 ± 0.1 °C.

Preparation of the CPE

Graphite powder (0.098 g) was added to DQDS (0.002 g) and about 0.06 ml of liquid paraffin and mixed well in a mortar with a pestle to obtain a paste. A portion of the paste was taken and used to fill the top of a glass tube; the surface of the electrode was then smoothed with the end of a spatula. The active surface area of the electrode used was 0.07 cm^2.

Reagents

Di-8-quinolyl disulphide was purchased from Dojindo Chemical Laboratories and used without further purification. A 1×10^{-2} mol dm^{-3} stock solution of copper(II) was prepared by dissolving copper metal (99.999%, Mitsuwa Chemicals) in 5% HNO_3. The supporting electrolyte was acetic acid–sodium acetate buffer (pH 4.5). High-quality nitrogen was used for de-aeration. All other reagents were of analytical-reagent grade.

Procedure

After de-aerating the supporting electrolyte containing copper(II), the latter was accumulated on the electrode for 5 min at −0.05 V. After a rest time of 15 s, the potential was scanned in the negative direction and voltammograms were recorded by differential-pulse polarography (pulse amplitude, 50 mV; pulse interval, 1 s; and scan rate, 5 mV s^{-1}).

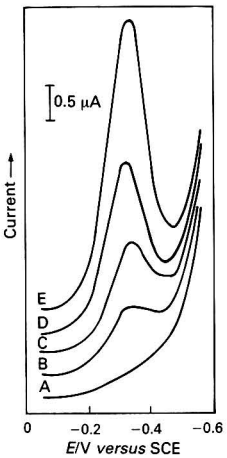

Fig. 1 Accumulation voltammograms of the copper(II)–DQDS complex. Accumulation on a CPE containing 2% DQDS at −0.05 V for 5 min in 0.1 mol dm^{-3} acetate buffer. A, Blank; B, 5×10^{-8}; C, 1×10^{-7}; D, 2×10^{-7}; and E, 4×10^{-7} mol dm^{-3} copper(II). Pulse amplitude, 50 mV; pulse interval, 1 s; and scan rate, 5 mV s^{-1}

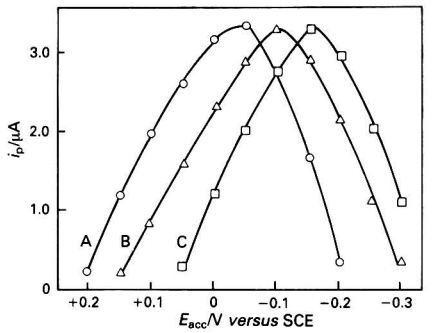

Fig. 2 Dependence of the peak current (i_p) on the accumulation potential (E_{acc}). Accumulation on a CPE containing 2% DQDS for 5 min in various supporting electrolytes of concentration 0.1 mol dm^{-3} in the presence of 4×10^{-7} mol dm^{-3} copper(II). A, Acetate buffer (pH 4.5); B, phosphate buffer (pH 7.0); and C, ammonia buffer (pH 9.0)

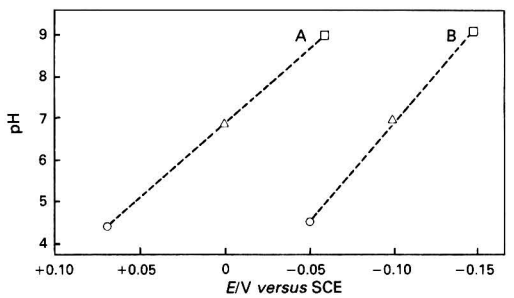

Fig. 3 Relationship between reagent peak and maximum of the accumulation potential. A, Potential of reagent peak at which DQDS was reduced to quinoline-8-thiol; and B, optimum potential in various supporting electrolytes. ○, Acetate buffer (pH 4.5); △, phosphate buffer (pH 7.0); and □, ammonia buffer (pH 9.0)

Results and Discussion

The voltammograms obtained with the CPE modified with DQDS are shown in Fig. 1. In the supporting electrolyte solution, no peak appeared in the potential range between −0.05 and −0.55 V and the residual current was stable in this range. When the accumulation process was carried out for 5 min at −0.05 V in a solution containing 5.0×10^{-8}, 1.0×10^{-7}, 2.0×10^{-7} or 4.0×10^{-7} mol dm^{-3} copper(II), the reduction wave appeared at about −0.30 V. The peak current was proportional to the concentration of copper(II) and the accumulation time. At an unmodified CPE, the reduction peak of copper(II) was not observed. It is thought that the accumulation of copper(II) in solution occurs because of the formation of a complex between copper(II) and the reagent (DQDS) on the electrode.

Relationship Between the Accumulation Potential and pH

The reduction peak current of copper(II) obtained with the CPE modified with DQDS depends on the accumulation potential and on the pH of the supporting electrolyte. Therefore, the relationship between the peak current and the accumulation potential was investigated at various pH values using acetate (pH 4.5), phosphate (pH 7.0) and ammonia (pH 9.0) buffers. As shown in Fig. 2, the reduction current of copper(II) could be observed over a wide range, *viz.*, +0.2 to −0.20 V, in the acetate buffer (Fig. 2, A), demonstrating that copper(II) could be accumulated on the electrode over this range of accumulation potential. The largest and most reproducible peak current was obtained at −0.05 V (optimum potential). In phosphate (Fig. 2, B) and ammonia (Fig. 2, C) buffers, the same relationship as that for the acetate buffer was obtained, but the potential was shifted in a negative direction. However, no significant current was obtained in hydrochloric acid (pH 1.0) or sodium hydroxide (pH 13) solution. When the accumulation was carried out at a more positive potential than the optimum potential, the peak current decreased. The accumulation potential is also related to the reduction of DQDS to quinoline-8-thiol. It appeared that the amount of copper(II)–quinoline-8-thiol which was accumulated on the electrode was very small because the reduction of DQDS to quinoline-8-thiol was difficult at more positive potentials. At a more negative potential than the optimum potential, the peak current decreased sharply because the reduction of the complex had already occurred at the optimum potential. When copper(II) was accumulated at each optimum potential, the peak current was independent of the nature of the supporting electrolyte and the same peak currents were observed. However, because the residual current increased with an increase in pH, acetate buffer, in which the residual current was relatively small, was used.

Mechanism of the Electrode Reaction

As mentioned above, a dependence of the peak current on the accumulation potential was observed, showing that a potential must be applied to the electrode in order to accumulate copper(II). Further, the optimum accumulation potential shifted to a more negative value as the pH of the solution increased (Fig. 3). The shift of optimum accumulation potential was analogous to the shift of peak potential at which DQDS was reduced to quinoline-8-thiol. Consequently, it appears that an accumulation potential is necessary to reduce DQDS to quinoline-8-thiol.

Therefore, the mechanism of the electrode reaction could be as follows: DQDS is first reduced to quinoline-8-thiol [reaction (1)]; copper(II) is then accumulated on the electrode as the copper(II)–quinoline-8-thiol complex by the reaction between copper(II) and the quinoline-8-thiol now present on the electrode [reaction (2)].

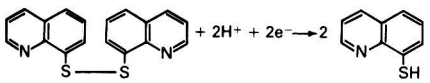

(1)

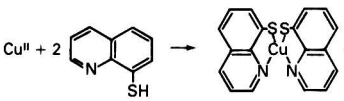

(2)

The copper(II)–quinoline-8-thiol complex on the electrode is reduced at −0.30 V to give copper metal and 'free' quinoline-8-thiol [reaction (3)].

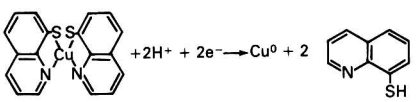

(3)

Effect of the Accumulation Time

The relationship between the peak current and the accumulation time is shown in Fig. 4. The peak current increased linearly over a period of 10 min on increasing the accumulation time in both 1×10^{-7} and 5×10^{-7} mol dm^{-3} copper(II) solutions. However, the accumulation time was kept at a constant value greater than 10 min for the 5×10^{-7} mol dm^{-3} solution because the amount of reagent on the surface of the electrode was saturated for copper(II) ions.

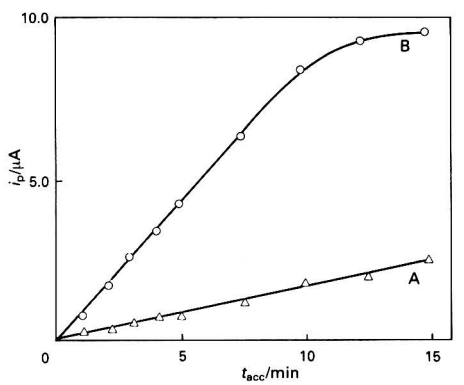

Fig. 4 Dependence of the peak current (i_p) on the accumulation time (t_{acc}). Accumulation on a CPE containing 2% DQDS at −0.05 V in 0.1 mol dm^{-3} acetate buffer containing A, 1×10^{-7}; and B, 5×10^{-7} mol dm^{-3} copper(II)

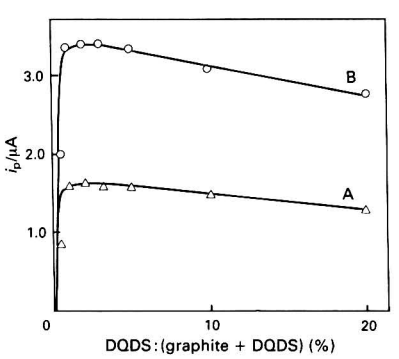

Fig. 5 Effect of amount of DQDS. Accumulation at −0.05 V for 5 min in 0.1 mol dm^{-3} acetate buffer containing A, 2×10^{-7}; and B, 4×10^{-7} mol dm^{-3} copper(II)

Effect of the Amount of DQDS

The effect of altering the ratio of DQDS to graphite powder in the paste on the peak current was investigated (Fig. 5). The peak current increased with increasing amounts of DQDS up to 1% and decreased above 3%. This might be related to the destruction of the mechanical integrity of the paste. It is thought that electron transfer at the CPE is adversely affected by increasing the amount of DQDS. The ratio of DQDS to graphite in the paste was fixed at 2% so that the peak current was constant.

Calibration Graph

When accumulation was carried out for 5 min at −0.05 V in 0.1 mol dm^{-3} acetate buffer followed by a potential scan using differential-pulse polarography, the calibration graph was linear over the range 3×10^{-9}–2×10^{-6} mol dm^{-3} copper(II) with a correlation coefficient of 0.997. The detection limit was 8×10^{-10} mol dm^{-3} at an accumulation time of 5 min. The relative standard deviation for five determinations of 5×10^{-8} and 5×10^{-7} mol dm^{-3} copper(II) was 3.5 and 2.5%, respectively.

Influence of Concomitant Ions

The influence of concomitant ions is shown in Table 1. It is known that Ag^{I}, Bi^{III}, Co^{II}, Fe^{III}, Pt^{IV}, Ru^{III}, Sb^{III}, Se^{IV} and Zn^{II} can form complexes with quinoline-8-thiol. Measurements were carried out for concomitant ions at concentrations of 50 and 100 times that of copper(II). The values in Table 1 show the ratio of the peak current in the presence of the

Table 1 Influence of concomitant ions on the peak current of copper(II). Accumulation on a CPE containing 2% DQDS at −0.05 V for 5 min in 0.1 mol dm^{-3} acetate buffer (pH 4.5) containing 4×10^{-7} mol dm^{-3} copper(II)

Ion	Concentration of concomitant ion/ μmol dm^{-3}	Signal ratio (%)
Ag^{I}	20	100
	40	99
Bi^{III}	20	95
	40	89
Co^{II}	20	103
	40	99
Fe^{III}	20	102
	40	101
Hg^{II}	20	98
	40	99
Pt^{IV}	20	102
	40	97
Ru^{III}	20	100
	40	100
Sb^{III}	20	102
	40	102
Se^{IV}	20	97
	40	98
Zn^{II}	20	103
	40	100

Table 2 Determination of copper(II) in Geological Survey of Japan rock standard reference materials

Sample	Concentration of copper(II)/μg g^{-1} Proposed method ± SD*	Recommended value
JA-1 (Andesite)	204 ± 7	203
JB-1 (Basalt)	58 ± 2	56
JG-1 (Granite)	1.6 ± 0.1	1.5

* n = 12.

concomitant ions to that in their absence (as a percentage). When Bi^{III} was added in a 100-fold excess it interfered in the determination of copper(II). As bismuth ions form a complex with the reagent, the reduction peak for the copper(II) complex may decrease. However, the reduction peak for bismuth was not observed. In anodic stripping voltammetry, the presence of an equivalent amount of Bi^{III} caused an interference in the determination of copper(II). In the proposed method, the peak current was not affected even by the addition of a 50-fold excess of Bi^{III} to the solution. Also, other ions in Table 1 did not interfere up to 40 μmol dm^{-3}. This is because the accumulation of copper(II) on the electrode occurs selectively.

Application of the Method to Rock Standard Reference Materials

The method was applied to the determination of copper(II) in rock reference materials prepared by the Geological Survey of Japan. The sample was decomposed with a mixture of HNO_3, $HClO_4$ and HF under pressure at 150 °C using a PTFE bomb. After the solution had been evaporated to dryness, the residue obtained was dissolved in dilute HNO_3. An aliquot of this solution was taken for the determination. The results are shown in Table 2. The values obtained using the proposed method agree with the recommended values; hence the proposed method is suitable for the determination of copper(II) in rocks.

Conclusion

Di-8-quinolyl disulphide was reduced to quinoline-8-thiol by applying a suitable potential. By using the reaction between copper(II) and the quinoline-8-thiol produced, the former could be selectively accumulated on the electrode as the copper(II)–quinoline-8-thiol complex. A highly sensitive and selective method for measuring copper(II) was developed using accumulation voltammetry. The method was applied to the determination of copper(II) in rock samples.

References

1 Isutsu, K., Nakamura, T., Takizawa, R., and Hanawa, H., *Anal. Chim. Acta*, 1983, **149**, 147.
2 Chastel, O., Kauffman, J.-M., Patriarche, G. J., and Christian, G. D., *Anal. Chem.*, 1989, **61**, 170.
3 Baldwin, R. P., Christensen, J. K., and Kryger, L., *Anal. Chem.*, 1986, **58**, 1790.
4 Cheek, G. T., and Nelson, R. F., *Anal. Lett.*, 1978, **A11**, 393.
5 Guadalupe, A. R., Jhaveri, S. S., Liu, K. E., and Abruna, H. D., *Anal. Chem.*, 1987, **59**, 2436.
6 Tanaka, S., and Yoshida, H., *Talanta*, 1989, **36**, 1044.
7 Prabhu, S. V., and Baldwin, R. P., *Anal. Chem.*, 1987, **59**, 1074.
8 Guadalupe, A. R., and Abruna, H. D., *Anal. Chem.*, 1985, **57**, 142.
9 Bankovsky, Yu. A., Ievins, A. F., Luksha, E. O., and Bochkans, P. Ya., *Zh. Anal. Khim.*, 1961, **16**, 150.
10 Toropova, V. G., Budnikov, K., and Zhiyangulova, F. G., *Zh. Obshch. Khim.*, 1976, **46**, 1125.
11 Toropova, V. G., Budnikov, K., and Zhiyangulova, F. G., *Zh. Obshch. Khim.*, 1977, **47**, 1148.
12 Nakabayashi, Y., Masuda, Y., and Sekido, E., *J. Electroanal. Chem.*, 1986, **205**, 209.

Paper 0/02862B
Received June 26th, 1990
Accepted September 21st, 1990

Comparative Performance of 14-Crown-4 Derivatives as Lithium-selective Electrodes

Ritu Kataky, Patrick E. Nicholson and David Parker*
Department of Chemistry, University of Durham, South Road, Durham DH1 3LE, UK
Arthur K. Covington
Department of Chemistry, University of Newcastle, Newcastle-upon-Tyne, UK

A series of neutral ionophore-based lithium-selective liquid-membrane electrodes have been prepared and the electrode performance compared with similar electrodes based on the lithium ionophores ETH 1810–*ortho*-nitrophenyl octyl ether (oNPOE) and ETH 2137–bis(1-butylpentyl) adipate (BBPA). By using a diamide substituted 14-crown-4 macrocycle, selectivities for Li^+ in the presence of Na^+ of log $k^{pot}_{Li,Na} = -3.25$ and -2.92 were obtained for diisobutylamide–oNPOE and di-*n*-butylamide–oNPOE derivatives. The di-*n*-butylamide–oNPOE based electrode functioned satisfactorily in serum, exhibiting a fast response time (10–15 s), an acceptable lifetime of 50 d and minimal protein interference.

Keywords: *Lithium; ion-selective electrode; selectivity; crown ether; serum*

An ideal Li^+ ionophore for use in monitoring the concentration of Li^+ ions in blood during manic depressive psychosis therapy has yet to be found. The search is imperative as a close monitoring of lithium concentration during treatment is required in order to secure a therapeutic effect and to avoid an overdose of lithium which could lead to fatal poisoning.[1] There is a narrow gap between therapeutic and toxic levels (Fig. 1). A series of chiral 14-crown-4 derivatives have been systematically synthesized and characterized (Table 1). Their performance, in serum, has been compared with the performance of commercial Li sensors and with results obtained by atomic absorption measurements. A diisobutylamide and a di-*n*-butylamide 14-crown-4 based sensor exhibit high selectivity for Li^+ over Na^+ with log $k^{pot}_{Li,Na}$ values of -3.25 and -2.92, respectively. These are superior to the best Li^+ in Na^+ selectivities reported previously (ETH 1810, log $k^{pot}_{Li,Na} = -2.45$).[2–11] The diisobutylamide derivative, however, behaves poorly in serum. The di-*n*-butylamide based electrode functions satisfactorily in serum, exhibits a fast response time (about 10–15 s) and has an acceptable lifetime.

Table 1 14-Crown-4 derivatives studied

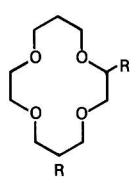

2. $14C_4$Thio $[CH_2OCH_2$ 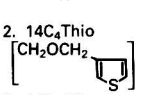 $S]$
3. $14C_4$ Monobenz (CH_2OCH_2Ph)
5. $14C_4$ ol (CH_2OH)
7. $14C_4$ Est (CH_2CO_2Me)
9. $14C_4$ Butam (CH_2CONBu_2)

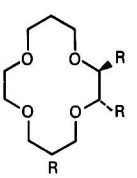

4. $14C_4$ Dibenz (CH_2OCH_2Ph)
6. $14C_4$ Diol (CH_2OH)
8. $14C_4$ Diest (CH_2CO_2Me)
10. $14C_4$ Dibutam (CH_2CONBu_2)
11. $14C_4$ Diibutam $[CH_2CON(iBu)_2]$

* To whom correspondence should be addressed.

Experimental

Design of the Ionophores

A 14-crown-4 skeleton has been the basis of previous Li^+ ionophores, as it has an optimum cavity size for incorporating Li^+ ions.[4–8] The substituents in these earlier sensors were chosen for their effect in improving the lipophilicity of the sensor rather than their effect in enhancing Li selectivity in

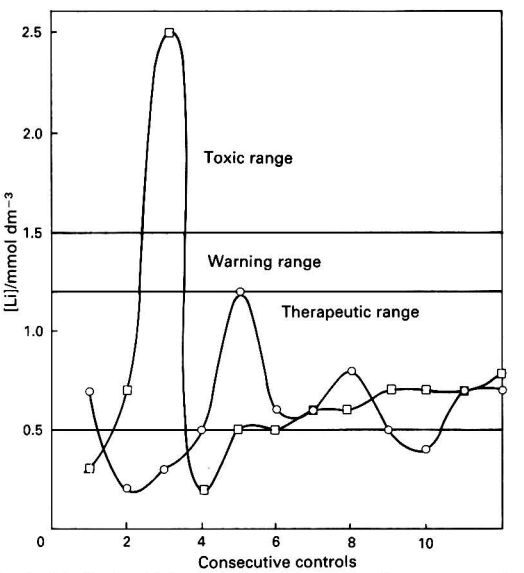

Fig. 1 Monitoring Li levels during therapy. The first two controls were made once a week after patient A, ○, was started on 800 mg d^{-1} of Li_2CO_3. Side effects were detected and the patient was taken off Li therapy for 3 months. Therapy was restarted at 400 mg d^{-1} (third control) and gradually increased to 600 mg d^{-1} (fourth control). The fifth control showed a high Li level of 1.2 mmol dm^{-3} corresponding to a dosage of 1200 mg d^{-1}. The following controls correspond to once every month while the dosage was maintained at 800 mg d^{-1}. Patient B, □, was started on 250 mg d^{-1} of Li_2CO_3 (first control) which was increased to 750 mg d^{-1} (second control). The toxic level at control 3 corresponds to administration of a diuretic. The treatment was stopped and restarted after 3 months at 250 mg d^{-1} (fourth control), gradually increased to 500 mg d^{-1} (controls 5 and 6) and then maintained at 800 mg d^{-1} (controls 7–12). (Blood samples were taken 12 h after administering Li_2CO_3 tablets. The instrument used was a Corning 405 flame photometer)

binding. Improving the selectivity for complexing Li^+ in the presence of excess of Na^+ has been the central aim of our recent work.

The Li^+ ion may exhibit octahedral coordination. This suggested the possibility that by incorporating additional 'axial' donor sites on the 14-crown-4 ring, 1 : 1 complexation with Li^+ would be favoured, while the formation of 2 : 1 complexes ($Li^+ : M^+$) would be suppressed. This tendency to form 2 : 1 complexes is particularly important for Na^+ and K^+, and is suppressed with the sterically demanding 'axial' substituents incorporated in the 14-crown-4 ring. The length of the side chains was chosen bearing in mind, not only purely geometric considerations for optimizing amide oxygen–Li^+ interactions, but also the fact that a chelate-ring size of six intrinsically favours Li^+ complexation whereas a five-membered ring favours binding by the larger K^+ and Na^+ ions. Furthermore, Li^+ is a small, 'hard', polarizing ion, hence 'hard' σ-donors with large dipole moments, such as amide or phosphonate groups, should enhance Li^+ in Na^+ selectivity.[10,11] Taking these factors into account, the 14-crown-4 derivatives shown in Table 1 were synthesized according to published procedures.[11]

Reagents and Chemicals

Chloride salts of lithium, sodium, potassium and magnesium (BDH AnalaR) were dried at 50 °C and stored over silica gel. Calcium chloride solution (BDH AnalaR, 1 mol dm^{-3}) was used. All standard solutions were prepared in de-ionized water and their cation concentrations checked by atomic absorption spectrometry. The 3-morpholinopropanesulphonic acid (MOPS) and 4-(2-hydroxyethyl)piperazine-1-ethanesulphonic acid (HEPES) buffers[12] and their sodium salts were obtained from Sigma.

The materials for the electroactive membranes were: high relative molecular mass poly(vinyl chloride) (PVC); *ortho*-nitrophenyl octyl ether (oNPOE); bis(1-butylpentyl) adipate (BBPA); potassium tetrakis(*p*-chlorophenyl)borate (K-T*p*ClPB); and lithium ionophore IV (ETH 2137), all obtained from Fluka; and a Philips Li ionophore (IS, 561). Tetrahydrofuran (THF) was of spectroscopic grade, distilled from sodium benzophenone ketyl.

Serum was collected from healthy volunteers and was not stabilized by addition of heparin, but was used immediately.

Apparatus

Calibration and selectivity measurements

A Philips IS (561) electrode body was used to mount the electroactive membranes. The filling solution was 1×10^{-3} mol dm^{-3} LiCl. The electrodes were fitted in a constant-volume cell made from a water-jacketed glass tube with a B19 ground-glass joint. The cell was incorporated in a flow system (Fig. 2). The reference electrode (porous plug, calomel, filled with 3.5 mol dm^{-3} KCl, REI Petiacourt) was placed, downstream, in a reference cell made from a water-jacketed glass tube from which a short capillary fitted with a ceramic plug had been drawn out. This formed a constrained diffusion junction with the sample. The temperature of the system was maintained at 37 °C by using a Techne Tempette Junior TE-85 thermostatically controlled bath. The solution was drawn at a constant rate (about 3 ml min^{-1}) using an RS 330-812 peristaltic pump. The ion-selective and reference electrodes were connected to a digital multimeter (Keithley 197, Autoranging Microvolt DMM) *via* a buffer amplifier. A flat-bed Linseis 17100 chart recorder, provided with back-off facilities, was used for monitoring potential differences. A suitable capacitance was connected across the input of the chart recorder to smooth out residual noise.

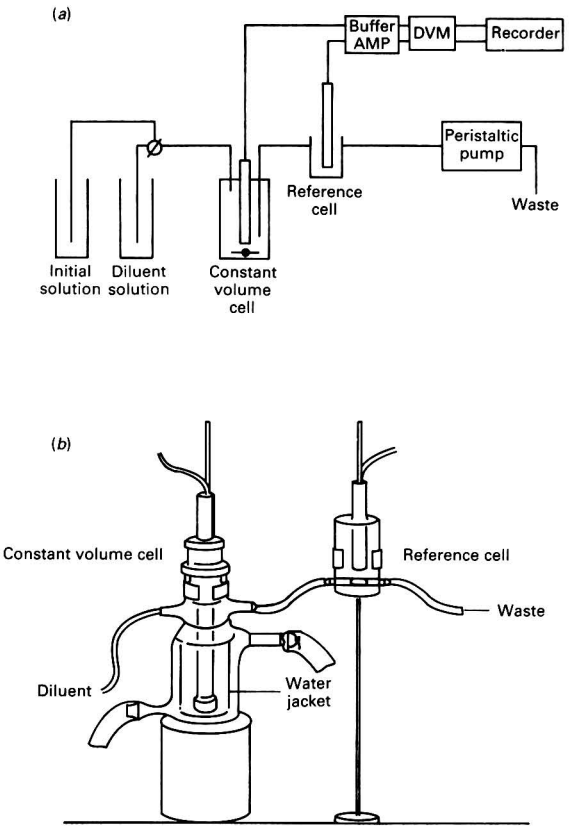

Fig. 2 (*a*) Flow system in which the cell was incorporated. (*b*) Constant volume cell and reference cell

Blood plasma studies

The electroactive membranes were mounted on polycarbonate stems, according to published procedures.[13] The cells were connected to a multiple switch (Fig. 3). The solution was injected into the system by use of disposable 1 ml syringes. The signal monitoring system was similar to that described above. Measurements were made at ambient temperature.

Atomic absorption measurements were carried out on a Perkin-Elmer (5000) instrument. A Corning 654 (Na^+, K^+, Li^+) analyser was used for comparative studies.

The determinations of refractive indices of serum for plasma water were made on a Goldberg AO, TS meter and concentrimeter.

Membrane preparation

The oNPOE-based membranes were composed of 1.2% ionophore, 65.6% oNPOE, 32.8% PVC and 0.4% KT*p*ClPB in 6 cm^3 of THF. The ETH 2137 and a 14-C-4 di-*n*-butylamide sensor were also made into membranes consisting of 2.0% ionophore, 65.6% BBPA and 32.4% PVC in 6 cm^3 of THF. The membranes were cast according to published procedures.[14]

Procedure

Calibration and selectivity measurements

The ion-selective electrodes (ISEs) were calibrated using a constant dilution technique.[15] A fixed interference method was used for selectivity coefficient measurements. In order to

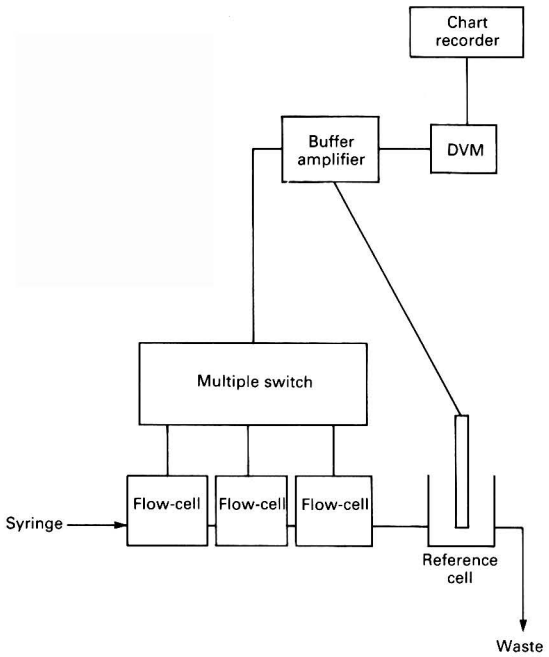

Fig. 3 Flow diagram showing the cells connected to the multiple switch

establish the behaviour of the electrodes in the ionic concentrations present in blood, a background interferent solution of 150 mmol dm^{-3} NaCl, 4.3 mmol dm^{-3} KCl and 1.26 mmol dm^{-3} LiCl was used and all of the measurements were made at 37 °C.

Blood plasma studies

Initial studies were carried out using three different dilutions of serum (serum + diluent: 1 + 1, 1 + 4 and 1 + 9) each containing a range of LiCl concentrations, 0.25, 0.50, 0.75 and 1.00 mmol dm^{-3}. The diluent was 145.0 mmol dm^{-3} NaCl, 5.0 mmol dm^{-3} NaMOPS, 6.7 mmol dm^{-3} MOPS and 4.0 mmol dm^{-3} KCl (pH = 6.86). The Corning 654 (Na^+, K^+, Li^+) analyser was used, according to the manufacturer's instructions, for comparative studies.[16]

Further tests were carried out with the best ionophore and ETH 2137 (the ionophore used in the Corning analyser). An aqueous solution of 140.0 mmol dm^{-3} NaCl, 4.0 mmol dm^{-3} KCl, 1.2 mmol dm^{-3} $CaCl_2$ (20 ml) and a serum sample (20 ml) were dosed with 0.1 mol dm^{-3} LiCl solution to give Li^+ concentrations ranging from 0.5–5.0 mmol dm^{-3} (AQ1-7 and PL1-7, Table 4). The calibration solutions used were: Cal 1 [135.0 mmol dm^{-3} NaCl, 3.6 mmol dm^{-3} KCl, 1.0 mmol dm^{-3} LiCl, 5.0 mmol dm^{-3} NaMOPS, and 6.7 mmol dm^{-3} MOPS, pH = 6.86, ionic strength (I) = 144.6] and Cal 2 (135.0 mmol dm^{-3} NaCl, 3.6 mmol dm^{-3} KCl, 2.5 mmol dm^{-3} LiCl, 5.0 mmol dm^{-3} NaMOPS, and 6.7 mmol dm^{-3} MOPS, pH = 6.86, I = 146.1). The cells were flushed with de-ionized water and air and calibrated with Cal 1 and Cal 2 prior to each sample injection. Atomic absorption measurements were performed in parallel.

Results and Discussion

The results of the calibrations of the various 14-crown-4 based ionophores in comparison with those used by Philips and Corning both in aqueous LiCl and in LiCl in the presence of interferents (150.0 mmol dm^{-3} Na^+, 4.3 mmol dm^{-3} K^+, and 1.26 mmol dm^{-3} Ca^{2+}) are given, (Table 2). These preliminary tests revealed that the alcohol derivatives behaved very poorly. The di-substituted derivatives were better behaved than their mono-substituted analogues. The dibenzyl, di-*n*-butylamide and diisobutylamide derivatives performed well even in aqueous solutions containing serum levels of sodium, potassium and calcium, the last two showing a significant improvement over the ETH 2137 and Philips (IS 561) Li^+ sensors (Fig. 4).

Table 2 Characteristics of Li ionophores. Theoretical slope at 37 °C = 61.54 mV decade^{-1}

	LiCl in de-ionized water		LiCl in a solution of (150 NaCl, 4.3 KCl, 1.26 $CaCl_2$)/ mmol dm^{-3}		
	Slope	LD*	Slope	LD*	Log k_{ij}^{pot}
Philips	62.0	−4.5	47.0	−2.6	−1.89
14-crown-4-thio	60.0	−5.1	44.0	−2.0	−1.14
14-crown-4-monobenz	53.1	−4.9	45.0	−2.2	−1.35
14-crown-4-dibenz	60.0	−4.6	62.0	−2.6	−1.77
14-crown-4-ol	37.3	—	—	—	—
14-crown-4-diol	32.0	—	—	—	—
14-crown-4-est	54.5	−4.6	—	—	—
14-crown-4-diest	62.0	−3.2	25.0	—	—
14-crown-4-nbutam	56.0	−3.9	36.0	—	—
14-crown-4-dinbutam	60.0	−5.0	61.0	−3.8	−2.92
14-crown-4-diibutam	50.0	−5.0	61.0	−4.1	−3.25
ETH 2137	62.0	−4.4	60.0	−2.7	−1.90

* LD = Log (limit of detection).

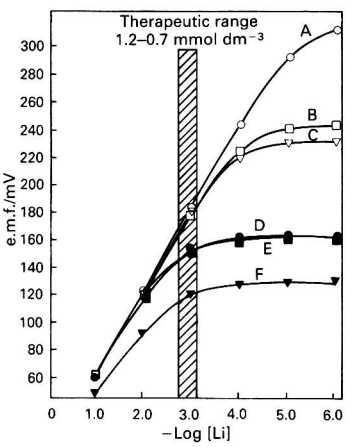

Fig. 4 Li ISE slopes in the presence of interferents: Na^+, 150; K^+, 4.3; and Ca^{2+}, 1.26 mmol dm^{-3}. A, Ideal; B, diisobutylamide C, di-*n*-butylamide; D, ETH 2137; E, dibenzyl; and F, Philips

The selectivity coefficients of the most promising ionophores were determined in interferent concentrations of 0.1 mol dm^{-3}. The only exception was proton interference, in which a 1×10^{-3} mol dm^{-3} HCl solution was used. The values obtained are shown in Table 3. The target selectivity coefficients were calculated using the Nikolsky–Eisenman equation based on a contribution of less than 1%, by the activity of the interferent ion, in comparison with the activity of the primary ion.[17] The values for the 'best' lithium ionophore, to date, (ETH 1810) are included for comparison. The diisobutylamide and the di-*n*-butylamide ionophores meet the target selectivities for K^+, Ca^{2+} and Mg^{2+}. As the pH of plasma is 7.3–7.4, the proton interference measured at pH 3 is not important.The selectivity observed with respect to Na^+ is superior to ETH 1810 and ETH 2137.

Preliminary tests with the two amide ionophores exhibiting the best selectivities *in vitro*, were performed with diluted serum to give an indication of their stability in biological media. The results were compared with those obtained using a Corning 654 (Na^+, K^+, Li^+) analyser in both the concentration and millivolt mode. Voltage readings were converted to concentrations using the equation

$$E_u - E_{Cal1} = S \log\{[c_{Li(u)} + k^{pot}_{Li,Na}\, c_{Na(u)}]/[c_{Li(Cal1)} + k^{pot}_{Li,Na}\, c_{Na(Cal1)}]\} \quad (1)$$

where E_u, $c_{Li(u)}$ and $c_{Na(u)}$ are the voltage reading, Li^+ concentration and sodium concentration, respectively, in the unknown sample and E_{Cal1}, $c_{(Cal1)}$ and $c_{Na(Cal1)}$ are the

Table 3 Selectivity coefficients of Li ionophores in 0.1 mol dm^{-3} interferent background

	Log k^{pot}_{ij}				
	Na	K	Ca	Mg	H*
Target values	<−4.3	<−2.8	<−3.0	<−3.5	<−2.1
Philips	−1.3	−2.15	−3.22	−3.7	−1.0
14-crown-4-dibenz	−1.4	−2.3	−4.5	−5.8	−3.5
14-crown-4-dinbutam	−3.0	−3.5	−4.2	−5.7	−0.9
14-crown-4-diibutam	−2.9	−4.3	−4.3	−5.3	1.1
ETH 1810†	−2.45	−2.6	−2.7	−4.0	−1.0
ETH 2137 (Corning)	−1.9	—	—	—	—

* Proton interference in 0.001 mol dm^{-3} HCl (pH = 3).
† Values from the Fluka Selectophore catalogue.

Table 4 Protein interference. Error (%) = $\{[c_{(actual)} - c_{(expected)}]/[c_{(expected)}]\} \times 100$. k^{pot}_{ij} = 1.2 × 10^{-2} Corning, 1.2 × 10^{-3} di-*n*-butylamide, 6.3 × 10^{-4} diisobutylamide

		Error (%)			
Plasma : water ratio	[Li]/ mol dm^{-3}	Corning*	Corning†	Di-*n*-butyl-amide	Diiso-butyl-amide
1 : 10	0.22	0	−58.8	0	−30.6
	0.40	0	−6.7	0	−24.0
	0.60	−1.3	−6.0	0	+5.4
	0.80	−2.1	−5.0	−1.2	+12.9
1 : 5	0.20	0	−46.7	0	−100.0
	0.35	−0.3	−11.1	0	−100.0
	0.54	−2.8	−8.9	−3.0	−65.0
	0.72	−4.8	−5.2	−4.2	−30.7
1 : 2	0.125	−100.0	−52.6	−44.0	−100.0
	0.22	−17.4	−9.1	−6.8	−91.3
	0.34	−18.1	−9.1	−7.8	−82.8
	0.42	−18.9	−7.9	−7.4	−52.2

* Concentration mode.
† Millivolt mode.

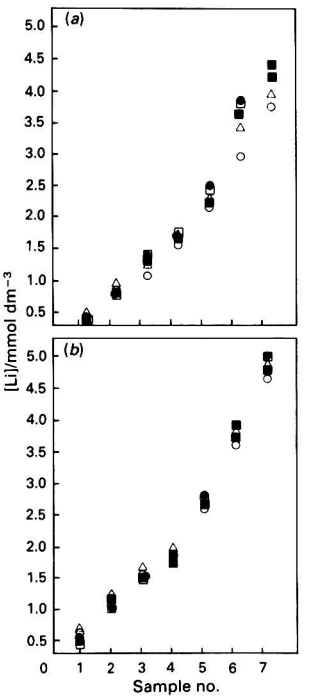

Fig. 5 Comparison of atomic absorption spectrometry, ETH 2137–BBPA and di-*n*-butylamide–oNPOE ISEs in (*a*) aqueous solution and (*b*) plasma. ○, ETH 2137; ■, di-*n*-butylamide; ●, flame; △, ETH 2137; and □, di-*n*-butylamide. ○ and ■, Using concentrations; and △, and □, using activities

Table 5 Comparison of flame photometry, ETH 2137–BBPA ISE and di-*n*-butylamide–oNPOE ISE, using concentrations directly. Concentration units, mmol dm^{-3}; c_{un}, uncorrected concentrations; c_{cr}, concentrations corrected for plasma water; refractive index for plasma sample = 1.354; plasma water = 91.5%; [Na] in plasma determined by atomic absorption spectrometry = 148 mmol dm^{-3}; error (%) = $(c_{ISE} - c_{Flame})/c_{Flame} \times 100$

	ETH 2137*			Di-*n*-butylamide*			Flame†
Solution	*c*		Error (%)	*c*		Error (%)	*c*
AQ1	0.40		+1.1	0.40		+1.1	0.39
AQ2	0.86		+6.2	0.78		−3.7	0.81
AQ3	1.24		−13.9	1.39		−3.5	1.44
AQ4	1.58		−9.2	1.70		−2.3	1.74
AQ5	2.19		−14.0	2.41		−5.5	2.55
AQ6	3.28		−15.0	3.67		−4.9	3.86
AQ7	3.79		−14.4	4.22		−4.7	4.43
	c_{un}	c_{cr}	Error (%)	c_{un}	c_{cr}	Error (%)	
PL1	0.57	0.62	+19.2	0.46	0.50	−3.8	0.52
PL2	0.97	1.06	+0.9	0.99	1.08	+2.8	1.05
PL3	1.43	1.56	+3.3	1.37	1.50	−0.7	1.51
PL4	1.69	1.85	+0.5	1.65	1.81	−1.6	1.84
PL5	2.40	2.62	−7.1	2.43	2.66	−5.6	2.82
PL6	3.34	3.65	−6.6	3.39	3.71	−5.1	3.91
PL7	4.29	4.69	−6.6	4.37	4.78	−4.8	5.02

* Error on ISE values, about 1% (equivalent to ±0.3 mV).
† Error on flame values, about 3%.

corresponding values in calibration solution, Cal 1. $k^{pot}_{Li,Na}$ is the appropriate selectivity coefficient and S is the slope of the electrode at ambient temperature. Concentrations were corrected[18] for 93% plasma water. Expected values were based on atomic absorption measurements of Li^+ in the diluents (Table 4). The diisobutylamide based derivative behaved very poorly, whereas the performance of the di-*n*-butylamide based electrode is better than that of the Corning ETH 2137 electrode. Errors are larger in solutions with higher serum and lower lithium concentrations. The approximate 18% error (Table 4) observed in the Corning concentration mode, which is the commonly used mode, is disconcerting.

To substantiate these results, further tests were performed on the di-*n*-butylamide–oNPOE based electrode and an ETH 2137–BBPA based electrode made from the parent ionophore. (Calibrations with electrodes based on the opposite combination, *viz.*, di-*n*-butylamide–BBPA and ETH 2137–oNPOE in aqueous solutions containing Na^+, K^+, Ca^{2+} and Li^+ at levels normally present in blood, showed that these combinations were unsuitable for use as clinical sensors.) Aqueous samples AQ1–AQ7 and plasma samples PL1–PL7 were injected into the flow cells and readings were taken as before. Atomic absorption measurements, on each sample, were performed in parallel. The results, shown in Table 5, were corrected for the presence of protein using refractive index measurements. The di-*n*-butylamide electrodes, again, appeared to be superior to the ETH 2137 electrode. The errors are higher for plasma samples containing >2.0 mmol dm^{-3} Li^+.

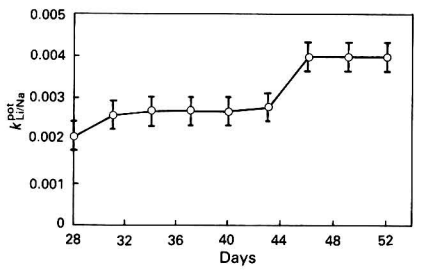

Fig. 6 Lifetime of a 14-crown-4 di-*n*-butylamide ISE used in serum for 4 weeks

Activity coefficients for Cal 1, Cal 2 and solutions AQ1–AQ7 were calculated using the Pitzer equation[19] (Table 6). Concentrations were calculated using

$$E_u - E_{Cal\,1} = S \log\{[c_{Li(u)}\,\gamma_{Li(u)} + k^{pot}_{Li,Na}\,c_{Na(u)}\,\gamma_{Na(u)}]/[c_{Li(Cal\,1)}\,\gamma_{Li(Cal\,1)} + k^{pot}_{Li,Na}\,c_{Na(Cal\,1)}\,\gamma_{Na(Cal\,1)}]\} \quad (2)$$

where $c\gamma = a$, 'a' being the activity of the appropriate ion and γ the corresponding activity coefficient. The other symbols have the same significance as in equation (1). The results given in Table 7 show marked improvement when activity coefficient corrections are made for the solutions of higher lithium concentrations (AQ3–AQ7 and PL4–PL7). The behaviour of the di-*n*-butylamide electrode is significantly improved by using activities [Fig. 5(*a*) and (*b*)].

The stability of a di-*n*-butylamide–oNPOE based ionophore used for 4 weeks in serum was monitored for a further 3 weeks with Cal 1 and Cal 2. The results are shown in Fig. 6. The selectivity coefficient was 1.26×10^{-3} for the fresh membrane. After 4 weeks it decreased to 2.0×10^{-3} and after a further 2.5 weeks to 3.96×10^{-3}. The fresh ETH 2137–BBPA membrane has a selectivity coefficient of 1.26×10^{-2}, much higher than that of the di-*n*-butylamide sensor.

Table 6 Activity coefficients based on the Pitzer equation. Solutions AQ1–AQ7 contain 0.140 mol dm^{-3} Na^+, 0.004 mol dm^{-3} K^+ and 0.0012 mol dm^{-3} Ca^{2+}; Cal 1 and Cal 2 contain 0.140 mol dm^{-3} Na^+ and 0.004 mol dm^{-3} K^+

Solution	[Li]/ mol dm^{-3}	I	γ_{Li}	γ_{Na}
AQ1	0.0005	0.1457	0.7758	0.7542
AQ2	0.001	0.1462	0.7757	0.7540
AQ3	0.0015	0.1467	0.7756	0.7537
AQ4	0.002	0.1472	0.7754	0.7535
AQ5	0.003	0.1482	0.7752	0.7533
AQ6	0.004	0.1492	0.7749	0.7529
AQ7	0.005	0.1502	0.7747	0.7526
Cal 1	0.001	0.1440	0.7765	0.7751
Cal 2	0.0025	0.1455	0.7761	0.7546

Conclusion

The best clinically relevant Li ionophore reported, to date, is ETH 1810–oNPOE, with a log $k^{pot}_{Li,Na} = -2.45$; well below the target value of −4.3 required for less than 1% interference. This ionophore is reported to have a slow response and limited lifetime when used in serum.[20,21] The preferred ionophore, ETH 2137–BBPA has log $k^{pot}_{Li,Na} = -1.9$.

The target ionophore with $k^{pot}_{Li,Na} = 5.0 \times 10^{-5}$ has a potential difference (ΔE) of 24.5 mV at 37 °C when transferred from Cal 1 to Cal 2. The ETH 2137–BBPA electrode has a ΔE of 11.9 mV ($k^{pot}_{Li,Na} = 1.2 \times 10^{-2}$) corresponding to a correction factor of 12.6 mV whereas the di-*n*-butylamide–

Table 7 Comparison of flame photometry, ETH 2137–BBPA ISE and di-*n*-butylamide–oNPOE ISE, making activity coefficient corrections

	ETH 2137			Di-*n*-butylamide			Flame
Solution	c		Error (%)	c		Error (%)	c
AQ1	0.45		+15.4	0.38		−2.6	0.39
AQ2	0.92		+13.6	0.78		−3.7	0.81
AQ3	1.33		−7.6	1.42		−1.4	1.44
AQ4	1.69		−2.9	1.75		+0.6	1.74
AQ5	2.30		−9.8	2.50		−2.0	2.55
AQ6	3.45		−10.6	3.83		−0.8	3.86
AQ7	3.97		−10.4	4.41		−0.5	4.43
	c_{un}	c_{cr}	Error (%)	c_{un}	c_{cr}	Error (%)	
PL1	0.63	0.69	+32.7	0.44	0.48	−7.7	0.52
PL2	1.04	1.14	+8.6	1.00	1.09	+3.8	1.05
PL3	1.52	1.66	+9.9	1.40	1.53	−1.3	1.51
PL4	1.80	1.97	+7.1	1.70	1.85	+0.5	1.84
PL5	2.54	2.77	−1.8	2.52	2.75	−2.5	2.82
PL6	3.52	3.85	−1.5	3.53	3.86	−1.3	3.91
PL7	4.51	4.93	−1.8	4.56	4.99	−0.6	5.02

oNPOE electrode has a ΔE of 18.5 mV ($k^{pot}_{Li,Na} = 2.4 \times 10^{-3}$) requiring a correction factor of 6.0 mV.

The sensor is stable in serum, has a short response time (about 10–15 s) and a lifetime of at least 50 d. These factors demonstrate that this ionophore is reliable for the assay of Li.

We thank SERC for support, Dr. C. T. G. Flear (Royal Victoria Infirmary, Newcastle-upon-Tyne) and Dr. C. J. Fischer (County Hospital, Durham) for useful discussions and Robert Coult for carrying out the atomic absorption measurements.

References

1 Amdisen, A., in *Handbook of Lithium Therapy*, ed. Johnson, F. N., MTP Press, Lancaster, 1986, ch. 2.
2 Metzger, E., Dohner, R., and Simon, W., *Anal. Chem.*, 1987, **59**, 1600.
3 Oggenfuss, P., Morf, W. E., Oesch, U., Ammann, D., Pretsch, E., and Simon, W., *Anal. Chim. Acta*, 1986, **180**, 299.
4 Kimura, K., Kitazawa, S., and Shono, T., *Chem. Lett.*, 1984, 639.
5 Metzger, E., Aeschmann, R., Egli, M., Suter, G., Dohner, R., Ammann, D., Dobber, M., and Simon, W., *Helv. Chim. Acta*, 1986, **69**, 1821.
6 Attiyat, A. S., Christian, G. D., Xie, R. Y., Wen, X., and Bartsch, R. A., *Anal. Chem.*, 1988, **60**, 2561.
7 Gadzekpo, V. P. Y., Moody, G. J., and Thomas, J. D. R., *Analyst*, 1986, **111**, 567.
8 Kimura, K., Yano, H., Kitazawa, S., and Shono, T., *J. Chem. Soc., Perkin Trans. 2*, 1986, 1945.
9 Metzger, E., Ammann, D., Schefer, U., Pretsch, E., Simon, W., *Chimia*, 1984, **38**, 440.
10 Kataky, R., Nicholson, P. E., and Parker, D., *Tetrahedron Lett.*, 1989, **30**, 4559.
11 Kataky, R., Nicholson, P. E., and Parker, D., *J. Chem. Soc., Perkin Trans. 2*, 1990, 321.
12 Good, N. E., Winget, G. D., Winter, W., Connolly, T. N., Izawa, A., and Singh, R. M. M., *Biochemistry*, 1966, **5**, 467.
13 Covington, A. K., Kelly, P. M., and Maas, A. H. J., in *Methodology and Clinical Applications of Ion-Selective Electrodes*, eds. Maas, A. H. J., Buckley, B. M., Manzoni, A., Moran, R. F., Siggaard Andersen, O., and Sprokholt, R., Davies Printing Co., Rochester, 1989, vol. 10, p. 4.
14 Craggs, A., Moody, G. J., and Thomas, J. D. R., *J. Chem. Educ.*, 1974, **51**, 541.
15 Horvai, G., Toth, K., and Pungor, E., *Anal. Chim. Acta*, 1976, **82**, 45.
16 Corning 654 (Na^+, K^+, Li^+) Analyser Reference Manual, Corning, 1988.
17 Ammann, D., Anker, P., Metzger, E., Oesch, U., and Simon, W., in *Ion Measurements in Physiology and Medicine*, eds. Kessler, M., Harrison, D. K., and Höper, J., Springer Verlag, Berlin, 1985, p. 102.
18 Czaban, J. D., and Legg, K. D., in *Proceedings of the Workshop on Direct Potentiometric Measurements in Blood*, ed. Koch, W. F., Gaithersburg, MD, 1983, p. 63.
19 Covington, A. K., and Ferra, M. I. A., *Scand. J. Clin. Lab. Invest.*, 1989, **49**, 667.
20 Metzger, E., Dohner, R., Simon, W., Voncherschmitt, D. J., and Gautschi, K., *Anal. Chem.*, 1987, **59**, 1600.
21 Gadzekpo, V. P. Y., Hungerford, J. M., Kadry, A. M., Ibrahim, Y. A., Xie, R. Y., and Christian, G. D., *Anal. Chem.*, 1986, **58**, 1948.

Paper 0/03204B
Received July 17th, 1990
Accepted August 20th, 1990

Magnesium as a Modifier for the Determination of Barium in Offshore Oil-well Waters by Direct Current Plasma Atomic Emission Spectrometry and Flame Atomic Absorption Spectrometry

Mohammad Jerrow and Iain Marr
Department of Chemistry, University of Aberdeen, Meston Walk, Old Aberdeen, AB9 2UE, UK
Malcolm Cresser
Department of Plant and Soil Science, University of Aberdeen, Meston Walk, Old Aberdeen, AB9 2UE, UK

It is shown that the addition of magnesium (5 mg ml^{-1}) to samples for the determination of barium by d.c. plasma atomic emission spectrometry enhances the sensitivity of the analysis and dramatically reduces interference from calcium and strontium at both atomic and ionic emission wavelengths. In the presence of high concentrations of sodium, magnesium is a slightly less effective plasma modifier, but still allows the determination of barium with a precision that is adequate for most practical purposes. Magnesium (in both the presence and absence of sodium) also reduces the interference of alkaline earth concomitants in the determination of barium by atomic absorption spectrometry using a fuel-rich dinitrogen oxide–acetylene flame.

Keywords: *Barium; oil-well water; direct current plasma atomic emission spectrometry; flame atomic absorption spectrometry; magnesium*

The determination of barium in offshore oil-well waters is important because of the risk of precipitation of barium sulphate scale as a consequence of mixing with sea-water pumped downhole to maintain hydrostatic pressure and assist oil production. Thus, there is a need for a reliable procedure for the measurement of barium in the mg l^{-1} range in the presence of large excesses of sodium and magnesium and variable amounts of calcium and strontium.

Although it is widely accepted that the determination of barium by flame atomic absorption spectrometry (FAAS) requires the use of a high temperature, dinitrogen oxide–acetylene flame to minimize interferences and give the required sensitivity, the determination is not straightforward. In the presence of high concentrations of alkali or alkaline earth elements, at least five potential mechanisms exist for interference.

Barium has a low ionization potential, and its determination at low concentrations is thus susceptible to ionization interference from concomitant elements with low ionization potentials. Generally, the lower the ionization potential of the concomitant element at any given molar excess, the greater the ionization suppression and enhancement of atomic absorbance (or suppression of ionic absorbance). This effect has been extensively investigated by Maruta *et al.*,[1] although these workers did not report the tolerance limits for concomitants in the presence of ionization buffers.

Capacho-Delgado and Sprague[2] and Koirtyohann and Pickett[3] investigated the strong molecular absorbance of CaOH in air–acetylene flames at the main barium resonance line, 553.6 nm, and showed that the absorption spectrum of CaOH closely resembled the emission spectrum of barium in this vicinity. In the dinitrogen oxide–acetylene flame, the formation of free atoms is increased, and that of polyatomic oxgyen-containing species reduced, especially in the fuel-rich flame. Thus, for example, using potassium naphthenate as an ionization buffer, Holding and Rowson[4] were able to determine barium in used lubricating oils in the presence of a modest excess of calcium, following dilution of samples with 2-methylpropan-2-ol plus toluene (3 + 2) containing small amounts of water. Concentrations of molecular species such as CaOH tend to be greatest at the flame edges.[5] The extent of molecular absorption interference therefore depends critically upon flame stoichiometry,[4] flame geometry and the optical path of the hollow cathode lamp beam through the flame. It further depends upon the performance of the nebulizer and spray chamber used. Thus, often different results are obtained in spectral interference studies on different instruments, or even on the same instrument, operated under slightly changed conditions.

Rooney and Woolley[6] suggested that much of the spectral interference attributed to CaOH could be an instrumental artefact, reflecting the inadequate ability of detectors to discriminate between a.c. and d.c. signals when the latter were excessively large. They suggested that the calcium–barium system could be a valuable test of this aspect of instrument performance. However, they did not apparently consider the point outlined above; namely the variation between instruments with regard to the flame width effectively used and the flame geometry. This could undoubtedly be reflected in the differences between performance in the series of instruments which they studied.

The other potential contributing factors to net interference, when using high salt matrices, are aerosol ionic redistribution, the AIR effect,[7] and other transport interferences related to changes in aspiration rate or to primary aerosol generation by the nebulizer. To date, AIR effects have apparently not been studied for ternary cation mixtures, but their possible occurrence for samples with a concentrated sodium chloride matrix certainly warrants investigation.

When Cioni *et al.*,[8] in 1976, reviewed interference effects in the determination of barium in silicates by AAS, they did not consider all the mechanisms outlined briefly above, but they nevertheless concluded that the separation of barium from concomitant elements was an essential prerequisite to reliable analysis. Numerous other workers have reached the same conclusion, and separation techniques suggested include ion exchange[9,10] and co-precipitation.[11] Solvent extraction has not been used much for barium, but its use, prior to furnace AAS determination, has been recommended.[12]

The low excitation potential for barium suggests that the determination of the element by atomic emission spectrometry (AES) should be highly sensitive if a high-temperature excitation source is employed. In practice, a detection limit of 0.3 μg l^{-1} has been reported for the analysis of hard water by inductively coupled plasma atomic emission spectrometry (ICP-AES) after 10-fold evaporative preconcentration, with no spectral interference from up to 200 mg l^{-1} of magnesium.[13] Other inter-element effects were not con-

sidered. The effects of easily ionizable elements (EIEs) in ICP-AES are more complex than in FAAS. Blades and Horlick[14] showed that the EIEs enhanced emission of both atomic and ionic lines in the lower regions of the plasma, but depressed emission for both species in the upper regions. The mechanism in the lower region was attributed to enhanced collisional excitation as a result of an increased number of electrons with sufficient energy to cause excitation of atomic or ionic species. The enhancement increased slightly as the concomitant element ionization potential decreased. A similar conclusion was drawn by Gunter *et al.*[15] Thompson and Ramsey[16] used a twin-nebulizer technique to demonstrate that calcium matrix effects were a consequence of something happening to the plasma itself, and not to a transport, volatilization or atomization phenomenon. They compared three techniques for minimizing calcium matrix effects, and found interactive matrix matching to be the most useful. Correction by the parameter-related internal standard method (PRISM) was partially successful only for some determinands. They suggested that calcium might prove a useful excitation buffer for other matrix elements. Maessen *et al.*[17] studied the separate and combined matrix effects of selected alkali and alkaline earth metals on net ICP-AES emission line and background intensities for a series of elements, and showed that composite matrix effects were less than the sums of individual matrix effects. These results show that great care is needed if reliable results for barium determination by ICP-AES in complex and variable alkali and alkaline earth element matrices are to be obtained.

Collins[18] advocated the use of a d.c. plasma (DCP) as early as 1967 for the determination of five elements, including barium, in oilfield waters. Although sodium, magnesium and calcium all interfered in the determination of barium, he found that, by appropriate, approximate matrix matching using a synthetic brine and adding propionic acid, matrix effects could be kept within acceptable limits (±10%). Johnson *et al.*[19] showed that phosphate did not interfere significantly in the determination of barium by DCP-AES.

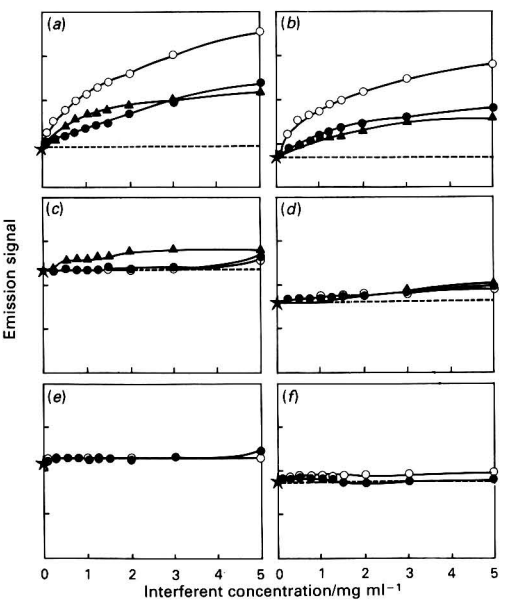

Fig. 1 Effects of increasing concentrations of ○, Ca; ●, Sr; and ▲, Mg on the determination of barium (emission from 1 μg ml^{-1}) at (*a*) (*c*) and (*e*) 553.6 nm and (*b*), (*d*) and (*f*) 455.4 nm in the absence of other cations [(*a*) and (*b*)] and in the presence of 3 g l^{-1} Na [(*c*) and (*d*)] or 5 g l^{-1} Mg [(*e*) and (*f*)]

The above consideration suggested that further investigation of the potential of DCP-AES for the determination of barium in oilfield waters should prove worthwhile, in order to see if a suitable excitation buffer could be found to allow simple, rapid and reliable determination.

Experimental

Apparatus

Atomic and ionic absorption measurements were made at 553.6 and 455.4 nm, respectively, by using a Philips SP9 atomic absorption spectrometer with a fuel-rich dinitrogen oxide–acetylene flame at a spectral bandwidth of 0.2 nm. Emission measurements for the same transitions were made using a Spectraspan III d.c. plasma échelle optical emission spectrometer, with 200 nm high, 100 nm wide slits.

Reagents

Stock solutions of sodium, magnesium, strontium and barium were made from analytical-reagent grade salts and a calcium stock solution from calcium carbonate, following dissolution in the minimum possible volume of dilute hydrochloric acid. The stock solutions, other than that for barium, were analysed by AES by scanning through the emission from the DCP, to check that they did not contain significant amounts of barium.

Results and Discussion

The graphs in Fig. 1(*a*) and (*b*) show the effects of increasing amounts of calcium, strontium and magnesium upon the apparent barium emission signals when solutions containing these cations plus 1 μg ml^{-1} of barium were nebulized into the DCP. The enhancements in emission signal are broadly comparable at both the atomic line [Fig 1(*a*), (*c*) and (*e*)] and the ionic line [Fig. 1(*b*), (*d*), and (*f*)]. This confirms that the effect is not significantly attributable to the suppression of the ionization by the concomitant elements. Thus, the DCP in this respect behaves much as the ICP, as discussed earlier. The atomic and ionic absorption results, on the other hand [Fig. 2(*a*)] show that as the atomic absorption signal increased with increasing concomitant concentration and increasing ioniza-

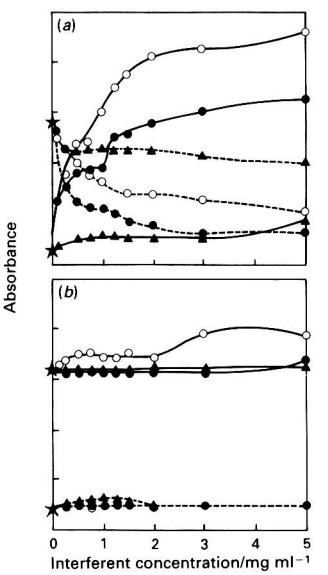

Fig. 2 Effects of ○, Ca; ●, Sr; and ▲, Mg on the atomic (solid line) and ionic (broken line) absorbance from barium at 1 μg ml^{-1}, (*a*) in the absence of other cations and (*b*) in the presence of Na at 3 g l^{-1}

tion suppression, the ionic absorption signal decreases. The decrease is not *pro rata*, however, because of the spectral interference from the CaOH species. Thus, while the order of suppression of ionization is Sr > Ca > Mg, as would be expected from the respective ionization potentials, the order of apparent atomic absorption enhancement is Ca > Sr > Mg.

The close relationship between the graphs in Fig. 1(*a*), (*b*), (*c*) and (*d*) suggests in fact that ionization suppression by concomitant elements is of minor importance in the DCP, and that the effects of calcium, strontium and magnesium are probably *via* changes induced in the plasma and enhanced collisional excitation.

The effects of magnesium and strontium are similar, but calcium has a more substantial impact, which is not the trend that would be expected for an ionization suppression effect. Another possible contributing factor could be ionic redistribution which sometimes occurs upon aerosol generation, the AIR effect. This seems unlikely to be a major factor here, however, because hitherto AIR effects have only been observed at higher alkali metal concentrations, and because of the disparate behaviour in DCP-AES and FAAS. In FAAS, the presence of an excess of sodium, as expected, largely suppresses the ionization interference of magnesium, calcium and strontium on the determination of barium, although the calcium spectral interference from CaOH absorbance is still discernible [Fig. 2(*b*)]. Background compensation is clearly essential if FAAS is to be used for the determination of barium in the presence of variable amounts of calcium on the instrument used here. However, the output from continuum sources at this wavelength is so low on some instruments that the background correction is inoperable.

Sodium at a concentration of 3 g l^{-1} also substantially reduces the extent of interference from magnesium, calcium and strontium in the determination of barium by DCP-AES [Fig. 1(*c*) and (*d*)].

At the wavelength of the barium atomic emission, 553.6 nm, magnesium still has a significant effect, and barium could not be reliably determined by DCP-AES if only the sodium concentrations were matrix matched, and magnesium concentration was variable between samples. Thus, although an excess of sodium apparently stabilizes the excitation conditions, the effect is inadequate for reliable routine work.

The results given above suggest that magnesium has a greater effect on plasma excitation conditions than does sodium, which in turn suggests that magnesium might be a more useful plasma modifier for the DCP than sodium. The graphs in Fig. 1(*e*) and (*f*) confirm that magnesium may indeed be used to prevent interference from calcium and strontium in barium determinations. At the ion line, however, calcium still causes a small enhancement in barium emission [Fig. 1(*f*)].

As most samples of interest are likely to contain sodium at a fairly high concentration, the effect of magnesium (5 g l^{-1}) was also studied in the presence of sodium (3 g l^{-1}). The results (Fig. 3) show that the mixture is less efficient than magnesium alone in stabilizing the plasma against the effects of calcium and strontium. However, they confirm that a concentration of up to 2 g l^{-1} of calcium or strontium can be tolerated, and that if samples contain a few hundred or a few thousand mg l^{-1} of calcium and/or strontium, the subsequent analysis will be more accurate if a sodium plus magnesium modifier is used than if sodium alone is used.

If magnesium is added as a modifier in FAAS, the effects of calcium and strontium on barium absorbance are much reduced (compare Fig. 4 with Fig. 2). Surprisingly, in the presence of 5 g l^{-1} of magnesium, low concentrations (<800 mg l^{-1}) of calcium and strontium depress the atomic absorption signal of barium [Fig. 4(*a*)], an effect not echoed in the ionic absorbance graphs. This is possibly an incomplete volatilization interference, observed because it is low in the red feather zone. In the presence of sodium (3 g l^{-1}) plus magnesium (5 g l^{-1}), high concentrations of calcium and strontium both significantly enhance the barium atomic absorbance [Fig. 4(*b*)].

In order to confirm that the beneficial effects observed for magnesium in DCP-AES were not confined to the specific set of operational parameters used, observations were made at different heights in the plasma analytical zone and at different aspiration rates. Fig. 5(*a*) shows that increasing the aspiration rate from 1.45 to 2.60 ml min^{-1} did not adversely influence the enhancement of barium emission caused by magnesium. It is notable that this increase in aspiration rate had a very small effect upon the size of the barium signal, almost certainly

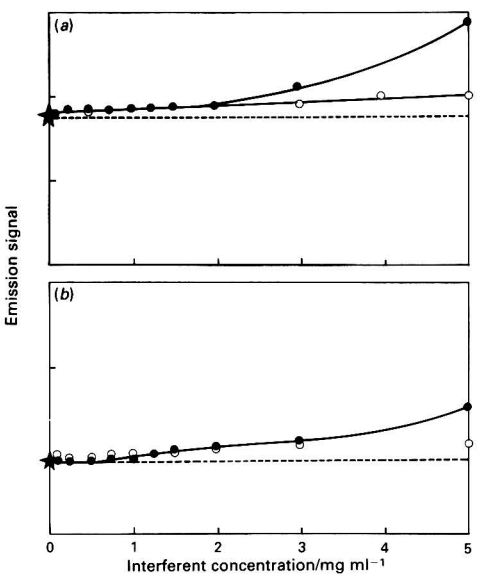

Fig. 3 Effects of increasing concentrations of ○, Ca; and ●, Sr on the emission from barium at 1 μg ml^{-1} at (*a*) 553.6 nm and (*b*) 455.4 nm, in the presence of Mg at 5 g l^{-1} plus Na at 3 g l^{-1}

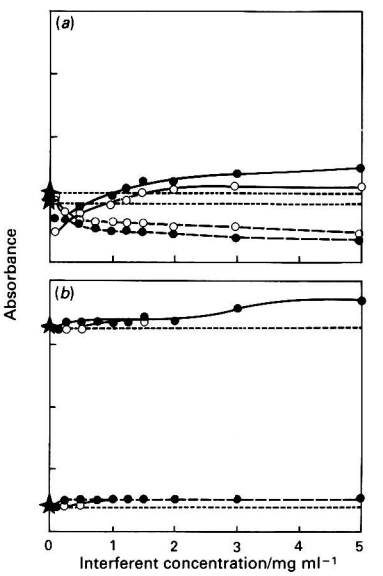

Fig. 4 Effects of increasing concentrations of ○, Ca; and ●, Sr on the atomic (solid line) and ionic (broken line) absorbance from barium at 1 μg ml^{-1} in the presence of (*a*) Mg at 5 g l^{-1} and (*b*) Mg at 5 g l^{-1} plus Na at 3 g l^{-1}

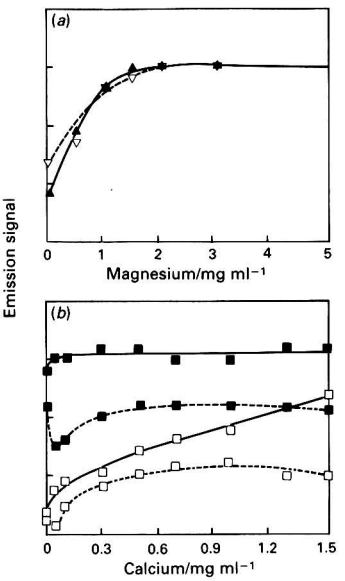

Fig. 5 Effects of aspiration rate on interferences in the signals from barium at 1 μg ml^{-1}; solid lines = 1.45 ml min^{-1}, broken lines = 2.60 ml min^{-1}. (*a*) Effect of increasing amounts of Mg; (*b*) effects of increasing amounts of Ca □, in the absence; and ■, presence of Mg at 5 g l^{-1}

because of the less favourable aerosol size distribution produced. Magnesium was effective in dramatically reducing interference from increasing amounts of calcium at both aspiration rates [Fig. 5(*b*)]. It is interesting to note that low concentrations of calcium depressed the barium emission at 455.4 nm at the higher aspiration rate, but not at the lower rate, even when magnesium was present. This, plus the relative shapes of the graphs in Fig. 5(*a*), indicate that the effect of magnesium as a plasma modifier or excitation buffer is greater when the water loading to the plasma (or posssibly the aerosol size distribution reaching the plasma) is lower. Changing the height of observation in the plasma had very little effect upon the benefits of using magnesium as an excitation buffer.

It is a common misconception that ionization buffers in FAAS totally suppress the ionization of the determinand, but this is not always so. Fig. 2, for example, shows that 3 g l^{-1} of sodium is approximately as effective as 3 g l^{-1} of strontium. Adding calcium or strontium at high concentrations to solutions containing sodium and magnesium may further enhance atomic absorbance signals. Great care is therefore needed when selecting ionization buffers for use in FAAS for samples such as oilfield brines.

Conclusions

Magnesium is an excellent excitation buffer for the determination of low concentrations of barium at 553.6 nm by DCP-AES, eliminating the effects of up to 4 g l^{-1} of both calcium and strontium. However, tolerance of these elements is reduced to about 2 g l^{-1} in the presence of sodium at a concentration of 3 g l^{-1}, and, even at only 2 g l^{-1} of a concomitant, a 5% change in signal is still observed. Clearly, therefore, great care is needed when determining barium by DCP-AES to ensure that whatever excitation buffer is used can cope with the conceivable range of concomitant elements present. Magnesium has the further advantage that it is less expensive than the more commonly used high-purity lithium salts for DCP-AES.

Care is also needed when determining barium in offshore oilfield waters by flame AAS. It should not be presupposed that the sodium will be totally adequate as an ionization buffer if other easily ionized concomitants are present. The presence of magnesium may drastically alter the effects of calcium and strontium on the determination of barium by FAAS, and it appears that incorporation of both sodium and magnesium into standards is required, as well as background compensation for CaOH absorbance.

M. Jerrow is grateful to the Iraq Ministry of Higher Education for financial support for this work.

References

1 Maruta, T., Takeuchi, T., and Suzuki, M., *Anal. Chim. Acta*, 1972, **58**, 452.
2 Capacho-Delgado, L., and Sprague, S., *At. Absorpt. Newsl.*, 1965, **4**, 363.
3 Koirtyohann, S. R., and Pickett, E. E., *Anal. Chem.*, 1966, **38**, 585.
4 Holding, S. T., and Rowson, J. J., *Analyst*, 1975, **100**, 465.
5 Cresser, M. S., Keliher, P. N., and Kirkbright, G. F., *Selected Ann. Rev. Anal. Sci.*, 1973, **3**, 139.
6 Rooney, R. C., and Woolley, J. F., *Analyst*, 1978, **103**, 1100.
7 Borowiec, J., Boorn, A. W., Dillard, J. H., Cresser, M. S., Browner, R. F., and Matteson, M. J., *Anal. Chem.*, 1980, **52**, 1059.
8 Cioni, R., Mazzucotelli, A., and Ottonello, G., *Analyst*, 1976, **101**, 956.
9 Sixta, V., Miksovsky, M., and Sulek, Z., *Fresenius Z. Anal. Chem.*, 1975, **273**, 193.
10 Strasheim, A., Strelow, F. W. A., and Norval, E., *J. Chem. South Afr. Chem. Inst.*, 1967, **20**, 25.
11 Bano, F. J., *Analyst*, 1973, **98**, 655.
12 Sugiyama, M., Fujino, O., and Matsui, M., *Bunseki Kagaku*, 1984, **33**, E123.
13 Thompson, M., Ramsey, M. H., and Pahlavanpour, B., *Analyst*, 1982, **107**, 1330.
14 Blades, M. W., and Horlick, G., *Spectrochim. Acta, Part B*, 1981, **36**, 881.
15 Gunter, W., Visser, K., and Zeeman, P. B., *Spectrochim. Acta, Part B*, 1985, **40**, 617.
16 Thompson, M., and Ramsey, M. H., *Analyst*, 1985, **110**, 1413.
17 Maessen, F. J. M. J., Balke, J., and de Boer, J. L. M., *Spectrochim. Acta, Part B*, 1982, **37**, 517.
18 Collins, A. G., *Appl. Spectrosc.*, 1967, **21**, 16.
19 Johnson, G. W., Taylor, H. E., and Skogerboe, R. K., *Anal. Chem.*, 1979, **51**, 2403.

Paper 0/03117H
Received July 11th, 1990
Accepted October 15th, 1990

Proposed Mechanism for the Action of Palladium and Nickel Modifiers in Electrothermal Atomic Absorption Spectrometry

Anatoly Volynsky*
V.I. Vernadsky Institute of Geochemistry and Analytical Chemistry, USSR Academy of Sciences, 19 Kosygin Street, 117975 Moscow, USSR

Sergei Tikhomirov and Anatoly Elagin
All-Union Research Institute of Organic Synthesis, 12 Radio Street, 107005 Moscow, USSR

By the use of Fourier transform infrared spectrometry it was found that palladium chloride decreased the temperature of the reduction of PbO and Ga_2O_3 with graphite; nickel chloride only catalysed the reduction of Ga_2O_3. A hypothesis is proposed that nickel and palladium salts promote the reduction of compounds (in atomic absorption measurements) at relatively low ashing temperatures. The resultant free elements form intermetallic compounds or solid solutions with metallic Pd and Ni, thus reducing or almost eliminating loss of analyte due to sublimation of halides, oxides, dimers and other compounds. The high efficiency and universal action of Pd modifiers are because the Pd metal can be easily formed from its compounds and also by the unique catalytic properties of metallic Pd.

Keywords: *Electrothermal atomic absorption spectrometry; palladium modifier; nickel modifier; mechanism of action; Fourier transform infrared spectrometry*

The compounds of nickel[1] and palladium and platinum[2] were introduced as modifiers in 1975 and 1979, respectively. At present, nickel compounds, platinum group metals (PGMs) and various different mixtures based on these are widely used for the determination of a great number of elements in various samples.[3–5] Palladium and nickel are known to form intermetallic compounds and solid solutions with the determined elements in the graphite furnaces.[6–9] The formation of such compounds causes an increase in the maximum permissible ashing temperature during the determination of elements of high- and mid-volatility. However, the mechanism of formation of the intermetallic compounds and solid solutions in graphite atomizers, when using such modifiers, is still rather vague. It is clear that Pd interacts in its metallic form. According to Morikawa *et al.*,[10] activated carbon partially reduces palladium chloride to the metal at room temperature. However, virtually all other elements detectable by electrothermal atomic absorption spectrometry (ETAAS) (with the exception of the noble metals), exist in the graphite atomizer in the form of oxides, chlorides[11] or other salts, within the temperature range 300–800 °C. It is still not clear why Pd is the most efficient modifier in the majority of instances.[5,12]

The supposition has been made,[12,13] that Ni and PGM modifiers catalyse some processes that occur in graphite atomizers for ETAAS. It might be that in the first stage of the process of the formation of solid solutions and intermetallic compounds, the graphite of the atomizer catalytically reduces the oxide analytes at low temperatures.[14] Nickel and PGMs are known as efficient catalysts for the reduction of the oxides of Mo, V, Cu, Sn, Re, Pb, W, Fe and Ni (other oxides have not yet been studied) with hydrogen, carbon monoxide and some hydrocarbons.[15,16]

By the use of X-ray photoelectron spectrometry,[17] it has been found that lead chloride is thermostable in a graphite atomizer at up to 600 °C; at higher temperatures it sublimes, whereas, in the presence of palladium chloride, metallic Pb is already apparent at 200 °C. This paper describes the investigation of the reduction of Pb and Ga oxides with graphite in the temperature range 100–1000 °C using Fourier transform infrared (FTIR) spectrometry.

Table 1 Initial (T_{in}) and final (T_f) temperatures of the reduction of Pb and Ga oxides with graphite

Experimental conditions	PbO		Ga_2O_3	
	T_{in}/°C	T_f/°C	T_{in}/°C	T_f/°C
Without catalyst	430	740	735	990
$NiCl_2 \cdot 6H_2O$ present	520	780	600	840
$PdCl_2$ present	340	500	360	720

* Present address: Laboratory of Organic Analysis, Department of Chemistry, Moscow State University, 119899 Moscow, USSR.

Experimental

Apparatus

For the identification of the gaseous products of the reactions, a Bruker FTIR spectrometer, Model IFS-113v, with a gas chromatographic interface was used. A JEOL pyrolyser, Model PL-722, was connected to the interface and the carrier gas flow (Ar, 30 ml min^{-1}) was controlled by a Carlo Erba Fractovap 4200 chromatographic block. The carrier gas was additionally purified, for traces of water vapour and free oxygen, with the aid of a Supelco high capacity gas purifier. The temperature of the pyrolytic oven was controlled by a thermocouple and registered on an analogue recorder with a 10 mV scale.

Procedure

Electrographite was pounded in a vibration mill. Just before the experiment, the graphite powder was heated in an Ar atmosphere for 40 min at 800 °C to remove adsorbed gases. The pre-heated graphite powder was mixed with the oxides (PbO, 3.5 mg; Ga_2O_3, 1.6 mg) with a mass ratio of approximately 5 : 1. The catalyst ($PdCl_2$ or $NiCl_2 \cdot 6H_2O$) was added to the reaction mixture in an atom ratio of carbon to metal of approximately 25 : 1. The maximum mass of the reaction mixture (about 25 mg) was limited by the size of the quartz crucible. The oxide mass in the mixture resulted in absorbance values of up to,0.3 during the measurements. The identification of the gaseous products of the reaction was performed within the following spectral windows: 2200–2100 cm^{-1} for carbon monoxide; 2380–2300 cm^{-1} for carbon

dioxide; 1700–1500 cm^{-1} for water; and 1860–1800 cm^{-1} for phosgene. The sensitivity for carbon dioxide is about 1.5-fold higher than that for carbon monoxide.

Results

As can be seen from Table 1, the reduction of lead monoxide in the absence of a catalyst starts at 430 °C. Below this temperature carbon dioxide is formed [Fig. 1(*a*)] due to the decomposition of the traces of $PbCO_3$ (t_{dec} = 315 °C).[18] The preliminary heating of PbO (10 min at 400 °C in an Ar atmosphere), although significantly reducing the area of this peak, fails to eliminate it completely. The interaction of Ga_2O_3 with graphite starts when the temperature is raised to 735 °C (Table 1). The erratic baseline shown in Fig. 1(*b*) is due to the temperature fluctuation of the light-pipe.[19] The effect appears to be pronounced in this particular instance because of the relatively high expansion of the ordinate axis.

The addition of nickel chloride substantially decreases the temperature of the reduction of Ga_2O_3 with graphite (Table 1) and changes the mechanism of the process towards the formation of carbon dioxide (Fig. 2). Nickel chloride does not produce a catalytic effect on the reduction of lead monoxide with graphite (Table 1). No traces of phosgene or water vapour are registered within the temperature interval examined (Fig. 3). Obviously, chlorine from nickel chloride evolves in the form of HCl,[20] but absorption bands due to HCl (3000–2800 cm^{-1}) lie beyond the limits of the interval examined. Water contained in $NiCl_2 \cdot 6H_2O$ apparently adsorbed on to the graphite starts to interact (at 800 °C) forming carbon dioxide (Fig. 2).

Palladium chloride sharply decreases the temperature of the reduction of the metal oxides with the graphite (Table 1). It can be seen that the CO_2 evolution is entirely complete in 3 min [Fig. 4(*a*)]. Carbon monoxide formation during the reduction of Ga_2O_3 becomes negligible [Fig. 4(*b*)]. A special 'blank' experiment was performed by heating the powdered graphite with palladium chloride in the absence of both lead and gallium oxide and neither CO_2 nor CO formation was detected.

Discussion

The results obtained corroborate the theory of the catalytic action of some modifiers on the reduction of the oxides of certain metals by graphite. It is necessary to note that these results have been obtained using electrographite powder as the reductant. Pyrolytic graphite is a much more inert material than electrographite, therefore, the reduction with pyrolytic graphite proceeds significantly slower. Hence, in the most popular graphite tubes with a pyrolytic graphite coating the catalytic effect should be more discernible. The direct experimental verification of this proposition is impossible by the procedure used. The main peculiarities of the pyrolytic graphite are the high degree of crystalline order and low concentration of active sites on its surface.[21] After severe pounding these peculiarities are lost.

Another difference of our experimental conditions from those used for ETAAS is the amount of lead and gallium oxides used, *i.e.*, mg instead of the μg and ng levels which are typical for ETAAS. The chemical and physical properties of clusters usually differ significantly from the properties of the bulk materials. This is a typical problem in the study of the processes that occur in the graphite tubes used in ETAAS, excluding the instances of usage of mass spectrometry or radioactive isotopic analysis. Thus, the temperatures of the reduction in the graphite tubes might differ from those obtained in our experiments.

We considered the principal processes occurring in graphite atomizers in the presence of the PGM modifiers with palladium chloride as an example. When a reductant (*e.g.*, the graphite of the atomizer) is present, palladium chloride

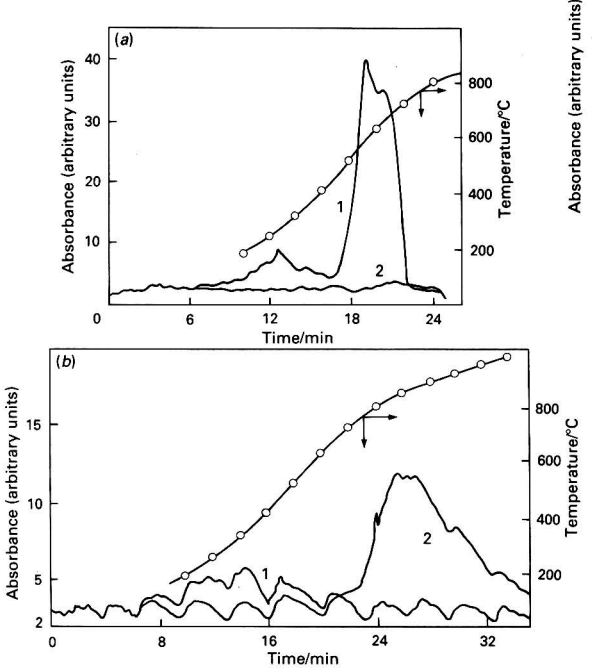

Fig. 1 Interaction of graphite with (*a*) PbO and (*b*) Ga_2O_3. 1, CO_2; and 2, CO

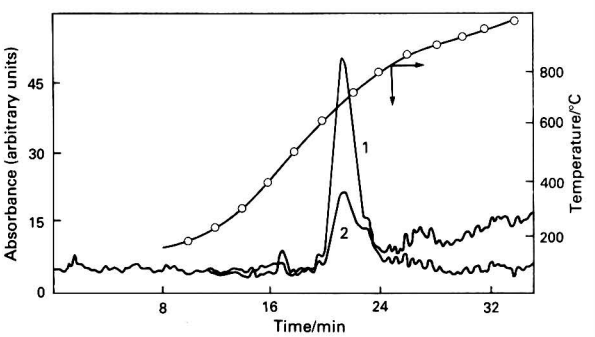

Fig. 2 Interaction of graphite with Ga_2O_3 in the presence of $NiCl_2 \cdot 6H_2O$. 1, CO_2; and 2, CO

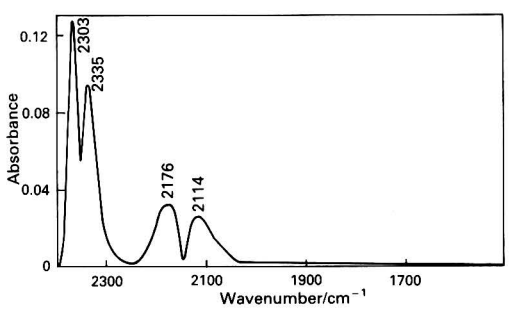

Fig. 3 Typical IR spectrum of a mixture of Ga_2O_3, graphite and $NiCl_2 \cdot 6H_2O$; T = 680 °C

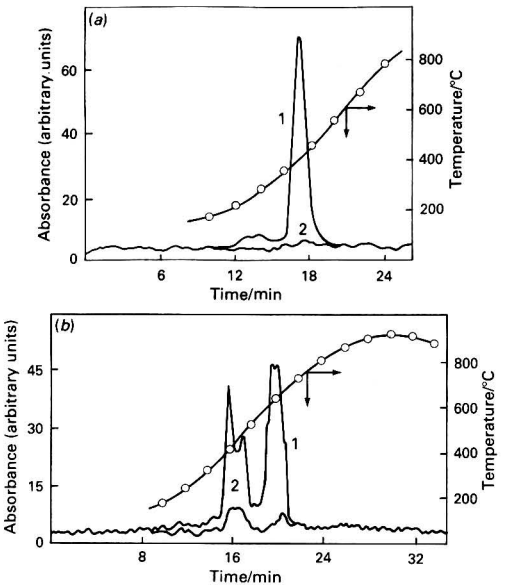

Fig. 4 Interaction of graphite with (*a*) PbO and (*b*) Ga_2O_3 in the presence of $PdCl_2$. 1, CO_2; and 2, CO

decomposes at the relatively low temperatures used during the ashing stage. The metallic Pd produced catalyses the reduction of the lead and gallium oxides and the lead chloride[17] with the graphite. The reduced metals dissolve in the Pd forming intermetallic compounds[7–9] or solid solutions.[6] Such a process is promoted in the graphite tube due to the amount of the modifier being 100–1000-fold higher than the amount of analyte. The increase in the sensitivity of the determination in the presence of such modifiers is caused by the formation of compounds of low volatility at the relatively low ashing temperatures. This formation decreases or eliminates any losses of analyte due to the sublimation of volatile chlorides,[17,22] oxides,[7,23] dimers,[7] hydrides[24] and other compounds.

Sometimes the catalyst not only decreases the temperature of the reduction for the compounds being determined, but also simultaneously changes the mechanism of the reduction. Without the catalyst, the products of Ga_2O_3 reduction are CO [Fig. 1(*b*)] and possibly Ga_2O[25] or GaO.[26] In the presence of $NiCl_2$ and especially $PdCl_2$ the main gaseous product of the reaction is CO_2 [Figs. 2 and 4(*b*)]. The marked increase in the maximum ashing temperature and sensitivity for gallium[26] suggests that in the presence of Pd and Ni modifiers, Ga_2O_3 is reduced to non-volatile products, *e.g.*, to the free metal. This supposition is verified by the absence of GaO in the electrothermal atomizer gas phase at the ashing stage in the presence of Ni compounds.[26]

Nickel forms compounds that are more thermostable than those of the PGMs (Table 2). The lack of elemental Ni in the reaction mixture at 300–400 °C is probably the main reason for the absence of the catalytic effect of nickel chloride on the reduction of PbO. According to thermodynamic calculations, nickel chloride is stable in an argon atmosphere in the graphite atomizer in the temperature range 230–630 °C.[24] Free hydrogen can reduce it to the metal at these temperatures; however, below 1000 °C the reaction between graphite and water, which produces free hydrogen, proceeds slowly without a catalyst. Nickel in the form of its compounds does not act as a catalyst for this process.[27] At 600 °C thermohydrolysis results in transformation of the nickel chloride into the oxide.[20]

Table 2 Thermal properties of the most thermostable chlorides and oxides of the PGMs and nickel[18]

Chloride	*T*/°C	Oxide	*T*/°C
$PdCl_2$	dec.* 500	PdO	m.p. 870
$PtCl_2$	dec. 581	PtO	dec. 550
$RuCl_3$	dec. >500	IrO_2	dec. 1100
$IrCl_2$	dec. 773	Rh_2O_3	dec. 1100–1150
$RhCl_3$	dec. 450–500	NiO	m.p. 1984
$NiCl_2$	subl.† 973–987		

* Dec. = decomposes.
† Subl. = sublimes.

Data from the literature, on the conditions for metallic Ni formation from the nitrate and oxide in the graphite atomizer, seem to be contradictory. According to thermodynamic calculations, nickel oxide is stable in the atomizer at temperatures between 230 and 630 °C under a partial pressure of free oxygen of 1×10^{-6} bar.[24] By the use of mass spectrometry it has been shown that metallic Ni is formed in the graphite atomizer in substantial amounts only at about 1500 °C.[7,23] It has been found by thermal and X-ray diffraction analysis that graphite reduces $Ni(NO_3)_2 \cdot 6H_2O$ to Ni metal in an argon atmosphere at 1150 °C.[28] Catalysts significantly decrease the reduction temperature (down to 630 °C for CuCl).[29] At the same time less than 1% of the nickel nitrate is reduced to nickel dicarbide at 330 °C.[23] Nickel nitrate is partially reduced to the free metal at relatively low ashing temperatures; thus it is necessary to introduce 1000 times as much Ni into the graphite atomizer as Pd in order to create a concentration sufficient for the effective catalysis of the reduction of the analyte.[12] In our experiments it would appear that significant amounts of catalytically effective metallic Ni were formed from $NiCl_2 \cdot 6H_2O$ at temperatures between 520 and 600 °C (Table 1). Nickel metal catalyses the reduction of Ga_2O_3 with graphite to free Ga, and the oxidation of graphite with water vapour. It is known that graphite readily reacts with water at 800 °C in the presence of metallic Ni.[27] Nickel metal and nickel oxide are also efficient catalysts for the oxidation of carbon monoxide to carbon dioxide; hence, carbon dioxide is the final product of graphite oxidation (Fig. 2).

Mixed oxide formation is a possible mechanism for the stabilization of highly volatile elements in the presence of nickel nitrate, at ashing temperatures below 600 °C. Such compounds are known for Ga, Tl, Ge, As, Sb, Bi, Se and Te; ZnO and NiO form solid solutions.[30] At elevated temperatures these compounds can be reduced to the corresponding intermetallic compounds. Evidently such a mechanism for stabilization is marginally possible using nickel chloride as the modifier.

The high efficiency and universality of Pd modifiers can be explained not only by the ease of formation of Pd metal from its compounds but also by the unique catalytic properties of Pd. In particular the catalytic properties of Pd are only slightly dependent on the particle size, because Pd electron configuration depends weakly on cluster size.[31] The electron configuration of Pd_2 is $4d^{9}5s^{1}$. This configuration approaches $4d^{9.45}5s^{0.6}$ at eight to ten atoms where only minor changes take place with increasing particle size. The configuration determined from experimental measurements on bulk Pd is $4d^{9.65}5s^{0.4}$. Sample matrix and the parameters of determination (especially the temperature and heating rate of the atomizer during the drying stage) can significantly affect the size and the structure of the catalytically effective particles, thus restricting the field of efficient use of the PGM modifiers (except Pd).

Excellent results have been reported by Dahl *et al.*[32] on the use of a mixture of Pd, Rh and Ir compounds for Sb determination in different matrices. They can probably be explained by the successful combination of the unique catalytic properties of Pd with the high melting points of Rh

(m.p. = 1960 °C) and Ir (m.p. = 2450 °C). This prevents the loss of Sb and enables ashing at extremely high temperatures.

The authors thank E. M. Sedykh and G. N. Takhtarova for their valuable assistance.

References

1 Ediger, R. D., *At. Absorpt. Newsl.*, 1975, **14**, 127.
2 Shan, X.-q., and Ni, Z.-m., *Huaxue Xuebao*, 1979, **37**, 261; *Chem. Abstr.*, 1980, **92**, 220474x.
3 Voth-Beach, L. M., and Shrader, D. E., *J. Anal. At. Spectrom.*, 1987, **2**, 45.
4 Schlemmer, G., and Welz, B., *Spectrochim. Acta, Part B*, 1986, **41**, 1157.
5 Ni, Z.-m., and Shan, X.-q., *Spectrochim. Acta, Part B*, 1987, **42**, 937.
6 Shan, X.-q., and Wang, D.-x., *Anal. Chim. Acta*, 1985, **173**, 315.
7 Styris, D. L., *Fresenius Z. Anal. Chem.*, 1986, **323**, 710.
8 Teague-Nishimura, J. E., Tominaga, T., Katsura, T., and Matsumoto, K., *Anal. Chem.*, 1987, **59**, 1647.
9 Wendl, W., and Müller-Vogt, G., *J. Anal. At. Spectrom.*, 1988, **3**, 63.
10 Morikawa, K., Shirasaki, T., and Okada, M., in *Advances in Catalysis and Related Subjects*, ed. Eley, D. D., Academic Press, New York, 1969, vol. 20, p. 98.
11 Frech, W., Lundberg, E., and Cedergren, A., *Prog. Anal. At. Spectrosc.*, 1985, **8**, 257.
12 Brzezinska-Paudyn, A., and Van Loon, J. C., *Fresenius Z. Anal. Chem.*, 1988, **331**, 707.
13 Rettberg, T. M., and Beach, L. M., *J. Anal. At. Spectrom.*, 1989, **4**, 427.
14 Volynsky, A. B., XXVI Colloquium Spectroscopicum Internationale, Sofia, 1989, Abstracts Volume I, p. 95.
15 Il'chenko, N. I., *Usp. Khim.*, 1972, **41**, 84.
16 Charcosset, H., and Delmon, B., *Ind. Chim. Belge.*, 1973, **38**, 481.
17 Sakurada, O., Takahashi, H., and Taga, M., *Bunseki Kagaku*, 1989, **38**, 407.
18 *CRC Handbook of Chemistry and Physics*, ed. Weast, R. C., CRC Press, Boca Raton, 68th edn., 1987.
19 White, R., *Chromatography/Fourier Transform Infrared Spectroscopy and its Applications*, Marcel Dekker, New York, 1990, pp. 57 and 58.
20 Welz, B., Akman, S., and Schlemmer, G., *Analyst*, 1985, **110**, 459.
21 Huettner, W., and Busche, C., *Fresenius Z. Anal. Chem.*, 1986, **323**, 674.
22 Sedykh, E. M., and Belyaev, Yu. I., *Prog. Anal. At. Spectrosc.*, 1984, **7**, 373.
23 Droessler, M. S., and Holcombe, J. A., *Spectrochim. Acta, Part B*, 1987, **42**, 981.
24 Dědina, J., Frech, W., Cedergren, A., Lindberg, I., and Lundberg, E., *J. Anal. At. Spectrom.*, 1987, **2**, 435.
25 McAllister, T., XXVI Colloquium Spectroscopicum Internationale, Sofia, 1989, Abstracts Volume IV, p. 55.
26 Shan, X.-q., Yuan, Z.-n., and Ni, Z.-m., *Anal. Chem.*, 1985, **57**, 857.
27 McKee, D. W., in *Chemistry and Physics of Carbon*, eds. Walker, P. L., Jr., and Thrower, P. A., Marcel Dekker, New York, 1981, vol. 16, p. 1.
28 Richardson, R. T., and Rowston, W. B., *Proceedings of the Second European Symposium on Thermal Analysis*, Aberdeen, 1981, p. 355.
29 Pushkarev, V. A., in *Physical Chemistry of Oxides*, ed. Men, A. N., Nauka, Moscow, 1971, p. 87 (in Russian).
30 *Landolt-Bornstein. Zahlenwerte und Funktionen aus Naturwissenschaften und Technik, Neue Serie*, ed. Hellwege, K.-H., Springer-Verlag, Berlin, 1975, Gesamtherausgabe, Gruppe III, Band 7, Teil a-f.
31 Hamilton, J. F., and Baetzold, R. C., *Science*, 1979, **205**, 1213.
32 Dahl, K., Martinsen, I., Salbu, B., Radziuk, B., and Thomassen, Y., XXVI Colloquium Spectroscopicum Internationale, Sofia, 1989, Abstracts Volume I, p. 91.

Paper 0/01009J
Received March 6th, 1990
Accepted July 23rd, 1990

Determination of Nickel Tetracarbonyl by Gas Chromatography

Alexander Harper
AEA Technology, Harwell Laboratory, Oxfordshire OX11 0RA, UK

Capillary gas chromatography, with use of an electron-capture detector, has been assessed as a detection technique for nickel tetracarbonyl in gas samples. Detection limits as low as 1 part in 10^{11} can be achieved under the appropriate conditions.

Keywords: *Gas chromatography; electron-capture detector; nickel tetracarbonyl*

Nickel tetracarbonyl is a volatile, thermally unstable material, which may be formed by the direct reaction of CO with nickel or nickel-containing alloys. Interest in the analysis of gases for $Ni(CO)_4$ at low concentrations arises both from the toxicity of the material and from its role in the transport of catalytically active nickel in gas circuits.

The carcinogenic behaviour associated with the chronic inhalation of $Ni(CO)_4$ is reflected in the exposure guidelines recommended for this material, 100 vppb (parts per 10^9 by volume) short term exposure limit (STEL) (10 min).[1] Even more stringent controls have been applied in the past; the American Conference of Industrial Hygienists set a value of 1 vppb in 1959, although this was subsequently increased to 0.05 mg m^{-3} of nickel [equivalent to 20 vppb of $Ni(CO)_4$].[2] These low values clearly point to the need for a reliable method for the determination of $Ni(CO)_4$ vapour at vppb levels for environmental monitoring.

The transport of catalytic nickel in gas circuits involves the formation of $Ni(CO)_4$ in relatively cool portions of the system and its subsequent thermal decomposition in regions of the circuit at higher temperatures. The catalytic nickel thereby formed can lead to the decomposition of hydrocarbon materials with the resulting formation of carbonaceous deposits in undesirable places. For example, in the primary cooling circuits of Advanced Gas-Cooled Reactors, where CO is maintained in the CO_2 coolant to inhibit corrosion of the graphite moderator, the phenomenon could lead to the formation of layers of material of relatively low thermal conductivity on heat-transfer surfaces. In systems such as this, where the rate of gas flow is high, even trace concentrations of $Ni(CO)_4$ in the gas phase can result in the transport of significant amounts of catalyst.

Analysis of gases for $Ni(CO)_4$ has been accomplished by two techniques: adsorption of the component of interest on to a substrate and subsequent assay of the substrate for nickel,[3] and by exploitation of the chemiluminescent reaction between $Ni(CO)_4$ and ozone.[4–7] Adsorption techniques possess the advantage that they may be calibrated without resource to gas standards containing $Ni(CO)_4$. Determinations by such methods are, however, time consuming and require large samples of gas, especially at low concentrations. Further, the ultimate sensitivity is limited by the inevitable nickel contamination of suitable adsorbents. Chemiluminescence possesses the merit of sensitivity, but commercially available equipment is expensive, and the method can be subject to interference from the chemiluminescent reactions of other components of the sample matrix.[6]

Gas chromatography, coupled with a suitable detection system, offers the potential for good selectivity and sensitivity combined with a modest sample volume and analysis time. This paper describes the evaluation of gas chromatography, with electron-capture detection, for the determination of $Ni(CO)_4$ in CO–CO_2 gas mixtures.

Experimental

Gas Chromatograph

The gas chromatograph used in the present study was a Hewlett-Packard Model 5890, fitted with a six-port gas-sampling valve and a constant-current electron-capture detector (ECD). A facility was available to allow operation of the oven at sub-ambient temperatures. Data acquisition, storage and analysis were effected by using a Hewlett-Packard Model 59970 workstation.

All the experiments described were performed with the use of a 10 m × 0.53 mm capillary column, coated with a 2.65 μm film of 5% diphenyl–95% dimethyl polysiloxane gum (Hewlett-Packard). The use of a capillary column restricts carrier gas flow-rates to values too low to allow operation of the ECD on carrier gas alone. A subsidiary gas feed (make-up gas) was therefore supplied to the detector. This has the advantage that carrier gas composition is not limited to those gases suitable for ECD operation.

The analytical conditions finally adopted for the assessment of sensitivity are summarized in Table 1.

Materials

Nitrogen (high purity, oxygen free) was obtained from Air Products. Carbon monoxide (99.5%) was obtained from the same source and passed over active charcoal to remove traces of $Ni(CO)_4$ and $Fe(CO)_5$ before use. Gaseous CO_2 was obtained from converters charged with solid carbon dioxide (Distillers). Nickel tetracarbonyl (>97%) was obtained in liquid form from Pfaltz and Bauer, and was used without further purification.

Table 1 Summary of chromatographic conditions

Parameter	Isothermal	Non-isothermal
Sample volume	0.25 ml	3.0 ml
Column	10 m × 0.53 mm coated with 2.65 μm film of 5% diphenyl–95% dimethyl polysiloxane gum	10 m × 0.53 mm coated with 2.65 μm film of 5% diphenyl–95% dimethyl polysiloxane gum
Injector temperature	30 °C	30 °C
Column temperature	30 °C	−30 °C for 1 min then ramp at 40 °C min^{-1} to 10 °C
Detector temperature	60 °C	60 °C
Make-up gas	Nitrogen	Nitrogen
Make-up gas flow-rate	60 ml min^{-1}	60 ml min^{-1}
Carrier gas	CO	CO
Carrier gas flow-rate	2 ml min^{-1}	2 ml min^{-1}

Standard Gases

Stock mixtures of $Ni(CO)_4$ in $CO–CO_2$ were prepared by transferring between 0.8 and 1.0 kPa of $Ni(CO)_4$ vapour into an evacuated aluminium cylinder. The cylinder was then pressurized, with as little delay as possible, to 4 MPa with a gas mixture of 2% v/v CO in CO_2. Carbon monoxide was maintained in the mixture to suppress the decomposition of $Ni(CO)_4$ to metallic nickel and CO. Although this mixture was not analysed directly, dilutions made from it suggest an $Ni(CO)_4$ concentration in the range 150–200 parts per million by volume (vppm).

Standards in the range 1–5 vppm were prepared by transferring about 60 kPa of the stock mixture into an evacuated cylinder and pressurizing to 4 MPa as before. Subsequent dilutions of this standard provided mixtures with nominal $Ni(CO)_4$ concentrations as low as 5 vppb.

Cylinders with nominal $Ni(CO)_4$ concentrations greater than 0.5 vppm were standardized by passing a known volume of gas over active charcoal and assaying the charcoal for nickel. The method has been described in detail elsewhere.[3] This technique allows the standardization of gas mixtures independently of any $Ni(CO)_4$ source. Gas mixtures containing 4.5 and 1.2 vppm of $Ni(CO)_4$ were analysed again after 3700 and 2850 h, respectively, at laboratory temperature (20 ± 2 °C). No significant change in $Ni(CO)_4$ concentration was observed, indicating the stability of these gas mixtures. Gas mixtures analysed in this way were, therefore, regarded as primary standards.

Analysis of mixtures with nominal concentrations below 0.5 vppm was effected by gas chromatography. A calibration graph was prepared by dynamic dilution of a primary standard with CO_2 by using commercially available electronic mass flow meters (Brooks Instruments Model 5850). This graph was used to standardize mixtures with concentrations down to 50 vppb. Dilution of this mixture allowed the standardization of more dilute mixtures in the same manner.

Dynamic dilution and a series of standards allowed the production of a continuous range of concentrations, covering several orders of magnitude, for the assessment of instrument performance.

Results

Column Performance

Experiments involving the use of a 0.25 ml gas sample with a helium carrier gas flow-rate of 2 ml min^{-1} showed that, on the column described above at 30 °C, the major components of the mixture (CO and CO_2) were essentially not retained. Nickel tetracarbonyl was clearly separated from these materials, and was eluted as a clean, Gaussian peak. Experiments with carbon monoxide samples, which were known to contain both $Ni(CO)_4$ and $Fe(CO)_5$, showed $Fe(CO)_5$ to be eluted much later than $Ni(CO)_4$, as might be expected from their relative boiling points [$Ni(CO)_4$ 43 °C; $Fe(CO)_5$ 102.8 °C].[8,9] The column, therefore, provides adequate resolution of the two carbonyl compounds formed by the direct reaction of CO with a metallic substrate. Similar results were obtained with a CO carrier.

Although the studies described in this paper were performed with $CO–CO_2$ as the sample matrix, the same chromatographic conditions should provide satisfactory resolution for the investigation of gaseous environmental samples, as the major components of air are not retained on the type of column used here.

Carrier Gas Composition

The significance of this parameter lies in the possibility of premature decomposition of $Ni(CO)_4$ on the column or in the detector. This phenomenon could be reduced by the addition of CO to the carrier gas.

The response of the detector to a 10 vppb gas standard was measured by using pure helium and CO as carrier gases. With the exception of the detector temperature, which was 105 °C, the other conditions were those shown in Table 1 for the isothermal example. With helium as the carrier gas the peak area obtained was 90 arbitrary units, whereas with carbon monoxide the peak area was 890 arbitrary units. These results indicate that detector response can be substantially enhanced by using CO as the carrier gas.

Detector Temperature

The sensitivity of the ECD is known to be a function of temperature.[10] The significance of detector temperature in these analyses was assessed from the response of the detector to a 0.25 ml sample of a 19 vppb $Ni(CO)_4$ standard. The carrier gas was pure carbon monoxide and the make-up gas pure nitrogen.

Peak area is shown as a function of detector temperature in Fig. 1. Detector response decreases steadily with temperature. It is therefore clear that, for optimum response, the detector should be operated at a relatively low temperature, but that the temperature should be constant to ensure reproducibility. The latter criterion requires operation at temperatures significantly above ambient; a value of 60 °C was adopted.

Oven Temperature

The most straightforward mode of operation is to maintain a constant column temperature throughout the analysis. In the present situation, adequate temperature control could be maintained at an oven temperature of 30 °C. The use of an isothermal column, however, limits the maximum sample size that can usefully be employed. The need to maintain satisfactory resolution limits carrier gas flow-rate, and, hence, the rate at which the sample loop can be purged. An excessive sample volume results in malformed peaks and poor resolution. Under isothermal conditions, a 0.25 ml sample was the largest that could be used reliably.

One strategy for increasing sample size is to operate the column at low temperature during the flushing of the sample loop. Under these conditions, $Ni(CO)_4$ progresses extremely slowly through the column and is concentrated in a narrow band at the start of the column. Raising the temperature then allows elution of this material as a sharp peak. Fig. 2 shows the effect of this strategy on a 1.0 ml gas sample containing 19 vppb of $Ni(CO)_4$. In this example, the column temperature was kept at −20 °C for 1 min, then ramped at 40 °C min^{-1} to a

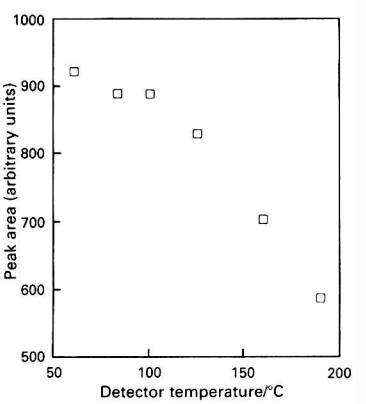

Fig. 1 Effect of detector temperature

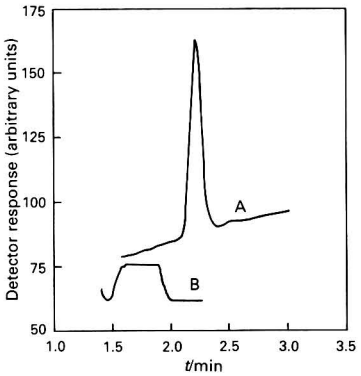

Fig. 2 Effect of temperature programme on peak shape. A, Temperature programmed; and B, not temperature programmed

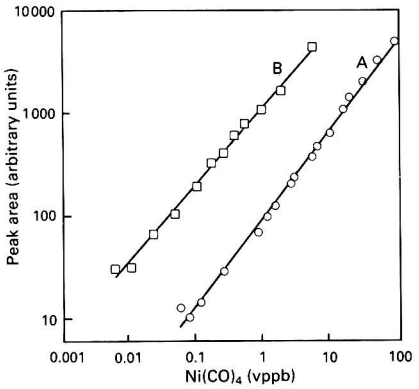

Fig. 3 Calibration graphs. A, 0.25 ml loop size (isothermal); and B, 3 ml loop size (non-isothermal)

Table 2 Calibration data at low concentration

	Isothermal	Non-isothermal
Slope	87.72	2046
Standard error of slope	0.90	56
Intercept	5.5	17
Standard error of intercept	3.1	12
Correlation coefficient	1.00	0.99
Number of data	9	20
Detection limit (vppb)	0.08	0.01

constant temperature of 10 °C. A maximum sample size of 3 ml could be accommodated by using the temperature programme given in Table 1.

Sensitivity

Calibration graphs prepared under both isothermal and non-isothermal conditions, as defined in Table 2, are shown in Fig. 3. Over the range of concentrations considered the graphs are significantly non-linear. The relationships between peak area (A) and concentration (c) in vppb are given by: $A = 105c^{0.87}$, for the isothermal example; and $A = 1158c^{0.81}$, for the non-isothermal example.

In order to establish the detection limit, only data with peak areas of less than about 300 arbitrary units were considered. Over this restricted range the linearity was excellent in both instances. Unweighted linear regression by least squares was used to determine the slope and intercept of the best line through the data. These values, together with the associated standard errors and correlation coefficients, are given in Table 2. Also shown in Table 2 are the values for the detection limits. These have been defined as those concentrations at which the lower 95% confidence limit becomes equal to the calculated y-intercept.[11] The results of this exercise are summarized in Table 2. The sensitivity of the method is clear from the detection limits quoted. That the difference in detection limit between isothermal and non-isothermal examples is not *pro rata* with sample size reflects the greater degree of scatter in the non-isothermal data.

Conclusions

Gas chromatography with an ECD has been shown to be an effective technique for the determination of $Ni(CO)_4$ in CO–CO_2 gas mixtures. Appropriate choice of carrier gas and chromatographic conditions allows detection limits as low as 0.01 vppb to be obtained. Although the method has been devised for the analysis of CO–CO_2 gas mixtures, the technique should also be appropriate for the analysis of air samples. In the latter instance, however, consideration would have to be given to the stability of the gas sample if analysis and sampling took place at different locations.

This work was jointly funded by the United Kingdom Atomic Energy Authority and Nuclear Electric plc under the Thermal Reactor Agreement. The author is grateful to these bodies for permission to publish this paper.

References

1 *Occupational Exposure Limits*, HSE Document 40/90, HM Stationery Office, London, 1986.
2 American Conference of Governmental Industrial Hygienists List, 1989–90.
3 Eller, P. M., *Appl. Ind. Hyg.*, 1986, **1**, 115.
4 Stedman, D. H., Tammaro, D. A., Branch, D. K., and Pearson, R., *Anal. Chem.*, 1979, **51**, 2340.
5 Stedman, D. H., and Tammaro, D. A., *Anal. Lett.*, 1976, **9**, 81.
6 Houpt, P. M., van der Waal, A., and Langeweg, F., *Anal. Chim. Acta*, 1982, **136**, 421.
7 Hikade, D. A., Stedman, D. H., and Walega, J. G., *Anal. Chem.*, 1984, **56**, 1629.
8 *Handbook of Chemistry and Physics*, ed. Weast, R. C., CRC Press, Boca Raton, FL, 60th edn., 1980, B-101.
9 *Handbook of Chemistry and Physics*, ed. Weast, R. C., CRC Press, Boca Raton, FL, 60th edn., 1980, B-86.
10 Grob, R. L., *Modern Practice of Gas Chromatography*, Wiley-Interscience, New York, 1985, p. 262.
11 Sharaf, M. A., Illman, D. L., and Kowalski, B. R., *Chemometrics*, Wiley-Interscience, New York, 1986, p. 128.

Paper 0/02273J
Received May 22nd, 1990
Accepted September 27th, 1990

Assessment of Procedures for the Determination of Nitrate and Nitrite in Vegetable Extracts

David J. Lyons, Leith E. McCallum, William J. Osborne and Peter E. Nobbs
Agricultural Chemistry Branch, Department of Primary Industries, Indooroopilly, Queensland 4068, Australia

The aim of this work was to establish a method that would preferably afford simultaneous extraction and determination of nitrate and nitrite in vegetables. Both high-performance liquid chromatography (HPLC), with ultraviolet (UV) and conductivity detection, and automated spectrophotometry (AS) were available. The effects of ascorbic acid on nitrate and nitrite, as determined by AS, were investigated. Ascorbic acid significantly reduced the concentration of nitrite in solution, particularly when the solutions were heated. It was concluded that this interference was not occurring during colour development, but was occurring before the analytical determination. Nitrate could be quantitatively recovered from vegetables that were heated or blended with water or extracted under alkaline conditions. Nitrite could only be recovered from alkaline extracts because of the instability of nitrite under acidic conditions. These observations suggest that extraction of nitrite from vegetables with water, as carried out in some surveys, could lead to underestimations of nitrite content. Use of HPLC with conductivity detection was impractical and error prone owing to the long analysis times and interference from sulphate and phosphate, but HPLC with UV detection was about ten times more sensitive than with conductivity detection and AS, and hence has potential in ultra-trace analysis. However, the AS method was preferred for vegetables as it was more time and labour efficient.

Keywords: *Vegetable; nitrate; nitrite; automated spectrophotometry; high-performance liquid chromatography*

Methods for the determination of nitrate and nitrite in fresh vegetables are required to service a survey of nitrate and nitrite residues in vegetables from Queensland.

Currently, the routine method in use in this laboratory for nitrate-N in plants is based on automated spectrophotometry (AS) and is the same as that described by Spann and Lyons.[1] Nitrite can be determined with use of the same method by eliminating the nitrate reduction step (*i.e.*, without hydrazine sulphate).

The instability of nitrite can present problems during sample preparation of fresh vegetables. Nitrites tend to be decomposed under acidic conditions, and losses have been reported on extraction of plant tissues.[2,3] Reducing agents such as ascorbic acid can attack nitrite. Several workers have shown that nitrite can be successfully extracted from foods under alkaline conditions.[4,5]

The aim of this work was to establish a suitable extraction procedure and analytical determination for fresh vegetables that would preferably afford simultaneous extraction and allow the determination of nitrate and nitrite in the same extract. Both AS and high-performance liquid chromatographic (HPLC) methods were available.

Experimental

Three extraction procedures were assessed, *viz.*, boiling and blending with water and an alkaline extraction. Two analytical methods were available and tested, *viz.*, AS and HPLC. Both conductivity and ultraviolet (UV) detection were used to measure anion response by HPLC.

Unless specified otherwise, all reagents were of analytical-reagent grade, and the term 'water' implies de-ionized water.

Effects of Reducing Agents Likely to be Present in Vegetable Extracts on the Spectrophotometric Determination of Nitrate and Nitrite

The effects of ascorbic acid on the determination of nitrate and nitrite by AS were assessed, as interference from ascorbic acid during colour development has been reported in the literature.[6] A range of solutions containing separate and combined amounts of nitrate and nitrite, with and without additions of ascorbic acid, were analysed by using both nitrate and nitrite manifolds. Solutions, both heated and unheated, were analysed. The degree of reduction from nitrate- to nitrite-N was assessed by running nitrite-N standards on the nitrate manifold.

pH and Conductivity of Vegetable Blends

Measurements of the pH and conductivity of vegetable blends were carried out in order to obtain an indication of which extraction procedure and extraction ratio would best suit determination by HPLC.

Assessment of Extraction Procedures

Vegetables (brussels sprouts, carrots, celery, lettuce and beetroot), purchased from local supermarkets, were diced to less than 1 cm after inedible parts were removed. Three extraction procedures were tested.

Heating

A 10 g sample of diced vegetable, plus 60 ml of water, were heated to gentle boiling for 1 h, and the mixture was diluted to 120 ml on cooling. Extracts were filtered before analysis through Whatman No. 41 filter-papers. The first 40–50 ml of filtrate were discarded in order to overcome possible nitrate contamination from the filter-papers.

Blending

Vegetables were homogenized with a Waring blender, and a 100 g sample of the homogenate was blended with 400 ml of water for 2 min. The blends were filtered through Whatman No. 41 filter-papers, again discarding the first 40–50 ml of filtrate.

Alkaline extraction

The method described by Sen and Donaldson[4] was used. Extracts were centrifuged before analysis.

Combined additions of nitrate- and nitrite-N were made to diced vegetables, and the recovery was calculated from the slope of the linear regression of analyte found (Y) *versus* analyte added (X) in each instance.

Comparison of Spectrophotometric and HPLC Methods

AS method

The AS method used was as described by Spann and Lyons.[1] They used a modification of the Griess–Ilosvay reaction.[6] Nitrite was determined in undiluted extracts by eliminating the nitrate-reducing agent (hydrazine sulphate). The extracts were diluted 1 + 9 with water before the determination of nitrate-N.

HPLC method

An IC-PAK anion-exchange column (Waters–Millipore) was used for the separation of anions. All the samples were filtered through a Millipore filter (0.45 μm) before injection. The solvents used were of high-purity HPLC grade.

Conductivity detection

Water blends and alkaline extracts were undiluted for nitrite determination and diluted 1 + 24 for nitrate determination with use of a Bio-Rad conductivity monitor. Operating parameters were: injection volume, 20 μl; eluent pump speed, 1.2 ml min^{-1} (Kortec pump); conductivity meter settings, 200 range, 200 sensitivity; and chart recorder settings, 0.2 V, 30 cm h^{-1}. The eluent stream was a borate–gluconate mixture, prepared as follows:

Stock solution. Sodium gluconate (16 g), 18 g of boric acid and 25 g of sodium tetraborate decahydrate were dissolved in 500 ml of water. About 250 ml of glycerol were added and the mixture was diluted to 1 l with water.

Eluent stream. Stock solution (20 ml), 20 ml of butanol (minimum assay 99.8%) and 120 ml of acetonitrile (minimum assay 99.8%) were mixed, and the mixture was diluted to 1 l with water.

Ultraviolet detection

Alkaline extracts were undiluted for nitrite determination and diluted 1 + 9 for nitrate determination with use of a Cecil Model CE 212A UV/visible detector.

Operating parameters were: injection volume, 90 μl; eluent pump speed, 1.2 ml min^{-1}; detection wavelength, 214 nm; chart recorder speed, 20 cm h^{-1}; and eluent, 0.025 mol dm^{-3} KOH.

Extracts of vegetables used for the recovery tests were analysed for nitrate- and nitrite-N by all the methods described. The methods were compared in terms of sensitivity, precision, ease, cost and speed of analysis.

Results and Discussion

Effect of Ascorbic Acid

Results of the experiments carried out to test the interference of ascorbic acid on nitrate and nitrite as determined by AS are shown in Table 1.

Solutions containing either nitrate or nitrite, without ascorbic acid, were stable after gentle boiling. When ascorbic acid was present, a loss of nitrite was observed and the rate of loss was dependent on the concentration of ascorbic acid. This interference was exacerbated with heating; *e.g.*, solutions 4 and 8 lost more than 80% of added nitrite.

There was no evidence of a loss of nitrate when ascorbic acid was present in the solution (Table 1, solutions 9–16), in spite of interference from ascorbic acid during colour development being reported in the literature.[6] This interference was

Table 1 Effect of ascorbic acid on nitrate-N and nitrite-N spectrophotometric response

	Known composition of solution/μg ml^{-1}			Analyte response/μg ml^{-1}					
				A*		B†		C‡	
No.	Nitrite-N	Nitrate-N	Ascorbic acid	U§	H¶	U§	H¶	U§	H¶
1	2	0	0	1.96	1.94	1.97	1.96	3.24	3.27
2	2	0	5	1.91	1.78	1.93	1.86	3.20	3.11
3	2	0	10	1.88	1.53	1.93	1.65	3.22	2.74
4	2	0	100	0.34	ND‖	1.5	0.18	1.93	0.28
5	5	0	0	4.95	4.96	4.97	4.97	**	**
6	5	0	5	4.88	4.57	4.92	4.64	**	**
7	5	0	10	4.83	4.41	4.87	4.53	**	**
8	5	0	100	4.06	0.74	4.32	1.06	**	1.69
9	0	2	0	ND	ND	1.27	1.32	1.94	2.07
10	0	2	5	ND	ND	1.26	1.30	1.95	2.07
11	0	2	10	ND	ND	1.27	1.28	2.00	2.03
12	0	2	100	ND	ND	1.22	1.27	1.95	2.07
13	0	5	0	ND	0.03	3.13	3.20	4.90	5.02
14	0	5	5	0.02	0.03	3.14	3.19	4.96	4.97
15	0	5	10	0.04	0.02	3.12	3.18	4.98	5.00
16	0	5	100	0.03	ND	3.09	3.17	4.91	5.02
17	2	5	10	1.88	1.49	4.97	4.78	**	**
18	5	2	10	4.9	4.46	**	5.82	**	**
19	0	0	10	ND	0.03	0.02	0.03	ND	0.07
20	0	0	100	ND	0.03	ND	0.02	ND	0.03

* A = No hydrazine sulphate, run against nitrate-N standards.
† B = With hydrazine sulphate, run against nitrite-N standards.
‡ C = With hydrazine sulphate, run against nitrate-N standards.
§ = Unheated.
¶ = Heated (gentle boiling).
‖ ND = Not detected. Less than 0.01 μg ml^{-1} of nitrite-N and 0.016 μg ml^{-1} of nitrate-N, respectively.
** = Response exceeded that of the highest standard (6.0 μg ml^{-1} of N).

confirmed in the present study, when ascorbic acid was introduced into the recipient dialyser stream and significant effects on nitrate determinations were observed. It was concluded that ascorbic acid was not passing across the dialyser membrane in the proposed system. The results suggest that the interference from ascorbic acid in the determination of nitrite (Table 1, solutions 1–8), which is the reactive nitrogen form during colour development, was occurring before the autoanalyser step and was independent of the analytical determination. This was confirmed when a similar loss of nitrite was observed when using HPLC determination. Interference in the determination of nitrite by reactive metabolites, such as ascorbic acid, have been reported by Klepper[2] and by Fox and Nicholas.[7] These observations suggest that the extraction of nitrite from vegetables with water, as carried out in a survey by Siciliano *et al.*,[8] and with hot water as reported by Wootton *et al.*,[9] could lead to an underestimation of the nitrite content.

Results in columns B and C (Table 1) demonstrate that the reduction of nitrate to nitrite with hydrazine sulphate, before colour development, was incomplete. The degree of reduction was typically about 62%, but was consistent throughout the extent of this work. This reduction efficiency is closely monitored during analyses of routine samples for nitrate-N in this laboratory.

pH and Conductivity of Vegetable Blends

Blends were prepared from one part of vegetable plus four parts of water. Values for the pH of carrot, lettuce, celery, brussels sprouts, silverbeet and beetroot blends ranged from 6.0 to 6.5, and conductivity values were 1970, 940, 2910, 2300, 3960 and 3270 μS cm^{-1}, respectively, which is equivalent to 1260, 600, 1860, 1470, 2530 and 2090 μg ml^{-1} of total dissolved ions. This is based on the conversion: 1 μS cm^{-1} approximates to 0.64 μg ml^{-1} of total dissolved ions.

Table 2 Recovery estimates derived from the linear regression of Y mg kg^{-1} of nitrite-N found *versus* X mg kg^{-1} of nitrite-N added to fresh vegetables before alkaline extraction (AS). Parameters shown with 95% confidence interval

	Linear regression parameters*			
Vegetable†	b_1	Recovery (%) ($b_1 \times 100$)	b_0/mg kg^{-1} of nitrite-N	R^2
Carrots (0, 1, 2, 5, 10)	0.963 ± 0.156	96.3 ± 15.6 (NSD‡ from 100)	0.33 ± 0.8 (NSD from 0)	0.992
Lettuce (0, 0.33, 0.66, 1.66, 3.33)	1.086 ± 0.14	108.6 ± 14 (NSD from 100)	0.04 ± 0.45 (NSD from 0)	0.995
Celery (0, 0.33, 0.66, 1.66, 3.33)	0.957 ± 0.134	95.7 ± 13.4 (NSD from 100)	0.11 ± 0.22 (NSD from 0)	0.994
Brussels sprouts (0, 1, 2, 5, 10)	0.897 ± 0.088	89.7 ± 8.8	0.07 ± 0.44 (NSD from 0)	0.986
Beetroot (0, 0.33, 0.66, 1.66, 3.33)	1.055 ± 0.07	105.5 ± 7.0 (NSD from 100)	0.21 ± 0.12	0.999

* $Y = b_0 + b_1X$, where Y = mg kg^{-1} of nitrite-N found, and X = mg kg^{-1} of nitrite-N added.
† The levels of nitrite-N (mg kg^{-1}) added to each vegetable are shown in parentheses.
‡ NSD = not significantly different ($p = 0.05$).

Table 3 Recovery of nitrate from vegetables extracted by using three techniques (AS)

	Linear regression parameters*			
Vegetable†	b_1	Recovery (%) ($b_1 \times 100$)	b_0/mg kg^{-1} of nitrate-N	R^2
Extracted by heating with water: ‡				
Carrots (0–120)	1.135 ± 0.333	113.5 ± 33.3	− 1.9 ± 26	0.957
Lettuce (0–600)	1.03 ± 0.175	103 ± 17.5	122 ± 68	0.985
Celery (0–600)	1.005 ± 0.36	100.5 ± 36	444 ± 140	0.937
Beetroot (0–2400)	0.983 ± 0.12	98.3 ± 12	286 ± 183	0.992
Extracted by blending with water: ‡				
Carrots (0–80)	1.075 ± 0.15	107.5 ± 15.0	11.9 ± 7.0	0.989
Lettuce (0–400)	0.98 ± 0.129	98.0 ± 12.9	122.6 ± 33	0.99
Celery (0–400)	1.04 ± 0.208	104 ± 20.8	425.2 ± 53	0.979
Beetroot (0–1600)	0.878 ± 0.28	87.8 ± 28.0	310 ± 280	0.95
Extracted under alkaline conditions: §				
Carrots (0–50)	0.965 ± 0.486	96.5 ± 48.6	14.4 ± 13.0	0.973
Lettuce (0–500)	1.143 ± 0.04	114.3 ± 4.4	100 ± 13	0.998
Celery (0–500)	0.999 ± 0.07	99.9 ± 7.0	354 ± 19	0.999
Brussels sprouts (0–500)	1.056 ± 0.37	105.6 ± 37	−0.6 ± 10.6	0.987
Beetroot (0–500)	1.255 ± 0.493	125.5 ± 49.3	528 ± 140	0.984
Silverbeet (0–500)	1.27 ± 0.162	127 ± 16	282 ± 46	0.998

* $Y = b_0 + b_1X$, where Y = mg kg^{-1} of nitrate-N found, and X = mg kg^{-1} of nitrate-N added. Parameters shown with 95% confidence interval.
† The range of nitrate-N (mg kg^{-1}) added to each vegetable is shown in parentheses.
‡ Purchased and analysed in 1987; recovery determined from replicate additions of nitrate-N.
§ Purchased and analysed in 1989; recovery determined from unreplicated additions of nitrate-N.

Provided that the extracts are not more concentrated than one part of vegetable plus four parts of water, the IC-PAK column should not be overloaded with salt.

Assessment of Extraction Procedures

Recovery of nitrite-N from water blends was highly variable. Levels of nitrite found in 'spiked' blends were sometimes lower than those found in unspiked blends, particularly for vegetables high in nitrate. For carrots, nitrite could not be detected in spiked blends even though additions were much higher than the detection limit for nitrite-N. It was concluded that nitrite was lost from vegetables when blended with water owing to the instability of NO_2^- in acidic solutions.

Under alkaline conditions, recovery of nitrite-N was 100% or close to 100%. Table 2 shows recovery estimates derived from five unreplicated additions of nitrite-N to each vegetable before alkaline extraction.

Nitrate was recovered without loss from vegetables that were heated or blended with water and from vegetables that were extracted under alkaline conditions (Table 3).

Alkaline extraction, although more labour intensive than simply heating or blending with water, afforded simultaneous quantitative extraction of nitrate and nitrite and hence was the preferred extraction technique.

Comparison of Spectrophotometric and HPLC Methods

AS versus *HPLC* (*conductivity detection*)

The response for nitrate- and nitrite-N by HPLC with conductivity detection was similar to that obtained by the AS method. Detection limits, based on twice the standard deviation of ten injections of a blank solution into the chromatograph, were estimated to be 0.042 μg ml^{-1} for nitrite-N and 0.12 μg ml^{-1} for nitrate-N. The recovery of added nitrate was not significantly different from 100%. However, the severe slope of the background made determination of nitrite very difficult for undiluted blends. Large peaks arising from phosphate, sulphate and chloride compounded the problem. Consequently, analysis times were between 12 and 15 min per sample and hence impractical for surveys with medium to large sample numbers.

When extracts were diluted 1 + 24, it was possible to determine nitrate accurately as the background slope was much less severe, but the conditions were too insensitive for nitrite. Resolution of phosphate and sulphate peaks was achievable.

Table 4 shows a comparison of the results for nitrate, by HPLC and AS, determined in both diluted water blends and alkaline extracts. Generally, agreement between the two methods was acceptable, except in one instance, the water blend for silverbeet. Interference from high levels of sulphate and chloride and errors in reading the background are likely to have contributed to the high result obtained for this sample by HPLC.

AS versus *HPLC* (*UV detection*)

Sensitivities for nitrate- and nitrite-N with UV detection were about ten times higher than those achievable with conductivity detection. Moreover, the baseline was steady and there were no interfering peaks. Fig. 1 shows the nitrate-N and nitrite-N response for standards and the relative response of each in alkaline extracts of two vegetables. It was possible to achieve a sensitivity with the proposed system similar to that reported for a Waters ion–liquid chromatograph system.[10]

A comparison of nitrate levels determined by both methods is shown in Table 5. Again, agreement between the two methods was acceptable.

During this study, nitrite was not detected in freshly prepared vegetables in all instances. Only when vegetables were stored for more than two months were detectable levels of nitrite found and then only in those vegetables high in nitrate, *e.g.*, silverbeet and beetroot.

The HPLC method with UV detection is the best choice for trace analyses of agricultural waters for nitrate- and nitrite-N, because of improved sensitivity and because both can be determined in a single extract. However, the AS procedure is preferable for medium to large sample loads of vegetables and plants, in spite of the need to split each sample and carry out two separate determinations. This is still less labour intensive

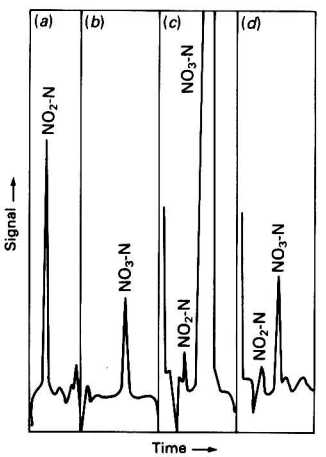

Fig. 1 HPLC scans using UV detection of alkaline standards and spiked extracts of vegetables. (*a*) 0.25 μg ml^{-1} of nitrite-N (a.u.f.s. = 0.02); (*b*) 0.25 μg ml^{-1} of nitrate-N (a.u.f.s. = 0.05); (*c*) beetroot, 1 + 9 dilution (a.u.f.s. = 0.05); and (*d*) carrots, 1 + 9 dilution (a.u.f.s. = 0.05)

Table 4 Comparison of nitrate-N levels in fresh vegetables determined by AS and HPLC (conductivity detection) methods

	Nitrate-N in vegetable/mg kg^{-1}			
	Water blend*		Alkaline extraction†	
Vegetable	AS	HPLC	AS	HPLC
Carrots	ND‡	0.2	1.8	ND
Lettuce	101	95	90	63
Celery	318	312	315	340
Brussels sprouts	31	24	18	20
Beetroot	436	414	504	478
Silverbeet	224	324	243	265

* Purchased and analysed on 8.2.89.
† Same vegetables stored frozen and analysed on 27.2.89.
‡ ND = not detected.

Table 5 Comparison of HPLC (UV detection) and AS methods for nitrate-N in vegetables

	Nitrate-N in vegetable*/ mg kg^{-1}	
Vegetable	AS	HPLC
Celery	70	100
Celery + 250 mg kg^{-1} of nitrate-N	315	330
Beetroot	925	867
Beetroot + 250 mg kg^{-1} of nitrate-N	1145	1077
Carrots	18	15
Carrots + 25 mg kg^{-1} of nitrate-N	38	41

* Purchased and analysed on 2.5.89.

and more time efficient than HPLC, which requires that each sample be filtered through a Millipore filter and which has long analysis times (6–7 min per sample). The method of Sen and Donaldson[4] offers simultaneous extraction of both nitrate and nitrite.

Other countries have already set maximum permissible threshold concentrations for nitrate in vegetables,[11] indicating increasing concern about nitrate toxicity. Levels of nitrite found in fresh vegetables in most surveys have been low. Pallotti *et al.*[12] reported a tolerance of 7 mg kg^{-1} for nitrite in vegetables, while Garcia-Roche and I'lnitskii[13] claimed that 2.7 mg kg^{-1} of nitrite in vegetables has no toxicological significance.

References

1 Spann, K. P., and Lyons, D. J., *Queensl. J. Agric. Anim. Sci.*, 1985, **42**, 35.
2 Klepper, L. A., *J. Agric. Food Chem.*, 1979, **27**, 438.
3 Usher, C. D., and Telling, G. M., *J. Sci. Food Agric.*, 1975, **2**, 1793.
4 Sen, N. P., and Donaldson, B., *J. Assoc. Off. Anal. Chem.*, 1978, **61**, 1389.
5 Vdovina, T. A., and Medvedeva, N. A., *Agrokhimiya*, 1979, **1**, 123.
6 Fox, J. B., *Anal. Chem.*, 1979, **51**, 1493.
7 Fox, J. B., and Nicholas, R. A., *J. Agric. Food Chem.*, 1974, **22**, 302.
8 Siciliano, J., Krulick, S., Heisler, E. G., Schwartz, J. H., and White, J. W., *J. Agric. Food Chem.*, 1975, **23**, 461.
9 Wootton, M., Kok, S. H., and Buckle, K. A., *J. Sci. Food Agric.*, 1985, **36**, 297.
10 Wildman, B., Scarchilli, D., and Jagoe, L. *Water Ion Briefs*, 1989, Method B1011, No. 88111.
11 Pushkareva, M. M., Chechetkina, L. V., Il'nitskii, A. P., Vlasenko, N. L., Ivanitskii, A. M., Zaichenko, A. I., and Selivanova, L. V., *Khim. Sel'sk. Khoz*, 1983, **11**, 19.
12 Pallotti, G., Bencivenga, B., Antonacci, T., and Rondinelli, R., *Boll. Chim. Unione Ital. Lab. Prov. Parte Sci.*, 1982, **33**, 137.
13 Garcia-Roche, M. O., and I'lnitskii, A. P., *Rev. Agroquim. Technol. Aliment.*, 1986, **26**, 115.

Paper 0/02903C
Received June 27th, 1990
Accepted September 21st, 1990

Sensitizers for the Room Temperature Phosphorescence of Biacetyl in Fats

L. Sargi, P. Prognon and G. Mahuzier
Laboratoire de Chimie Analytique II, Faculté de Pharmacie, Rue J.B. Clément, 92290 Châtenay-Malabry, France

A. Cepeda and M. L. Vazquez
Departemento de Quimica Analitica, Nutricion y Bromatologia, Facultad de Farmacia, Universidad de Santiago de Compostela, Spain

J. Blais
Laboratoire de Physique et Chimie Biomoléculaire (CNRS URA 198), Institut Curie et Université Paris VI, 11 rue Pierre et Marie Curie, 75231 Paris Cedex 05, France

E. Bisagni
Laboratoire de Synthèse Organique, Institut Curie, Centre Universitaire, 91400 Orsay, France

The determination of the biacetyl concentration in fats can be achieved by measuring the phosphorescence emission of biacetyl at room temperature. The biacetyl phosphorescence can be sensitized using suitable donors by means of a triplet–triplet energy transfer. The spectroscopic characteristics of four newly synthesized coumarin derivatives, which are soluble in non-polar solvents, have been studied. In order to determine whether a triplet–triplet energy transfer is possible, the energy of the lowest triplet state of these derivatives was determined by using phosphorescence spectroscopy. Their ability to sensitize the biacetyl phosphorescence has been investigated and the 6,7-dihydro-3-ethoxycarbonylpsoralen appeared to be the best sensitizer. In this instance, a biacetyl concentration as low as 0.05 ppb (μg kg^{-1}) can be determined in butter samples.

Keywords: *Furocoumarin derivative; spectrofluorimetry; phosphorescence spectroscopy; triplet–triplet energy transfer; biacetyl fats*

Biacetyl (2,3-butanedione) is an important compound in food chemistry (fats, beer, *etc.*). Its production in large amounts during the fermentation of beer is responsible for the bitterness.[1] In fats, biacetyl derives from fermented milk and contributes to the natural flavour of butters and margarines. When this flavour is poor or absent because of an unsuccessful fermentation, biacetyl can be added to fats as an aromatizing agent at concentrations of about 1 ppm (μg g^{-1}).[2] However, concentrations above 20 μg g^{-1} are responsible for an unpleasant flavour and lead to a rapid alteration of the fat.[3]

In contrast to most of the organic compounds, biacetyl exhibits phosphorescence emission at room temperature[4] which can be sensitized by way of a triplet–triplet (T–T) energy transfer. This property can be used for analytical purposes and has been shown to be fairly sensitive for the determination of the concentration of biacetyl in the fermentation juice of beer.[5] However, owing to the lack of donor compounds which are soluble in apolar media, this method has not been developed for fats.

One of the main parameters which must be considered in a T–T energy transfer process is the energy level of the lowest triplet state of the donor molecule which has to lie above that of the acceptor molecule, *i.e.*, biacetyl. The efficiency of the triplet formation and its lifetime have to be considered also.[6,7] Furocoumarin derivatives, which have been previously studied in this laboratory,[8] seemed to comply with these requirements.[9,10] They are further characterized by a high solubility in apolar media. This prompted the study of some derivatives that were synthesized in this laboratory as possible sensitizers.

The chemical structures of the four derivatives studied are shown in Fig. 1. Three are furocoumarins or psoralens: the 3-ethoxycarbonylpsoralen (**I**); its dihydro derivative, 6,7-dihydro-3-ethoxycarbonylpsoralen (**II**); and 6,7-dihydro-6,7,9-trimethyl-3-ethoxycarbonylpsoralen (**III**). The fourth derivative is a coumarin: 7-hydroxy-8-methyl-3-ethoxycarbonylcoumarin (**IV**).

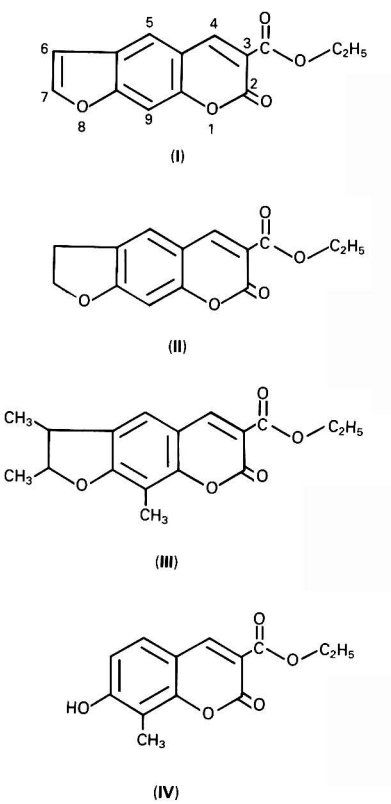

Fig. 1 Chemical structures of the four derivatives studied

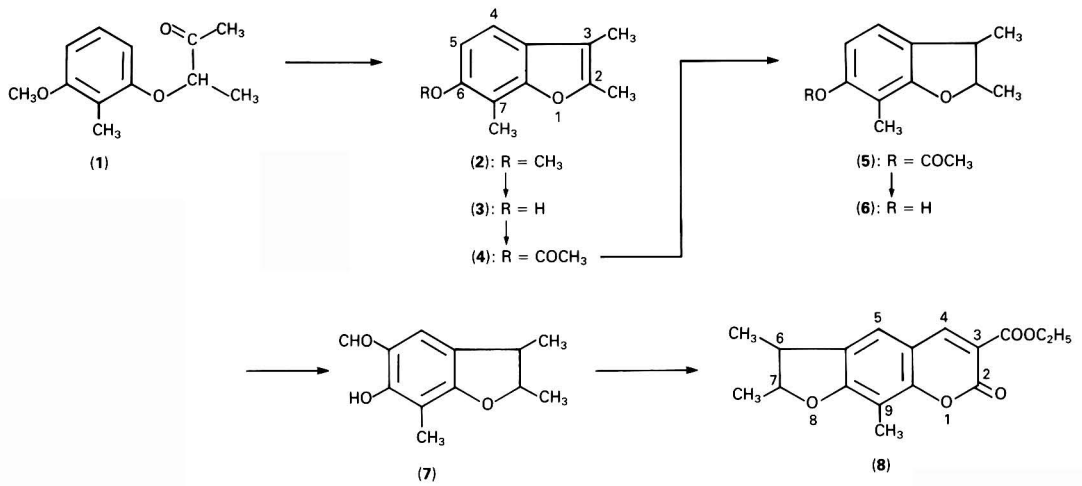

Scheme 1

The phosphorescence emission of these potential sensitizers has been studied in liquid nitrogen at 77 K in order to determine the energy of the lowest triplet state. Their ability to sensitize the biacetyl phosphorescence at room temperature has been investigated and an analytical procedure proposed.

Experimental

Chemicals

All solvents used were of analytical-reagent grade and were doubly distilled before use. Quinine sulphate and biacetyl were purchased from Merck. 3-Ethoxycarbonylpsoralen or 3-ethoxycarbonylfuro[3,2-*g*]coumarin (**I**) and 6,7-dihydro-3-ethoxycarbonylpsoralen or 3-ethoxycarbonyl-6,7-dihydrofuro[3,2-*g*]coumarin (**II**) were synthesized as described in references 11 and 12 and used after checking the purity by thin-layer chromatography (TLC) and high-performance liquid chromatography (HPLC). 6,7-Dihydro-6,7,9-trimethyl-3-ethoxycarbonylpsoralen or 3-ethoxycarbonyl-6,7-dihydro-6,7,9-trimethylfuro[3,2-*g*]coumarin (**III**) was synthesized as follows (see Scheme 1).

A mixture of 103.5 g (0.75 mol) of 3-methoxy-2-methylphenol, 87.8 g (0.825 mol) of 3-chlorobutan-2-one, 138 g (1 mol) of potassium carbonate and 500 ml of acetone was heated under reflux for 30 h. The mixture was poured into water, acidified with hydrochloric acid and extracted with chloroform. The extract was dried over sodium sulphate and the chloroform evaporated. The residue was then distilled to produce 105 g (65%) of an oil corresponding to 3-(3-methoxy-2-methylphenoxy)butan-2-one (**1**), b.p. = 136–139 °C (8 mmHg), n_D24 1.5204. Found: C, 69.03; H, 7.74. Calc. for $C_{12}H_{16}O_3$: C, 69.21; H, 7.74%.

At a temperature fixed between 0 and 15 °C, 105 g of sulphuric acid (sp. gr. = 1.84) were added very slowly to 103 g of **1**. Solidification of the mixture occurred on addition of about half the amount of sulphuric acid. After complete addition, the mixture was left at room temperature for 15 min and poured into cold water. It was then extracted with chloroform, washed with water, 1 mol dm^{-3} sodium hydroxide and again with water. After drying over sodium sulphate and filtration, the solvent was evaporated and the residue distilled twice to produce 86.4 g (90.4%) of an oil corresponding to 6-methoxy-2,3,7-trimethylbenzofuran (**2**), b.p. = 128–129 °C (7 mmHg). Found: C, 75.84; H, 7.39. Calc. for $C_{12}H_{14}O_2$: C, 75.76; H, 7.41%.

A mixture of 73 g of **2** and 150 g of pyridine hydrochloride was heated under reflux for 30 min and poured into water, which led to the formation of a solid which was filtered, air-dried, purified by distillation [b.p. = 158–160 °C (12 mmHg)] and recrystallized from cyclohexane to yield 57.5 g (87.7%) of pale yellow needles of 6-hydroxy-2,3,7-trimethylbenzofuran (**3**), m.p. = 107–108 °C. Found: C, 75.03; H, 6.86. Calc. for $C_{11}H_{12}O_2$: C, 74.97; H, 6.86%.

A mixture of 30 g of **3** and 100 ml of acetic anhydride was heated under reflux for 1 h and evaporated to dryness. The residue was distilled [b.p. = 156–158 °C (7 mmHg)] to yield 33 g (88.8%) of a colourless liquid corresponding to 6-acetoxy-2,3,7-trimethylbenzofuran (**4**) which crystallizes progressively. Compound **4** was dissolved in 300 ml of glacial acetic acid and hydrogenated at room temperature and atmospheric pressure with continuous stirring with 1.5 g of 10% palladium on charcoal catalyst in a hydrogen atmosphere, until a theoretical amount of hydrogen had been absorbed (6–7 h). The catalyst was filtered off and the solvent evaporated. The residue was distilled (b.p. 162–164 °C, 12 mmHg) yielding 30.5 g (91.6%) of a colourless oily liquid corresponding to 6-acetoxy-2,3,7-trimethyl-2,3-dihydrobenzofuran (mixture of *cis*- and *trans*-isomers) (**5**). Found: C, 70.71; H, 7.15. Calc. for $C_{13}H_{16}O_3$: C, 70.89; H, 7.32%.

Saponification of **5** was carried out by heating 24 g of the compound in 50 ml of ethanol, with 8 g of sodium hydroxide in 20 ml of water under reflux for 30 min. The reaction mixture was allowed to cool and was diluted in 100 ml of water. It was then acidified with concentrated hydrochloric acid. The residue was distilled (b.p. 152–154 °C, 9 mmHg) to yield 18.1 g (93%) of a viscous brown liquid corresponding to 6-hydroxy-2,3,7-trimethyl-2,3-dihydrobenzofuran (*cis*- and *trans*-mixture) (**6**). Dried hydrogen chloride was passed for 30 min through a stirred, cooled (about 0 °C) mixture of 14.24 g (0.08 mol) of **6**, 14.4 g (0.12 mol) of zinc cyanide and 400 ml of dry diethyl ether. The reaction mixture was stirred for 2 h at room temperature and hydrogen chloride was again passed through the mixture for 30 min. The solid formed was filtered off, washed with dry diethyl ether and hydrolysed to the aldehyde in 300 ml of boiling water. The mixture was allowed to cool and extracted with chloroform. After evaporation, the residue was distilled [b.p. = 165 °C (7 mmHg)] giving 14 g (89.3%) of a component which recrystallized from cyclohexane leading to the formation of colourless prisms of 5-formyl-6-hydroxy-2,3,7-trimethyl-2,3-dihydrobenzofuran (**7**), m.p. = 103–

104 °C. Found: C, 70.05; H, 6.88. Calc. for $C_{12}H_4O_3$: C, 69.88; H, 6.84%.

A mixture of 5.16 g (25 mmol) of **7**, 5 g (31 mmol) of diethyl malonate and 0.5 g (5.8 mmol) of piperidine was heated until homogeneity was achieved. The mixture was dissolved in chloroform, washed with 0.1 mol dm^{-3} HCl and water and evaporated. The residue was recrystallized (three times) from cyclohexane giving 3.7 g (48.9%) of an amorphous yellowish powder corresponding to 3-ethoxycarbonyl-6,7-dihydro-6,7,9-trimethylfuro[3,2-*g*]coumarin (**8**), m.p. = 128–130 °C. Found: C, 67.36; H, 5.94. Calc. for $C_{17}H_{18}O_5$: C, 67.54; H, 6.00%. NMR (dimethyl sulphoxide)[$(CD_3)_2SO$]: 1.12 (3 H, d, 6-CH_3), 1.35 (6 H, m, 7-CH_3 + CH_3–CH_2), 2.15 (3 H, s, 9-CH_3), 3.55 (1 H, m, 6-H), 4.25 (2 H, q, –CH_2–CH_3), 5.1 (1 H, m, 7-H), 7.55 (1 H, s, 5-H), 8.64 (1 H, s, 3-H).

The 7-hydroxy-8-methyl-3-ethoxycarbonylcoumarin was synthesized as follows (see Scheme 2). A mixture of 124 g

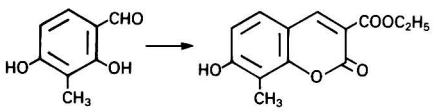

(**9**) (**10**)

Scheme 2

(1 mol) of 2-methylresorcinol and 73 g (1 mol) of dimethylformamide was heated until homogeneity was achieved. Phosphorus oxychloride (92 g, 0.6 mol) was added very slowly resulting in an exothermic reaction. When addition was completed, the reaction mixture was allowed to cool for 2 h at room temperature and a saturated solution of sodium acetate (500 ml) was added. The mixture was stirred, heated to boiling for 5 min and cooled. The solid obtained was filtered, and recrystallized from water to produce 80 g (53%) of pale yellow needles corresponding to 2,4-dihydroxy-3-methylbenzaldehyde (**9**), m.p. = 150 °C.

A mixture of 60.8 g (0.4 mol) of **9** and 70.4 g (0.44 mol) of diethyl malonate was heated until it was homogeneous. Piperidine (0.5 ml) and 20 ml of pyridine were added and the mixture was heated under reflux for 2 h and cooled. The solid was filtered, washed with ethanol and recrystallized from ethanol giving 27 g (27.2%) of yellow crystals corresponding to 7-hydroxy-8-methyl-3-ethoxycarbonylcoumarin (**10**); m.p. = 246 °C. Found: C, 62.71; H, 4.79. Calc. for $C_{13}H_{12}O_5$: C, 62.9; H, 4.87. NMR [$(CD_3)_2SO$]: 1.27 (3 H, t, CH_3–CH_2), 2.12 (3 H, s, 8-CH_3), 4.22 (2 H, q, –CH_2–CH_3), 6.88 (1 H, d, 6-H, $J_{6,7}$ = 8.5 Hz), 7.6 (1 H, d, 5-H), 8.6 (1 H, s, 4-H).

Methods

Absorption spectra were recorded with an ultraviolet(UV)–visible Hewlett-Packard HP 8898 spectrophotometer. Room temperature fluorescence spectra were obtained with a Perkin-Elmer LS5 luminometer. The fluorescence quantum yield was determined according to Parker and Rees.[13]

Fluorescence and phosphorescence measurements at 77 K were obtained with a spectrofluorimeter specially built for the detection of very weak luminescences.[14] Total luminescence (fluorescence plus phosphorescence) was measured. The use of a phosphoroscope made it possible to record only the emissions with lifetimes longer than 1×10^{-3} s (phosphorescence). The fluorescence spectrum was inferred from the difference between the total luminescence and the phosphorescence after normalization in the 500 nm spectral region where there is no contribution from the fluorescence emission. The energy of the $T_1 \rightarrow S_0$ transition (triplet energy E_{T_1}) was determined from the energy of the blue edge of the phosphorescence emission. The ratio of the phosphorescence and fluorescence emissions (P : F) was calculated from the areas under the respective spectra.

A Quickfit micro-distillation apparatus made of Pyrex glass was used for the distillation of the fatty samples. About 2 g of fat (margarine or butter) were homogenized with 18 ml of hexane, introduced into the flask of the micro-distillation apparatus and distilled at 69 °C for 10 min.[15]

The HPLC system consisted of a Shimadzu LC 9A pump, a Rheodyne 7125 injector with a 20 µl loop, a Cyclobond (25 cm × 4.6 mm i.d.) Astec column and a Perkin-Elmer LS 5 luminometer used in the phosphorescence mode (gating time = 0.1 ms, delay time = 0.05 ms), equipped with an 8 µl flow cell. The separation was performed in isocratic conditions with a de-oxygenated 1×10^{-4} mol dm^{-3} solution of the derivative **II** in hexane–ethanol (9 + 1 v/v) at a flow-rate of 1 ml min^{-1}. De-oxygenation of the eluent was performed with a special device that has been previously described.[7]

Results and Discussion

Absorption and Fluorescence Spectra

The absorption of the derivative **I** in methanol–water (3 + 7 v/v) shows a main absorption band (313 nm) with a 'shoulder' at about 350 nm. In an apolar solvent (hexane), the absorption band is shifted to a shorter wavelength and the shoulder is better resolved [Fig. 2(*a*)]. This spectral behaviour is consistent with the ππ* nature of the lowest electronic transitions of psoralen derivatives.[16]

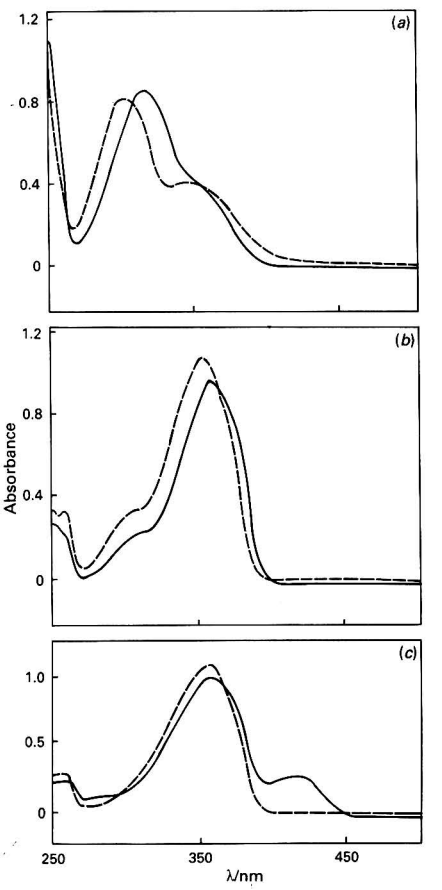

Fig. 2 Absorption spectra of the derivatives in hexane (broken line) and in methanol–water (3 + 7) (solid line). (*a*) **I** (5×10^{-5} mol dm^{-3}); (*b*) **II** (4×10^{-5} mol dm^{-3}); and (*c*) **IV** (5×10^{-5} mol dm^{-3})

On saturation of the 6,7 furan double bond (derivatives **II** and **III**), the absorption spectrum is strongly modified, becoming similar to that of the coumarin derivative, **IV** [Fig. 2(*c*)] with a main absorption band with a maximum at 350 nm and a shoulder at about 310 nm [Fig. 2(*b*)]. The methylation has little affect on the absorption spectrum.

The absorption spectrum of the derivative **IV** in a protic solvent shows an additional band at 410 nm [Fig. 2(*c*)] which is also observed for alkaline solutions. Such a transition could be attributed to an enhancement of the electronic resonance by charge transfer from the phenolic O–H bond to the coumarin nucleus. The fluorescence excitation and emission maxima are reported in Table 1. The observed increase of the quantum yield with the solvent polarity is in good agreement with the so called proximity effect described for heterocyclic carbonyl compounds such as furocoumarins.[17]

The shift of the fluorescence maximum to a longer wavelength, observed on increasing the solvent polarity, is consistent with the $\pi\pi^*$ nature of the fluorescent state of these compounds. A larger Stoke's shift (Table 2) is observed with derivative **I** indicating a larger polarizability of this derivative which could result from the higher aromatic character related to the presence of the double bond between carbon atoms 6 and 7 of the furan ring. From a comparison of the values reported in Table 1, it can be seen that the fluorescence quantum yield, ϕ_f, decreases in the order: **IV** > **III** > **II** > **I**. The presence of the 6,7 double bond in the furan ring leads to a decrease in the ϕ_f values. The highest quantum yields of the coumarin molecule, **IV**, can result from the possibility of resonance which has been reported for the 7-hydroxy-coumarins.[18]

Table 1 Fluorescence emission characteristics of the four derivatives

Derivative	Solvent	$\lambda_{ex(max)}$*/ nm	$\lambda_{em(max)}$†/ nm	$E_{s_1}(0.0)$‡/ eV	ϕ_f
I	Hexane	306	444	3.15	5.3×10^{-3}
	Ethanol	310	464	3.14	1.3×10^{-2}
II	Hexane	356	416	3.24	3.1×10^{-2}
	Ethanol	362	422	3.16	9.7×10^{-2}
III	Hexane	358	422	3.23	9.2×10^{-2}
	Ethanol	364	421	3.14	0.26
IV	Hexane	351	411	3.23	5.1×10^{-2}
	Ethanol	357	413	3.20	0.29

* The wavelength of the maximum of the fluorescence excitation spectrum. The fluorescence excitation spectrum is identical with the absorption spectrum in each instance.

† The wavelength of the maximum of the fluorescence emission spectrum.

‡ The energy of the lowest singlet state S_1.

Table 2 Stoke's shifts for the four compounds in different solvents

	$\nu_a - \nu_f$/cm^{-1}		
Derivative	Hexane	Acetonitrile	Ethanol
I	10157	10799	10706
II	4051	4181	3928
III	3661	3871	3720
IV	4159	3363	3798

Phosphorescence Spectroscopy at 77 K

A typical luminescence spectrum of the derivative **I** obtained at 77 K in a hexane matrix is displayed in Fig. 3. The phosphorescence band always shows vibrational structures whereas the fluorescence emission is structureless. The energy values of the lowest triplet state E_{T_1} of the four compounds (Table 3) are found to be fairly close, lying from 0.2 to 0.3 eV above the T_1 state of biacetyl.

The P:F ratio gives a quantitative indication of the magnitude of the inter-system crossing efficiency making possible a comparison between the different compounds studied. The P:F ratio is found to be very high for the derivative **I** indicating a high efficiency in the populating of the T_1 state. This is consistent with the high triplet quantum yield value ϕ_T reported for this compound by Ronfard-Haret *et al.*[19] [ϕ_T (**I**) = 0.44 in ethanol]. The saturation of the 6,7 furan double bond leads to a decrease in the ϕ_T value [ϕ_T (**II**) = 0.17 in ethanol[20]].

Table 3 Emission characteristics at 77 K of the four derivatives studied. An E_{T_1} value of 2.43 eV has been measured for biacetyl under the same experimental conditions

Derivative	Fluorescence maximum/nm	Phosphorescence maximum/nm	E_{T_1}/eV	P:F ratio
I	438	466	2.73	4.89
II	408	490	2.60	0.06
III	409	488	2.65	0.24
IV	400	484	2.65	0.16

Table 4 Intensity of phosphorescence of biacetyl sensitized by the four compounds (25 °C). Each value represents the mean of three measurements

	Sensitized phosphorescence (arbitrary units)	
Derivative	Hexane–ethanol (9 + 1 v/v)	Methanol–water (3 + 7 v/v)
I	4.8	3.1
II	99.4	39.8
III	79.6	34.1
IV	None	None

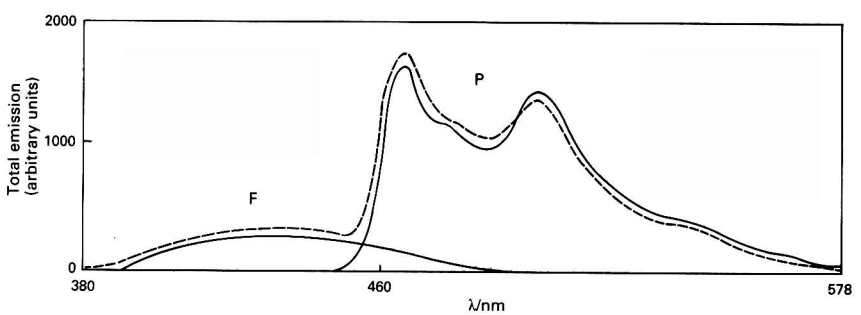

Fig. 3 Luminescence spectrum of the derivative **I** at 77 K in a hexane matrix. Solid lines (recorded separately): F = Fluorescence emission; P = phosphorescence emission. The excitation wavelength was 330 nm. Broken line = total emission spectrum

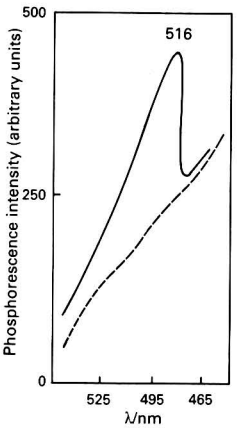

Fig. 4 Sensitized phosphorescence signal obtained with a butter sample (solid line) containing 73 ng g^{-1} of biacetyl. The broken line represents the emission of the blank under the same conditions (residual fluorescence of the donor, derivative **II**). The excitation wavelength was 357 nm

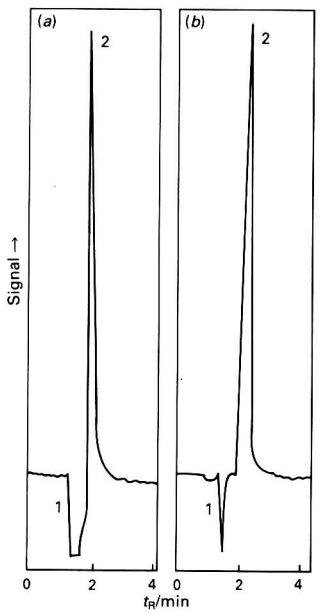

Fig. 5 (*a*) Chromatogram of a butter sample containing 0.69 μg g^{-1} of biacetyl recorded without previous de-oxygenation. (*b*) Chromatogram of the same sample recorded after de-oxygenation for 1 min. 1, Oxygen; and 2, biacetyl. The excitation and emission wavelengths were 357 and 516 nm, respectively

Sensitization of the Biacetyl Room Temperature Phosphorescence by the Derivative Studied

As the T_1 state of biacetyl (2.43 eV) lies below the T_1 state of the four compounds studied, a T–T energy transfer could be expected between the furocoumarin or coumarin donors and the acceptor, biacetyl. The ability of these derivatives to sensitize the biacetyl phosphorescence in both apolar [hexane–ethanol, 9 + 1 (v/v)] and polar [methanol–water (3 + 7 v/v)] solvents was investigated. As can be seen in Table 4, marked differences were observed in the ability of the four molecules to sensitize the biacetyl phosphorescence. Derivative **II** appears to be the best sensitizer although the E_{T_1} value of this compound is only 0.17 eV above that of biacetyl. Efficient T–T energy transfers have been reported involving energy gaps as low as 0.22 eV (21 kJ mol^{-1}).[21] It should be noted that the P : F value is lower for derivative **II** than for the three other compounds.

Another parameter to consider in a T–T energy transfer process is the triplet lifetimes. The triplet lifetime of **II** is four times lower than that of derivative **I** (6 and 27 μs, respectively, in ethanol at room temperature).[19,20] However, this difference alone cannot be responsible for the higher efficiency in the energy transfer observed for derivative **II** compared with **I** (Table 4). The results suggest that close lying triplet levels of the donor and acceptor (ΔE_T <21 kJ mol^{-1}) allow a more efficient energy transfer, probably because of the resonance effect produced by the overlap of their vibrational levels.

Table 5 Determination of the biacetyl concentration in fats by using two sensitized phosphorescence methods. Analytical characteristics of the 'direct' and chromatographic methods

Method	LOD (signal to noise ratio = 3)/ ng g^{-1}	Reproducibility at 100 ng g^{-1} [RSD (%)] (n = 3)	Linearity/ng g^{-1} (n = 3)
Direct	0.05	3.5	0.1–1000 r = 0.9989
Chromatographic	5	1.09	5–5000 r = 0.9998

Table 6 Comparison of the LOD values of various methods for the determination of biacetyl

Method	LOD/ng g^{-1}	Reference
Spectrophotometric*	500	22
Spectrophotometric†	1000	23
Polarographic	250	24
Head-space gas chromatography	50	25
HPLC–UV	20000	1
HPLC–direct phosphorescence	1000	1
HPLC–sensitized phosphorescence	1	1
Sensitized phosphorescence–direct method	0.05	This work
HPLC–sensitized phosphorescence–chromatographic method	5	This work

* Spectrophotometric reaction with creatine and α-naphthol in alkaline medium.

† As an ammine(dimethylglyoximato)iron(II) complex.

Determination of Biacetyl Concentrations in Fats

An attempt has been made to determine the biacetyl concentration in fats (butter and margarine) using derivative **II** as a phosphorescence sensitizer. Two methods have been used for comparison: a so called 'direct method' and a chromatographic method.[15] In both instances, the direct extraction of biacetyl from a butter sample with hexane produced no phosphorescence signal at room temperature. This was attributed to the presence in the extract of some fat constituents which can act as strong inhibitors of the biactyl phosphorescence. Hence, distillation of the butter sample was necessary.

In the direct method, the distillate (see under Experimental) was collected in an ethanolic solution of derivative **II** (1×10^{-4} mol dm^{-3}). The emission of biacetyl in the distillate was recorded after nitrogen bubbling and compared with the emission of a standard solution of known concentration of biacetyl in ethanolic (1×10^{-4} mol dm^{-3}) derivative **II**. Nitrogen bubbling is necessary to remove dissolved oxygen which acts as a powerful quencher of phosphorescence at room temperature because of its low lying triplet state (121 kJ mol^{-1}).

In the chromatographic method, the distillate was directly injected into the HPLC system (see under Experimental) after nitrogen bubbling. The peak height was compared with that obtained with a standard solution of biacetyl. Nitrogen bubbling prior to injection was found to reduce the negative peak in the solvent front caused by the oxygen dissolved in the sample. Under these conditions, complete resolution (R_S = 3.8) of oxygen and biacetyl (capacity factor k' = 0.59) was achieved (Fig. 5).

The sensitized phosphorescence signals observed with a butter sample, when the direct or chromatographic method is used, are shown in Figs. 4 and 5, respectively. The analytical characteristics of both methods are summarized in Table 5. The limits of detection (LOD) obtained in the experiments can be compared with the currently used detection techniques (Table 6). It should be noted that the LOD values correspond to the determination of biacetyl concentration in various matrices (beer, fat, fermentation juice, *etc.*). From an analysis of the LOD values (Table 6), it is clear that the methods reported in this paper compare favourably with the other procedures both from a specificity and sensitivity point of view.

In conclusion, biacetyl can be sensitively detected in fats by sensitized room temperature phosphorescence using a new suitable energy donor, derivative **II**. The exceptional selectivity is due to the T–T energy transfer between donor and acceptor. Of the two distinct methods used, the HPLC method is simple and rapid and compares favourably with other analytical methods.

References

1 Baumann, R. A., Gooijer, C., Velthorst, N. H., and Frei, R. W., *Anal. Chem.*, 1985, **57**, 1815.
2 Coustille, J. L., and Prevot, A., *Rev. Fr. Corps Gras*, 1985, **11**, **12**, 447.
3 Lecoq, R., *Manuel d'Analyses Alimentaires*, Doin, Paris, 1965, p. 624.
4 Almgren, M., *Photochem. Photobiol.*, 1967, **6**, 829.
5 Baumann, R. A., Gooijer, C., Velthorst, V., Frei, R. W., Strating, J., Vermagen, L. C., and Veldhuyzen-Doorduin, R. C., *Int. J. Environ. Anal. Chem.*, 1986, **25**, 195.
6 Donkerbroek, J. J., Elzas, J., Gooijer, C., Frei, R. W., and Velthorst, N. H., *Talanta*, 1981, **28**, 717.
7 Donkerbroek, J. J., Van Eikema-Hommes, N. J. K., Gooijer, C., Velthorst, N. H., and Frei, R. W., *Chromatographia*, 1982, **15**, 218.
8 Blais, J., Prognon, P., Mahuzier, G., and Vigny, P., *J. Photochem. Photobiol.*, 1988, **2**, 455.
9 Bensasson, R. V., Chalvet, O., Lands, E. I., and Ronfard-Haret, J. C., *Photochem. Photobiol.*, 1984, **39**, 287.
10 Craw, M., Bensasson, R. V., Ronfard-Haret, J. C., Sae Melo, M. T., and Truscott, T. G., *Photochem. Photobiol.*, 1983, **37**, 611.
11 Queval, P., and Bisagni, E., *Eur. J. Med. Chem. Chim. Ther.*, 1974, **9**, 335.
12 Morning, E. C., and Reisner, D. B., *J. Am. Chem. Soc.*, 1948, **70**, 3019.
13 Parker, C. A., and Rees, W. T., *Analyst*, 1960, **85**, 587.
14 Vigny, P., and Duquesne, M., *Photochem. Photobiol.*, 1974, **20**, 15.
15 Cepeda-Saez, A., Vazquez, M. L., Sargi, L., Prognon, P., Mahuzier, G., and Bisagni, E., *Anal. Chim. Acta*, 1989, **227**, 319.
16 Moore, T. A., Harter, M. L., and Song, P. L., *J. Mol. Spectrosc.*, 1971, **40**, 144.
17 Lai, I., Lim, B. T., and Lim, E. C., *J. Am. Chem. Soc.*, 1982, **104**, 7631.
18 Mattoo, B. N., *Trans. Faraday Soc.*, 1956, **52**, 1134.
19 Ronfard-Haret, J. C., Averbreck, D., Bensasson, R. V., Bisagni, E., and Land, E. J., *Photochem. Photobiol.*, 1982, **35**, 479.
20 Blais, J., Ronfard-Haret, J. C., Vigny, P., Cadet, J., and Voituriez, L., *Photochem. Photobiol.*, 1985, **42**, 599.
21 De Luccia, F. J., and Clinelove, L. J., *Anal. Chem.*, 1984, **56**, 2811.
22 Mattessich, J., and Cooper, J. R., *Anal. Biochem.*, 1989, **180**, 349.
23 Cogan, T. M., *J. Dairy Sci.*, 1972, **55**, 382.
24 Fukal, L., Smid, F., Davidek, J., and Velisek, J., *Sb. Vys. Sk. Chem. Technol. Praze, Potraviny*, 1979, **E50**, 225; *Chem. Abstr.*, 1980, **93**, 68800m.
25 Marsili, R. T., *J. Chromatogr. Sci.*, 1981, **19**, 451.

Paper 0/02563A
Received June 8th, 1990
Accepted September 24th, 1990

Development of a Non-radioactive Iodine Label-based Method for the Determination of Proteolytic Activity

Paula Keating, Fiona Anderson, Garret Donnelly and Richard O'Kennedy
School of Biological Sciences, Dublin City University, Glasnevin, Dublin 9, Ireland

A method for the determination of proteolytic activity is described, based on the use of non-radioactive iodine-labelled bovine serum albumin (BSA) as the substrate for proteolytic activity. Iodinated BSA catalyses the Sandell–Kolthoff reaction, involving the oxidation of arsenic(III) by cerium(IV), and the degree of catalysis can be used to detect proteolytic activity. The assay is simple and sensitive, allowing the detection of 100 ng ml^{-1} of proteinase.

Keywords: *Non-radioactive proteinase assay; iodinated Bolton–Hunter reagent; Sandell–Kolthoff reaction; protease assay*

Many assays involving the use of radioactively labelled compounds (*e.g.*, ^{125}I) have been described, but there are many hazards associated with the use of radioactive materials. However, the chemistry involved in the iodination of proteins and other molecules is well characterized. In this paper, we describe the development of a non-radioactive iodine-based assay for the determination of proteinase activity. The substrate used was bovine serum albumin (BSA), which was iodinated using the Bolton–Hunter reagent (IBHR).

Sandell and Kolthoff[1] reported that small amounts of iodide catalysed the reaction:

$$2Ce^{IV} + As^{3+} \rightarrow 2Ce^{3+} + As^{V}$$
(yellow) (colourless)

This reaction can be monitored spectrophotometrically and has been used to develop a micro-assay for I^- and iodine-conjugated proteins.[2]

In the present assay, iodinated BSA is adsorbed onto the bottom of the wells of 96-well micro-titre plates. Following addition of protease, the amount of iodinated substrate remaining can be determined and, hence, the level of activity measured.

Experimental

Materials

Ammonium cerium(IV) sulphate, arsenic trioxide, BSA, *N,N*-dimethylformamide (DMF), trypsin (from bovine pancreas) and pepsin (from porcine stomach mucosa) were obtained from Sigma (Poole, Dorset, UK). Ultrogel AcA44 was obtained from IBF Biotechnics (Villeneuve-la-Garenne, France). Flat-bottomed 96-well micro-titre plates were obtained from Nunc (Denmark). Sulphuric acid was obtained from BDH (Poole, Dorset, UK). Collagenase (from *Clostridium histolyticum*) was obtained from Boehringer (Mannheim, Germany). Papain (from *Papaya latex*) was obtained from Chemcon (Cork, Ireland). The bicinchoninic acid (BCA) protein-assay reagent was obtained from Pierce Chemicals (Rockford, IL, USA).

Reagent Solution

Ammonium cerium(IV) sulphate (0.1 mol dm^{-3}) was made up in 2.5 mol dm^{-3} H_2SO_4. As the intensity of the yellow colour is a function of acid concentration, fresh dilutions of this stock solution were made with 10% H_2SO_4 daily. Arsenious acid (0.075 mol dm^{-3}) was prepared by dissolving 14.84 g of arsenic trioxide in 700 ml of distilled water containing 28 ml of concentrated H_2SO_4. The mixture was heated to near boiling, with constant stirring, until virtually all the As_2O_3 had dissolved (precipitation of arsenious oxide may occur). After cooling to room temperature, the solution was filtered and the filtrate was made up to 1 l with distilled water.[2]

Preparation of Mono-iodinated Bolton–Hunter Reagent

This was prepared as previously described.[2]

Conjugation of IBHR to BSA

A 1 ml aliquot of a solution of BSA (2 mg ml^{-1}) was added to a solution containing 2 mg of IBHR in 200 μl of DMF. The reaction was allowed to proceed on ice for 2 h.

Gel Filtration

The labelled product was chromatographed on a column (245 × 16 mm i.d.) of Ultrogel AcA44, and elution was effected with 0.01 mol dm^{-3} phosphate buffered saline (PBS) (pH 9) at a flow-rate of approximately 1 ml min^{-1}; 1 ml fractions were collected.

Assay Procedure

The 96-well micro-titre plates were pre-coated with 100 μl of iodinated BSA (10 μg ml^{-1}, diluted with 50 mmol dm^{-3} carbonate–hydrogen carbonate buffer, pH 9.6) per well by incubation at 37 °C for 2 h. The wells were washed three times (for 10 min each time) with PBS (pH 7.2), incubated at 37 °C for 2 h with PBS, and then washed a further three times. Duplicate 100 μl samples of enzyme, at various dilutions, were placed in the wells and incubated for 16 h at 37 °C. All the enzymes were diluted with PBS (pH 7.2). Wells incubated with 100 μl of PBS served as zero controls. The supernatant solutions were aspirated from the plate, and the I^- remaining was detected by the addition of 60 μl of 0.075 mol dm^{-3} arsenious acid and 25 μl of 0.028 mol dm^{-3} ammonium cerium(IV) sulphate, made up in 10% H_2SO_4. Absorbance readings at 414 nm were recorded after a 10 min incubation. With increasing enzyme concentration, the amount of iodinated BSA remaining bound to the wells was reduced.

Results and Discussion

The BSA used was labelled with IBHR. Gel filtration on Ultrogel AcA44 produced a labelled product free from unbound IBHR (Fig. 1). The extent of hapten conjugation was found to be up to approximately 27 μmol of IBHR per μmol of BSA. The Ce^{IV}–As^{III} reaction was used to determine the IBHR content of the conjugate. Hapten conjugation by IBHR introduces groups into the protein,[3] which absorb at 280 nm,

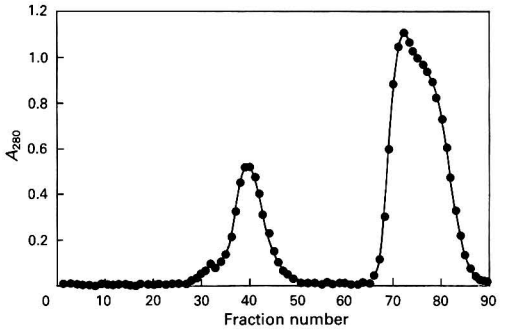

Fig. 1 Isolation of BSA by chromatography on Ultrogel AcA44. The eluent was 0.01 mol dm^{-3} PBS, pH 9.0. The flow-rate was 1 ml min^{-1} and 1 ml fractions were collected. Fractions were monitored at 280 nm (A_{280}). The first peak represents iodinated BSA; the protein content was measured by the BCA assay. No protein was present in the second peak which is due to non-conjugated IBHR

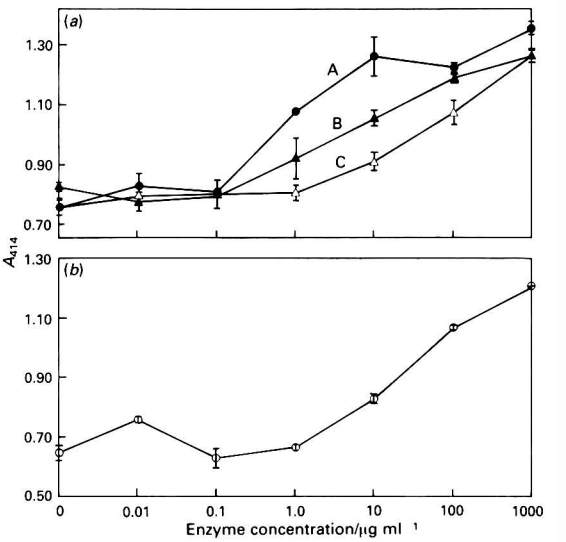

Fig. 2 Absorbance at 414 nm (A_{414}) after incubating different enzymes as indicated in microtitre wells with iodinated BSA. Each enzyme was assayed in duplicate at 10-fold dilutions. (*a*): A, Papain; B, pepsin; and C, collagenase. (*b*): Trypsin

so that the use of absorbance at 280 nm as a measure of protein concentration is no longer accurate. Similarly, IBHR was found to affect the BCA assay method of protein determination. Estimates of protein concentration were made, using the BCA protein assay, by 'spiking' the standards with a known amount of IBHR.

In order to establish if iodination influenced the adsorption characteristics of BSA onto poly(vinyl chloride), two microtitre plates were pre-coated, one with BSA and the second with iodinated BSA, both at a concentration of 50 μg ml^{-1}, and the amount of protein bound to the plates was determined. A coating efficiency of approximately 10% was found, and this is in accordance with work carried out by Walsh and Gosling,[4] who used polystyrene tubes. There was no significant effect resulting from iodination on BSA binding.

Non-ionic detergents, such as Tween 20 and Triton X-100, are commonly used in washing buffers for many immunological and biochemical assays. However, they were excluded from this assay because of their possible effects on the action of proteolytic enzymes. Hence, a stringent washing procedure with PBS was adopted, based on the method of Robertson *et al.*[5]

A range of commercially available enzymes were tested to establish the sensitivity of the assay and to ascertain the classes of enzyme to which the substrate was susceptible. Enzymes were tested over a range of dilutions from 1 mg ml^{-1} to 1 pg ml^{-1}. The amount of iodinated BSA remaining adsorbed on the wells was then determined by measuring the absorbance of the contents of each well at 414 nm, following addition of the reagents for the Ce^{IV}–As^{III} reaction. These data are presented in Fig. 2(*a*) and (*b*). With this assay it was possible to detect each enzyme at concentrations above background in the range 1–1000 μg ml^{-1}, with papain and pepsin detected at levels as low as 100 ng ml^{-1}. In an assay involving use of radio-iodinated gelatin as the substrate, detection of trypsin and collagenase at a level of 100 pg ml^{-1} and papain at 100 ng ml^{-1} is reported.[5] Currently, we are investigating ways to improve the sensitivity of this assay.

The endolytic enzymes trypsin and papain both cleave next to lysine and arginine; these residues are widely distributed in BSA. Collagenase has a relatively restricted substrate specificity, cleaving only at proline residues. Pepsin cleaves adjacent to aromatic or dicarboxylic L-amino acid residues. The ability of each enzyme to degrade the substrate reflects its sensitivity and susceptibility to a broad range of enzymes. The Bolton–Hunter reagent labels lysine residues, and BSA with 58 lysine residues, was chosen to achieve a high conjugation level. Gelatin radio-iodinated with IBHR has also been used because of its susceptibility to a broad range of enzymes.[5]

The iodination is simple to perform, and the Ce^{IV}–As^{III} reaction eliminates problems associated with radioactivity. The use of micro-titre plates allows large numbers of samples to be assayed on a small scale, which is economical both on substrate and, more importantly, on the samples being tested.

The financial support of BioResearch Ireland, Dublin City University, and the Cancer Research Advancement Board is gratefully acknowledged.

References

1 Sandell, E. B., and Kolthoff, I. M., *J. Am. Chem. Soc.*, 1934, **56**, 1426.
2 O'Kennedy, R., Bator, J. M., and Reading, C., *Anal. Biochem.*, 1989, **179**, 138.
3 Knight, L. C., and Welch, M. J., *Biochem. Biophys. Acta*, 1978, **534**, 185.
4 Walsh, J., and Gosling, J. P., *Anal. Biochem.*, 1986, **158**, 413.
5 Robertson, B. D., Kwan-Lim, G. E., and Maizels, R. M., *Anal. Biochem.*, 1988, **172**, 284.

Paper 0/03800H
Received August 21st, 1990
Accepted October 2nd, 1990

Determination of Creatine Kinase Activity Using a Co-immobilized Auxiliary Enzyme Reactor Coupled On-line With a Flow Injection System

J. M. Fernández-Romero and M. D. Luque de Castro*
Department of Analytical Chemistry, Faculty of Sciences, University of Córdoba, 14004 Córdoba, Spain

Two flow injection methods (based on spectrophotometric and spectrofluorimetric detection) were developed for the determination of over-all creatine kinase activity. Despite the complexity of the reactions involved (both include three enzyme-catalysed steps), the manifold is very simple because the two auxiliary enzymes which catalyse the two-step indicator reaction are co-immobilized on controlled-pore glass. The features of the proposed methods (calibration ranges between 0.1 and 2.0 and 0.01 and 1.0 U l^{-1}, relative standard deviation 0.93 and 0.53% for the spectrophotometric and spectrofluorimetric methods, respectively) allow the successful determination of the analyte activity in serum samples (recoveries better than 95–105% for both methods).

Keywords: *Creatine kinase activity; enzyme; flow injection; serum*

Creatine kinase [CK, adenosine triphosphate (ATP): creatine *N*-phosphotransferase E.C. 2.7.2.1] occurs in serum as a dimer. The monomers are labelled B and M and the three isoenzymes detected in serum are denoted by CK–BB, CK–MB and CK–MM; each of them is indicative of certain health disorders. Thus, myocardial infarction usually results in increased CK–MB in serum; CK–MM in serum is also increased in patients with Duchenne's muscular dystrophy, Reye's syndrome and carbon monoxide poisoning, among others; and finally, CK–BB is increased in cerebral diseases. These facts have fostered the development of chromatographic,[1–7] electrophoretic[8] and immunochemical[9,10] methods for the separation and determination of these isoenzymes. Nevertheless, a method for the over-all determination of CK activity should be very useful for fast screening, because separation steps are usually rather time-consuming and thus impractical whenever fast result delivery is mandatory.

This paper reports simple methods for the determination of the over-all activity of CK based on the following reaction sequence:

$$\text{Creatine phosphate} + \text{ADP} \xrightarrow{\text{CK}} \text{Creatine} + \text{ATP} \quad (1)$$

$$\text{ATP} + \text{D-glucose} \xrightarrow{\text{HK}} \text{D-glucose-6-phosphate} + \text{ADP} \quad (2)$$

$$\text{D-glucose-6-phosphate} + \text{NADP}^+ \xrightarrow{\text{G6PD}} \text{D-glucono-}\delta\text{-lactone-6-phosphate} + \text{NADPH} + \text{H}^+ \quad (3)$$

where CK, HK and G6PD are creatine kinase, hexokinase and glucose-6-phosphate dehydrogenase, respectively, and ATP and ADP adenosine triphosphate and adenosine diphosphate, respectively. The reduced form of the coenzyme, nicotinamide adenine dinucleotide phosphate (NADPH), can be monitored spectrophotometrically (λ_{max} 340 nm), or spectrofluorimetrically (λ_{ex} 340 nm, λ_{em} 470 nm).

The proposed methods were implemented in a flow-injection (FI) configuration in which the two auxiliary enzymes were co-immobilized on controlled-pore glass in a reactor that was coupled on-line with the FI manifold.

* To whom correspondence should be addressed.

Experimental

Reagents

Tris(hydroxymethyl)aminomethane (Tris) acetate buffer solution (100 mmol dm^{-3}, pH 7.00) alone or also containing magnesium acetate (20 mmol dm^{-3}), ethylenediaminetetraacetic acid (EDTA) (1 mmol dm^{-3}), P^1P^5-di(adenosin-5′-yl) pentaphosphate (AP5A) (10 μmol dm^{-3}) (Boehringer Mannheim 737020 trilithium salt), adenosine 5′-monophosphate (0.5 mmol dm^{-3}) (Sigma A-2002, free acid from yeast, type IV), and *N*-acetyl-L-cysteine (10 mmol dm^{-3}) (Sigma A-7250). Substrate solution containing adenosine 5′-diphosphate (1.5 mmol dm^{-3}) (Sigma A-275 sodium salt, grade IV), phosphocreatine (10 mmol dm^{-3}) (Sigma P-6502, disodium salt), α-D-(+)-glucose (1.5 mmol dm^{-3}) (Sigma G-5000) and β-nicotinamide adenine dinucleotide phosphate (2 mmol dm^{-3}) (Sigma N-0505 from yeast β-NAD, sodium salt). Enzymes: G6PD (Sigma G-8878 from torula yeast, type XI), HK (Sigma H-5750 from yeast, type C-301), creatine phosphokinase (Sigma C-3755 from rabbit muscle, type I, C-78886 from bovine muscle, type III, and C-6638 from rabbit brain, type IV), isotrol-CK 18F-6148 (Sigma C-0153), and isotrol-CK MB/LD 69F-6231 (Sigma C-5410). Controlled-pore glass (CPG 120–200 mesh from Electronucleonics) was used to immobilize the auxiliary enzymes as described by Masoom and Townshend.[11]

Apparatus

A Pye Unicam SP-500 single-beam spectrophotometer equipped with a Hellma 178-12QS flow cell (18 μl inner volume) connected to a Radiometer recorder and a Perkin Elmer LS-1 spectrofluorimeter equipped with a 4 μl flow cell and connected to a Perkin Elmer 56 recorder were used. A four-channel Gilson Minipuls-2 peristaltic pump with rate selector, Rheodyne 5041 injection valves, a Tecator TM III chemifold and a Selecta 382-S thermostat were also used.

Manifold and Procedure

Fig. 1 depicts the manifold used. The serum sample, diluted to an appropriate extent with Tris acetate buffer, is injected into a stream of the buffer, and subsequently merged with another stream containing all the ingredients of the main and auxiliary

reactions. The main reaction, which is catalysed by the enzyme analyte, takes place along the reactor L_1, after which it reaches the enzymic reactor (IMER). A signal is obtained as the sample plug reaches the flow cell as a result of the formation of NADPH; the signal can be related to the CK activity using the calibration graph.

Results and Discussion

Optimization of Variables

The variables influencing the system were divided into FI and chemical factors; the temperature was studied separately. The ranges over which they were studied and the optimum values found with spectrophotometric and spectrofluorimetric detection are listed in Table 1.

The temperature had a strong influence on the enzymic reactions; however, at temperatures >40 °C the analytical signal decreased because of denaturation of the biocatalysts.

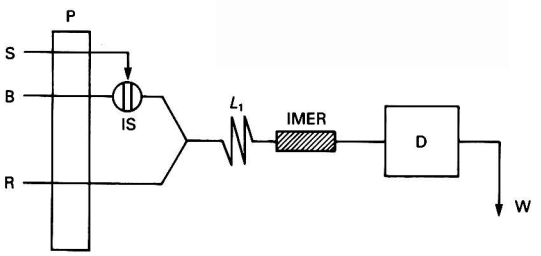

Fig. 1 FI manifold for the determination of CK activity: B, buffer solution; R, reagents solution; S, sample; P, peristaltic pump; IS, injection system; L_1, open reactor; IMER, enzymic reactor; D, spectrophotometric or spectrofluorimetric detector; and W, waste

Table 1 Study of variables

Variable	Range studied	Optimum value: Spectrophotometric method	Optimum value: Spectrofluorimetric method
Temperature/°C	25–50	40	40
Flow-rate/ml min^{-1}	1.19–2.34	1.64	1.64
Injected volume/µl	50–300	200	200
Reactor length/cm	10–350	200	200
Tris acetate buffer/mmol dm^{-3}	—	100	100
Tris acetate buffer/pH	—	7.00	7.00
Magnesium acetate/mmol dm^{-3}	5–30	20.0	20.0
EDTA/mmol dm^{-3}	0.5–2.5	1.0	1.0
AP5A/µmol dm^{-3}	—	10.0	10.0
AMP/mmol dm^{-3}	0–4.0	1.0	0.5
NAC/mmol dm^{-3}	0.5–30	10.0	10.0
ADP/mmol dm^{-3}	0.1–5.0	2.0	1.5
CP/mmol dm^{-3}	2.0–25.0	15.0	15.0
D-Glucose/mmol dm^{-3}	0.1–10.0	1.5	1.5
NADP$^+$/mmol dm^{-3}	0.1–3.0	1.5	2.0
IMER/cm	2.0–12.0	8.0	8.0

Flow injection variables

The reactor length, L_1; flow-rate, q; and injected volume, V_i had a similar influence on both types of detection. The optimum L_1 value listed in Table 1 was that providing a high signal; however, the optimum q and V_i values were a compromise between sampling rate sensitivity and sample consumption sensitivity, respectively.

Chemical variables

The buffer used was a complex solution including a series of modifiers such as (*i*) Mg^{II}, an activator for the ATP–ADP complex, (*ii*) EDTA to avoid the inhibitory effect of endogenous cations such as Ca^{II}, Fe^{III} and Cu^{II}, (*iii*) adenosine monophosphate (AMP), a competitive inhibitor of the activity of the other kinase (adenylate kinase, AK) and of the analyte itself. A compromise had to be made between maximum inhibition of AK and minimum inhibition of CK, (*iv*) AP5A, a competitive inhibitor for AK from erythrocyte and skeletal muscle, and (*v*) *N*-acetyl-L-cysteine (NAC), a reactivator of CK. All of these were included in the Tris acetate buffer solution at the concentrations listed in Table 1 and constituted the carrier into which the sample was inserted. The concentration and pH of the buffer were also optimized.

The solution merging with the sample carrier (R in Fig. 1) contained all the reagents of the main and auxiliary reactions except the auxiliary biocatalysts (HK and G6PD), which made up the IMER. These reagents were ADP, creatine phosphate (CP), D-glucose and $NADP^+$. The ranges over which their influence was studied and their optimum values are listed in Table 1. The length of the enzymic reactor (a hybrid FI–chemical variable) was also optimized.

Features of the Methods

Calibration graphs for both methods were constructed under the optimum working conditions. The results obtained and details of the reproducibility study are summarized in Table 2. The linear range achieved was more than adequate for the determination of the analyte in serum; the regression coefficient and precision, expressed as per cent. relative standard deviation (RSD), were excellent. The features of the spectrofluorimetric method are better than those of the spectrophotometric method (wider linear range, lower determination limit and higher precision).

Determination of CK Activity in Human Serum

The proposed methods were applied to the determination of the analyte activity in human serum. As the normal level of the enzyme in serum exceeded the linear range, dilution of the sample with the buffer acting as carrier was required in all instances. The activity results found compared with those corresponding to the conventional recommended method,[12] and those obtained on two standard additions are summarized in Table 3. Both testify to the usefulness of the two methods.

Conclusions

The two methods proposed for the determination of CK activity allow the fast, sensitive screening of this enzyme. The

Table 2 Features of the methods

Detection method	Equation*	Regression coefficient	Linear range/U l^{-1}	RSD† (%)	Sampling frequency/h^{-1}
Spectrophotometric	$A‡ = 0.2267\,[CK] + 3.3 \times 10^{-3}$	0.9990	0.1–2.0	0.93	48
Spectrofluorimetric	$I_f(\%) = 48.869\,[CK] - 0.9332$	0.9990	0.01–1.0	0.53	48

* [CK] in U l^{-1}.
† For 11 samples of 0.3 U l^{-1}, triplicate injection.
‡ Corrected absorbance.

Table 3 Determination of the enzymic activity of CK in serum. Results given in U l^{-1}

Sample No.	Reference method*	Dilution	Spectrophotometric method			Spectrofluorimetric method		
				Recovery† (%)		Recovery† (%)		
			Found	Addition 1	Addition 2	Addition 1	Addition 2	Found
1	64	1:99	0.63	105	100	103	95	0.66
2	116	1:999	0.116	101	101	100	100	0.118
3	98	1:99	0.96	99	101	101	101	0.98
4	39	1:99	0.38	104	101	103	102	0.38
5	208	1:999	0.208	102	101	96	98	0.210
6‡	800	1:999	0.798	104	100	105	103	0.799
7§	200	1:999	0.203	102	103	100	102	0.202

* See reference 12.
† Addition 1: 0.1 U l^{-1}; addition 2: 0.2 U l^{-1}.
‡ Control serum Isotrol-CK 18F-6148.
§ Control serum Isotrol-CK MB/LD 69F-6231.

simplicity of the FI manifold used with both methods arises from the use of co-immobilized enzymes, which in turn results in decreased analytical costs. The advantageous features of the methods were demonstrated by applying them to human serum samples.

The high sampling frequency, wide determination range and high reproducibility make these two methods suitable for screening by using very simple apparatus and any spectrophotometric or spectrofluorimetric detector commonly employed in laboratories.

The authors thank the Comisión Interministerial de Ciencia y Tecnología (CICyT) for financial support (Grant No. PA86-0146).

References

1 Mercer, D. W., and Varat, M. A., *Clin. Chem.*, 1975, **21**, 1088.
2 Nealon, D. A., and Henderson, A. R., *Clin. Chem.*, 1975, **21**, 1663.
3 Mercer, D. W., *Clin. Chem.*, 1975, **21**, 1102.
4 Mercer, D. W., *Clin. Chem.*, 1974, **20**, 36.
5 Nealon, D. A., and Henderson, A. R., *Clin. Chem.*, 1975, **21**, 392.
6 Chang, S. H., Noel, R., and Regnier, F. E., *Anal. Chem.*, 1976, **48**, 1839.
7 Klein, B., Foreman, J. A., Jeunelot, C. L., and Sheehan, J. E., *Clin. Chem.*, 1977, **23**, 504.
8 Yasmineh, W. G., and Hanson, N. Q., *Clin. Chem.*, 1975, **21**, 381.
9 Weiser, W. E., and Pardue, H. L., *Anal. Chem.*, 1986, **58**, 2523.
10 Toyoda, T., Kuan, S. S., and Guilbault, G. G., *Anal. Chem.*, 1985, **57**, 2346.
11 Masoom, A., and Townshend, A., *Anal. Chim. Acta*, 1984, **166**, 111.
12 American Association of Clinical Chemistry, *Selected Methods of Clinical Chemistry*, eds. Faulkner, W. R., and Meites, S., vol. 9, 1982, pp. 121–201.

Paper 0/03563G
Received August 6th, 1990
Accepted August 31st, 1990

Photochemical–Spectrofluorimetric Determination of Phenothiazine Compounds by Unsegmented-flow Methods

Danhua Chen,* Angel Rios, M. D. Luque de Castro and Miguel Valcarcel
Department of Analytical Chemistry, Faculty of Sciences, University of Córdoba, 14004 Córdoba, Spain

The properties of ultraviolet radiation were exploited to obtain fluorescent products from three phenothiazine compounds (chlorpromazine, promethazine and perphenazine). Photochemical reactions were studied and compared with chemical oxidation processes. After optimizing the working conditions, these reactions were applied to the determination of the analytes by stopped-flow injection methods (irradiation of the flow cell) and normal flow injection methods (irradiation of the reaction coil). The determination limits thereby achieved were 20 ng ml^{-1} (chlorpromazine and perphenazine) and 50 ng ml^{-1} (promethazine) with relative standard deviations of less than 2% in all instances ($n = 11$). Analyses for these compounds in pharmaceutical preparations were also carried out.

Keywords: *Phenothiazine; spectrofluorimetry; photochemical reaction; flow injection*

Phenothiazines and their derivatives are commonly used in pharmaceutical preparations such as tablets, injections and elixirs. They are extensively used as psychotropic drugs. From an analytical point of view, these compounds have been determined by chromatographic,[1–4] spectrophotometric[5–7] and, less often, spectrofluorimetric[8–10] methods, although spectrofluorimetric methods for the identification of phenothiazine drugs have been reported.[11–13] Many of these methods involve the use of a chemical oxidation reaction as the basis for such determinations, but several workers have shown the compounds to be photochemically unstable,[8,14] a feature that can be exploited for their determination.

Photochemical reactions have been used in the last few years for post-column derivatization in high-performance liquid chromatography (HPLC) to improve the detection of some types of solute.[15] However, to date, they have not been used very widely in other hydrodynamic analytical systems such as flow injection (FI). The amperometric determination of oxalate by a photochemical reaction taking place in the reaction coil of an FI system that was irradiated with visible light has been reported.[16] A second, more interesting, approach to the photochemical determination of this analyte was based on the use of an amperometric flow cell with several inlet optical fibre leads.[17] The optical fibres irradiated the sample only in the flow cell, thereby allowing the photochemical reaction to be monitored throughout.

This paper describes the similar use of a photochemical reaction in FI, with unstable compounds such as phenothiazines, under ultraviolet (UV) radiation. The methods described are simpler than those reported in the literature, particularly the method in which UV radiation from a spectrofluorimeter lamp is used, which induces the reaction in the flow cell (stopped-flow method). The results obtained are compared with those achieved by irradiation of the reactor coil of an FI system with a commercially available UV lamp [normal FI(nFI) method]. Both methods (stopped-flow and nFI) can be satisfactorily applied to authentic samples at high sampling rates.

Experimental

Reagents

Analytes. Chlorpromazine and promethazine were prepared in distilled water, and perphenazine in 5×10^{-3} mol dm^{-3} HCl. All stock solutions had a concentration of 1.000 mg ml^{-1} and were kept in a refrigerator in the dark. Working solutions were prepared by direct dilution with distilled water twice each working day and kept in the dark.

Carriers. Hydrochloric acid (1×10^{-3} mol dm^{-3}) was used as the carrier for chlorpromazine and perphenazine, and 1×10^{-3} mol dm^{-3} NaOH for promethazine.

Apparatus and Manifold

Fluorescence measurements were made on a Kontron SFM25 spectrofluorimeter equipped with a Knauer x–t recorder, a Gilson Minipuls-2 peristaltic pump, a Rheodyne 5041 rotary

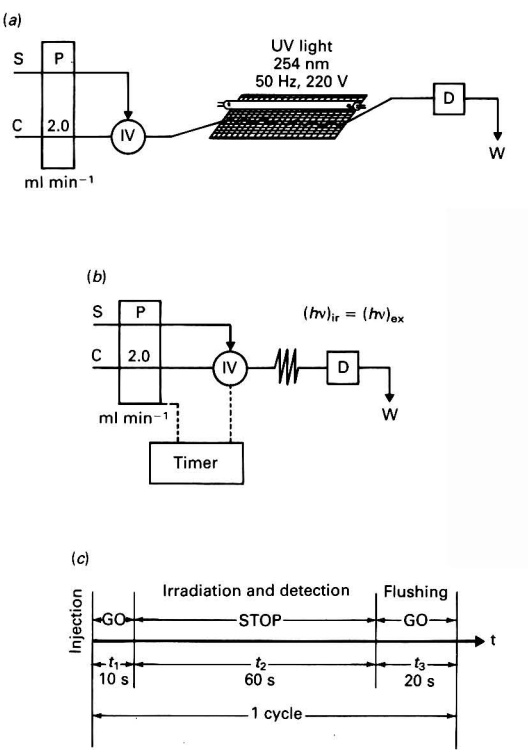

Fig. 1 Manifolds used for application of the photochemical methods for phenothiazines by (*a*) normal and (*b*) stopped-flow modes. (*c*) Time programme for the stopped-flow method. C, carrier; S, sample; P, pump; IV, injection valve; D, detector; W, waste; and t, time

* Permanent address: Department of Chemistry, Wuhan University, Wuhan, People's Republic of China.

valve with a loop volume of 65 μl and a fluorescence cell of 1.1 mm path length. Two manifolds (Fig. 1) were used to develop the methods.

In manifold (*a*), a Uvatom-70 UV lamp (which was equipped with a fan to cool the reactor to room temperature) was used to irradiate the reactor (0.5 mm i.d.) at 254 nm, with an energy of 50 Hz and 220 V. The portion of the reactor under UV irradiation was stitched through a frame of steel net and linked to the UV lamp. The injected sample plug was propelled by the carrier at a flow-rate of 2.0 ml min^{-1} and, as it passed to the detector, was irradiated by the UV lamp.

In manifold (*b*), a laboratory-built timer was used to control the pump and injection valve in the stopped-flow mode, and the injected sample plug was propelled along the 50 cm reactor (0.5 mm i.d.) at a flow-rate of 2.0 ml min^{-1}, halted in the flow cell and then irradiated directly by excitation radiation, the irradiation and detection process being enacted simultaneously.

All three phenothiazines were detected at an emission wavelength of 373 nm; in all instances, excitation was at 253 nm for chlorpromazine and perphenazine and at 295 nm for promethazine, with an energy of 50 Hz. The time programme for one cycle is shown in Fig. 1(*c*).

Results and Discussion

Both manual (by using a conventional cuvette) and flow methods for the photochemical determination of the phenothiazines were tested and compared. The obvious advantage of the flow method over its manual counterpart is illustrated in Fig. 2. A conventional fluorescence cell (1 cm optical path length and 18 μl inner volume), containing 1 μg ml^{-1} of analyte, was placed in the detector, and the fluorescence was detected and recorded. The signal increased gradually and did not reach a maximum within 10 min (*i.e.*, a steady state was not reached within 10 min) (it was even lower than that obtained with the flow cell, under the same conditions, within 5 min, although the light path of the fluorescence cell was nine times as long as that of the flow cell).

However, the kinetic curve was not smooth and the reproducibility was poor. A very smooth and reproducible kinetic curve was obtained with the flow cell and the signal reached a maximum within 1.5–2.0 min. This was the result of a small portion of the solution in the conventional cell being irradiated by the excitation radiation, and the photochemical product of the analyte diffusing into the other zones of the cell as it was formed and concentrated in the small zone under UV irradiation. This diffusion process was rather erratic. The physical kinetics of the system resulted in poor reproducibility and caused a weak signal to be obtained. On the other hand, all of the solution stopped in the flow cell was irradiated by the excitation radiation; therefore, only chemical kinetics were involved, which increased the efficiency, speed and reproducibility of the automated method.

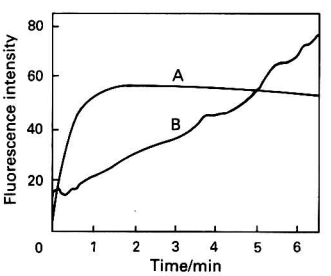

Fig. 2 Fluorescence–time recordings obtained by A, flow and B, batch methods

Study of the Reactions

The effect of the irradiation on the photochemical reaction was comprehensively studied in the stopped-flow mode (Fig. 3). The influence of the irradiation wavelength was investigated. Chlorpromazine stopped in the flow cell was irradiated at various wavelengths from 250 to 700 nm, at 100 V, for 1 min and then detected at an emission wavelength of 373 nm, with excitation at 253 nm and 550 V [Fig. 3(*a*)]. Hence, in the detection process the sample was continuously irradiated at 253 nm and 550 V. The photochemical reaction developed to an extent of about 90% at irradiation wavelengths below 320 nm, and no photochemical reaction was observed above 360 nm. Further experiments were performed by irradiating 1 μg ml^{-1} of chlorpromazine at 360 nm and 500 V for different periods of time; the irradiation energy was about 250 times higher at 500 V than at 100 V, hence the fluorescence was detected at an emission wavelength of 373 nm, with excitation at 253 nm and 550 V [Fig. 3(*b*)].

One minute of pre-irradiation had little effect on the photochemical reaction, and only about 60% of the photochemical product was formed after a 10 min irradiation. This small difference in the peak maxima arose from the different irradiation conditions used. The photochemical product would be easier to convert further, partially by use of stronger radiation (shorter wavelength or higher intensity). At 253 nm, irradiation at 100 V was sufficient for the photochemical reaction; similar results were obtained by using irradiation energies up to 100 times higher. From the above results it can be concluded that the irradiation wavelength was more influential than the irradiation time and energy, and that it must be equal to, or less than, 320 nm.

The spectra of the photochemical reaction products obtained from the three phenothiazines were recorded and compared with those of native fluorescence and those of the products resulting from oxidation with permanganate. The continuous-flow mode was used because the continuous

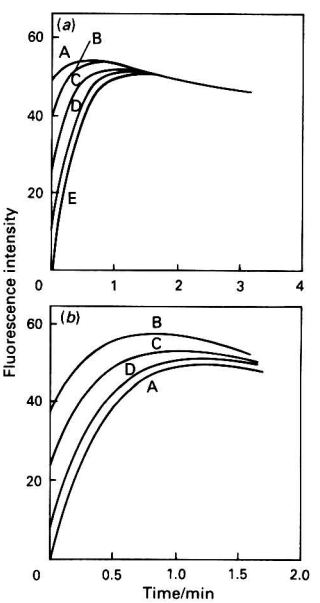

Fig. 3 Influence of the irradiation conditions on the fluorescence intensity of 1 μg ml^{-1} chlorpromazine irradiated at 550 V, λ_{ex} = 253 nm, λ_{em} = 373 nm. (*a*) After irradiation for 1 min (100 V) at the wavelengths (λ/nm) A, <320; B, 330; C, 340; D, 350; and E, >360. (*b*) After irradiation at 360 nm (500 V) for A, 1; B, 2; C, 5; and D, 10 min

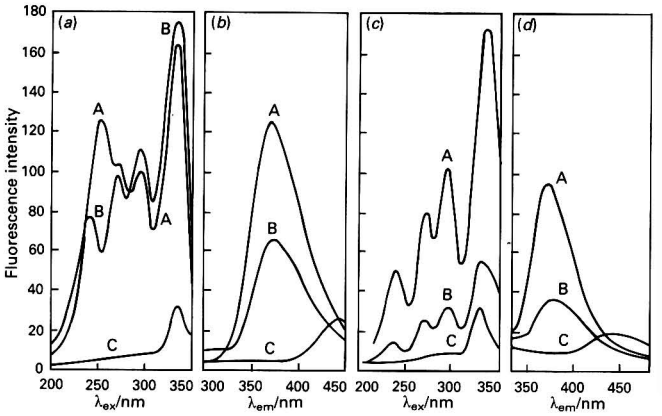

Fig. 4 Excitation and emission spectra of 1 μg ml^{-1} of (*a*) and (*b*) chlorpromazine and (*c*) and (*d*) promethazine. A, Photochemical reaction in the 50 cm reactor coil; B, oxidized by 0.01% $KMnO_4$; and C, native fluorescence

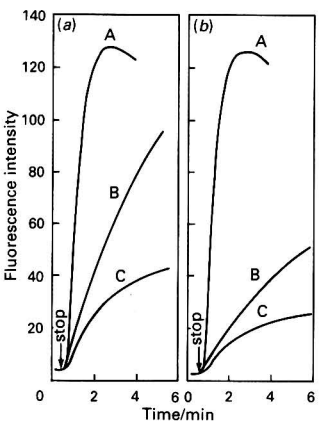

Fig. 5 Influence of oxygen in the development of the reactions. (*a*) Without removing dissolved oxygen and (*b*) after removing dissolved oxygen with argon: A, 1 μg ml^{-1} chlorpromazine in 1 × 10^{-3} mol dm^{-3} HCl; B, 0.5 μg ml^{-1} promethazine in distilled water; and C, 1 μg ml^{-1} chlorpromazine in distilled water

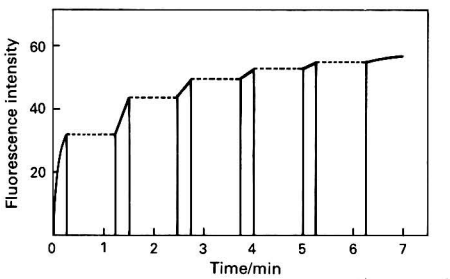

Fig. 6 Influence of the irradiation time on the fluorescence intensity of 1 μg ml^{-1} chlorpromazine (HV 550 V, λ_{ex} 253 nm, and λ_{em} 373 nm)

aspiration of the sample solution avoided further photochemical reaction induced by the excitation radiation of the detector and it kept the concentration of the photochemical product unaltered during the wavelength scan. A two-channel configuration, with a confluence point for the sample and the auxiliary stream, was used in this instance.

The sample solution contained either 2 μg ml^{-1} of chlorpromazine or perphenazine in 2 × 10^{-3} mol dm^{-3} HCl, or 1 μg ml^{-1} of promethazine in 2 × 10^{-3} mol dm^{-3} NaOH. The other stream contained distilled water for the photolysis and the native fluorescence, and 0.01% $KMnO_4$ for the chemical oxidation. Two streams at a flow-rate of 1 ml min^{-1} were merged, passed through a 100 cm reactor and then into the detector. The lamp was turned on to irradiate part of the reactor (50 cm) for the photochemical reaction and was off in other instances.

The spectra of chlorpromazine and promethazine are shown in Fig. 4(*a*) and (*b*), respectively. The spectra of perphenazine were similar in shape and position to those of chlorpromazine; hence, they have been omitted. Both the excitation and the emission spectra of the photochemical reaction shifted to shorter wavelengths, and the signal was more sensitive than that of the native fluorescence by about a factor of 10. The maximum emission wavelength appeared at 373 nm for all three phenothiazines. Four peaks were obtained in the excitation spectra. They were at 253, 273, 295 and 333 nm for chlorpromazine and perphenazine, and at 239, 273, 295 and 333 nm for promethazine. The excitation spectra of promethazine were identical in shape for both the photochemical reaction and the chemical oxidation, while with chlorpromazine and perphenazine, different shapes were obtained from the two reactions; hence, for the photochemical reaction, the first three peaks shown in Fig. 4(*a*) decreased in fluorescence with increasing wavelength, while the opposite effect was observed for the oxidation by permanganate. Moreover, the first excitation peak of the chemical oxidation shifted to shorter wavelengths than that of the photochemical reaction. The products of the two reactions could, therefore, be different.

The photochemical reaction is feasible with no other reagent except light. As the solution came into contact with air, it contained some dissolved oxygen. In order to investigate the nature of the photochemical reaction, the solution was continuously de-gassed with Ar under vibration and pumped through the reactor with continuous aspiration into a single-channel configuration. The kinetic curve was recorded while the pump was stopped and the photochemical reaction took place afterwards; the same solution, without removal of oxygen, was used as a reference for comparison (Fig. 5). In 1 × 10^{-3} mol dm^{-3} HCl medium, 1 μg ml^{-1} of chlorpromazine showed the same kinetic behaviour and sensitivity, irrespective of whether dissolved oxygen was removed or not. On the other hand, in distilled water, the sensitivity of the de-gassed solution decreased for 1.0 and 0.5 μg ml^{-1} of promethazine.

Table 1 Analytical parameters of the determination of phenothiazines by the normal FI (nFI) and stopped-flow modes

Parameter	nFI	Stopped-flow
Sampling volume/μl	65	65
Flow-rate/ml min^{-1}	2.0	2.0
Reactor length/cm	100*	50
Delay time (t_1)/s	—	10
Stop-time (t_2)/s	—	60
Flush time (t_3)/s	—	20
Sampling frequency/h^{-1}	90	40

* 50 cm of the reactor were exposed to UV irradiation.

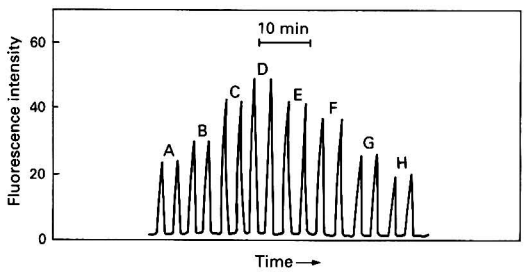

Fig. 7 Influence of the delay time of the FI peak for 1 μg ml^{-1} of chlorpromazine. Time (s): A, 7; B, 8; C, 9; D, 10; E, 11; F, 12; G, 13; and H, 14

The above results allow one to conclude that UV radiation acted as a 'reagent' in the photo-oxidation and that dissolved oxygen played some role in the neutral solution, although it was not indispensable because the photo-oxidation also took place in its absence. On the other hand, without UV radiation, the solution containing dissolved oxygen was very stable.

Further experiments were performed by adding the 'reagent' intermittently; 1 μg ml^{-1} of chlorpromazine was injected into the carrier stream and stopped at the flow cell. The kinetic curve was then recorded (Fig. 6). Irradiation periods of 15 s were followed by 1 min without irradiation, as shown by the broken line in the figure (the detection process was also halted meanwhile). The reaction stopped as irradiation was halted, and resumed on re-application. This is an obvious advantage of photochemical reactions over chemical reactions as UV radiation acts as a clean 'reagent' that can be removed altogether at any stage of the reaction.

Influence of Variables

Table 1 lists the optimum values of the variables for the normal and stopped-flow methods. Common variables such as the pH, injected volume and flow-rate had the same values for the two methods. These and variables whose values differed for both methods are commented on below.

The pH of the reaction medium was studied in the range from 1×10^{-1} to 1×10^{-5} mol dm^{-3} HCl and NaOH, pH 4.56 acetic acid–sodium acetate, pH 7.65 $H_2PO_4^-$–HPO_4^{2-}, pH 9.4 NH_4Cl–NH_3 and distilled water (neutral solution). The signal obtained for chlorpromazine and perphenazine was fairly weak with neutral and basic media and strong with acid media. The maximum value was achieved with 1×10^{-3} mol dm^{-3} HCl. The photochemical product of promethazine featured intense fluorescence with acid and neutral media, the highest value being obtained with NaOH in the range from 1×10^{-1} to 1×10^{-5} mol dm^{-3} (1×10^{-3} mol dm^{-3} NaOH was selected).

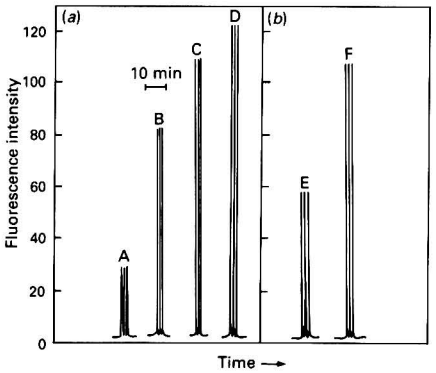

Fig. 8 Influence of the geometrical shape of the irradiated reactor on the FI peak. (*a*) UV lamp on (λ_{ex} = 253 nm; λ_{em} = 373 nm), 2 μg ml^{-1} perphenazine; (*b*) UV lamp off (λ_{ex} = 333 nm; λ_{em} = 450 nm), 20 μg ml^{-1} perphenazine; A and E, 50 cm of reactor around the lamp; B, C, D and F, 50 cm reactor stitched through a frame of steel net and placed near the UV lamp, at a distance of B, 3.0; C, 1.5; and D, 0 cm

Stopped-flow variables

The delay time is a major parameter in the stopped-flow mode because it allows the sample plug to be stopped in the flow cell for irradiation and detection in order to maximize the signal. The influence of the delay time is illustrated in Fig. 7; the maximum signal was obtained for an interval of 10 s between injection and halting of the pump. The irradiation time selected was 60 s as a compromise between sensitivity and efficiency, although the maximum value was obtained in 90–120 s for chlorpromazine and perphenazine, and equilibrium was not reached until after 4–5 min for promethazine. As the pump was restarted, the signal returned to the baseline immediately because the solution outside the flow cell received no irradiation, so no photochemical reaction occurred, except in the solution stopped in the flow cell. This provided a single peak in FI. However, a further 20 s were required to flush the trailing end of the injected sample plug to waste. This flushing step was required in order to render the flow cell ready for the next determination.

FI variables

The reactor length selected in the nFI method was 100 cm, 50 cm of which was UV irradiated. In photochemical detection in HPLC, the photochemical reactor is usually placed around the lamp and cooled with pressurized air pre-cooled by solid CO_2.[18] In this work, for simplicity, a fan was used to cool the reactor by air. Different geometrical reactor shapes were assayed (Fig. 8). Weak signals were obtained when the reactor was coiled around the lamp, while much improved sensitivity (4.4 times higher) was obtained as the reactor was stitched through a frame of steel net, which was placed near the UV lamp. The difference in sensitivity can be explained as follows.

(1) *Photochemical efficiency.* As the reactor was coiled around the lamp, it was heated by the contact surface, where the cooling air could not reach. The higher temperature reduced the yield of the photochemical reaction.

(2) *Effect of geometrical distortion.* The coil diameter of the reactor was 1.6 cm around the lamp and 0.4 cm when stitched onto the frame of steel net. Peak broadening (dispersion) was less obvious in the latter instance because the injected sample plug in the reactor changed its direction of flow more frequently. In order to distinguish between these two aspects, the native fluorescence of 20 μg ml^{-1} of perphenazine was measured at an emission wavelength of 450 nm, excited at 253 nm without UV irradiation. The signal obtained with the reactor stitched onto the steel net was 1.9

times as sensitive as that obtained with the reactor coiled around the lamp, which is exactly the contribution from the difference in dispersion. The influence of the distance of the steel net to the lamp was also investigated; the strongest signal was achieved by placing them almost in contact.

Analytical Features of the Methods

The features of the proposed methods for the determination of chlorpromazine, promethazine and perphenazine are summarized in Table 2. Each point in the calibration graphs was obtained from three replicate injections. The limits of determination were 20 ng ml^{-1} for chlorpromazine and perphenazine, and 50 ng ml^{-1} for promethazine. The relative standard deviations (RSDs) obtained for a concentration of 1 μg ml^{-1} in all instances ($n = 11$; $p = 0.05$) were less than 2%, the nFI method being more accurate (deviations of less than 1% for the three analytes).

Interferences

The influence of foreign species on the photochemical determination of the three phenothiazines was studied in the normal and stopped-flow modes (Table 3). The experiment was performed by adding specific amounts of interferent to 1 μg ml^{-1} of analyte; the tolerated level was taken as the measured signal variation ±5%. Glucose, sucrose and mannitol were tolerated in large amounts, and 10-fold excesses of acetopromazine were also tolerated in the determination of chlorpromazine and promethazine. Ascorbic acid and sodium sulphite interfered owing to their redox properties. Citric acid interfered in the determination of chlorpromazine and perphenazine, but not in that of promethazine (the interferent effect was probably due to the acid–base media used as the former determination was carried out in 1×10^{-3} mol dm^{-3} HCl, while promethazine was determined in 1×10^{-3} mol dm^{-3} NaOH).

Analysis of Authentic Samples

In order to confirm the applicability of the proposed methods, various drugs were determined in authentic samples (pharmaceuticals), in the normal and stopped-flow modes, by using normal and standard additions procedures. The results were consistent with one another and also agreed with values for the nominal contents (see Table 4).

Table 2 Features of the proposed methods for the determination of chlorpromazine, promethazine and perphenazine

Analyte	Method	Concentration range/μg ml^{-1}	Calibration equation	Regression coefficient	RSD (%)‡
Chlorpromazine	nFI	0.02–2.40	$F = 56.82c$† + 0.83	0.9989	0.92
	SF*	0.02–3.00	$F = 50.13c + 3.61$	0.9995	1.96
Promethazine	nFI	0.05–2.50	$F = 67.13c - 0.45$	0.9994	0.85
	SF	0.05–3.00	$F = 42.44c - 1.29$	0.9995	1.97
Perphenazine	nFI	0.02–2.00	$F = 70.96c + 11.01$	0.9843	0.58
	SF	0.02–2.50	$F = 40.17c + 2.24$	0.9984	1.45

* SF = stopped-flow.
† c = concentration in μg ml^{-1}.
‡ From 11 measurements of 1 μg ml^{-1} of analyte.

Table 3 Maximum levels of foreign species tolerated in the determination of 1 μg ml^{-1} of each phenothiazine compound

	Ratio of foreign species to analyte (m/m)					
	Chlorpromazine		Promethazine		Perphenazine	
Foreign species	nFI	Stopped-flow	nFI	Stopped-flow	nFI	Stopped-flow
Glucose	1000*	1000*	250	250	250	500
Ascorbic acid	1	<1	<1	1	<1	<1
Caffeine	10	10	10	2.5	5	2.5
Sucrose	100	200	15	20	500	500
Sodium sulphite	<1	8	<1	<1	<1	2
Citric acid	<1	<1	20	20	<1	<1
Mannitol	1000*	1000*	1000*	1000	1000*	1000*
Acetopromazine	40	70	50	20	5	2
Promethazine	<1	<1			<1	<1
Perphenazine	<1	<1	1	1		
Chlorpromazine			1	1	<1	<1

* Not the maximum allowed ratio.

Table 4 Application of the proposed methods to the determination of chlorpromazine, promethazine and perphenazine in pharmaceutical preparations

		nFI		Stopped-flow	
Pharmaceuticals*	Analyte	Normal	SAM†	Normal	SAM†
1. Largactil	Chlorpromazine	0.45[illegible]	0.4635	0.5857	0.5867
2. Largatrex	Chlorpromazine	0.[illegible]70	0.5778	0.5771	0.5831
3. Fenergan	Promethazine	[illegible].343	0.5231	0.5026	0.5257
4. Hemotripsin	Promethazine	0.5220	0.5541	0.5184	0.5349
5. Norfenazin '10'	Perphenazine	0.6182	0.6541	0.5244	0.5956
6. Mutabase 4–10	Perphenazine	0.4579	0.5064	0.5158	0.5315

* 0.50 μg reference value for 1, 2, 3, 5 and 6; 0.48 μg for 4.
† SAM = standard additions method.

Conclusions

Photochemical reactions used in unsegmented-flow systems have a great analytical potential not fully exploited to date. Light is an ideal 'reagent', available at various intensities, convenient and inexpensive, and rather flexible in relation to reaction times. By selecting a narrow wavelength band, the selectivity of a reaction can be increased at will. Light can be applied on to the reaction coil or in the flow cell, as shown in this work. A special, very simple application involves using light from the detector lamp, the intensity of which is sufficient to induce the photochemical reaction, which was used here for the spectrofluorimetric determination of various phenothiazine compounds in the stopped-flow mode. In other instances, optical fibres can be used to transmit the light to the flow cell.

Comisión Interministerial de Ciencia y Technología (CICyT) is thanked for financial support (Grant No. PA86-0146).

References

1 Larsen, N. E., Hansen, L. B., and Knudsen, P., *J. Chromatogr., Biomed. Appl.*, 1985, **42**, 244.
2 Melethil, S., Dutta, A., Chungi, V., and Dittert, L., *Anal. Lett.*, 1983, **16**, 701.
3 Bounine, J. P., and Guiochon, G., *Analusis*, 1984, **12**, 175.
4 Tebbett, I. R., *J. Chromatogr.*, 1986, **356**, 227.
5 Taha, A. M., El-Rabbat, N. A., El-Kommos, M. E., and Referat, I. H., *Analyst*, 1983, **108**, 1500.
6 Jayarama, M., D'Souza, V., Yathirajau, H. S., and Rangaswamy, *Talanta*, 1986, **33**, 352.
7 Ibrahim, E. A., Issa, A. S., Salam, M. A. A., and Mahrons, M. S., *Talanta*, 1983, **30**, 531.
8 White, V. R., Frings, C. S., Villafranca, G. E., and Fitzgerald, J. M., *Anal. Chem.*, 1976, **48**, 1314.
9 Gutiérrez, M. C., Gómez-Hens, A., and Pérez-Bendito, D., *Anal. Lett.*, 1987, **20**, 1847.
10 Clark, B. J., and Fell, A. F., *Pharm. Pharmacol.*, 1983, **35**, 22P.
11 Millinger, T. J., and Keelert, C. E., *Anal. Chem.*, 1963, **35**, 554.
12 Ragland, J. B., and Kinross-Wright, V. J., *Anal. Chem.*, 1964, **36**, 1357.
13 Mellinger, T. J., and Keeler, C. E., *Anal. Chem.*, 1964, **36**, 1841.
14 Scholten, A. H. M. T., Brinkman, U. A. Th., and Frei, R. W., *Anal. Chim. Acta*, 1980, **114**, 137.
15 Krull, I. S., and LaCourse, W. R., in *Reaction Detection in Liquid Chromatography*, ed. Krull, I. S., Marcel Dekker, New York, 1986, ch. 7, pp. 303–352.
16 León, L. E., Ríos, A., Luque de Castro, M. D., and Valcárcel, M., *Analyst*, 1990, **115**, 1549.
17 León, L. E., Ríos, A., Luque de Castro, M. D., and Valcárcel, M., *Anal. Chim. Acta*, 1990, **234**, 227.
18 Scholten, A. H. M. T., and Frei, R. W., *J. Chromatogr.*, 1979, **176**, 349.

Paper 0/02937H
Received June 29th, 1990
Accepted September 28th, 1990

Flow Injection Method for the Assay of Phenothiazine Neuroleptics in Pharmaceutical Preparations Using Ammonium Metavanadate

Salah M. Sultan
Chemistry Department, King Fahd University, KFUPM Box 2026, Dhahran 31261, Saudi Arabia

A simple flow injection method for the determination of chlorpromazine, promethazine, trimeprazine and perphenazine over wide ranges of concentrations is described. The method is based on the oxidation of phenothiazine with ammonium metavanadate in sulphuric acid media and subsequent measurement of the coloured, oxidized form of the product at the corresponding wavelength. A sampling rate of up to 160 h^{-1} was attained. Relative standard deviations for the standard samples were usually less than 0.5%. The method was applied to the determination of phenothiazines in proprietary drugs and the results were comparable to those obtained by the official methods in the British Pharmacopoeia.

Keywords: *Flow injection; chlorpromazine, promethazine, trimeprazine and perphenazine; ammonium metavanadate; pharmaceutical products*

The *N*-substituted phenothiazine tranquillizing agents are the best available drugs for the treatment of moderate and severe mental and emotional conditions. They are also known for their antiemetic effects, the potency of the effects of anaesthetics, analgesics and sedatives, and also as antihistamines.[1] The vast number of phenothiazine derivatives and the continued introduction of these drugs has instigated many workers to explore new methods for their determination. Many spectrophotometric methods have been proposed, some lacking sensitivity and specificity,[2–9] or requiring long heating times,[10–13] or involving non-aqueous media,[14,15] and some other spectrophotometric methods have very narrow limits of detection.[13,15,16] Few flow injection (FI) methods have been reported, one[17] requires the use of a very high concentration (10 mol dm^{-3}) of perchloric acid and another[10] uses synchronous luminescence spectroscopy. A titrimetric method[18] and two complexometric methods[19,20] have also been reported but they are only suitable for the determination of macro amounts of the drug. The majority of the methods described are chromatographic and have been reviewed,[21–32] all require the use of highly sophisticated equipment, involving tedious extraction procedures, and are time consuming. In the British Pharmacopoeia (BP) methods the four compounds are assayed spectrophotometrically and each is treated differently: chlorpromazine hydrochloride[2] in tablet form is triturated with ethanol and dissolved in HCl and the absorbance is measured at 254 nm; promethazine tablets[3] are triturated and dissolved in HCl and the absorbance of the resulting solution is measured at 249 nm; for the oral solution[3] palladium(II) is added, diluted and the absorbance is measured at 472 nm; trimeprazine tartrate[4] is dissolved in methanol and the absorbance is measured at 255 nm; and perphenazine[5] is treated with ethanol and the absorbance is measured at 258 nm.

Ammonium metavanadate is used for the first time in this study for oxidizing phenothiazines. Similar inorganic oxidants such as sodium cobaltinitrite,[12] tungsten,[8,13] and iron(III)[17] have been used previously. The wavelengths of the absorption maxima of the products, found experimentally, correspond to those reported in the literature[7,8,12,17] and support the present findings of this worker, which indicate that studies using the FI technique should be continued. In this work the phenothiazine is reacted on-line with the vanadate in sulphuric acid media and the oxidized form of the drug is measured spectrophotometrically at the corresponding wavelength of maximum absorbance.

Experimental

Apparatus

Apparatus obtained from the Alitea USA/FIA Laboratory (Sweden) was used for all experimental work. The apparatus consists of the following units. (*i*) Pump. A high quality peristaltic pump with cassette drive. It features eight stainless-steel rollers on individual bearings with individual cassettes for as many as four pump tubes and a gearbox with a double-bearing shaft. Pump tubing (PVC) of 1.02 mm i.d. was obtained from Cole Parmer (Chicago, IL, USA). (*ii*) Injector. A Rheodyne Model 5041 4-way PTFE rotary valve mounted on an angle bracket in the injector position of the FIA Laboratory apparatus was used. (*iii*) Reactor module. Consisting of 0.5 mm i.d. Micro-Line tubing available from Thermoplastic Scientifics (New Jersey, NY, USA). (*iv*) Detector. A Spectronic mini 20 spectrophotometer (Milton Roy, Analytical System Business, NY, USA) with a grating monochromator detector. A Unovic ultra-micro flow cell of 20 µl with a path length of 1.0 mm was used, which is available from Unovic Instruments (NY, USA). (*v*) Recorder. A Model 0555 single channel strip-chart recorder, from Cole Parmer, was used for peak absorbance–time recordings.

Prior to the FI measurements, absorbance–wavelength graphs were obtained using a Cary Model 2300 ultraviolet/visible/near infrared spectrophotometer connected to a Varian DS-15 data station and Epson LX-86 printer; 10.00 mm cells were used with this apparatus.

Reagents

Phenothiazine pure sample. Stock solutions of 2000 ppm were prepared by dissolving the pure analytical-reagent grade product (May & Baker, Rhone-Poulenc, Dagenham, Essex, UK) in hot water for chlorpromazine, promethazine and trimeprazine tartrate, and in dilute sulphuric acid for perphenazine. Working solutions were prepared by appropriate dilutions.

Phenothiazine tablets. Solutions with a concentration of 1000 ppm were prepared by dissolving an amount of crushed and powdered tablets equivalent to the required amount of phenothiazine in water; the mixture was heated in a water-bath for 15 min, filtered, washed and the filtrate then made up to volume in a 50 ml calibrated flask with water after cooling to room temperature. Working solutions were obtained by appropriate dilution.

Phenothiazine elixirs. Working solutions were prepared by appropriate dilution of the elixir as a stock solution without any treatment.

Sodium metavanadate. Ammonium metavanadate (8.00 g) (Fluka-Granite, Switzerland) was dissolved in the appropriate concentration of sulphuric acid solution and made up to volume with the same acid solution in a 2 l calibrated flask.

Sulphuric acid. Appropriate concentrations of sulphuric acid solutions were prepared by dilution from AnalaR concentrated sulphuric acid.

Water. Highly purified distilled water was used throughout.

Manifold and Procedure

The single-line manifold system used for the direct spectrophotometric FI determination of the phenothiazines is shown in Fig. 1. A 123 μl aliquot of the phenothiazine sample containing a definite amount calculated as ppm is injected through the injection valve into the carrier stream of the vanadate solution driven by the peristaltic pump. The stream passes through a reaction coil, 45 cm long, where the phenothiazine is oxidized and the colour is developed; the absorbance of this coloured solution is measured in the flow cell of the spectrophotometer and the peaks are recorded at a recorder speed of 0.5 cm min^{-1}.

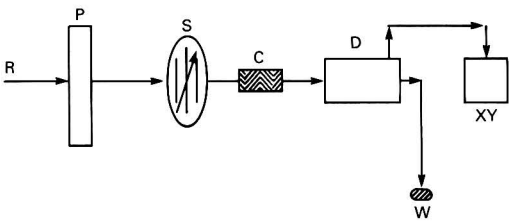

Fig. 1 Schematic diagram of the FI manifold used for the assay of phenothiazines: R, ammonium metavanadate solution; P, peristaltic pump; S, sample injector, 123 μl loop size; C, reactor, coil length 45 cm or 2 m; D, Spectronic 20 spectrophotometer adjusted to the corresponding wavelength of the oxidized form of the phenothiazine; XY, recorder; and W, waste

Results and Discussion

Chemical System

The FI method is based on the reaction of the vanadate with the phenothiazine (chlorpromazine hydrochloride, promethazine theoclate, trimeprazine tartrate and perphenazine). In sulphuric acid media, each gives a coloured product that absorbs at a different wavelength as shown in Table 1. The

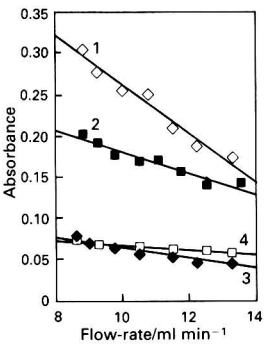

Fig. 2 Influence of the flow-rate (adjusted by the pump speed) (ml min^{-1}) on the peak absorbance. Phenothiazine concentration: 1, 900 ppm of chlorpromazine; 2, 890 ppm of promethazine; 3, 100 ppm of trimeprazine; and 4, 55 ppm of perphenazine

Table 1 Compounds investigated

Name	Structure	Batch No.	λ_{max}/nm
Chlorpromazine hydrochloride	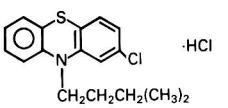	E99	526
Promethazine theoclate	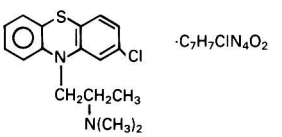	W3021	515
Trimeprazine tartrate	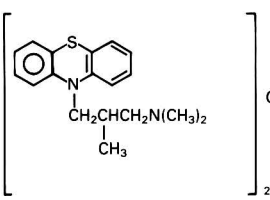	CD14014	510
Perphenazine	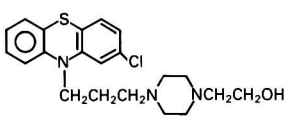	D11	525

Table 2 Analytical appraisals

Drug	Calibration equation	r	Range (ppm)	Frequency (f)/ samples h^{-1}	Peak width/s	RSD (%)	Flow-rate (Q)/ ml min^{-1}
Chlorpromazine	$A = 0.0125 + 4.58 \times 10^{-5} c$*	0.997	160–1000	129	6	0.3	8.6
Promethazine	$A = -0.00566 + 1.37 \times 10^{-4} c$	1.00	160–2100	150	5	0.5	8.6
Trimeprazine	$A = -0.0463 + 2.76 \times 10^{-4} c$	0.998	400–1200	129	6	0.4	8.6
Perphenazine	$A = -0.0109 + 7.38 \times 10^{-3} c$	0.997	0–200	138	5.5	0.4	12.5

* c = concentration.

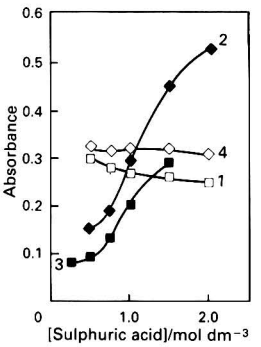

Fig. 3 Influence of acidity on the peak absorbance. Phenothiazine concentration: 1, 615 ppm of chlorpromazine; 2, 1150 ppm of promethazine; 3, 250 ppm of trimeprazine; and 4, 198 ppm of perphenazine

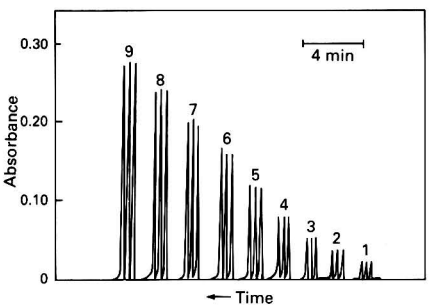

Fig. 4 Typical FI results (n = 3) for promethazine standard solutions of: 1, 178; 2, 297; 3, 416; 4, 594; 5, 892; 6, 1189; 7, 1486; 8, 1783; and 9, 2080 ppm

colour is attributed to the radical cation as the oxidized form of the phenothiazine. Oxidation of the phenothiazines to the radical cation has been reported previously.[7,12]

Optimization of Variables

The influence of the most critical FI variables, such as flow-rate, reaction coil length, injected volume and acidity of the reaction, on the magnitude of the peak absorbance and reproducibility of the results was studied carefully as indicated below.

Flow-rate and reaction coil length

Both parameters are closely related and variation of one or the other has a great influence on the peak absorbance. The flow-rate is conveniently controlled by the peristaltic pump with a speed of up to 999 ramps. The relationship of pump speed in ramps to flow-rate could be obtained by applying the following equation: flow-rate (Q) = 8.5 + 0.005 × ramps.

The reaction coil length, which is defined as the total length of tubing from the point of sample introduction to the detector, is interchangeable with longer or shorter tubing of the same type and diameter. The effect of flow-rate on the peak absorbance is shown in Fig. 2 for the four compounds. From the graphs obtained it is obvious that the four compounds behave similarly, in that as the flow-rate or pump speed is increased, there is a slight decrease in the peak absorbance, which is caused by a corresponding decrease in the residence time (t) of the sample in the reaction coil, indicating that equilibrium and full development of the colour of the oxidized form of the drug are not being achieved. The effect seems to be significant for chlorpromazine and promethazine, particularly the former, and insignificant for trimeprazine and perphenazine. This could be due to the comparatively low concentrations of these last two compounds; it is of note that the rate decreases with decreasing reactant concentrations for any system. It was therefore decided to fix the flow-rate at 8.6 ml min^{-1} and use a longer reaction coil. However, it was found that the peak absorbance was not significantly high and the peak heights were not reproducible for any of the compounds except perphenazine for which a 2.0 m reaction coil length was found to be adequate. It was therefore decided to use a 45 cm reaction coil with a flow-rate of 8.6 ml min^{-1} for chlorpromazine, promethazine and trimeprazine or a 2 m reaction coil with a flow-rate of 12.5 ml min^{-1} for perphenazine.

Sample volume

The sample volume was varied between 15 and 150 μl by changing the tube length, but it was found that the results were not reproducible when a volume of more than 123 μl was injected for any of the compounds. Hence, a tube of length 20 cm with a 0.5 mm i.d., injecting 123 μl of sample, was used.

Acidity effects

The effect of changing the sulphuric acid concentration in the system is rather complex because two different aspects should be considered from a theoretical point of view. Firstly, the redox potential of the vanadate increases with increasing acid concentration giving rise to an increase in the amount of oxidation products, which should consequently be reflected in an increase in peak absorbance. However, if the potential at any acid concentration is not sufficient to lead to full product formation, at a fixed time, peak absorbance is directly proportional to concentration, simply because measurements can be accurately monitored at a fixed time. Flow injection is the most suitable technique for quantitative determinations at fixed times. The fixed-time method has recently been discussed.[33] Secondly, the rate of degradation of the oxidation product of the radical cation should increase, resulting in a decrease of peak absorbance. The influence of sulphuric acid concentration in the range 0.2–2.5 mol dm^{-3} on the peak absorbance is shown in Fig. 3. As can be seen, the peak absorbance decreased slightly as the acid concentration was increased for chlorpromazine and trimeprazine, which indicates that the influence of acid degradation of the product predominates. Therefore, determinations were conducted in 0.5 and 0.6 mol dm^{-3} sulphuric acid for chlorpromazine and

Table 3 Statistical comparison of the results of the analysis of pharmaceutical products containing phenothiazine by the vanadate method with those obtained by the official BP method

Proprietary name of drug and supplier	Active materials as analysed (ppm)		Recovery ± SD* (%) FI	Recovery ± SD* (%) BP	t†
Phenergan tablet (Specia, France)	Promethazine,	250	99.9 ± 0.70	100.7 ± 0.8	2.6
		500	98.8 ± 0.51	99.1 ± 1.0	0.9
Phenergan elexir (Specia, France)	Promethazine,	250	99.8 ± 0.65	99.4 ± 0.9	1.4
		500	98.7 ± 0.44	99.2 ± 0.8	2.5
Cigan elexir, (Cimabrex, Denmark)	Promethazine,	250	100.8 ± 0.62	101.2 ± 0.6	1.4
		500	98.6 ± 0.75	99.3 ± 0.7	2.1
Largactil tablet (Specia, France)	Chlorpromazine,	250	102.4 ± 0.61	101.8 ± 0.9	0.82
		500	101.8 ± 0.82	102.4 ± 0.4	1.6
		1000	101.5 ± 0.6	100.8 ± 0.8	2.6

* Standard deviation calculated as the mean of five determinations.
† Calculated Student t test value [theoretical value = 2.78 (p = 0.05)].

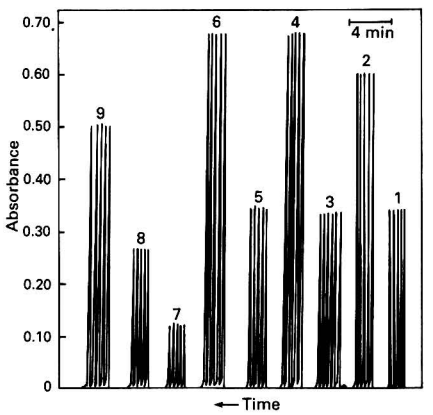

Fig. 5 Typical FI results (n = 5) for: 1, 250 ppm phenergan tablet; 2, 500 ppm phenergan tablet; 3, 250 ppm phenergan elexir; 4, 500 ppm phenergan elexir; 5, 250 ppm cigan; 6, 500 ppm cigan; 7, 250 ppm largactil; 8, 500 ppm largactil; and 9, 1000 ppm largactil

trimeprazine, respectively. For the promethazine and perphenazine systems, the peak absorbance increased as the acid concentration was increased, particularly between 1.5 and 1.25 mol dm^{-3} for both drugs, demonstrating that the influence of the increase of redox potential predominates. Promethazine was determined in 1.5 mol dm^{-3} sulphuric acid but the results for the determination of perphenazine in 1.25 mol dm^{-3} sulphuric acid were not reproducible, possibly due to the increase in residence time as a result of using the longer reaction coil of 2 m, thus allowing more degradation of the product to occur; therefore, lower concentrations were used and finally a concentration of 0.5 mol dm^{-3} was found to be acceptable.

Analytical Appraisals

Phenothiazine oxidation products were found in this and previous studies to be in high quantitative yield and to obey Beer's law.[7,8,12,13,17]

Series of standard solutions were run in triplicate for the four compounds as typically represented in Fig. 4 for promethazine. Peak absorbance *versus* concentration was found to be linear over a wide range of phenothiazine concentrations, with the corresponding calibration equations calculated by a computer, each with an insignificant intercept and a correlation coefficient (r) of approximately 1. The peak width (w) at 60% of the peak height was calculated as a measure of the total sample dispersion in the system.[34] The peak width at the baseline was also measured in order to define the maximum throughput or sample frequency (f). Repeatability for each system was confirmed by injecting one of the sample solutions seven times and estimating the relative standard deviation (RSD). All these statistical parameters are given in Table 2.

Application

In order to establish the validity of the proposed method, the proprietary drugs containing phenothiazines listed in Table 3 were analysed. Fig. 5 shows the FI recorder trace for these drugs. The same batch of samples was analysed by the BP method,[2-5] and per cent. recovery, standard deviation (SD) and Student t test values were calculated (Table 3). The results obtained reveal that a similar degree of accuracy is afforded by both methods. Excipients such as glucose, starch and other drug components such as sodium gentisate do not interfere.

The proposed method is superior to other conventional methods in that it is very fast, simple and specific. Other advantages of this method can be found elsewhere.[35]

The author expresses his gratitude to Rhone-Poulenc Ltd., Dagenham, Essex, for the gift of the pure analytical-reagent grade phenothiazine compounds.

References

1 Wilson, C. O., Gisvold, O., and Doerge, R. F., *Text Book of Organic Medicinal and Pharmaceutical Chemistry*, J. B. Lippincott, 7th edn., 1977, p. 384.
2 *British Pharmacopoeia*, HM Stationery Office, London, 5th edn., 1988, p. 918.
3 *British Pharmacopoeia*, HM Stationery Office, London, 5th edn., 1988, pp. 749 and 995.
4 *British Pharmacopoeia*, HM Stationery Office, London, 5th edn., 1988, p. 1015.
5 *British Pharmacopoeia*, HM Stationery Office, London, 5th edn., 1988, p. 982.
6 Gurka, F., Kolinski, R. E., Myrick, J. W., and Wells, C. E., *J. Pharm. Sci.*, 1980, **69**, 1069.
7 Ramappa, P. G., Gowda, H. S., and Nayak, A. N., *Analyst*, 1980, **105**, 663.
8 Ramappa, P. G., Gowda, H. S., and Nayak, A. N., *Fresenius Z. Anal. Chem.*, 1979, **298**, 160.
9 Ramappa, P. G., and Basavaiah, K., *Indian J. Pharm. Sci.*, 1985, **47**, 125.
10 Fell, A. F., and Clark, B. J., *J. Pharm. Pharmacol.*, 1983, **35**, 22.
11 El-Shabouri, S. R., Yousif, A. F., Mohamed, F. A., and Rageh, A. M. I., *J. Assoc. Off. Anal. Chem.*, 1986, **69**, 821.
12 Mahrous, M. S., and Abdel-Khalek, M. M., *Talanta*, 1984, **31**, 289.
13 Ramappa, P. G., Gowda, H. S., and Nayak, A. N., *Microchem. J.*, 1983, **28**, 586.

14 Rizk, M., Zakhari, N. A., Ibrahim, F., and Walash, M. I., *Mikrochim. Acta, Part I*, 1989, 355.
15 Rizk, M., Zakhari, N. A., Ibrahim, F., and Walash, M. I., *Talanta*, 1986, **33**, 111.
16 Gayarama, M., D'Souza, M. V., Yathirajan, H. S., and Rangaswam, Y., *Talanta*, 1986, **33**, 352.
17 Koupparis, M. A., and Barcuchova, A., *Analyst*, 1986, **111**, 313.
18 Nayak, A. N., Rangaswamy, Y. H. S., and Ramappa, P. G., *Indian Drugs*, 1982, **19**, 202.
19 Sane, R. T., and Ambardekar, A. B., *J. Indian Chem. Soc.*, 1982, **59**, 1201.
20 Burgot, J. L., *Ann. Pharm. Fr.*, 1979, **37**, 125.
21 Maurer, H., and Pfleger, K., *J. Chromatogr. Biomed. Appl.*, 1984, **306**, 125.
22 Curry, S. H., Brown, E. A., Hu, O. Y. P., and Perrin, J. H., *J. Chromatogr. Biomed. Appl.*, 1982, **231**, 361.
23 Kok, W. T., Voogt, W. H., Brinkman, U. A. Th., and Frei, R. W., *J. Chromatogr.*, 1986, **354**, 249.
24 Thoma, K., and Albert, K., *Arch. Pharm.*, 1984, **317**, 133.
25 Brinkman, U. A. Th., Welling, P. L. M., De Vries, G., Clolten, A. H. M. T., and Frei, R. W., *J. Chromatogr.*, 1981, **217**, 463.
26 Buhl, F., and Chwistek, M., *Chem. Anal. (Warsaw)*, 1980, **25**, 365.
27 Wheals, B. B., *J. Chromatogr.*, 1979, **177**, 263.
28 Maurer, H., and Pfleger, K., *J. Chromatogr. Biomed. Appl.*, 1984, **31**, 3.
29 Maurer, H., and Pfleger, K., *J. Chromatogr.*, 1983, **272**, 75.
30 Cabo, J., Gamez, M. J., and Jimenez, J., *Ars. Pharm. (Spain)*, 1988, **29**, 51.
31 Goldstein, S., A., and Van Vunakis, H., *J. Pharmacol. Exp. Ther.*, 1981, **217**, 36.
32 Douse, J. M. F., *J. Chromatogr.*, 1984, **301**, 137.
33 Sultan, S. M., *Analyst*, 1988, **113**, 149.
34 Růžička, J., and Hansen, E. H., *Anal. Chim. Acta*, 1978, **99**, 37.
35 Růžička, J., and Hansen, E. H., *Flow Injection Analysis*, Wiley, New York, 2nd edn., 1988.

Paper 0/02846K
Received June 25th, 1990
Accepted October 4th, 1990

Spectrophotometric Determination of Oxytetracycline by Flow Injection

A. A. Alwarthan, S. A. Al-Tamrah and S. M. Sultan*
Chemistry Department, College of Science, King Saud University, Riyadh-11451, Saudi Arabia

A flow injection spectrophotometric method is proposed for the determination of oxytetracycline. The method is based on the reaction of this drug with iron(III) in the presence of sulphuric acid to form a coloured complex. Less than 10 μg ml^{-1} of the drug (defined as the amount of the drug that gave a signal of twice the background noise) can be determined by measuring the absorbance at 435 nm of the complex formed. Parameters affecting the absorbance such as the acid concentration, sample volume and the reaction coil length were all studied in order to optimize them. The method was applied to the determination of oxytetracycline in real samples and some pharmaceutical preparations. The relative standard deviation was 1.7% for 80 μg ml^{-1} (for ten replicate injections). The sample throughput is 17 samples h^{-1}. The effect of some foreign species was also investigated.

Keywords: *Spectrophotometry; oxytetracycline; flow injection*

Oxytetracycline [(4*S*,4a*S*,5a*S*,6*S*,12a*S*)-4-dimethylamino-1,4,4a,5,5a,6,11,12a-octahydro-3,6,10,12,12a-hexahydroxy-6-methyl-1,11-dioxonaphthacene-2-carboxamide] is a compound which belongs to a large group of antibiotics which contain four rings in their structures capable of forming stable complexes with many metal ions.[1–4] Oxytetracycline hydrochloride (OTH), like other tetracyclines, has been determined in a variety of sample matrices. Many methods have been reported for the determination of tetracyclines, including spectrophotometric and chromatographic,[5–10] fluorimetric[11,12] and microbiological methods.[13]

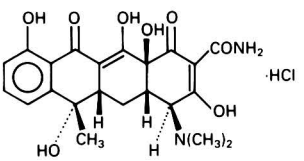

In recent years flow injection (FI) has been widely used for the determination of many organic and inorganic compounds.[14–18] Flow injection spectrophotometric methods have been shown to be reliable for the determination of trace metal ions and antibiotics with good reproducibility, selectivity and sensitivity.[19–26] Apart from the FI chemiluminescence method reported by Alwarthan and Townshend[27] for the determination of tetracycline, there is no FI spectrophotometric method described in the literature for the determination of this drug.

This paper describes the development of a simple and rapid FI spectrophotometric method for the determination of OTH and application of the proposed method to the determination of the drug in some pharmaceutical preparations.

Experimental

The FI system is shown in Fig. 1. A four-channel peristaltic pump (Gilson Minipuls 3MP4) was used to deliver the acidic ammonium iron(III) sulphate solution. Teflon tubing (0.3 mm i.d.) was used for the flow lines. The sample was injected into the acidic iron(III) stream through a 235 μl Teflon rotatory valve (Rheodyne RH 5020) and was propelled by the Gilson pump. The absorbance of the complex formed was measured at 435 nm using an LKB Model-4050 spectrophotometer with an 80 μl flow cell.

* Present address: Department of Chemistry, King Fahad University of Petroleum and Minerals, Dharan, Saudi Arabia.

Reagents

Sulphuric acid at a concentration of 0.01 mol dm^{-3} (Merck) was prepared by dissolving the appropriate amount of the concentrated acid in high-purity distilled water and ammonium iron(III) sulphate (1000 μg ml^{-1}) was prepared by dissolving 1 g of the salt in 1 l of 0.01 mol dm^{-3} H_2SO_4. A stock solution of 1000 μg ml^{-1} of OTH (Pfizer) was prepared by dissolving the appropriate amount of the drug in 0.01 mol dm^{-3} sulphuric acid.

Results and Discussion

Oxytetracycline reacts with ammonium iron(III) sulphate to form a stable complex. It is suggested that iron(III) chelates with tetracycline as follows:[6]

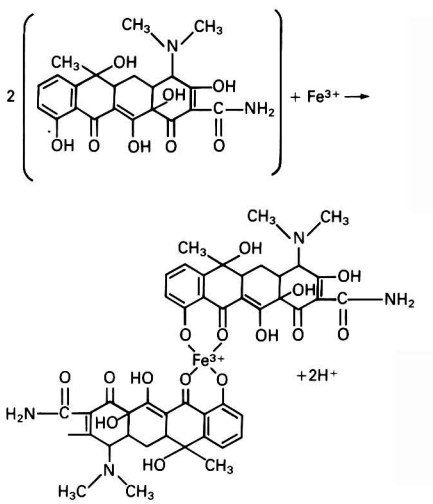

The yellowish brown complex formed from the reaction of oxytetracycline with iron(III) can be used for the spectrophotometric determination of oxytetracycline by measuring its absorbance at 435 nm. The intensity of the colour formed is related directly to the amount of oxytetracycline present and depends very much on the reaction conditions. Therefore, it is very important to optimize the reaction conditions such as the flow-rate, the sample volume, the reaction coil length, the

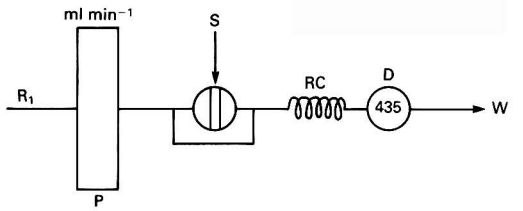

Fig. 1 Manifold used for the determination of oxytetracycline by flow injection: P, pump; S, injection valve; RC, reaction coil; D, detector; and W, waste

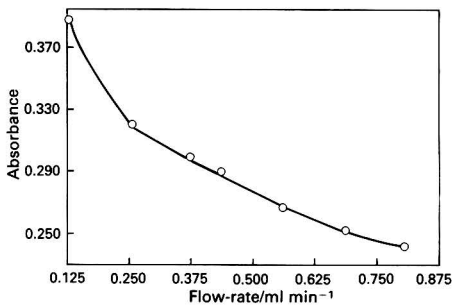

Fig. 2 Effect of flow-rate on the formation of the complex between iron(III) (200 ppm) and OTH (80 ppm)

acidity and the iron(III) concentration. The flow-rate of the solutions is very important and should be regulated. High flow-rates shorten the reaction time, hence the reaction is not allowed to reach completion[29] as indicated by the decrease in absorbance of the complex formed (Fig. 2). On the other hand, low flow-rates will decrease the sample throughput. The flow-rate was studied by keeping all other conditions constant; the iron(III) concentration at 200 μg ml^{-1}, the oxytetracycline concentration at 80 μg ml^{-1}, the coil length at 200 cm and the sample loop at 235 μl. The results obtained are summarized in Table 1, which shows that better sensitivity could be obtained at very low flow-rates (0.125 ml min^{-1}). As the flow-rate increases the absorbance decreases indicating that the reaction is incomplete. A flow-rate of 0.436 ml min^{-1} was chosen in order to obtain a reasonable sample throughput which is the essence of using a flow injection method. The effect of the sample volume was studied by changing the loop, *i.e.*, to give a sample volume in the range 50–285 μl in order to find the optimal sample volume. The results obtained show that small volumes of up to 100 μl give a low sensitivity as the reaction is incomplete owing to dispersion by the carrier stream. A 200 μl volume was found to be the optimum. Larger sample volumes did not give a significant increase in the absorbance and also gave a poorer reproducibility as shown in Table 2. The effect of the reaction coil length was investigated by varying the coil length from 20 to 400 cm. Maximum absorbance was obtained when the coil length was 50 cm. Increasing the coil length further caused a decrease in the absorbance due to dilution of the complex formed as shown in Table 3.

The effect of the acid concentration on the absorbance was also studied using different concentrations of sulphuric acid. The acidity appears to be a very important parameter. The low acidity of sulphuric acid (≤0.002 mol dm^{-3}) hydrolyses the iron(III) sulphate, and the high acidity (≥0.1 mol dm^{-3}) protonates the tetracycline molecule resulting in a gradual decrease of the absorbance. Therefore, 0.002 mol dm^{-3} sulphuric acid is suitable for the operating conditions as shown in Table 4. Other acids such as HCl, $HClO_4$ and HNO_3 can also be used while H_3PO_4 cannot, as it forms a white

Table 1 Effect of flow-rate on the absorbance of oxytetracycline

Flow-rate/ml min^{-1}	Absorbance*
0.125	0.378
0.258	0.320
0.370	0.301
0.436	0.290
0.560	0.268
0.680	0.252
0.800	0.242
0.900	0.238

* Average of three determinations.

Table 2 Effect of sample volume on the absorbance of oxytetracycline

Sample volume/μl	Absorbance*
50	0.096
100	0.132
150	0.209
200	0.277
235	0.299
285	0.335

* Average of three determinations.

Table 3 Effect of coil length on the absorbance of oxytetracycline

Reaction coil length/cm	Absorbance*
20	0.306
50	0.326
100	0.315
150	0.295
200	0.270
250	0.253
300	0.239
350	0.226
400	0.215

* Average of three determinations.

Table 4 Effect of H_2SO_4 concentration on the absorbance of oxytetracycline

H_2SO_4 concentration/mol dm^{-3}	Absorbance*
0.002	0.299
0.004	0.295
0.006	0.287
0.01	0.270
0.03	0.184
0.05	0.138
0.1	0.079
0.3	0.038

* Average of three determinations.

precipitate. With these optimized conditions, it is obvious that iron(III) sulphate (the complexation reagent) should be present in excess to ensure that the oxytetracycline reaction goes to completion. A two-fold excess of the reagent was found to be sufficient (Table 5). The effect of temperature on the formation of the complex was investigated, keeping other conditions constant, by immersing the reaction coil in a water-bath and varying the temperature from 25 to 70 °C (Table 6). It was observed that the absorbance increased with increasing temperature up to 55 °C. Higher temperatures decrease the absorbance probably due to the formation of the colourless appoxytetracycline.[28] Under the optimum operating conditions, the calibration graph of absorbance *versus* concentration was linear from 10 to 80 μg ml^{-1} of oxytetracycline. The correlation coefficient is 0.997 with an intercept of 0.001 and a slope of 0.003.

Table 5 Effect of iron(III) concentration on the absorbance of oxytetracycline

Iron(III) concentration (ppm)	Absorbance*
50	0.218
100	0.263
150	0.261
200	0.263
300	0.263

* Average of three determinations.

Table 6 Effect of temperature on the absorbance of oxytetracycline

Temperature/ °C	Absorbance*
25	0.225
40	0.245
55	0.256
70	0.185

* Average of three determinations.

Table 7 Determination of oxytetracycline

Amount of oxytetracycline/mg		
Added	Found*	Recovery (%)
80	80	100
100	99.9	99.9
200	201	100.5

* Average of three determinations.

Table 8 Determination of oxytetracycline in drug formulations

	Amount of oxytetracycline/mg		
	Claimed	Found*	Recovery (%)
Drug formulations—			
Sample 1	20	21.5	107.5
Sample 2	50	54.0	108
Sample 3	80	87.0	108.7
Terramycine—			
Sample 1	250	260	104
Sample 2	250	258	103
Sample 3	250	261	104.4

* Average of three determinations.

Interferences

The effect of copper, nickel, magnesium, lead, cobalt, zinc and cadmium on the absorbance of 50 μg ml^{-1} of oxytetracycline was studied. For up to 200 μg ml^{-1} of these metals, there was no interference. Vanadium, when present, caused a strong interference by forming an intense yellow colour. Other excipients which are normally added to pharmaceutical preparations such as starch, lactose and glucose did not interfere, although riboflavine, which used to be added to the drugs, showed a slight interference.

Determination of Oxytetracycline

The method was applied to the determination of oxytetracycline in three different samples Excellent results were obtained as shown in Table 7.

Application

The proposed method was applied to the determination of oxytetracycline in drug formulations. For the analysis of tetracycline capsules (Terramycine S.F., Pfizer, containing about 250 mg of oxytetracycline) the content of a capsule was mixed with 50 ml of 0.01 mol dm^{-3} sulphuric acid and the solution was warmed for 10 min whilst stirring. The solution was cooled to room temperature, filtered and made up to volume with 0.01 mol dm^{-3} sulphuric acid in a 250 ml calibrated flask. A 200 μl aliquot of the sample solution was injected into the flow system and the absorbance of the complex formed was measured as before. The results obtained are shown in Table 8. The relatively high results are probably due to the presence of riboflavine which absorbs at this wavelength.

Table 9 Determination of oxytetracycline in drug formulations using the standard additions method

	Amount of oxytetracycline/mg		
Sample	Claimed	Found*	Recovery (%)
Sample 1	20	21.5	107
Sample 2	50	55	110
Sample 3	80	90	112

* Average of three determinations.

Table 10 Effect of riboflavine on the absorbance of oxytetracycline using either iron(III) or water as the carrier

Amount of riboflavine added/ μg ml^{-1}	Absorbance*	
	Iron(III)	Water
5	0.045	0.044
10	0.085	0.083
20	0.168	0.166
40	0.336	0.329
60	0.500	0.468
80	0.657	0.611

* Average of three determinations.

Use of the standard additions method gave almost the same results, shown in Table 9. The effect of riboflavine was investigated by injecting different concentrations (5–80 μg ml^{-1}) into the flow system. It was found that the absorbance increased as the amount of riboflavine increased. Similar results were obtained when riboflavine alone was injected, using water as the carrier instead of the iron(III) reagent, as shown in Table 10, indicating that the absorbance is due to the coloured riboflavine solutions and is not a result of its reaction with the reagent [iron(III)] as was the case with oxytetracycline, where relatively high results were obtained. Fortunately, this effect is minimized by using dilute sample solutions, which significantly reduce this effect, giving better analytical results.

This research (Chem/1409/34) was supported by the Research Center, College of Science, King Saud University, Riyadh, Saudi Arabia.

References

1 *United States Pharmacopeia*, Mack, Easton, PA, 20th edn., 1980, pp. 780–782.
2 Rhoades, E. R., *J. Oklahoma State Med. Assoc.*, 1981, **74**, 31.
3 Neuvonen, P. J., *Drugs*, 1976, **11**, 45.
4 Tabbara, K. F., in *Antimicrobiological Agents in Ophthalmology*, eds. Smolin, G., and Okunmoto, M., Masson USA, New York, 1983, pp. 65–69.
5 Mahrous, M. S., and Abdel Khalek, M. M., *Talanta*, 1984, **31**, 289.
6 Sultan, S. M., Al-Zamil, I. Z., and Al-Arfaj, N. A., *Talanta*, 1988, **35**, 375.
7 Stankov, M. J., and Vese Linovic, D., *Analyst*, 1989, **114**, 714.

8 Oka, H., Matsumoto, H., and Uno, K., *J. Chromatogr.*, 1985, **325**, 265.
9 George, D. M., and Raymond, B. A., *J. Chromatogr. Sci.*, 1978, **16**, 93.
10 Netis, H. J. C. F., and de Leenheer, A. P., *J. Chromatogr.*, 1980, **195**, 35.
11 Regosz, A., and Swirydo, A., *Farm. Pol.*, 1978, **34**, 17.
12 Poiger, H., and Schlatter, Ch., *Analyst*, 1976, **101**, 808.
13 *The British Pharmacopoeia*, Pharmaceutical Press, London, 1968, pp. 923–925.
14 Hansen, E. H., Krug, F. J., Ghose, A. K., and Růžička, J., *Analyst*, 1977, **102**, 714.
15 Krug, F. J., Růžička, J., and Hansen, E. H., *Analyst*, 1979, **104**, 47.
16 Fukasawa, T., Kawakubo, S., and Unno, K., *Anal. Chim. Acta*, 1986, **183**, 269.
17 Al-Tamrah, S. A., *Anal. Chim. Acta*, 1987, **202**, 247.
18 Abdalla, M. A., and Al-Swaidan, H. M., *Analyst*, 1989, **114**, 583.
19 Holm, K. A., *Analyst*, 1986, **111**, 927.
20 Yerian, T. D., Hadjiioannou, T. P., and Christian, G. D., *Talanta*, 1986, **33**, 547.
21 Ahmed, A. S. K., Abdel-Mocty, E. M., Moustafa, A. A., and Gendy, A. E., *Arch. Pharm. Chem. Sci. Ed.*, 1986, **14**, 11.
22 Yamane, T., and Ogawa, T., *Bunseki Kagaku*, 1987, **36**, 625.
23 Zolotov, Y. A., Shpigun, L. K., Kolotyrkina, I. Y., Novikov, E. A., and Bazanova, O. V., *Anal. Chim. Acta*, 1987, **200**, 21.
24 Ohta, T., Goto, N., and Takitani, S., *Analyst*, 1988, **113**, 1333.
25 Mattos, I. L., Zagatto, E. A. G., and Jacintho, A. O., *Anal. Chim. Acta*, 1988, **214**, 247.
26 Masoom, M., *Anal. Lett.*, 1988, **21**, 2381.
27 Alwarthan, A. A., and Townshend, A., *Anal. Chim. Acta*, 1987, **196**, 135.
28 Chiccarelli, F. S., Woolford, M. H., Jr., and Avery, M. E., *J. Am. Pharm. Assoc.*, 1959, **XLVIII**, 263.
29 Seitz, W. R., Suydam, W. W., and Hercules, D. M., *Anal. Chem.*, 1972, **44**, 957.

Paper 0/00672F
Received February 13th, 1990
Accepted October 9th, 1990

Solvent Extraction–Spectrophotometric Determination of Berberine and Benzethonium in Drugs With Tetrabromophenolphthalein Ethyl Ester by Batchwise and Flow Injection Methods

Tadao Sakai
Department of Chemistry, Asahi University, 1851 Hozumi, Hozumicho, Gifu 501-02, Japan

A spectrophotometric method for the determination of berberine and benzethonium in drugs was studied using batchwise and flow injection techniques coupled with solvent extraction. Tetrabromophenolphthalein ethyl ester (TBPE·H) in 1,2-dichloroethane reacted with berberine and/or benzethonium to form a blue ion associate whose absorbance was determined at 610 nm. The extraction conditions were studied using a batchwise method. On the basis of the results obtained with the batchwise method, a three-line manifold was constructed. The sample was injected into a distilled water stream and the pH adjusted to 11 with a borate–phosphate buffer solution. Then the stream was mixed with the extracting TBPE·H reagent. The organic phase was separated with a polytetrafluoroethylene porous membrane (0.8 μm pore size). The sample throughputs were 45 h^{-1} for berberine and 30 h^{-1} for benzethonium. The calibration graphs were linear in the range 1×10^{-6}–1×10^{-5} mol dm^{-3} for berberine and/or benzethonium and the relative standard deviation ($n = 6$) was 0.9% for 1×10^{-6} mol dm^{-3} berberine and 1.2% for 4×10^{-6} mol dm^{-3} benzethonium. The proposed method was used for the rapid and selective determination of berberine and benzethonium in pharmaceuticals.

Keywords: *Berberine and benzethonium determination; ion-associate extraction with tetrabromophenolphthalein ethyl ester; spectrophotometry; flow injection*

Berberine and benzethonium, being quaternary ammonium salts, are widely used as medicines for stomach and bowel ailments and for internal use in the form of tablets, injections and liquids because of their sterilizing powers. Most methods for the extraction–spectrophotometric determination of quaternary ammonium salts are based on the formation of ion-association complexes with anionic dyes. Although compounds in the triphenylmethane series such as Bromophenol Blue (BPB),[1,2] Bromocresol Green (BCG)[3] and azo dyes such as Orange II[4] have been used as counter ions, the colour development and quantitative extractability of association complexes were poor, and their molar absorptivities had values of 20 000–30 000 dm^3 mol^{-1} cm^{-1}. Moreover, the linear ranges of the calibration graphs were very narrow, and the graphs did not pass through the origin.

In previous work,[5,6] it has been reported that quaternary ammonium salts (R_4N^+) could be successfully extracted with BPB and/or BCG(A^{2-}) into organic solvents in neutral media only in the presence of quinine; the R_4N^+–A^{2-} associate could not be completely extracted in the absence of quinine in the above media. In the method described above, extractability and selectivity were enhanced by the formation of a bulky ternary ion associate, R_4N^+–A^{2-}–[quinine]$^+$. The molar absorptivity[5] obtained for berberine was 4.35×10^4 dm^3 mol^{-1} cm^{-1}. However, sensitivity was not satisfactory compared with that of the monoprotic acid dye tetrabromophenolphthalein ethyl ester ([TBPE]$^-$);[7] the molar absorptivity obtained for berberine in this study was 9.8×10^4 dm^3 mol^{-1} cm^{-1}. Of the anionic dyes investigated, [TBPE]$^-$ has the highest sensitivity, best extractability and provides good reproducibility. However, it is not suitable for the selective determination of quaternary ammonium compounds and amines. Therefore, a new technique using the thermochromism of ion associates[8] was developed in order to enhance the selectivity when the TBPE anion is used. In the above situation, TBPE was used as an anionic monovalent reagent in an aqueous buffered solution at pH 8.5. However, it was not possible to use TBPE in alkaline media of pH >12 because TBPE was hydrolysed at this pH.

Fortunately, it was found that the hydrolysis of TBPE could be depressed even in highly alkaline media when a molecular form of TBPE (TBPE·H) was dissolved in organic solvents, and that TBPE·H–dichloroethane was useful as an ion-association reagent for the selective extraction of quaternary ammonium salts in highly alkaline media, where ion associates with amines were not formed.

This paper describes the rapid and selective determination of berberine and benzethonium in multicomponent mixtures with a TBPE·H–dichloroethane solution by solvent extraction coupled with flow injection (FI).

Experimental

Reagents

All reagents were of analytical-reagent grade and were used without further purification.

Standard berberine solution. A standard solution of 1×10^{-3} mol dm^{-3} berberine was prepared by dissolving 0.4078 g of berberine hydrochloride (dried at 105 °C, Nakarai Chemicals, Kyoto, Japan) in hot water and diluting to 1 l. The stock solution was standardized by the official method.[9]

Standard benzethonium solution. A stock solution of 1×10^{-2} mol dm^{-3} benzethonium was prepared by dissolving 0.397 g of benzethonium chloride (Nakarai Chemicals) in distilled water and diluting to 100 ml.

Working solutions were prepared by accurate dilution of the above solutions.

Buffer solution. Buffer solutions (pH 3.4–12.8) were prepared by mixing equal volumes of 0.3 mol dm^{-3} potassium dihydrogen phosphate and 0.1 mol dm^{-3} sodium borate. The pH was adjusted with 1 mol dm^{-3} sodium hydroxide or 0.5 mol dm^{-3} sulphuric acid.

Procaine and dibucaine solutions. Appropriate amounts of procaine (Daiichi Seiyaku, Tokyo, Japan) and dibucaine (Santen Seiyaku, Osaka, Japan) hydrochlorides were dissolved in distilled water to obtain 1×10^{-2} mol dm^{-3} solutions.

Tetrabromophenolphthalein ethyl ester (TBPE). A 4×10^{-3} mol dm^{-3} solution of TBPE was prepared by dissolving 0.2800 g of tetrabromophenolphthalein ethyl ester potassium salt (Tokyo Kasei Kogyo, Tokyo, Japan) in 100 ml of ethanol by

heating on an electrical heater. This anionic dye ([TBPE]$^-$) is usually used as the counter ion for the extraction of cationic compounds in aqueous media buffered at pH 7–10. However, in this work, TBPE·H–dichloroethane solution was used in colour development based on the formation of ion-association complexes with quaternary ammonium ions in the organic phase. A dichloroethane solution of TBPE·H was prepared as follows. In a separating funnel, 5 ml of 4×10^{-3} mol dm^{-3} TBPE–ethanol solution, 15 ml of sodium acetate–acetic acid buffer (pH 3) and 30 ml of water were mixed, and the solution was then shaken for 10 min with 100 ml of 1,2-dichloroethane. The organic phase was filtered through a filter-paper and the aqueous phase discarded. The TBPE anion in the aqueous phase, buffered at a pH <3, was completely extracted into 1,2-dichloroethane. Consequently, a TBPE·H–dichloroethane solution was obtained.

Apparatus

A Hitachi Model 556 double-beam spectrophotometer and a Hitachi Model 057 *x–y* recorder were used with 10 mm light-path cells for absorption measurements. Extractions were carried out by shaking with an Iwaki Model KM shaker. A Hitachi-Horiba pH meter with a glass electrode, Model M-5, was used to measure the pH of the aqueous phase after extraction.

Procedure for the Batchwise Method

Extraction is carried out as follows. Place an appropriate amount of berberine, procaine and/or dibucaine solution into a 50 ml calibrated flask, add 10 ml of buffer solution and dilute the mixture to the mark with distilled water. Transfer the solution into a 100 ml separating funnel and shake with 10 ml of 6×10^{-5} mol dm^{-3} TBPE·H–dichloroethane solution for 5 min, then centrifuge the organic phase to remove water droplets. After separation of the organic layer, measure the absorbance of the organic phase at 610 nm against 1,2-dichloroethane as a reference.

Procedure for the FI Method

A diagram of the flow system used is shown in Fig. 1. The absorbance was measured at 610 nm with a Soma Kogaku Model S-3250 double-beam spectrophotometer with a 10 mm micro flow cell (8 μl) and recorded as peak-shaped signals using a Toa Electronics Model FBR-251A recorder. Two double-plunger micropumps (Sanuki Kogyo, DM2U-1026) were used for propelling the buffer solution, the carrier solution and the TBPE·H–dichloroethane solution. The samples were injected into the carrier stream with a six-way injection valve (dead volume, 80 μl) to which a volume control loop was attached. Flow lines were made of polytetrafluoroethylene (PTFE) tubing (0.5 mm i.d.).

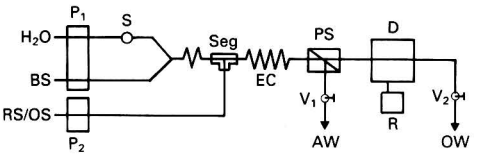

Fig. 1 Schematic diagram of the extraction–FI system. BS, Phosphate buffer (pH 11); RS/OS, 1×10^{-5} mol dm^{-3} TBPE·H–1,2-dichloroethane solution; P_1 and P_2, pumps (0.8 ml min^{-1}); S, sample injection valve; Seg, segmentor; EC, extracting coil (2 m × 0.5 mm i.d.); PS, phase separator; D, detector (610 nm); R, recorder; V_1 and V_2, needle valves, AW, aqueous-phase waste; and OW, organic-phase waste

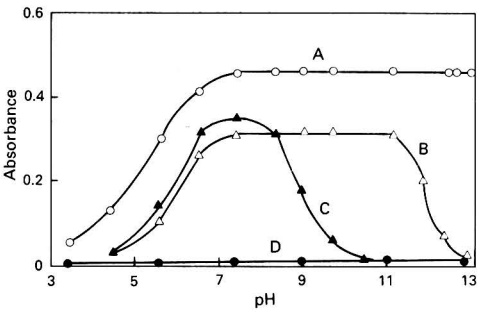

Fig. 2 Effect of pH on extraction of ion associates with TBPE·H–1,2-dichloroethane solution using the batchwise method. A, 1×10^{-6} mol dm^{-3} berberine; B, 2×10^{-5} mol dm^{-3} dibucaine; C, 1×10^{-5} mol dm^{-3} procaine; and D, reagent blank. Wavelength, 610 nm; TBPE·H, 6×10^{-5} mol dm^{-3}; reference, 1,2-dichloroethane

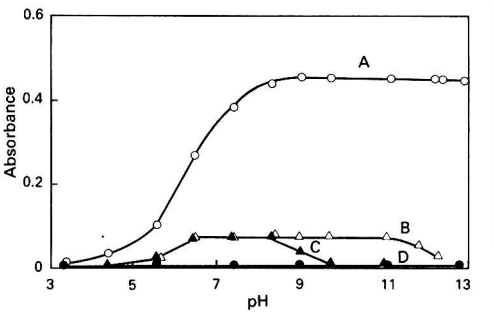

Fig. 3 Effect of pH on extraction of ion associates with TBPE·H–1,2-dichloroethane solution using the batchwise method. A, 1×10^{-6} mol dm^{-3} berberine; B, 2×10^{-5} mol dm^{-3} dibucaine; C, 1×10^{-5} mol dm^{-3} procaine; and D, reagent blank. Wavelength, 610 nm; TBPE·H, 1×10^{-5} mol dm^{-3}; reference, 1,2-dichloroethane

Results and Discussion

Batchwise Study

Effect of pH on extraction of quaternary ammonium compounds and amines in the batchwise method

The effect of pH on the extraction of berberine (R_4N^+), procaine and dibucaine (amines) was examined in the pH range 3.4–12.8 with TBPE·H–dichloroethane solution. As can be seen in Fig. 2, at a pH >7.4, absorbance of the berberine associate was maximum and constant. On the other hand, absorbance of the dibucaine association complex considerably decreased with an increase in pH and, at pH 12.8, its absorbance was reduced almost to zero, although that of the dibucaine association complex was constant in the pH range between 7.4 and 11. Although the procaine associate showed the highest absorbance at pH 7.4, absorbance decreased drastically with only a slight change in pH and was almost zero at pH 10.5. The absorbance of the reagent blank was about 0.02 at pH 9–11. The effect of pH on the extraction of the same associates was also investigated using dilute, 1×10^{-5} mol dm^{-3}, TBPE·H–dichloroethane (Fig. 3). Although the absorbance of the berberine associate was the same as that in Fig. 2, the absorbance of the amine associates decreased considerably because the concentration of TBPE·H was not high enough to form ion-association complexes with the amines. As a result, it was found that it was necessary to use 1×10^{-5} mol dm^{-3} TBPE·H–dichloroethane and to adjust the pH to 12.8 for the selective determination of berberine and benzethonium. The extraction behaviour of other amines such as diphenhydramine, ephedrine, methylephedrine and eserine showed the same tendency as procaine.

Table 1 Interferences of organic substances with different concentrations of TBPE·H using the batchwise method. Berberine concentration, 1×10^{-6} mol dm^{-3}; extracting solvent, 1,2-dichloroethane; wavelength, 610 nm; reference, reagent blank; and pH, 12.8

	[TBPE·H]/mol dm^{-3}							
	2×10^{-4}		6×10^{-5}		2×10^{-5}		1×10^{-5}	
Compound	[Amine]: [Ber]	Recovery (%)	[Amine]: [Ber]	Recovery (%)	[Amine]: [Ber]	Recovery (%)	[Amine]: [Ber]	Recovery (%)
Procaine	10	101.0	20	101.3	20	102.2	40	102.8
Papaverine	100	101.3	100	100.7	100	101.1	100	99.0
Dibucaine	10	99.4	20	101.3	40	101.6	100	102.6
Diphenhydramine	10	101.6	10	100.6	20	101.8	40	102.1
Chlorpheniramine	0.5	102.0	2	99.6	4	102.9	10	102.6
Ephedrine	20	101.6	40	102.4	60	102.9	100	102.8
Methylephedrine	20	102.0	20	102.8	20	101.9	100	102.1
Eserine	40	102.7	60	102.8	100	100.9	100	100.5
Trimethylamine	10	102.4	40	101.7	60	102.0	80	103.0
Triethylamine	0.2	102.2	0.5	100.0	0.5	101.0	1	101.0
Triethanolamine	100	102.1	100	99.0	100	98.5	100	100.5

Interferences

Foreign organic substances, as shown in Table 1, were added to berberine and their interferences with the determination of berberine were studied. In previous papers[7,8] when the TBPE anion was used in the aqueous phase, inorganic compounds such as sodium chloride, potassium chloride, calcium chloride, magnesium chloride, sodium nitrate and sodium acetate did not cause any interference. However, amines such as procaine, dibucaine, diphenhydramine, chlorpheniramine and ephedrine caused large interferences in the conventional TBPE method[7,8] because the TBPE concentration was sufficient to form ion associates with amines and the pH of the aqueous phase was kept relatively low to prevent hydrolysis of TBPE. Therefore, the effect of the TBPE·H concentration on the formation of the ion-association complexes was investigated. The concentration of TBPE·H was varied from 1×10^{-5} to 2×10^{-4} mol dm^{-3}. The higher the TBPE·H concentration, the lower was the tolerable concentration of amines in the determination of berberine; the absorbance of the berberine associate was maximum and constant for all of the TBPE·H concentrations examined (Table 1). As a result, the interferences from amines were partially eliminated by adjusting the pH for the extraction to 12.8 and using 1×10^{-5} mol dm^{-3} TBPE·H–dichloroethane.

Extracting solvents

Seven solvents, *viz.*, 1,3-dichlorobenzene, 1,2-dichlorobenzene, 1,1,1-trichloroethane, chlorobenzene, dichloromethane, 1,1-dichloroethane and 1,2-dichloroethane, were tested in the extraction system. Of these solvents, dichloromethane, 1,2-dichloroethane and 1,2-dichlorobenzene showed higher absorbances, however, 1,2-dichloroethane was the best in terms of colour stability of the organic phase and reproducibility of the extraction. The molar absorptivity of the berberine associate with 1×10^{-5} mol dm^{-3} TBPE·H solution was 89 000 dm^3 mol^{-1} cm^{-1} at 610 nm and the absorbance of the reagent blank was about 0.01.

Flow Injection Study

Phase segmentor and separator in an FI system coupled with solvent extraction

By considering the various conditions in the batchwise method described above, the solvent extraction–FI system using TBPE·H–dichloroethane was examined. Motomizu and Oshima[10] have examined some phase segmentors and phase separators in the solvent extraction–FI system. In this work, a T-shaped segmentor, in which the extracting solvent flows into the aqueous solution at 90°, was used. In addition, the same type of phase separator as described in reference 10, which has a sloped groove, was used for efficient phase separation, and a porous PTFE membrane (0.8 μm pore size) was used to recover the organic phase efficiently. Moreover, the effect of pH on extraction in the flow system was examined. Although a pH of 12.8 was suitable to eliminate the interferences from amines in the batchwise method, the baseline was noisy and unstable and the membrane permeability of the associate was not constant when the pH of the aqueous phase was adjusted to 12.8. This is probably because most of the TBPE·H transfers into the aqueous phase at pH 12.8 and the TBPE anion easily adsorbs on to the PTFE membrane filter. Accordingly, a pH of 11 was chosen for this work.

Effect of extraction coil and sample injection volume

In order to examine the efficiency of extraction the length of the extracting tubing was varied. The maximum peak heights were obtained when the tubing was over 2 m in length. In this work, 2 m long tubing was used. In addition, the effect of sample injection volume on peak shape was investigated. The volume of sample injected was varied by changing the length of the sample loop in the injection valve. Consequently, 140 μl of sample were injected for the rapid determination of berberine and benzethonium.

Effect of flow-rate on peak shape

Holding the flow-rate of the extracting solvent constant (0.8 ml min^{-1}), the flow-rates of the carrier and the buffer solutions were varied from 1 to 2.3 ml min^{-1}. Recovery of the organic phase was kept at 97% using needle valves. At a flow-rate of 2.3 ml min^{-1} about a 30% augmentation in the peak height was observed compared with that at a flow-rate of 1.6 ml min^{-1} for the aqueous phase and the peak width became narrower. Considering consumption of reagents and unstable phase separation, a flow-rate of 1.6 ml min^{-1} (aqueous:organic = 2:1) was chosen in this work. Of the extracting solvents examined with the batchwise method, dichloromethane was the best for phase separation, but the flow-rate of dichloromethane was not constant because its vapour pressure was low compared with other solvents. Consequently, 1,2-dichloroethane was used.

Calibration Graphs for Berberine and Benzethonium

The calibration graphs obtained in the extraction–FI system showed good linear relationships over the range 1×10^{-6}–5×10^{-6} mol dm^{-3} of berberine and the range 2×10^{-6}–1×10^{-5} mol dm^{-3} of benzethonium when 140 μl of the standard solutions were injected. The relative standard deviation (n =

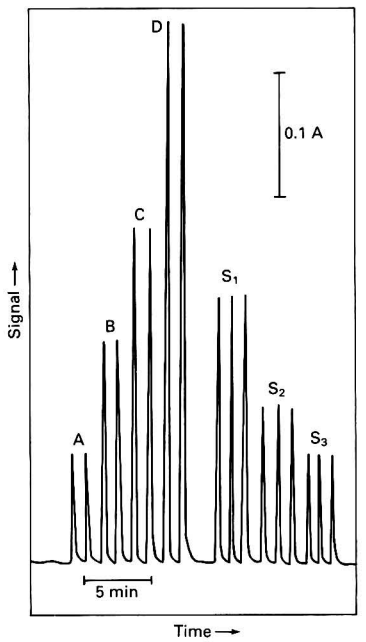

Fig. 4 Flow signals for berberine standard solutions and sample solutions containing berberine. A, 1×10^{-6}; B, 2×10^{-6}; C, 3×10^{-6}; and D, 5×10^{-6} mol dm^{-3}; and S_1, S_2 and S_3, sample solutions. TBPE·H concentration, 1×10^{-5} mol dm^{-3}

6) was 0.9% for 1×10^{-6} mol dm^{-3} berberine and 1.2% for 4×10^{-6} mol dm^{-3} benzethonium, and the sample throughputs were 45 h^{-1} for berberine and 30 h^{-1} for benzethonium.

Determination of Berberine and/or Benzethonium in Pharmaceuticals

The practical use of the method was assessed by applying it to the determination of berberine and benzethonium in pharmaceutical preparations. Tablets containing berberine were dissolved in hot water and the sample solutions were prepared after filtration and suitable dilution. Fig. 4 shows the flow signals for a berberine standard solution and sample solutions. The results obtained with the FI system are shown in Table 2. Small amounts of chlorpheniramine, ephedrine and dibucaine coexisting in the samples did not interfere. Berberine and/or benzethonium contents were all in good agreement with the declared amounts. In conclusion, the FI method coupled with solvent extraction in highly alkaline media has the advantages of sensitivity, selectivity and rapidity for the determination of berberine and benzethonium in complex mixtures.

Table 2 Determination of berberine and benzethonium in commercial samples by FI coupled with solvent extraction

	Berberine/mg		Benzethonium	
Sample	Declared	Found*	Declared	Found*
Tablet—				
A	100	104	—	—
B	37.5	36.8	—	—
C	200	207	—	—
Eyedrops—				
A	—	—	0.005%	0.0048%
B	—	—	0.1 mg	0.101 mg

* Average of three determinations.

References

1 Auerbach, E., *Ind. Eng. Chem., Anal. Ed.*, 1943, **15**, 492.
2 Kaneda, Y., and Iwaida, M., *Eisei Kagaku*, 1976, **22**, 370.
3 Irving, H. M. N. H., and Markham, J. J., *Anal. Chim. Acta*, 1967, **39**, 7.
4 Scott, G. V., *Anal. Chem.*, 1968, **40**, 768.
5 Sakai, T., *Analyst*, 1983, **108**, 608.
6 Sakai, T., *Anal. Chim. Acta*, 1983, **147**, 331.
7 Sakai, T., *Bunseki Kagaku*, 1975, **24**, 135.
8 Sakai, T., *J. Pharm. Sci.*, 1979, **68**, 875.
9 *The Japanese Pharmacopoeia, XI*, Hirokawa Publishing, Tokyo, 1986, p.C-315.
10 Motomizu, S., and Oshima, M., *Analyst*, 1987, **112**, 295.

Paper 0/03480K
Received July 31st, 1990
Accepted September 18th, 1990

Determination of Aluminium in Kaolins by Flow Injection

Anuchit Prownpuntu and Umaporn Titapiwatanakun*
Department of Chemistry, Chulalongkorn University, Bangkok 10330, Thailand

A flow injection spectrophotometric method is described for the determination of aluminium in kaolins, based on its complexation with Alizarin Red S. The flow injection system permits a throughput of 120 samples per hour with a precision (relative standard deviation) of 1.31% and without any carryover. The aluminium contents in various clay extracts as determined by the proposed flow injection method were in good agreement with those determined by a well established classical method.

Keywords: *Aluminium determination; Alizarin Red S; kaolins; flow injection; spectrophotometric detection*

Kaolin is a type of clay that contains large amounts of aluminium mostly in the form of hydrous aluminium silicates. It is an economic clay commodity having many industrial applications and new uses are still being discovered. Many grades of kaolin are specially designed for specific uses, in particular paper, paint, rubber, plastics and ceramics.[1] One method of classification is by determining the aluminium content, the higher the content the better the grade of kaolin.

The aluminium in kaolin is usually determined by a classical method, according to the American Society for Testing and Materials (ASTM) D 718–86.[2] Although this method is simple, accurate and precise, it is very laborious. Yoshinobu and Itsuma[3] determined the aluminium contents in kaolins by an X-ray fluorescence spectrometric method. The accuracy and precision of the method were reported to be 0.1 and 2%, respectively, however, sample preparation for the method was time consuming. This paper describes an attempt to develop a competitive method that has a high throughput and employs simple instrumentation.

Flow injection (FI), as developed by Růžička and Hansen,[4] has been widely used for automated continuous analysis in various fields.[5,6] The low sample and reagent consumptions, good sensitivity and reproducibility and high sample throughput are considered to be the main advantages of FI methods. Most applications of this technique have involved spectrophotometry based on the formation of coloured chelates.[5,6] Aluminon,[7] Bromopyrogallol Red,[8] Chrome Azurol S,[9] Eriochrome Cyanide R,[10] Pyrocatechol Violet[11] and Xylenol Orange[12,13] have been reported as spectrophotometric reagents for the determination of aluminium by flow analysis, however, the reported linear working ranges were rather low, *i.e.*, 0–0.1 ppm.[8] Although Alizarin was the first spectrophotometric reagent for aluminium, proposed in 1915,[14] there has been no report of an FI application. Therefore, it was decided to employ an FI technique with spectrophotometric detection for the determination of aluminium in kaolin samples with a high aluminium content. Alizarin Red S was used as the spectrophotometric reagent instead of Alizarin, owing to its high solubility in water.

Experimental

Reagents

All reagents used were of analytical-reagent grade. The Alizarin Red S and mercaptoacetic acid were obtained from Fluka. The other chemicals were obtained from BDH.

Aluminium stock solution (1000 μg ml^{-1}). Dissolve 1.00 g of pure aluminium wire in 20 ml of 6 mol dm^{-3} hydrochloric acid and then dilute to 1 l with triply distilled water.

Alizarin Red S solution (0.01%). Dissolve 0.10 g of Alizarin Red S in water, adjust to pH 4.5 with ammonium acetate buffer and dilute to 1 l.

Synthetic kaolin sample. Grind the reagents, consisting of 45.0% Al_2O_3, 50.0% SiO_2, 1.5% Fe_2O_3, 1.0% TiO_2, 0.5% MnO_2, 0.5% $CaCO_3$, 0.5% $MgSO_4$, 0.5% K_2CO_3 and 0.5% $(NH_4)_2HPO_4$, until they become homogeneous.

Apparatus

The FI system, shown in Fig. 1, consisted of a peristaltic pump (IPN/S Model 4–16, Ismatec), a laboratory-built injection valve, a spectrophotometer (Spectronic 21 Model MV, Bausch & Lomb) and a strip-chart recorder (Perkin-Elmer Model 56). The flow cell (volume 80 μl, 10 × 1 mm i.d.) was constructed of perspex. A single-line manifold for the FI measurements was employed with 1.0 mm i.d. PTFE tubing. All reported measurements were made at room temperature.

Procedures

Classical method

Sample decomposition, pre-treatment, and determination procedures for the classical method employed were based on the standard method of ASTM D 718–86.[2] A soil sample was fused with sodium carbonate in a platinum crucible. A series of procedures were then followed to determine the percentage amounts of iron oxide, titanium oxide and the total mixed oxides (Al_2O_3 + TiO_2 + Fe_2O_3). The percentage amounts of iron oxide and titanium oxide were then subtracted from the total percentage amount of the mixed oxides in order to obtain the percentage amount of the aluminium oxide.

Flow injection method

Decomposition. Sodium hydroxide (5.0 g) was fused in a zirconium crucible and left to cool in a desiccator. The soil sample (0.20 g) was added to the crucible and fused for 5 min. The cooled melt was extracted with water and all precipitates were dissolved in 6 mol dm^{-3} hydrochloric acid and then diluted to 250 ml.

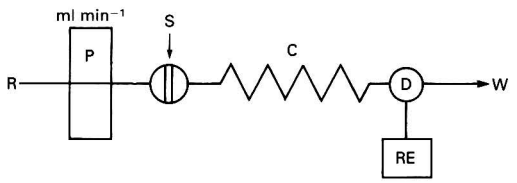

Fig. 1 Diagram of the FI system: R, reagent; P, pump; S, sample injection port; C, mixing coil (150 cm); D, detector; RE, recorder; and W, waste

* To whom correspondence should be addressed.

Pre-treatment of sample solution. An aliquot (10 ml) containing approximately 0.5–2.0 mg of aluminium was made alkaline with 3 mol dm^{-3} ammonia solution, until a hydroxide precipitate appeared, then acidified with 5 mol dm^{-3} acetic acid until the precipitate was completely redissolved, and finally, diluted to 100 ml.

Results and Discussion

Choice of Fixed Operating Wavelength

The absorption spectra of Alizarin Red S and aluminium–Alizarin Red S complex solutions were scanned between 350 and 650 nm (Fig. 2). The maximum absorbances of the reagent and the complex solutions were at 422 and 480 nm, respectively. The results agreed well with the values reported by Parker and Goddard.[15] Marked differences between the absorbances of the blank reagent and the test solutions were observed at 510 nm. Therefore, this wavelength, 510 nm, was chosen for the FI method of measurement for subsequent work.

Effect of pH

The effect of pH on the maximum absorption and sensitivity of this complex was investigated by varying the pH of the ammonium acetate buffer from 3.5 to 5.0. The results in Fig. 3 show that the absorption band of the complex shifts to a longer wavelength at a higher pH. At pH 5.0, the absorption peak was broad and the sensitivity was the lowest. It was found that the highest sensitivity (signal to background ratio) was obtained when the pH of the reagent solution was adjusted to 4.5; the rate of the reaction also reached a maximum at this pH.

Effect of Concentration of Reagent

The effect of the concentration of reagent on sensitivity is shown in Fig. 4 which gives the calibration graphs for the determination of aluminium using FI at various concentrations of Alizarin Red S. The sensitivity increased with an increase in the concentration of the reagent, however, precipitation of Alizarin Red S occurred at concentrations greater than 0.015%. It was found that the background, when using 0.015% Alizarin Red S, was high and difficult to adjust to zero on the Spectronic 21 instrument. A concentration of 0.010% Alizarin Red S was, therefore, used in order to obtain a high sensitivity with low background.

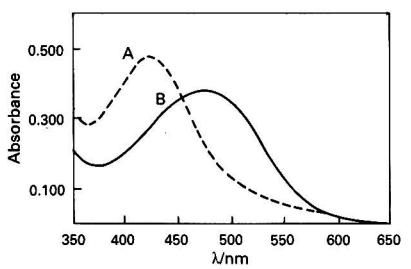

Fig. 2 Absorption spectra of Alizarin Red S and its aluminium complex: A, 0.01% Alizarin Red S at pH 4.5; and B, 50 μg of aluminium in 50 ml of 0.01% Alizarin Red S

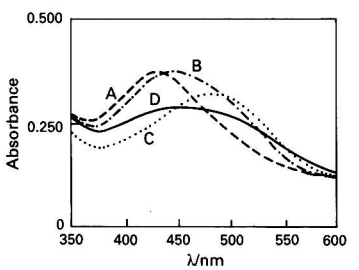

Fig. 3 Effect of pH on the absorption spectra of the aluminium complex (50 μg of aluminium in 50 ml of 0.01% Alizarin Red S solution): pH: A, 3.5; B, 4.0; C, 4.5; and D, 5.0

Effect of Injection Volume, Flow-rate and Length of Tubing

Dispersion is the most important parameter that must be optimized, when using FI, in order to attain maximum sensitivity and sampling rate. Dispersion can be adjusted by altering many of the flow parameters including injection volume, flow-rate and length of tubing.

Fig. 5 shows the absorbance changes recorded at a fixed concentration of aluminium (50 ppm) using aliquots of 10–250 μl injected into the reagent stream with a 5.0 ml min^{-1} flow-rate, using a 100 cm tube length between the injection port and the flow cell. Both peak height and peak width were found to increase with increasing injection volume.

The effect of the flow-rate was investigated by injecting a fixed volume of a standard aluminium solution into the flow system at various flow-rates (see Fig. 6). The resulting peak

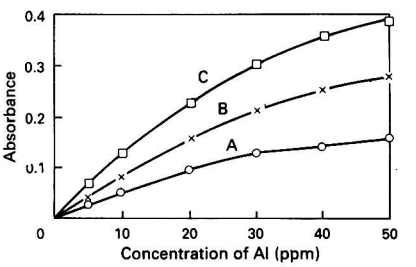

Fig. 4 Effect of reagent concentration on the sensitivity of aluminium determination: A, 0.005; B, 0.010; and C, 0.015% Alizarin Red S, for a 75 μl injection at a flow-rate of 5.0 ml min^{-1}

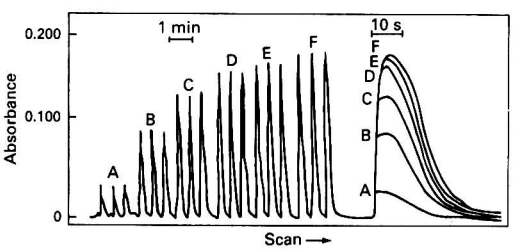

Fig. 5 Effect of sample injection volume on sample peaks at a flow-rate of 5.0 ml min^{-1}: A, 10; B, 50; C, 100; D, 150; E, 200 and F, 250 μl of 50 ppm aluminium

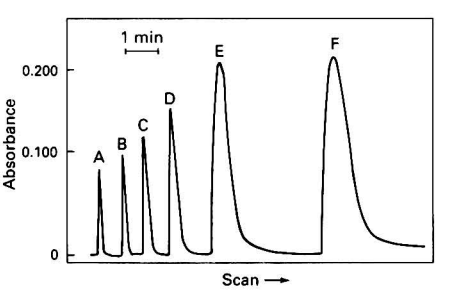

Fig. 6 Effect of flow-rate on sample peaks: A, 5.0; B, 4.0; C, 3.0; D, 2.0; E, 1.0; and F, 0.5 ml min^{-1}

Table 1 Effect of flow-rate on sample peaks

Flow-rate/ ml min^{-1}	Peak-height absorbance	Peak width/ min	Sampling rate/samples per hour
1.00	0.252	3.00	20
2.00	0.166	1.20	50
3.00	0.133	0.75	80
4.00	0.109	0.60	100
5.00	0.091	0.45	133

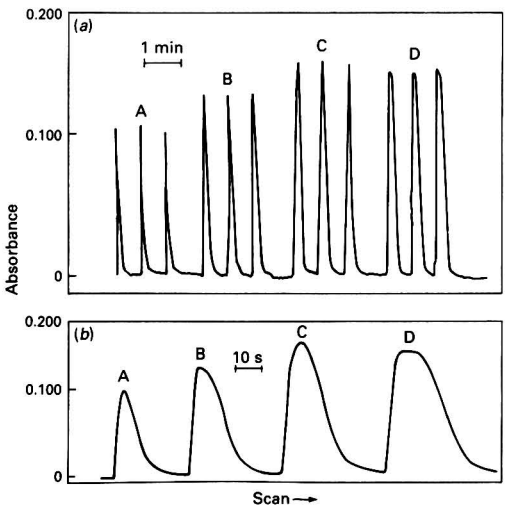

Fig. 7 Effect of tube length on sample peaks at a fixed flow-rate of 5.0 ml min^{-1}: A, 50; B, 100; C, 150; and D, 200 cm, using different time-scales as shown

heights and peak widths are summarized in Table 1, together with the calculated change in sampling rate. When the flow-rate was reduced to between 5.0 and 0.5 ml min^{-1}, an increase in peak height was observed; a reduction in the maximum number of sample analyses per hour was also observed. The effect of changing the flow-rate is contrary to the effect observed with increasing path length or residence time, in an FI system that is solely controlled by dispersion, as described by Růžička and Hansen.[5] In the proposed system, where it took 9 min for the reaction rate to reach a maximum at room temperature, there was competition between dispersion and chemical kinetics. An increase in dispersion would decrease peak height, however, chemical kinetics had the opposite effect. The cumulation of these effects led to an increase in peak height when the flow-rate was reduced. It can be concluded, therefore, that the effect of the chemical kinetics is more significant than that of the dispersion in the FI system described here. However, the effect of dispersion on peak width can still be seen, as in Fig. 6 which shows that an increase in dispersion gives a wider peak.

In addition to varying the flow-rate, the effect of the residence time on dispersion was also investigated by varying the tube length between the injection port and the flow cell (Fig. 7). In Fig. 8, the graph of absorbance *versus* tube length (5–200 cm), shows that the effect of changing the tube length is similar to the effect of a decreased flow-rate. Peak height increased with increasing tube length (or residence time) up to a tube length of 150 cm. However, a decrease in peak height was observed when the tube length was increased from 150 to 200 cm. Thus, it can be deduced that the effect of dispersion became more influential than the effect of the chemical kinetics when a tube length of 200 cm was employed.

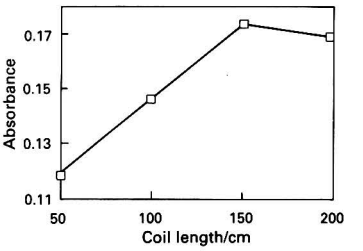

Fig. 8 Peak heights plotted at various tube lengths

Table 2 Effect of sampling rate on precision and carryover

Sampling rate/ samples per hour	RSD* (%)	Carryover (%)
60	0.49	0
90	0.66	0
120	1.31	0
180	1.41	0.75

* For ten sample replicates.

Table 3 Interference effects on aluminium determination at a concentration of 20 ppm

Ion	Added as	Maximum added without interference effect (ppm)
Ba^{2+}	$BaCl_2$	200
Ca^{2+}	$CaCl_2$	200
Co^{2+}	$Co(NO_3)_2$	50
Cu^{2+}	$CuSO_4$	200
Fe^{3+}	$FeCl_3$	2
K^+	KCl	200
Li^+	LiCl	200
Mg^{2+}	$Mg(NO_3)_2$	200
Mn^{2+}	$MnSO_4$	200
Zn^{2+}	$Zn(NO_3)_2$	100
NO_3^-	KNO_3	200
PO_4^{3-}	$(NH_4)_2HPO_4$	100
SiO_3^{2-}	Na_2SiO_3	100

Effect of Sampling Rate

The effect of sampling rate on precision and carryover is shown in Table 2. The results indicate that sampling at rates of up to 120 samples per hour was possible with no carryover and with <1% carryover between consecutive low and high samples when the sampling rate was raised to 180 samples per hour. Precision with a relative standard deviation (RSD) of <1.5% was attained when sampling at less than 180 samples per hour.

Interference Study

Possible sources of interference in kaolin such as calcium, magnesium, lithium, barium, potassium, zinc, cobalt, manganese, iron, silicate, nitrate and phosphate were investigated at concentrations of up to ten times that of aluminium, the major element in kaolin. The interference study was carried out by using a standard solution of 20 ppm of aluminium and an ion was considered to interfere if it altered the detector response by more than 2%. The results of this study are given in Table 3. It was found that barium, calcium, copper, lithium, manganese, magnesium, potassium and nitrate caused no interference even at ratios of 1:10. Zinc, phosphate and silicate showed no interference effect provided the concentra-

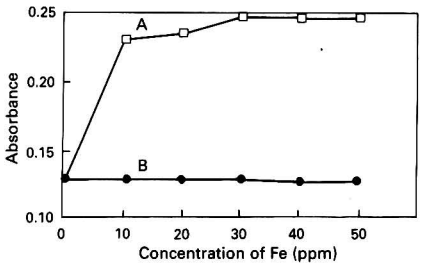

Fig. 9 Effect of the addition of 0.04% mercaptoacetic acid to A, the reagent solution and B, the sample solution, on the interference of iron in the determination of aluminium (20 ppm)

Table 4 Determination of aluminium in a synthetic sample (45.00% Al_2O_3)

Method	Al_2O_3 (% m/m)	Error (%)	RSD (%)	Recovery (%)
Proposed	45.10	0.20	1.29	100.02
Classical	44.90	0.20	1.88	99.78

Table 5 Determination of aluminium in kaolins from various parts of Thailand

Sample No.	Al_2O_3 (% m/m) Proposed FI method	Classical method
1	41.45	41.60
2	40.12	40.62
3	39.44	39.50
4	39.78	39.94

tion did not exceed five times that of aluminium. Cobalt at concentrations greater than 50 ppm (2:5 ratio) would be a positive interferent. However, the amounts of these ions in kaolin were very low compared with that of aluminium and, therefore, had no effect on aluminium determination. The presence of iron at a ratio of greater than 10:1 also caused serious interference which could be eliminated by adding 0.04% mercaptoacetic acid to a sample solution, but not to the reagent solution (Fig. 9).

Linearity and Detection Limit

The calibration graph obtained for the determination of aluminium with a 75 µl sample injection volume, when injected into 0.01% Alizarin Red S in ammonium acetate buffer at pH 4.5, gave a linear working range for injections of 0–25.0 ppm of aluminium with a correlation coefficient of 0.999; it also passed through the origin. This linear range was very high compared with previous reports.[7–12] Alizarin Red S, therefore, was suitable for the determination of aluminium in samples with a high aluminium content. The detection limit (defined as three times the standard deviation of ten replicate peak measurements near the blank reading) of the proposed method was found to be 0.8 ppm. However, no peak was detected when this concentration of aluminium was injected into the flow system. The lowest concentration recommended for quantitative analysis was 2.0 ppm.

Determination of Aluminium in Kaolins

Accuracy, precision and percentage recovery of the proposed FI method for the determination of aluminium in the synthetic kaolin, conducted with a 75 µl sample injection into a reagent stream with a 5 ml min^{-1} flow-rate and a 50 cm mixing coil at 120 samples per hour, are compared with those of the classical method in Table 4. The results suggest that the FI method has a similar accuracy with better precision and percentage recovery. The feasibility of the proposed method was then tested by determining aluminium in kaolin from various parts of Thailand. The results are summarized in Table 5 and show good agreement between the two methods.

Conclusion

The determination of aluminium in kaolin formerly required a time-consuming decomposition step.[2,3] The proposed NaOH fusion procedure not only enables adequate decomposition of the inorganic matrix but also requires less time. In the determination step, Alizarin Red S has been shown, in this study, to be a suitable spectrophotometric reagent for determining high levels of aluminium by FI as the reaction proceeds slowly at room temperature. The proposed FI spectrophotometric method is as accurate for determining aluminium in kaolin as the classical method. However, the classical method is very laborious and requires a long analysis time for each sample. The proposed method gives more precise results and a sample throughput of 120 samples per hour can be attained with no carryover.

While the aim of this work was to investigate the practicability of using an FI method with a simple spectrophotometric detector for the determination of aluminium in kaolin, it is apparent that the proposed method will also have direct application to a wide variety of samples that contain high levels of aluminium such as lateritic soil, feldspar, ball clay and bauxite.

References

1 Huber, J. M., in *Kaolin Clays and Their Industrial Uses*, J. M. Huber Corporation, New York, 2nd edn., 1955.
2 American Society for Testing and Materials, *Method of Analysis of Aluminium Silicate Pigment*, American Society for Testing and Materials, Philadelphia, 1987, Method D 718–86.
3 Yoshinobu, U., and Itsuma, S., *Hokkaido Kogya Kaihatsu Shikensho Hokoku*, 1984, **28**, 17.
4 Růžička, J., and Hansen, E. H., *Anal. Chim. Acta*, 1975, **78**, 145.
5 Růžička, J., and Hansen, E. H., *Flow-Injection Analysis*, Wiley, New York, 2nd edn., 1988.
6 Růžička, J., and Hansen, E. H., *Anal. Chim. Acta*, 1986, **179**, 1.
7 Bertsch, P. M., Alley, M. M., and Ellmore, T. L., *Soil Sci. Soc. Am. J.*, 1981, **45**, 666.
8 Wyganowski, C., Motomizu, S., and Toei, K., *Anal. Chim. Acta*, 1982, **140**, 313.
9 Zoeltzer, D., and Schwedt, G., *Fresenius Z. Anal. Chem.*, 1984, **317**, 422.
10 Reis, B. F., Bergamin, H., Zagatto, E. A. G., and Krug, F. J., *Anal. Chim. Acta*, 1979, **107**, 309.
11 Grigg, J. L., and Morrison, J. D., *Commun. Soil Sci. Plant Anal.*, 1982, **13**, 351.
12 Mochizuki, T., Toda, Y., and Kuroda, R., *Talanta*, 1982, **29**, 659.
13 Edwards, A. C., and Cresser, M. S., *Talanta*, 1983, **30**, 702.
14 Atack, F. A., *J. Soc. Chem. Ind., London*, 1915, **34**, 936.
15 Parker, C. A., and Goddard, A. P., *Anal. Chim. Acta*, 1950, **4**, 517.

Paper 0/03537H
Received August 1st, 1990
Accepted September 27th, 1990

Stray Radiant Energy Test Method in Spectrophotometry Based on Direct Transmittance Spectrometry

Paddy Fleming and John O'Dea
Sligo Regional Technical College, Ballinode, Sligo, Ireland

A sample-based stray radiant energy (SRE) test method in spectrophotometry which takes the attenuation of the SRE by the sample into account is described. The proposed test method allows the SRE transmittance of the sample and the true relative SRE level of the spectrophotometer to be determined by measuring the absorbances of concentrated food dye samples such that the monochromatic transmittances are much less than the relative SRE level. The proposed test method was applied to a double-beam spectrophotometer, *i.e.*, a Shimadzu 260 instrument, at two slit-heights while maintaining the spectral slit-width and wavelength constant. The ensuing SRE values were compared with those obtained previously *via* transmittance ratio spectrometry on the same food dye samples under identical instrumental conditions.

Keywords: *Spectrophotometer; stray radiant energy; transmittance ratio spectrometry*

Spectrophotometric absorbance is, under ideal conditions, directly proportional to the product of sample concentration and cell path length. Conditions are ideal when the incident radiation is monochromatic, *e.g.*, if the effective spectral slit-width (ESW) of the monochromator is less than 12% of the natural band-width (NBW) of the absorbing peak then 99% of true peak absorbance will be reproduced, according to Burgess and Knowles.[1] If the radiant intensity of the exit slit *versus* wavelength distribution is assumed to be triangular then the wavelength range centred about the nominal wavelength setting of the monochromator which contains 50% of the emergent radiant energy is termed the ESW. The ratio of ESW:SSW = $(1 - 1/\sqrt{2})$, where SSW represents the spectral slit-width, *i.e.*, the total wavelength region isolated by the monochromator. The relative radiant intensity leaving the monochromator at the ESW wavelength limits is $1/\sqrt{2}$. The non-linearity of absorbance *versus* sample concentration for a fixed cell path length, which is observed as the sample concentration increases, may be attributed to stray radiant energy (SRE) and transmittance readings at very high concentrations may be ascribed solely to SRE. If the SRE test method is sample based, then the very act of introducing a sample into the spectrophotometer alters the relative SRE level present unless the sample is transparent to SRE. Otherwise, the SRE transmittance of the test sample must be determined experimentally and accommodated in the theoretical analysis so as to be in a position to report the true relative SRE level in a spectrophotometer.

The proposed SRE test method involves determining the actual absorbances (A') of a series of concentrated solutions whose monochromatic transmittances are at least a factor of 50 lower than the relative SRE level to be determined, *e.g.*, if the relative SRE level is 0.005, then the monochromatic transmittances of the test solutions should be less than 0.0001 so that the detected radiation consists of more than 98% SRE and less than 2% monochromatic radiation. This enables the investigation of the SRE behaviour of samples of various concentrations. If the absorbance readings encountered exceed full-scale deflection on the spectrophotometer, then an absorbing blank of known absorbance may be employed to maintain on-scale readings. The gradual increase in absorbance with increasing concentration, observed in the non-Beer–Lambert concentration range, is due to the absorption of the SRE. The true relative SRE level can be determined from this region of the actual absorbance *versus* concentration plot by extrapolation to zero concentration and the SRE transmittance of the sample can be calculated from its slope. The monochromatic absorbance of a concentrated solution in a 10 mm quartz cell cannot be measured directly but it may be calculated from its measured monochromatic absorbance in a 1 mm quartz cell. The path-length ratio of the pair of 10 mm matched quartz cells used in this experiment was determined by measuring the absorbance of a dilute food dye solution placed in the 10 mm sample cell against a water blank placed in a matched 10 mm reference cell. The sample and reference cells were then interchanged and the absorbance measurement described above was repeated. The experiment was repeated for the pair of 1 mm cells with the same solution. Each pair of cells was found to be matched to within 0.5%. The average path-length ratio of a 10 mm cell to a 1 mm cell was hence calculated to be 10.00 ± 0.05.

The proposed SRE test method and the transmittance ratio spectrometry test method[2] developed by Fleming were applied to a Shimadzu 260 spectrophotometer under identical sample and instrumental conditions and the results were compared.

Formulation of Experimental Quantities

The observed transmittance (T') of a sample may be expressed as a combination of the monochromatic transmittance (T) and the relative SRE level (s), according to Burgess and Knowles[1] and Slavin[3] for $s \ll 1$, as follows

$$T' = (1 - s)T + s \approx T + s \quad (1)$$

This equation does not allow for the absorbance of the stray light by the sample and therefore it needs to be modified by the introduction of a factor that encompasses the attenuation of SRE with increasing absorbance of the sample. Such a factor is given by t^A, where t is the SRE transmittance of a sample whose monochromatic absorbance is unity and equation (1) becomes

$$T' = T + st^A \quad (2)$$

The contribution by the SRE to the transmitted light intensity is negligible at low absorbances, *i.e.*, at low concentrations, compared with the contribution by the monochromatic light since $s \ll T$ and equation (2) approximates to

$$T' = T \text{ or } \log_{10} T' = -A \quad (3)$$

However, the contribution by the SRE predominates at high concentrations where $s > 50T$ and equation (2) approximates to

$$T' = st^A \quad (4)$$

Taking the $\log_{10}$ of equation (4) gives

$$\log_{10}T' = \log_{10}s + A\log_{10}t \quad (5)$$

If the observed transmittance (T') is plotted against the monochromatic absorbance (A) on semilog axes then a plot of two linear parts separated by an 'elbow' is obtained. The elbow arises in the monochromatic absorbance region where the monochromatic transmittance is of the same order of magnitude as the SRE. At lower monochromatic absorbances, where $s \leqslant 0.02T$, equation (3) yields a linear plot with a negative slope of unity, and at higher monochromatic absorbances, where $T \leqslant 0.02s$, equation (5) yields a linear plot with a slope of $\log_{10}t$ which may be extrapolated to give an intercept on the ordinate log axis equal to s. Thus, by ensuring that the monochromatic radiation is less than 2% of the total detected radiation, it becomes possible to determine the SRE by this method.

Spectrophotometers may not directly read the large absorbances required by this method. Therefore, if A_{fsd} (the full-scale absorbance reading) is less than $-\log_{10}s$, then a blank of finite absorbance A'_b must be used to keep these large absorbance readings on-scale. Therefore, the relative transmittance R' of a concentrated solution of transmittance T' with respect to an absorbing blank of transmittance T'_b (= $10^{-A'b}$) is given by

$$R' = T'/T'_b \tag{6}$$

The transmittance ratio (r) of a sample-beam solution whose concentration or cell path length is α-times greater than a similar reference-beam solution is given by[2]

$$r = \frac{T^{\alpha} + s't^{\alpha A}}{T + s't^{A}} \tag{7}$$

where $s' = s/(1 - s)$.

This transmittance ratio function has a minimum, $r(\min) = \rho$, at a monochromatic reference transmittance value, $T = \tau$, which is determined by the relative SRE level prevailing, by the SRE transmittance of the reference sample whose monochromatic transmittance, T, is 0.1 and by the concentration ratio, α, chosen. If it is assumed that $t = 1$ then the SRE is given by[2]

$$s = \left[1 + \frac{(1-\rho)(\rho/\alpha)^{\alpha/(1-\alpha)}}{(\alpha - 1)}\right]^{-1} \tag{8}$$

Experimental

An arithmetic concentration series of aqueous solutions was prepared from a 10 g l^{-1} stock solution of Orleans Blue food dye (E123); its minimum concentration was 0.5 g l^{-1} and its maximum concentration was 10 g l^{-1}. The arithmetic concentration series had a concentration increment of 0.25 g l^{-1} up to a sample concentration of 3.5 g l^{-1} and 0.5 g l^{-1} at sample concentrations above 3.5 g l^{-1}. The NBW of the peak of a solution centred at 630 nm was 50 nm. The absorbance of each solution relative to a distilled water blank, at its 630 nm peak wavelength and using a 5 nm SSW, was determined in a pair of matched 1 mm cells using a Shimadzu 260 spectrophotometer. This gave an average absorptivity of 0.10013 ± 0.0005 l mm^{-1} g^{-1} (Fig. 1). Hence the monochromatic absorbances of the test solutions in a 10 mm cell may be calculated.

The absorbance relative to water of each of the samples in the above arithmetic concentration series was determined in a pair of matched 10 mm quartz cuvettes using the Shimadzu 260 spectrophotometer set at 630 nm and the 5 nm SSW setting. The experiment was repeated but with the actual slit-height halved, *i.e.*, the 05 nm SSW setting on this particular instrument. The observed absorbance (A') increased with concentration in step with the monochromatic absorbance (A) at low concentration, however, as the concentration increased the observed absorbances gradually deviated from the expected linear behaviour with the monochromatic absorbance, as the SRE began to predominate over the monochromatic radiation. The monochromatic absorbance values of interest in this experiment were in the range $A \geqslant 1.7 - \log_{10}s$ where the detected SRE contributed more than 98% of the radiation detected. The full-scale absorbance reading on the Shimadzu 260 instrument ($A_{fsd} = 4$) was less than $-\log_{10}s$, therefore, an absorbing blank, A'_b (= 2.003 ± 0.002) was used to produce on-scale differential absorbance readings in the range $0 < \Delta A' < 3$ for samples whose observed absorbances were greater than A'_b. The absolute observed absorbance values (A') of such samples were then given by

$$A' = \Delta A' + A'_b \tag{9}$$

where $\Delta A' = -\log_{10}R'$.

Each differential absorbance reading of interest fluctuated randomly about an average value and so a sufficient number of observations of each was recorded such that each average can be quoted with a standard error of less than ±0.5%. The calibration mode of operating the Shimadzu 260 instrument facilitated the recording of the randomly fluctuating differential absorbance readings from whence an average and standard error value were calculated. The ensuing observed absorbance readings (A') are recorded in Table 1 for monochromatic absorbance values greater than 7.

The actual transmittance, $T' = 10^{-A'}$, of each solution was plotted against the corresponding monochromatic absorbance on semilog axes (Fig. 2) for the two slit-heights investigated.

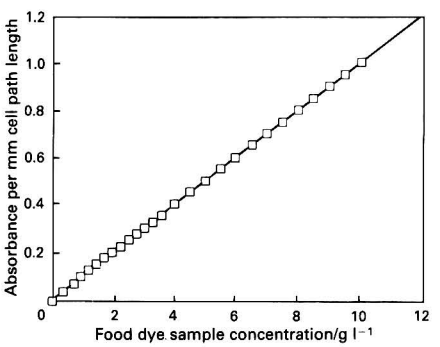

Fig. 1 Absorbance (at λ = 630 nm, SSW = 5 nm and with reference to a distilled water blank) of aqueous solutions of Orleans Blue food dye (E123) measured in a pair of matched 1 mm quartz cells plotted against food dye concentration. The equation of the line of best fit is given by $A_c = 0.10013(\pm 0.0005)c + 0.0084(\pm 0.0026)$ and the correlation coefficient is 1.000

Table 1 Direct transmittance SRE test method measurements for the two slit-heights (5 nm and 05 nm) in a Shimadzu 260 spectrophotometer*

Monochromatic absorbance (A)	Observed absorbance (±0.007) ($A' = \Delta A' + A'_b = \Delta A' + 2.003$)		Observed transmittance (×10^{-5}) ($T' = 10^{-A'}$)	
	5 nm	05 nm	5 nm	05 nm
7.032	4.347	4.620	4.50 ± 0.07	2.40 ± 0.04
7.534	4.367	4.640	4.30 ± 0.07	2.29 ± 0.04
8.036	4.390	4.663	4.07 ± 0.07	2.17 ± 0.03
8.538	4.409	4.682	3.90 ± 0.06	2.08 ± 0.03
9.040	4.432	4.704	3.70 ± 0.06	1.98 ± 0.03
9.543	4.452	4.721	3.53 ± 0.06	1.90 ± 0.03
10.045	4.474	4.746	3.36 ± 0.06	1.79 ± 0.02

* If the observed transmittance (T') is plotted on semilog axes against the monochromatic absorbance (A) on linear axes for the two slit-heights (5 nm and 05 nm) investigated, then the following exponential regression equations of best fit ensue: 5 nm: $T' = 8.93 \times 10^{-5} \times 10^{-0.0423A}$; 05 nm: $T' = 4.70 \times 10^{-5} \times 10^{-0.0415A}$

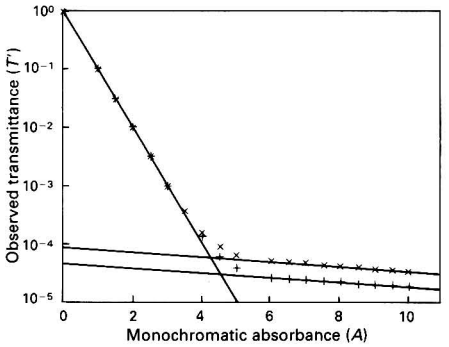

Fig. 2 Plot on semilog axes of the observed transmittance (T') *versus* the monochromatic absorbance (A) for two slit-heights (×, 5 nm; and +, 05 nm) at 630 nm. The measurements were made using a pair of matched 10 mm quartz cells and a Shimadzu 260 instrument. The analyte samples were derived from a 10 g l^{-1} stock solution of Orleans Blue food dye (E123) diluted with water

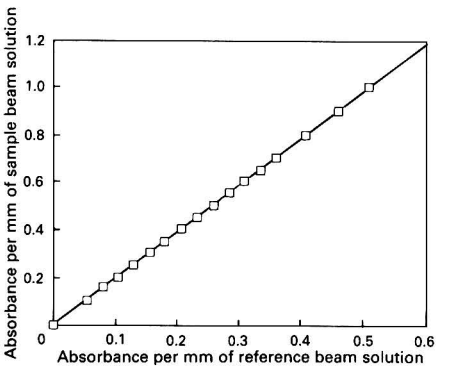

Fig. 3 Absorbances (taken from Fig. 1) of the concentration ratio pairs used in transmittance ratio spectrometry plotted against each other, *i.e.*, $A_{\alpha c}$ *versus* A_c. The concentration ratio (α) was nominally 2. The equation of the line of best fit is $A_{\alpha c} = 1.983(\pm 0.014)A_c - 0.0013(\pm 0.008)$ and the correlation coefficient is 0.9999

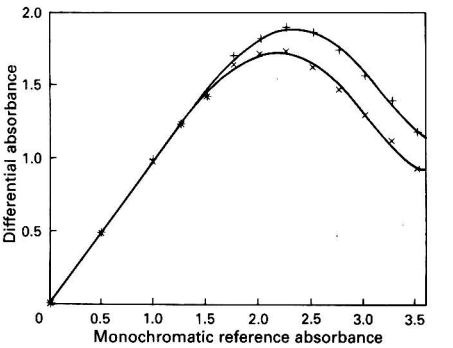

Fig. 4 Two plots of the differential absorbance ($\Delta A'$) *versus* the monochromatic reference absorbance (A_r) of a series of pairs of Orleans Blue food dye (E123) solutions whose concentration ratios (α_c) were kept constant. The experimental concentration ratio was found (*cf.* Fig. 3) to be 1.983 ± 0.014. The differential absorbance measurements were made with a pair of matched 10 mm quartz cells and a Shimadzu 260 instrument. The experiment was replicated for two slit-heights (×, 5 nm; and +, 05 nm) at 630 nm

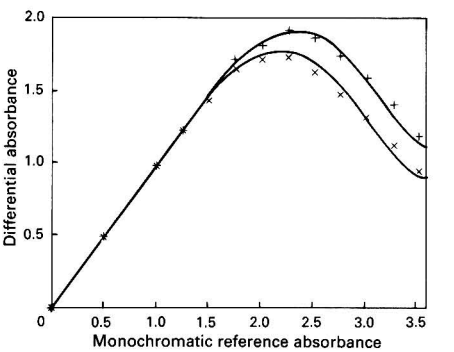

Fig. 5 Simulated full line plots based on equation (7) for $\alpha_c = 1.983$, $s = 0.0000893$ (lower curve) and 0.0000470 (upper curve), and $t = 0.907$ (lower curve) and 0.909 (upper curve). The experimental points indicated by × and + were taken from Fig. 4

The prepared concentration series had many sample pairs with a nominal concentration ratio of 2 and an average experimental concentration ratio (α_c) of 1.983 ± 0.014 (Fig. 3).

This sub-set of sample pairs was used to determine the relative SRE level at 630 nm using the transmittance ratio spectrometry method of Fleming.[2] The differential absorbance of the more concentrated of each sample pair was determined relative to its less concentrated partner in a pair of matched 10 mm quartz cuvettes. This experiment was carried out for the 5 nm slit-width at normal height and at half height. Fig. 4 shows experimental graphs constructed using this method, *i.e.*, differential absorbance against the monochromatic reference absorbance.

Results

Each curve in Fig. 2 has three distinct regions, *i.e.*, two linear regions which are bridged by a non-linear elbow. The Beer–Lambert law applied to monochromatic radiation solely accounts for linearity at low monochromatic absorbances while the Beer–Lambert law applied to SRE solely explains linearity at very high monochromatic absorbances. The non-linear elbow at intermediate absorbances arises where the ratio of monochromatic radiation to SRE, *i.e.*, T/s, is in the range $50 \geqslant T/s \geqslant 0.02$. Measurements on the linear region of each graph in Fig. 2 at monochromatic absorbances greater than 6 yielded the following values for the SRE quantities of interest [see equation (5)]: for the 5 nm slit the SRE = 8.93 (± 0.15) × 10^{-5} and $t = 0.907$ (± 0.005); for the 05 nm slit the SRE = 4.70 (± 0.15) × 10^{-5} and $t = 0.909$ (± 0.005).

Equation (8) was applied to the maximum of the experimental differential absorbance measurements in Fig. 4 and the following values for the relative SRE level were obtained: for the 5 nm slit the SRE = 7.80 (± 0.25) × 10^{-5}; for the 05 nm slit the SRE = 3.50 (± 0.25) × 10^{-5}. Note that a transmittance ratio minimum is synonymous with a differential absorbance maximum.

Conclusion

The direct transmittance spectrometric SRE test method developed here enables the true relative SRE level in spectrophotometers to be determined, albeit being sample based. Slavin[3] reported that Vandenbelt *et al.*[4] plotted absorptivity *versus* monochromatic absorbance for three substances measured at the same ultraviolet wavelength on the same spectrophotometer. The ensuing experimental curves showed the apparent decrease in absorptivity at high monochromatic absorbance that is characteristic of the presence of SRE. But the deviation from the Beer–Lambert linearity law differed for the three substances and this fact suggests that the three substances had absorbed different proportions of the instrumental SRE.

The transmittance ratio SRE values are significantly lower than the corresponding values from the proposed method. This discrepancy between the two methods would have been reconciled had the transmittance of the food dye to SRE, which is the thesis of the proposed method, been known when the transmittance ratio analysis was undertaken.

The full line plots traversing the experimental points in Fig. 5 were numerically derived from equation (7) for α_c = 1.983 and using the experimental values for the SRE (0.0000893 and 0.0000470) and t (0.907 and 0.909) yielded by the proposed SRE test method. The good fit of the line graphs based on equation (7) to the experimental measurements from Fig. 2 suggests that the proposed method is a valid SRE test method.

The relative SRE level and the transmittance of samples to SRE may vary from wavelength to wavelength within a given instrument and from instrument to instrument at a given wavelength. The increased relative SRE level with the increased slit-height was due to the increased probability of detecting a scattered or spurious ray among the peripheral rays of the optical system of the spectrophotometer as the slit-height was symmetrically expanded. The proposed test method was easier to apply than the transmittance ratio test method, it had the same precision but was more accurate because it took the non-transparency of test samples to SRE into account.

The proposed SRE test method exploits the supposedly non-linear region of the Beer–Lambert quantitative graph which has been ignored heretofore. The analysis herein shows that at high concentration (or long cell path length) the said quantitative graph becomes linear again with a slope which is determined by the SRE transmittance of the sample.

The authors are grateful for the critical and valuable comments of Dr. C. Burgess.

References

1 *Techniques in Visible and Ultraviolet Spectrometry, Volume 1, Standards in Absorption Spectrometry*, eds. Burgess, C., and Knowles, A., Chapman and Hall, London, 1st edn., 1981, pp. 9 and 98.
2 Fleming, P., *Analyst*, 1990, **115**, 375.
3 Slavin, W., *Anal. Chem.*, 1963, **35**, 561.
4 Vandenbelt, J. M., Forsyth, J., and Garrett, A., *Ind. Eng. Chem., Anal. Ed.*, 1945, **17**, 235.

Paper 0/03289A
Received July 20th, 1990
Accepted October 9th, 1990

Determination of Humic Acid and Iron(III) by Solid-state Spectrophotometry to Study Their Interactions

Kunio Ohzeki, Miyoko Tatehana, Ishoshi Nukatsuka and Ryoei Ishida
Department of Chemistry, Faculty of Science, Hirosaki University, 036 Hirosaki, Japan

A simple and sensitive method for the determination of humic acid has been developed. The method is based on the adsorptive enrichment of humic acid using a finely divided anion-exchange resin, collection of the resin on a membrane filter by filtration as a circular thin-layer, and direct measurement of the absorbance of the resultant thin-layer of resin by densitometry at 470 nm. Up to 80 μg of humic acid in 100 ml of sample solution can be determined, the limit of detection being 1.3 μg. The effect of iron(III) is masked with ethylenediaminetetraacetic acid (EDTA). Iron(III) is also determined by densitometry at 600 nm after enrichment on the thin-layer of resin as a complex with ammonium pyrrolidine dithiocarbamate (ammonium pyrrolidin-1-yldithioformate) (APDC), the limit of detection being 0.06 μg of iron(III). In the presence of humic acid, the blank value is obtained by masking the iron(III) as the EDTA complex, and calculating the net absorbance due to the APDC complex. The methods have been used to investigate the effect of humic acid on the formation of filterable iron(III) species, which can pass through a 0.45 μm membrane filter. The possibility of characterizing humic acid based on the formation of a complex with iron(III) has been shown.

Keywords: *Humic acid determination; iron(III) determination; densitometry; interaction between iron(III) and humic acid; filterable iron species*

The importance of speciation in a water sample for understanding the toxicity, bioavailability, bioaccumulation and transport of a particular element has been previously evaluated.[1] Filtration with a 0.45 μm membrane filter is a universally applied first step to separate the particular element into the fractions termed dissolved and particulate.[1,2] Humic acid has been recognized to play an important role in the mobilization, transportation and immobilization of metals in water.[3] As iron is the most abundant heavy metal in water, the interactions between iron and humic acid have been widely investigated.[3–9] While the association of colloidal particles of iron hydroxide with humic substances and the existence of iron hydroxide coated with humic substances have been widely accepted,[1,7] the formation of dissolved complexes or chelates between the functional groups of the humic substances and iron has also been accepted as significant in order to keep the iron in solution.[3–5] The solubility of humic acid–iron complexes has been found to be dependent on the humic acid:iron ratio.[6] To understand the speciation of iron in water, it is important to study the effect of humic acid on the formation of filterable iron species which pass through a 0.45 μm membrane filter.

The aims of this work were to develop simple methods for the determination of humic acid and iron(III) at the hundred ppb level and to carry out fundamental studies of the interactions between humic acid and iron(III).

Experimental

Apparatus

A Shimadzu CS-920 chromatoscanner was used for the densitometric measurement of the resin-phase absorbance. The apparatus has the capacity to transform convex calibration graphs into linear graphs. A Hitachi-Horiba Type M-7$_{II}$ pH meter was also used. Toyo KG-25 and KG-47 filter holders with Toyo 0.45 μm membrane filters of cellulose nitrate and 0.40 μm Nucleopore filters were used for the filtration of the sample solution. A Toyo KG-25 filter holder with Toyo 0.65 μm membrane filters was used to collect the anion-exchange resin particles for the preparation of the thin-layer of resin.

Reagents

Unless stated otherwise, all reagents used were of analytical-reagent grade. Water, purified using an osmotic membrane, was distilled twice and used.[10]

Iron(III) standard solution, 1000 ppm, *pH* 1. Prepared from ammonium iron(III) sulphate dodecahydrate. A working solution, containing 10 μg ml^{-1} of iron, was prepared by dilution of the standard solution with dilute sulphuric acid, maintaining a pH of about 1.

Ammonium pyrrolidine dithiocarbamate (ammonium pyrrolidin-1-yldithioformate) (APDC) solution, 0.4% *m/v*.

Sodium acetate solution, 30% *m/v*.

Sodium perchlorate solution, 4 mol dm^{-3}.

Humic acid solutions. Humic acids obtained from Wako Pure Chemical and Nacalai-tesque were used as received. The sodium salt of humic acid obtained from Aldrich was converted to the acid form by precipitation from 0.1 mol dm^{-3} hydrochloric acid. About 0.1 g of each humic acid was accurately weighed and dissolved in 50 ml of a 0.1 mol dm^{-3} sodium hydroxide solution using sonication for 30 s. The pH was adjusted to between 6 and 7 by the addition of hydrochloric acid and the solution was then filtered using a 0.45 μm membrane filter of 47 mm diameter. As the filters clogged rapidly, four or five were required to filter 50 ml of the solution. The resultant filtrate was diluted to 500 ml with water. The used membrane filters were air-dried and the amount of residue on each weighed. The concentration of humic acid in the filtrate solution was determined by subtracting the residue on the filters.[11] The concentrations of humic acid solutions from Wako, Nacalai-tesque and Aldrich were 142, 120 and 158 ppm, respectively.

Anion-exchange resin suspension (ARS), 7.8 μequiv ml^{-1}. Prepared from a macro-reticular type Amberlyst A-27 resin in the chloride form according to the method reported.[10]

General Procedure for the Determination of Humic Acid in the Presence of Iron(III)

A 45 ml aliquot of an acidified sample solution (pH about 1.2) containing less than 80 μg of humic acid and less than 5.0 μg of iron(III) is placed in a 100 ml beaker. A 0.5 ml portion of 10 mmol dm^{-3} ethylenediaminetetraacetic acid (EDTA), 1.25 ml of 4 mol dm^{-3} sodium perchlorate and 2 ml of 30% sodium

acetate solutions are added successively. The final volume is adjusted to 50 ml with water. The pH of the resultant solution is 4.7. Then 1.3 ml of ARS are added to the solution and the mixture is stirred for 5 min. The resin particles are collected on a 0.65 μm membrane filter by filtration under suction and a circular thin-layer of approximately 17 mm diameter and 0.03 mm thick is prepared. The wet membrane filter holding the thin-layer of the anion-exchange resin is placed on a white plastic plate in the densitometer. The integrated absorbance of the humic acid concentrated in the resin phase is measured, with the use of the linearizer, at 470 and 600 nm by scanning the thin-layer over an area of 24 × 30 mm^2. The absorbance measured at 470 nm is used for the determination of humic acid; the absorbance measured at 600 nm is used as the blank value for the determination of iron(III), as described below.

General Procedure for the Determination of Iron(III) With APDC in the Presence of Humic Acid

The procedure for the determination of iron(III) as the APDC complex is the same as for the determination of humic acid, except that a 0.5 ml portion of 0.4% APDC is added to the sample solution in place of the EDTA solution, and the absorbance of the resultant coloured thin layer of the anion-exchange resin is measured at 600 nm. The net absorbance due to the iron(III)–APDC complex is determined by subtracting the blank value obtained in the presence of EDTA, as described above.

General Procedure to Study the Effect of Humic Acid on the Formation of Filterable Iron Species

A 45 ml aliquot of the sample solution containing 500 μl of the 10 ppm iron(III) solution and 1.25 ml of a 4 mol dm^{-3} sodium perchlorate solution is placed in a 100 ml beaker and various amounts of humic acid are added up to about 80 μg. The solution is then stirred for 1 min using a magnetic stirrer. A 0.3 ml aliquot of a 30% sodium acetate solution is added and the final volume adjusted to 50 ml with water, the pH value of the resultant solution being 5.6. After stirring for 1 min the solution is filtered through a 0.45 μm membrane filter of cellulose nitrate under suction from a water pump. The filter is then removed from the filter support and the support washed with 0.5 ml of 6 mol dm^{-3} hydrochloric acid and 5 ml of water. The washings are combined with the filtrate and the whole is allowed to stand for 30 min. Duplicate experiments are carried out to obtain a set of filtrates and then each filtrate is subjected to the determination of humic acid and iron(III).

Results and Discussion

Determination of Humic Acid

Humic acid has been determined by various methods, including ultraviolet/visible spectrophotometry,[3,6,8,9,12–14] fluorimetry,[15,16] chemiluminescence,[17] and thermal-lens spectrometry.[18] Of these, spectrophotometry has been the most widely used. As there are similarities in the absorption spectra of humic acid and iron(III) hydroxide, masking the effect of the iron[12] or removal of the iron altogether[14] is usually required before the determination of humic acid is possible. The simultaneous determination of iron and humic acid is carried out by measuring the absorbances at different wavelengths.[19]

In this paper, a method of determination based on the enrichment of humic acid with the use of a finely divided anion-exchange resin followed by the densitometric measurement of the resin-phase absorbance is proposed. The details of the method are studied according to the general procedure described under Experimental, both with and without the addition of iron(III).

Absorption spectra

Absorption spectra of humic acid collected in the resin phase showed an absorption maximum at 470 nm, as shown in Fig. 1, whereas, the absorbance of a humic acid solution obtained by the usual spectrophotometric method simply decreased with increasing wavelength in the visible range, no maximum being found in the spectrum.[3,19]

Effect of the amount of ARS

The effect of the amount of ARS was investigated according to the general procedure, with the addition of different amounts of ARS of up to 2.0 ml. With increasing amounts of added ARS, the absorbance of the resultant thin-layer of resin increased sharply and reached a maximum at 0.5 ml of ARS. The absorbance then gradually decreased with increasing amounts of added ARS; this was probably because the resultant thin-layer of resin became thicker than the effective optical path length.

Effect of pH

The absorbance of humic acid collected in the resin phase from solutions with various pH levels was found to increase slightly with increasing pH in the range studied (1.5–7.5) as reported.[13] The absorbance, however, was almost constant in the pH range 3.4–5.8. The pH of the solution for the determination of humic acid was, therefore, fixed at pH 4.7 and the determination of iron(III) with APDC was carried out at pH 4.7, as described later.

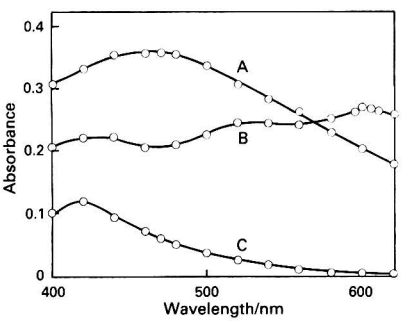

Fig. 1 Absorption spectra of humic acid and iron(III)–APDC complex in the thin layer of the anion-exchange resin: A, humic acid from Wako, 71.0 μg; B, iron(III)–APDC complex, iron(III) 5.00 μg; C, resin blank

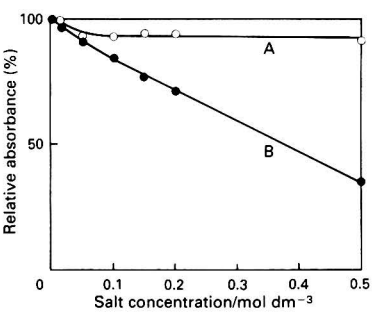

Fig. 2 Effect of salt concentration on the fixation of humic acid to the thin-layer of the anion-exchange resin. Humic acid (Wako), 71.0 μg; anion-exchange resin, Amberlyst A-27, 10.1 μequiv (1.3 ml of ARS of 7.8 μequiv ml^{-1}); sample volume, 50 ml. A, Sodium chloride; B, sodium perchlorate. The absorbance of the thin-layer of resin prepared without the addition of the salt was taken as 100%

Effect of sodium perchlorate

The effect of salt concentration on the resin-phase absorbance was investigated using sodium chloride and sodium perchlorate. While a constant absorbance was observed in the presence of sodium chloride in the range from 0.05 to 0.5 mol dm^{-3}, as shown in Fig. 2, it decreased markedly with increasing amounts of added sodium perchlorate. Consequently, it was clear that the fixing of humic acid was suppressed in the presence of the perchlorate ion. Although the adsorption of humic acid on the anion-exchange resin of styrene–divinylbenzene copolymer was reported to be irreversible,[12,21] the above results indicated that there was competition between the perchlorate ion and the anion of humic acid for the ion-exchange sites. The recovery could be improved by increasing the amount of added ARS to more than 1.3 ml, however, the use of large amounts of resin could result in the following disadvantages: firstly, a longer time period for the collection of the resin particles by filtration; and secondly, the decrease of the absorbance of the resultant thin-layer of resin with increasing thickness, as already described. As the interactions between iron(III) and humic acid were investigated in the presence of 0.1 mol dm^{-3} sodium perchlorate, the calibration graph for the determination of humic acid was prepared in the presence of 0.1 mol dm^{-3} sodium perchlorate in order to compensate for the recovery loss of humic acid due to the perchlorate ion.

Effect of sample volume

The recovery of humic acid was examined for various volumes of sample solution ranging from 30 to 100 ml, all containing 71.0 μg of humic acid from Wako in the presence of 0.1 mol dm^{-3} sodium perchlorate. A constant recovery of the humic acid was obtained from each of the different sample volumes.

Effect of iron(III)

The absorbance of the thin-layer of resin prepared from sample solutions containing a known amount of humic acid and various amounts of iron(III) was found to increase with increasing amounts of added iron(III); this is probably owing to the formation of iron(III) hydroxide and the iron(III) complex with humic acid.[19] The effect of iron(III) was successfully masked by the addition of EDTA. The resultant iron(III)–EDTA complex was not retained by the anion-exchange resin in the presence of 0.1 mol dm^{-3} perchlorate ion.

Calibration graph

A calibration graph was prepared for the determination of humic acid using the general procedure without the addition of iron(III). A graph showing good linearity was obtained for levels of up to about 80 μg of each humic acid. The regression lines of the calibration graph for the determination of humic acid from Nacalai-tesque, Wako and Aldrich were: $y = 1293x + 7558$; $y = 1125x + 7646$; and $y = 1056x + 7394$, respectively, where y is the integrated absorbance in arbitrary units including the blank value due to the anion-exchange resin, and x is the amount of humic acid in μg. The relative standard deviation (RSD) for 42.6 μg of humic acid from Wako was 3.2% ($n = 5$) and the limit of detection (LOD) was 1.3 μg, based on three times the standard deviation of the blank value. As stated above, the recovery of humic acid was independent of the sample volume for values of up to 100 ml, accordingly, the regression equation was valid for sample volumes of up to 100 ml.

Determination of Iron(III) With APDC

Ammonium pyrrolidine dithiocarbamate has been widely used as a solvent extraction reagent and a spectrophotometric reagent for copper and other metals.[22,23] Iron(III) was reported to form a black precipitate of $Fe(PDC)_3$ on reaction with APDC.[22] The determination of iron with APDC by thin-layer spectrophotometry has already been reported,[24] but the details of the method were not revealed. The details of the method are according to the general procedure described above, both with and without addition of humic acid.

Absorption spectrum

The absorption spectrum of the iron(III)–APDC complex in a thin-layer of the anion-exchange resin showed a small maximum at about 600 nm, while the absorbance spectrum of the blank thin-layer decreased with increasing wavelength, as shown already in Fig. 1. Accordingly, the subsequent measurements were carried out at 600 nm.

Effect of amount of ARS

The effect of the amount of ARS on the absorbance of the iron(III)–APDC complex in the resultant thin-layer of the anion-exchange resin was examined with the addition of various amounts of ARS up to 2.0 ml. Although the iron(III)–APDC complex could be collected on the membrane filter directly, without the addition of the anion-exchange resin, reproducible absorbance was only obtained by fixing the complex in the thin-layer of the anion-exchange resin. The resin-phase absorbance increased with increasing amounts of added ARS, up to 0.5 ml and then gradually decreased. The increase in the absorbance with increasing amounts of added ARS, up to 0.5 ml, was probably because the optical path-length would be increased with the increasing thickness of the resultant thin-layer. The decrease in the absorbance with increasing amounts of added ARS, above 0.5 ml, was probably because the resultant thin-layer became thicker than the optical path-length. These tendencies are characteristic of absorption measurements by densitometry. When the absorbance is measured with the use of a conventional spectrophotometer it increases with increasing thickness of the thin-layer.

Effect of pH

The effect of pH on the absorbance of the iron(III)–APDC complex was studied according to the general procedure described above, in the pH range 1.3–6.9. The absorbance of the complex in the thin-layer of the anion-exchange resin was found to be constant and maximum in the pH range 3.0–5.5, as was observed in the extraction of the iron(III)–APDC complex with 2,6-dimethylheptan-4-one.[25]

Effect of sodium perchlorate

The absorbance of the iron(III)–APDC complex in the thin-layer of the anion-exchange resin showed a constant and maximum value in the presence of sodium chloride or sodium perchlorate in the range 0.05–1.0 mol dm^{-3}.

Effect of sample volume

The effect of sample volume on the fixing of iron(III), as the APDC complex, to the anion-exchange resin was examined with various sample volumes ranging from 20 to 100 ml. The recovery of iron was independent of the sample volume studied. Hence, the calibration graph was valid for sample volumes of less than 100 ml. The sensitivity of the densitometric determination of iron with bathophenanthrolinedisulphonate (BPS)[26] is higher than with the proposed method, but the reduction of iron(III) to iron(II) is essential before the colour producing reaction with BPS can occur.

Effect of foreign ions

The effect of iron(II), copper(II), nickel(II), cobalt(II) and zinc(II) on the determination of 3.0 μg of iron(III) was examined. The results are summarized in Table 1. Iron(II) was

Table 1 Effect of foreign ions on the determination of iron(III). Amount of iron(III), 3.00 μg; sample volume, 50 ml

Ion	Amount added/μg	Iron(III) found*/μg	Error (%)
Fe^{II}†	3.00	2.99	−0.3
Cu^{II}	3.00	2.86	−4.6
	1.00	2.98	−0.7
Ni^{II}	3.00	2.81	−6.3
	1.00	3.08	2.7
Co^{II}	3.00	3.03	1.0
	1.00	2.98	−0.7
Zn^{II}	6.00	3.08	2.7
	3.00	2.95	−1.7

* Results of duplicate determinations.
† In the presence of hydroxylamine hydrochloride.

Table 2 Effect of humic acid on the determination of iron(III)

Amount of iron(III)/μg	Humic acid added*/μg	Iron found/μg	Number of experiments
2.00	14.2	2.06	2
	42.6	2.00	2
	71.0	2.08	2
		Mean 2.05	6
		SD† 0.21	
5.00	14.2	5.10	3
	42.6	5.11	3
	71.0	5.02	2
		Mean 5.08	8
		SD 0.09	

* Humic acid from Wako.
† SD = standard deviation.

found to react with APDC in a similar manner to iron(III). Consequently, in the presence of iron(II) the total amount of iron can be determined. A small negative error was observed in the presence of the same amount of copper(II) and nickel(II), however, the concentrations of these ions in common water samples are much lower than that of iron(III).[27]

Effect of humic acid

In the presence of humic acid, the sum of the absorbances from the iron(III)–APDC complex and humic acid was measured at 600 nm. The absorbance of humic acid was measured with the use of another aliquot of the sample solution after masking the iron(III) with the EDTA complex and the difference calculated. The effect of humic acid was thus effectively eliminated, as shown in Table 2.

Calibration graph

The calibration graph for the determination of iron(III) was prepared according to the general procedure without the addition of humic acid. The calibration graph showed good linearity, the correlation coefficient (r) being 0.9998 in the concentration range 1.0–5.0 μg of iron(III). The regression equation of the calibration graph was $y = 21878x - 4774$, where y is the net value of the integrated absorbance in arbitrary units and x the amount of iron(III) in μg. For the determination of less than 1.0 μg of iron(III) the regression equation of $y = 17969x$ was used. The RSD for 4.0 μg of iron(III) was 2.4% ($n = 5$) and the LOD was 0.06 μg, based on three times the standard deviation of the blank value.

Absorption of Iron(III) on the Membrane Filter

Effect of pH on the formation of iron(III) hydroxide

The effect of pH on the formation of the filterable iron(III) species was investigated by the use of a 0.45 μm membrane filter of cellulose nitrate. The solution pH was adjusted with the use of sodium hydroxide and dilute hydrochloric acid solutions. The amount of iron(III) in the filtrate was determined by the proposed method and plotted against the pH of the filtrate, as shown in Fig. 3. Iron(III) was almost quantitatively collected on the membrane filter as a pale yellow precipitate from solutions in the pH range of about 6–10. The results of the calculation to estimate the effect of pH on the formation of iron(III) hydroxide are also illustrated in Fig. 3. There were good similarities between the pH dependence of the formation of iron(III) hydroxide and the adsorption of iron(III) on to the membrane filter.

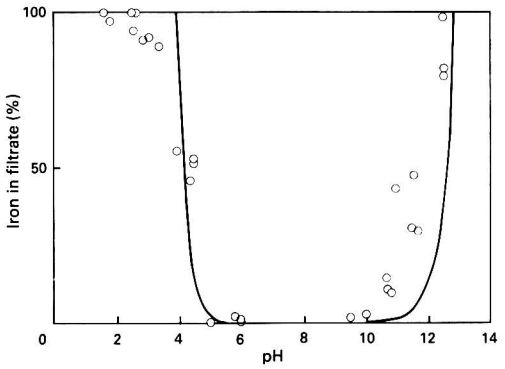

Fig. 3 Effect of pH on the adsorption of iron on to a 0.45 μm membrane filter of cellulose nitrate from 50 ml of solution containing 5.00 μg of iron(III) and 0.1 mol dm^{-3} sodium perchlorate. Solid line indicates the theoretical curve for the formation of iron(III) hydroxide. The following equilibria and the stability constants were used for the calculation, the ionic strength being 0.1 mol dm^{-3}[20]

$Fe(OH)_3(s) = Fe(OH)^{2+} + 2OH^-$ $\log K_{s1} = -26.16$
$Fe(OH)_3(s) = Fe(OH)_2^+ + OH^-$ $\log K_{s2} = -16.74$
$Fe(OH)_3(s) + OH^- = Fe(OH)_4^-$ $\log K_{s4} = -5$
$2Fe(OH)_3(s) = Fe_2(OH)_2^{4+} + 4OH^-$ $\log K = -50.8$

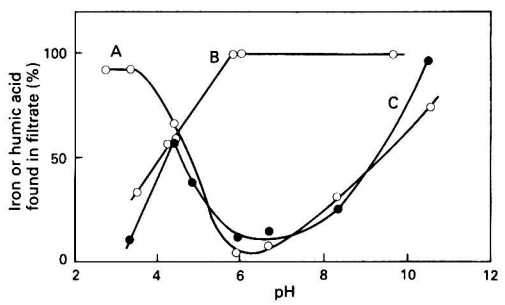

Fig. 4 Effect of pH on the fixing of the humic acid and iron on to the 0.45 μm membrane filter of cellulose nitrate. Amount of iron(III), 5.00 μg; amount of humic acid (Wako), 14.2 μg; sample volume, 50 ml. A, Adsorption of iron(III) in the presence of humic acid; B, adsorption of humic acid in the absence of iron(III); C, adsorption of humic acid in the presence of iron(III)

Effect of pH on the adsorption of humic acid on the membrane filter

The effect of pH on the adsorption of humic acid on to the membrane filter of cellulose nitrate was examined both in the absence and presence of iron(III). The solution pH was adjusted with the use of hydrochloric acid, sodium acetate, ammonium acetate and sodium hydroxide solutions. Humic acid was not retained by the membrane filter from solutions with a pH of above about 6, as shown in Fig. 4. In the presence of iron(III), however, some of the humic acid became fixed on to the membrane filter together with iron(III) above about pH

4.5. As the solution pH increased above 8, most of the humic acid added appeared in the filtrate together with iron(III). When each sample solution of different pH was allowed to stand for 20 min before the filtration, no significant difference was found in the pH dependence of the formation of the filterable iron species in the presence of humic acid. It was safely concluded that there are strong interactions between iron(III) and humic acid above about pH 4.5.

Effect of humic acid concentration

The effect of the concentration of humic acid on the formation of the filterable iron(III) species was examined at pH 5.6 and 8.4, respectively. The results obtained with the use of humic acid from Nacalai-tesque are shown in Fig. 5. Until the added amount of humic acid reached a certain level, both iron and humic acid were not found in the filtrate, however, after that, the amount of filterable iron(III) species was found to increase with increasing added amount of humic acid and then reached a constant and maximum value. Almost the same results were obtained at pH 8.4 except that the plot was shifted to the left of that obtained at pH 5.6. As it was postulated that the iron found in the filtrate was accompanied by a fixed amount of humic acid (as shown in Table 3) it was expected that the complexation between iron(III) and humic acid occurred in a fixed molar ratio. Assuming the formation of a 1 : 1 complex, the relative molecular mass of humic acid could be calculated, as shown in Table 3, in which the results obtained with humic acids from Wako and Aldrich are also included. Among the humic acids examined, that of Aldrich was found to be most effective for the formation of the filterable iron(III) species; in the presence of about twice the amount of humic acid over 5 μg of iron(III), more than 90% of the iron was converted to the filterable species. As the average relative molecular mass of humic acid was estimated to be in the range 600–1000,[28] the formation of iron–humic acid complexes with molar ratios of 2 : 1 and 3 : 1 could also be expected.[3]

Effect of other complexing agents

The effect of complexing agents, other than humic acid, on the formation of the filterable iron(III) species was also examined at pH 5.6. As expected, nitrilotriacetic acid (NTA) was found to react with iron(III) to form a filterable 1 : 1 complex, as shown in Fig. 6. On the other hand, citrate, tartrate and pyrophosphate ions were much more effective than NTA, even when they were present at less than the stoichiometric amounts required for the formation of a 1 : 1 complex with iron(III), as considerable amounts of iron(III) were found in the filtrate. The effect of standing time on the formation of a filterable iron(III) species was examined with the use of 50 ml portions of a sample solution containing 5.0 μg (89.5 nmol) of iron(III) and 20 nmol of pyrophosphate. The amount of iron in the resultant filtrate was independent of standing time for up to 30 min. Accordingly, it was assumed that citrate, tartrate and pyrophosphate ions react with iron(III) to form filterable complexes in which the molar ratio of iron to each ligand

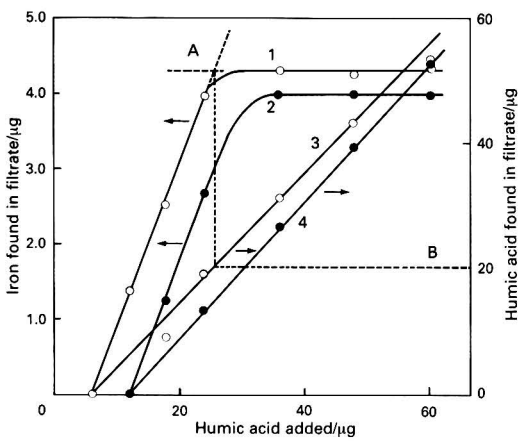

Fig. 5 Effect of humic acid concentration on the formation of the filterable iron(III) species: A, the maximum amount of iron(III) in the filtrate; B, humic acid in the filtrate which is expected to be complexed with iron(III) of A. 1 and 3, pH 8.4; and 2 and 4, pH 5.6. Initial amount of iron(III), 5.00 μg; sample volume, 50 ml; ionic strength, 0.1 mol dm^{-3}; and membrane filter, 0.45 μm cellulose nitrate

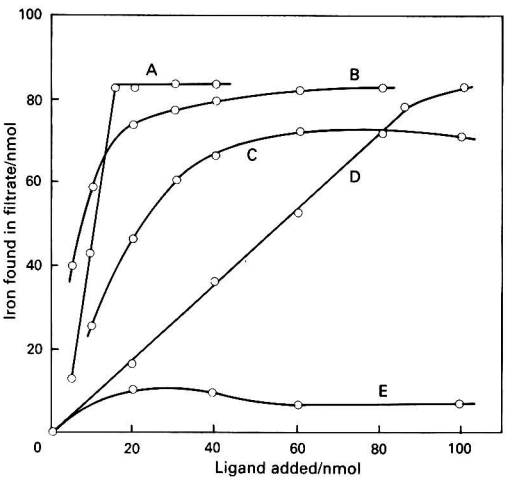

Fig. 6 Effect of complexing agents on the formation of the filterable iron(III) species: A, sodium pyrophosphate; B, sodium citrate; C, sodium tartrate; D, NTA; and E, sodium oxalate. pH 5.6, other conditions as in Fig. 5

Table 3 Results for the determination of iron and humic acid in 50 ml portions of sample solution containing 5.00 μg of iron(III) and various amounts of humic acid after filtration (see Fig. 5)

Source of humic acid	pH	Amount of iron in A*/μg	Amount of humic acid in B*/μg	Ratio of B to A	Relative molecular mass of humic acid†
Aldrich	5.6	4.53	12.0	2.6	142
	8.4	4.54	11.4	2.5	140
Nacalai-tesque	5.6	4.00	19.0	4.8	268
	8.4	4.29	20.3	4.7	262
Wako	5.6	3.25	18.4	5.7	318
	8.4	3.96	22.1	5.6	313

* A and B areas found in Fig. 5.

† The formation of a 1 : 1 iron–humic acid complex was assumed.

exceeded 1. However, oxalate, acetate and phosphate ions were not effective for the formation of filterable iron(III) species. More than 20 μmol of phosphate ion and 4.5 mmol of acetate ion were required for the conversion of 5.0 μg of iron(III) to the filterable species.

Effect of Sample Volume on the Determination of Filterable Iron(III)

The effect of sample volume on the determination of the filterable iron(III) species was examined in the presence of humic acid. The 50 ml portions of sample solution of pH 5.6, containing 5.0 μg of iron(III) and 35 μg of humic acid from Nacalai-tesque, were prepared and filtered successively through a 0.45 μm membrane filter of cellulose nitrate, with diameters of 25 and 47 mm, and a 0.4 μm Nucleopore filter with a 25 mm diameter under suction. The amount of iron(III) in each filtrate decreased throughout the number of filtration runs as shown in Fig. 7. As already shown in Fig. 4, about 20% of the iron(III) was fixed on to the membrane filter together with the humic acid from the 50 ml of sample solution, and consequently, the filter may be clogged with the particulate iron(III) species during successive filtrations. A marked decrease in iron(III) concentration in the filtrate was observed when a sample of water was filtered with the use of a Nucleopore filter.[2] A membrane filter of 47 mm diameter was much better than that of 25 mm diameter for preparation for the determination of filterable iron(III) species. The experiments were also carried out in the presence of citrate, tartrate, nitrilotriacetate and pyrophosphate ions. Each complexing agent was added to the sample solution such that a part of iron(III) was converted to the filterable species and the remainder was present as the particulate hydroxide. With the addition of citrate, tartrate and nitrilotriacetate ions the concentration of iron(III) in the resultant filtrate was constant regardless of filtered sample volumes for volumes of up to 400 ml (8 filtration runs). In the presence of pyrophosphate, however, the concentration of iron in the filtrate decreased with an increasing number of filtration runs, as was observed in the presence of humic acid.

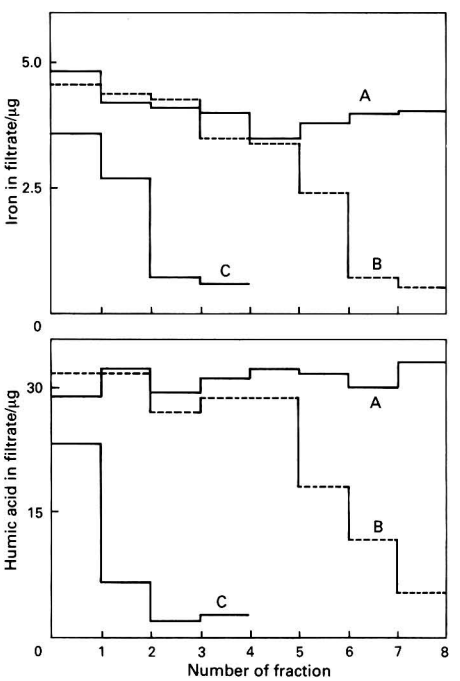

Fig. 7 Effect of filtration on the determination of the filterable iron(III) species and humic acid. Membrane filters used were; A, 0.45 μm cellulose nitrate of 47 mm diameter; B, 0.45 μm cellulose nitrate of 25 mm diameter; and C, 0.40 μm Nucleopore of 25 mm diameter. Initial amount of iron(III), 5.00 μg; and humic acid (Nacalai-tesque), 36.0 μg. Amount of each fraction, 50 ml

Determination of Iron and Humic Substances in River-water

An aliquot of a river-water sample was divided into 50 ml portions, and each portion was filtered successively through a 0.45 μm membrane filter of cellulose nitrate, of 47 mm diameter, within 3 h of sampling. Another series of filtrates was prepared with the use of a fresh membrane filter. A series of sets of filtrates was thus prepared. Each set of filtrates was then subjected to the procedure for the determination of iron and humic acid. Coloured species in each filtrate collected in the resin phase were determined as for humic acid with the use of a calibration graph prepared from the Aldrich humic acid. The results are shown in Table 4 (the results obtained for a tap-water sample are included for comparison). The amount of iron in each 50 ml filtrate of the river-water sample was almost constant for 6 filtration runs. As the total concentration of iron was found to be 81 ppb (Table 5), it was concluded that 85% of the iron in the river-water was from particulate species and 15% from filterable species. However, the classification of iron in the tap-water sample was meaningless because the concentrations of the filterable iron and therefore the particu-

Table 4 Effect of filtration on the determination of filterable iron and humic substances in river- and tap-water samples. The 50 ml portions of the water samples were successively filtered through a 0.45 μm membrane filter of 47 mm diameter

	River water*		Tap-water‡
Number of filtration runs	Iron found (ppb)	Humic substances found† (ppb)	Iron found (ppb)
1	11.2	75	24.1
2	12.2	87	8.5
3	11.3	82	0.0
4	12.8	81	0.0
5	13.3	82	—
6	12.3	88	—
7	9.3	70	—
8	10.0	77	—
9	7.6	70	—
10	5.4	54	—

* Collected from a tributary of the Iwaki river.

† Calibration graph prepared with the humic acid obtained from Aldrich was used.

‡ Collected after running for more than 30 min. The total concentration of iron was 102.4 ± 4.0 ppb (n = 6).

Table 5 Results of the determination of iron and humic substances in river-water

	Iron		Humic substances*	
River-water	Total (ppb)	Filterable (ppb)	Total (ppb)	Filterable (ppb)
A†	81.0 ± 1.6 n = 6	12.4 ± 0.7 n = 5	126 ± 7 n = 6	84 ± 3 n = 5
B	185.4 ± 3.1 n = 6	17.3 ± 0.7 n = 5	126 ± 3 n = 3	13 ± 2 n = 4

* Humic acid from Aldrich was taken as the standard.

† River-water A is a tributary of the Iwaki river B.

late iron were dependent on how much of the tap-water was filtered. The results also indicated that the hydroxide might be the predominant iron species in tap-water. The classification of humic substances in the river-water sample into filterable and particulate species was significant, as a constant amount of humic substances was found in the filtrate, see Table 4.

For the determination of the total concentration of iron, the water sample was acidified to pH 1.2 and filtered through a 0.45 μm membrane filter of cellulose nitrate of 47 mm diameter. On the other hand, the determination of total humic substances was carried out as follows. A 1 l portion of the water sample was acidified to pH 1.2 and 2.0 ml of 0.1 mol dm^{-3} EDTA solution were added. The solution was allowed to stand for 2 h, after which the pH was adjusted to approximately 11 by the addition of sodium hydroxide and the resultant solution was filtered through a 0.45 μm membrane filter. The pH of the filtrate was adjusted to 4.7 and the coloured species in the filtrate determined as described previously. The results are summarized in Table 5. The total concentration of humic acid in the river-waters was found to be almost the same, whereas a significant difference was found between the concentrations of filterable iron(III) species in each water.

Conclusion

Simple and sensitive methods for the determination of iron and humic acid have been developed and the effects of humic acid and other complexing agents, such as citrate, tartrate, pyrophosphate and nitrilotriacetate ions, on the formation of filterable iron(III) species were investigated. These ligands were found to be effective for the formation of filterable iron species. Except for the nitrilotriacetate ion which formed a 1 : 1 complex with iron(III), the formation of iron-rich complexes in which the molar ratio of iron to each ligand exceeded 1 was demonstrated. The total amount of iron and humic substances found in the river-waters examined could be classified into their respective filterable and particulate species.

References

1 Florence, T. M., *Talanta*, 1982, **29**, 345.
2 Lexen, D. P. H., and Chandler, I. M., *Anal. Chem.*, 1982, **54**, 1350.
3 Schnitzer, M., *Humic Substances in the Environment*, Marcel Dekker, New York, 1972, pp. 54 and 230.
4 Rashid, M. A., and Leonard, J. D., *Chem. Geol.*, 1973, **11**, 89.
5 Perdue, E. M., Beck, K. C., and Reuter, J. H., *Nature (London)*, 1976, **260**, 418.
6 Picard, G. L., and Felbeck, G. T., Jr., *Geochim. Cosmochim. Acta*, 1976, **40**, 1347.
7 Moore, R. M., Burton, J. D., Williams, P. J., and Yound, M. L., *Geochim. Cosmochim. Acta*, 1979, **43**, 919.
8 Tipping, E., *Geochim. Cosmochim. Acta*, 1981, **45**, 191.
9 Hiraide, M., Ishii, M., and Mizuike, A., *Anal. Sci.*, 1988, **4**, 605.
10 Ohzeki, K., Minorikawa, M., Yokota, F., Nukatsuka, I., and Ishida, R., *Analyst*, 1990, **115**, 23.
11 Hiraide, M., Tillekeratne, S. P., Otsuka, K., and Mizuike, A., *Anal. Chim. Acta*, 1985, **172**, 215.
12 Nagayama, M., Goto, K., and Yotsuyanagi, T., *Kogyo-Yosui*, 1963, (61), 24.
13 Hiraide, M., Arima, Y., and Mizuike, M., *Anal. Chim. Acta*, 1987, **200**, 171.
14 Nomizu, T., Sanji, M., and Mizuike, A., *Anal. Chim. Acta*, 1988, **211**, 293.
15 Almgren, T., Josefsson, B., and Nyquist, G., *Anal. Chim. Acta*, 1975, **78**, 411.
16 McCrum, W. A., *Anal. Proc.*, 1986, **23**, 307.
17 Marino, D. F., and Ingle, J. D., Jr., *Anal. Chim. Acta*, 1981, **124**, 23.
18 Power, J. F., and Langford, C. H., *Anal. Chem.*, 1988, **60**, 842.
19 Carpenter, P. D., and Smith, J. D., *Anal. Chim. Acta*, 1984, **159**, 299.
20 Snoeyink, V. L., and Jankins, D., *Water Chemistry*, Wiley, New York, 1980, pp. 264–267.
21 Miles, C. J., Tsuchall, J. R., Jr., and Brezonik, P. L., *Anal. Chem.*, 1983, **55**, 410.
22 Shindo, E., and Morito, M., *Kagaku no Ryoiki*, 1966, **21**, 206.
23 Cheng, K. L., Ueno, K., and Imamura, T., *Handbook of Organic Analytical Reagents*, CRC Press, Boca Raton, FL, 1982, p. 397.
24 Ohzeki, K., Toki, C., Ishida, R., and Saitoh, T., *Analyst*, 1987, **112**, 1689.
25 Bone, K. M., and Hibbert, W. D., *Anal. Chim. Acta*, 1979, **107**, 219.
26 Shriadah, M. M. A., and Ohzeki, K., *Analyst*, 1986, **111**, 555.
27 Martin, J.-M., and Mwybeck, M., *Mar. Chem.*, 1979, **7**, 173.
28 Wilson, M. A., Vasallo, A. M., Perdue, E. M., and Reuter, J. H., *Anal. Chem.*, 1987, **59**, 551.

Paper 0/02346I
Received May 25th, 1990
Accepted October 19th, 1990

Extraction–Spectrophotometric Determination of Sulphur Dioxide

N. Balasubramanian and B. S. M. Kumar
Department of Chemistry, Indian Institute of Technology, Madras-600 036, India

A sensitive spectrophotometric method for the determination of trace amounts of sulphur dioxide after fixing in a modified buffered formaldehyde solution is described. The reaction of iodate with sulphur dioxide in the presence of acid and excess of chloride leads to the formation of ICl which is stabilized as the ICl_2^- ion. The species formed reacts with 2′,7′-dichlorofluorescein to form 2′,7′-dichloro-4′,5′-diiodofluorescein and is extracted into a solvent mixture of 15% isopentyl acetate in isopentyl alcohol. The colour system obeys Beer's law in the range 0–40 μg of sulphur dioxide. The relative standard deviation is 3.5% for ten determinations of 15 μg of sulphur dioxide. The effect of interfering gases on the determination is discussed. The method has been applied to the determination of sulphur dioxide at low concentrations and the results obtained were compared with the widely used pararosaniline method. The method can be used to determine as low as 2 μg of sulphur dioxide.

Keywords: *Sulphur dioxide; 2′,7′-dichlorofluorescein; spectrophotometry; gas analysis; gas permeation device*

Air pollution due to sulphur dioxide has arisen mainly as a consequence of the widespread use of sulphur and its compounds in manufacturing and industrial processes and the increased use of fossil fuels as a source of energy. It has been estimated that the combustion of coal and petroleum products contributes 70 and 16%, respectively, to man-made sulphur dioxide pollution.[1] As the presence of sulphur dioxide in ambient air is known to be a health hazard, the development of analytical methods for its determination has attracted considerable attention.

The pararosaniline method,[2] after absorbing sulphur dioxide in 0.1 mol dm^{-3} tetrachloromercurate (TCM) solution, has been widely used for the colorimetric determination of sulphur dioxide in the atmosphere, because of its simplicity, sensitivity and specificity. However, the analysis must be carried out carefully with close attention to temperature, pH and dye purity.[3] Further, the TCM absorbent has some disadvantages, *e.g.*, the use of highly toxic and expensive mercury(II) chloride and the instability of the complex.[4] In order to overcome these disadvantages, Dasgupta *et al.*[5] advocated the use of a buffered formaldehyde solution for trapping sulphur dioxide. The trapped sulphur dioxide is stable for about 30 d without appreciable loss of fixed sulphur dioxide.

A highly sensitive method for the determination of sulphur dioxide, after trapping it in a buffered formaldehyde absorber solution, has been reported by Selvapathy *et al.*[6] The reaction of sulphur dioxide with iodate in an acidic medium containing chloride ions to produce ICl_4^- ions, formed the basis of their method. The ICl_4^- formed an ion pair with pyronine G and was extracted into benzene for spectrophotometric measurement at 535 nm. This approach, however, has the disadvantage of a high blank value and poor colour stability (10 min after extraction into benzene).

This paper describes the study and evaluation of the variables which govern the interaction of the ICl, generated by the reaction between iodate and sulphur dioxide, with 2′,7′-dichlorofluorescein in order to provide the basis for a selective and sensitive spectrophotometric method for the determination of sulphur dioxide.

Experimental

Apparatus

Absorbance measurements were made by using a Carl Zeiss PMQ II spectrophotometer with 10 mm quartz cells. Fritted glass bubblers with suitable suction devices were used for trapping sulphur dioxide from air. The air flow-rate was measured using a rotameter.

Reagents

All chemicals used were of analytical-reagent grade and distilled water was used for preparing the reagent solutions.

Standard sulphur dioxide solution, 350 μg ml^{-1}. Prepared by dissolving 0.4 g of anhydrous sodium sulphite in 500 ml of water and standardizing iodimetrically.[7] A suitable volume of this solution was diluted using a 7 mmol dm^{-3} solution of formaldehyde to give a solution containing 5 μg ml^{-1} of sulphur dioxide. This solution remained stable for at least 1 month.

Potassium iodate, 0.4% *m/v*.

Sodium chloride, 6% *m/v*.

Sulphamic acid, 2.5% *m/v*.

Mercury(II) *chloride*, 0.03% *m/v*.

Sodium hydroxide, 4.5 *and* 4 mol dm^{-3}.

The above solutions were prepared by dissolving appropriate amounts of the reagent in water.

2′,7′-*Dichlorofluorescein solution*, 0.01% *m/v*. Prepared by dissolving 0.1 g of the dye in 4 ml of 1 mol dm^{-3} sodium hydroxide and diluting to 1 l with water.

Acetate–acetic acid buffer (*pH* 6.20). Prepared by dissolving 29.6 ml of glacial acetic acid in about 200 ml of water. The pH was adjusted to 6.2 by the addition of ammonia solution using a pH meter. The solution was diluted to 250 ml with water.

Buffered formaldehyde trapping solution. Prepared by diluting 500 μl of formaldehyde solution, 1.36 g of sodium acetate trihydrate and 600 μl of glacial acetic acid to 1 l with water. The solution was 7 mmol dm^{-3} in formaldehyde and 10 mmol dm^{-3} in sodium acetate and acetic acid and had a pH of 4.76 at 25 °C.

Sulphuric acid, 4.25 mol dm^{-3}. Prepared by diluting 236.1 ml of sulphuric acid (sp.gr. 1.84) to 1 l with water.

Isopentyl acetate–isopentyl alcohol mixture, 15% *v/v*. Prepared by diluting 15 ml of isopentyl acetate to 100 ml with isopentyl alcohol.

Procedure

Sampling

Air samples were collected by drawing 10–100 l of air through a fritted glass bubbler containing 15 ml of buffered formaldehyde trapping solution for a period of 20–200 min at a rate of

0.5 l min^{-1}. The volume of the solution was made up to 50 ml with the trapping solution prior to determination.

Determination

Into a 50 ml calibrated flask were placed 5 ml of potassium iodate, 2 ml of 0.01% 2′,7′-dichlorofluorescein, 1 ml of 6% sodium chloride and 1 ml of 4.25 mol dm^{-3} sulphuric acid. A 15 ml aliquot of the buffered formaldehyde trapping solution containing not more than 40 μg of sulphur dioxide (fixed as the hydrogen sulphite addition compound) was treated with 1 ml of 4.5 mol dm^{-3} sodium hydroxide, used to decompose the complex. The solution was then introduced into the 50 ml calibrated flask through a long-stemmed funnel with the tip kept well immersed in the reagent solution to avoid the loss of sulphur dioxide. The solution was made up to about 40 ml with water, mixed thoroughly and allowed to stand for 5 min. Then, 1 ml of 4 mol dm^{-3} sodium hydroxide and 5 ml of acetate buffer (pH 6.20) were added and the solution was diluted to 50 ml with water and mixed thoroughly. It was then transferred into a 125 ml separating funnel and extracted with 5 ml of a solvent mixture containing 15% isopentyl acetate in isopentyl alcohol for 1 min. The organic layer was separated and transferred into a test-tube and treated with about 1 g of anhydrous sodium sulphate to remove trace amounts of water. The absorbance of the organic extract was measured at 535 nm in 10 mm cells against a reagent blank which was taken through the entire procedure. The concentration of sulphur dioxide was established by reference to a calibration graph which was prepared by treating 0–8 ml of standard sulphur dioxide solution (containing 0–40 μg of sulphur dioxide) with 15 ml of the buffered formaldehyde trapping solution and following the procedure described above.

Results and Discussion

Preliminary studies were carried out using 5 ml of a solution of 0.4% potassium iodate, 1 ml of 6% sodium chloride and 2 ml of 0.01% 2′,7′-dichlorofluorescein. The resulting solution was treated with 15 μg of sulphur dioxide (fixed as the hydrogen sulphite addition compound) in 15 ml of buffered formaldehyde trapping solution, after treating it with 1 ml of 4.5 mol dm^{-3} sodium hydroxide solution, used to decompose the formaldehyde–hydrogen sulphite complex.[5] After allowing it to stand for 5 min, the solution was treated with 1 ml of 4 mol dm^{-3} sodium hydroxide and 5 ml of acetate buffer and diluted to 50 ml with water. The solution was transferred into a 125 ml separating funnel and extracted for 1 min using a solvent mixture containing 15% isopentyl acetate in isopentyl alcohol. The result indicated that the extraction of the iodinated product into the solvent mixture was fairly selective as the absorbance of the blank at 535 nm was low and that of the sample was high (Fig. 1).

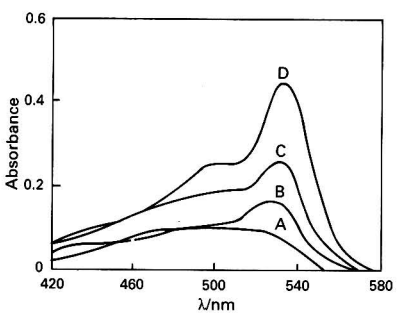

Fig. 1 Absorption spectra measured against solvent blank. A, Reagent; B, SO_2 (7.5 μg); C, SO_2 (15 μg); and D, SO_2 (30 μg)

The optimum acidity for the formation of the ICl_2^- species for subsequent reaction with 2′,7′-dichlorofluorescein to form 2′,7′-dichloro-4′,5′-diiodofluorescein was first established. A constant and maximum absorbance was obtained when the acidity of the reaction medium was greater than 0.04 mol dm^{-3}. Subsequent studies were carried out using solutions maintained at 0.05 mol dm^{-3} for the formation of 2′,7′-dichloro-4′,5′-diiodofluorescein.

Although the reaction was carried out in acidic medium for the formation of the dichlorodiiodo compound, the control of pH was essential for the selective extraction of 2′,7′-dichloro-4′,5′-diiodofluorescein. Different buffer solutions were investigated for the selective extraction and the optimum pH for the extraction was found to be in the range 6.0–6.4. This could be achieved by the use of 5 ml of acetate buffer (pH 6.20).

Similar studies revealed that 2.5 ml of 0.4% potassium iodate, 1 ml of 0.01% 2′,7′-dichlorofluorescein and 0.5 ml of 6% sodium chloride solution were sufficient to provide a constant and maximum absorbance.

The formation of 2′,7′-dichloro-4′,5′-diiodofluorescein was found to be almost instantaneous and mixing the phases for about 30 s was found to be sufficient for its quantitative extraction into the isopentyl acetate–isopentyl alcohol solvent mixture. The colour system, after extraction, was found to be stable for 1 h after which a gradual decrease in absorbance was observed.

A variety of solvents were investigated for the selective extraction of 2′,7′-dichloro-4′,5′-diiodofluorescein. In solvents such as benzene, hexane, isobutyl methyl ketone (IBMK), diisopropyl ether and isopentyl acetate, the absorbance values for the blank and sample were found to be almost zero. In solvents such as butan-1-ol, propan-2-ol and isopentyl alcohol, the absorbance values of the blank and sample were both very high. Hence solvent mixtures such as benzene–propan-2-ol, IBMK–propan-2-ol, acetone–butan-1-ol, IBMK–butan-1-ol, benzene–isopentyl alcohol, IBMK–isopentyl alcohol, benzene–acetone, IBMK–acetone and isopentyl acetate–isopentyl alcohol were investigated as extracting solvents. Binary mixtures of benzene with acetone, propan-2-ol, butan-1-ol and isopentyl alcohol produced high blank values. Similar results were obtained with the binary mixtures of IBMK with acetone, propan-2-ol, butan-1-ol and isopentyl alcohol. Only a solvent mixture consisting of isopentyl acetate and isopentyl alcohol proved to be satisfactory, as the extraction of the iodinated compound was found to be selective and maximum only in this instance, with low blank values. Constant absorbance was observed when the concentration of isopentyl acetate was in the range 10–19% in isopentyl alcohol. Above 19% of isopentyl acetate, the absorbance of the sample showed a gradual decrease while below 10% of isopentyl acetate an increase in the blank absorbance was observed. Hence, studies were carried out by extracting 2′,7′-dichloro-4′,5′-diiodofluorescein into 5 ml of a solvent mixture containing 15% of isopentyl acetate in isopentyl alcohol.

A linear calibration graph was obtained over the range 0–40 μg of sulphur dioxide. The precision of the proposed method was confirmed by establishing the concentration of ten samples containing 15 μg of sulphur dioxide. The mean recovery was found to be 14.5 μg with a relative standard deviation of 3.5%.

Nature of the Extracted Species

The formation of 2′,7′-dichloro-4′,5′-diiodofluorescein from 2′,7′-dichlorofluorescein under the experimental conditions described and the extraction of the former into the solvent mixture is responsible for the observed colour. The formation of the diiodo compound can be explained on the basis of the iodination of the dichloro compound as a result of the reaction

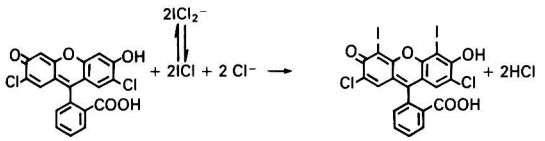

2′,7′-Dichlorofluorescein 2′,7′-Dichloro-4′,5′-diiodofluorescein

Fig. 2 Species responsible for the colour system

of potassium iodate with sulphur dioxide in acidic medium, to generate iodine in accordance with equation (1).

$$2IO_3^- + 5SO_2 + 2H^+ \rightarrow I_2 + 5SO_3 + H_2O \quad (1)$$

$$5SO_2 \equiv I_2$$

(320.31 μg of $SO_2 \equiv 253.81$ μg of I_2)

When experiments were carried out to iodinate 2′,7′-dichlorofluorescein using stoichiometric amounts of iodine solution (prepared by equilibrating solid iodine with water in the absence of iodide) in acidic medium, a very low absorbance (0.004 A) was obtained indicating that the iodination reaction was not taking place as expected. However, when the same reaction was carried out in the presence of potassium iodate and a stoichiometric amount of iodine, a high absorbance (0.195 A, for 11.88 μg of $I_2 \equiv 15$ μg of SO_2) was observed. This observation can be explained by the fact that the reaction of iodine with iodate in an acidic medium leads to the formation of ICl which is stabilized as ICl_2^- in the presence of chloride ions[8] in accordance with equations (2) and (3).

$$2I_2 + IO_3^- + 6H^+ + 5Cl^- \rightarrow 5ICl + 3H_2O \quad (2)$$

$$5ICl + 5Cl^- \rightleftharpoons 5ICl_2^- \quad (3)$$

Iodine monochloride is widely used as an iodinating agent in aromatic substitution reactions[9] and the formation of ICl under the experimental condition used here is highly favoured. When experiments were carried out using sulphur dioxide or equivalent amounts of iodine solution in the presence of potassium iodate and chloride ions, identical absorbance values were obtained, indicating that the species responsible for the iodination of 2′,7′-dichlorofluorescein is ICl, and the observed colour is due to the extracted 2′,7′-dichloro-4′,5′-diiodofluorescein in the solvent mixture, as shown in Fig. 2.

Trapping Solution

Tetrachloromercurate is one of the most widely used absorbing reagents for fixing atmospheric sulphur dioxide.[2] The TCM absorber has several disadvantages.[4] Several other reagents have been proposed for the absorption of atmospheric sulphur dioxide, including monoethanolamine,[10] hydroxamic acids,[11] ethylenediaminetetraacetic acid[12] and morpholine.[13] All these reagents have various advantages and disadvantages.

Dasgupta *et al.*[5] have advocated the use of a formaldehyde (7 mmol dm^{-3}) solution buffered at pH 4.2 using 1 mmol dm^{-3} potassium hydrogen phthalate (KHP) as trapping solution; the fixed sulphur dioxide is stable for about 30 d without appreciable loss. The trapping solution permits a sampling rate of 0.25–0.4 l min^{-1}, preferably at 0.3 l min^{-1},[14] for the quantitative collection of atmospheric sulphur dioxide. For the sampling of sulphur dioxide in ambient air a sampling rate higher than 0.4 l min^{-1} is preferred. Attempts were made to modify the trapping solution so that it could be used at a higher sampling rate and for a longer duration of sampling. In this study known amounts of sulphur dioxide were generated using an 'H'-type permeation device developed by Balasubramanian *et al.*[15] This simple permeation device, made with PTFE as the permeation medium, generates sulphur dioxide at 145.6 ng min^{-1} (214 ± 5 ppb) when dry air is passed through the system at a flow-rate of 0.26 ± 0.01 l min^{-1}. The air, containing sulphur dioxide being emitted from the permeation device, was mixed with clean dry air and this gas mixture was sampled through 15 ml of the trapping solution at various sampling rates, as desired for the experiments. The fixed sulphur dioxide, after sampling, was determined by following the proposed method. A sulphur dioxide recovery of >98% is taken as a sign of quantitative absorption in the trapping solution. Three approaches were investigated in an effort to improve the absorption efficiency of the trapping solution. First, the buffer (KHP) concentration of the absorbing solution was changed from 1 to 10 mmol dm^{-3} and further increased to 50 mmol dm^{-3}. This approach permitted a

Table 1 Collection efficiency of the trapping solutions. Sampling rate, 0.5 l min^{-1}

Trapping solution	Time/ h	Sulphur dioxide expected/ μg	Sulphur dioxide found/ μg	Recovery (%)
7 mmol dm^{-3} HCHO–1 mmol dm^{-3} KHP (pH 4.2)	1	8.74	8.61	98.51
	2	17.47	10.0	57.24
7 mmol dm^{-3} HCHO–10 mmol dm^{-3} KHP (pH 4.2)	2	17.47	17.15	98.16
	3	26.21	25.0	95.37
7 mmol dm^{-3} HCHO–50 mmol dm^{-3} KHP (pH 4.2)	3	26.21	25.8	98.44
	4	34.94	25.83	73.93
7 mmol dm^{-3} HCHO–10 mmol dm^{-3} KHP (pH 4.9)	3	26.21	25.83	98.55
	4	34.94	33.98	98.5
	5	43.68	26.15	74.84
7 mmol dm^{-3} HCHO–10 mmol dm^{-3} sodium acetate–acetic acid (pH 4.76)	4	34.94	33.99	98.5
	5	43.68	43.07	98.60
	6	52.42	51.67	98.57

* Average of three values.

Table 2 Variation of sampling rate. (Trapping solution, 7 mmol dm^{-3} HCHO–10 mmol dm^{-3} NaOAc–HOAc buffer pH 4.76.) Sampling period, 6 h. The amount of sulphur dioxide expected was 52.42 μg in all instances

Sample	Sampling rate/ l min^{-1}	Sulphur dioxide found*/μg	Recovery (%)
1	0.4	52.38	99.92
2	0.5	51.67	98.57
3	0.6	51.78	98.78
4	0.7	51.72	98.66
5	0.8	47.50	90.61
6	1.0	40.83	77.89

* Average of three values.

Table 3 Variation of absorption efficiency in the sampling period. (Trapping solution, 7 mmol dm^{-3} HCHO–10 mmol dm^{-3} NaOAc–HOAc buffer pH 4.76.) Sampling rate, 0.5 l min^{-1}

Sample	Time/ h	Sulphur dioxide expected/μg	Sulphur dioxide found*/μg	Recovery (%)
1	4	34.94	34.90	99.89
2	6	52.42	51.67	98.57
3	7	61.15	60.85	99.51
4	8	69.89	68.42	97.90

* Average of three values.

sampling rate of 0.5 l min^{-1} for 3 h. Second, keeping the buffer concentration at 10 mmol dm^{-3}, the pH of the trapping solution was adjusted to 4.9 (instead of 4.2). This approach permitted a sampling rate of 0.5 l min^{-1} for 4 h. Third, an attempt was made to replace the phthalate buffer system with 10 mmol dm^{-3} sodium acetate–acetic acid buffer (pH 4.76). This change permitted a sampling rate of 0.5 l min^{-1} for 6 h. The results of this study are given in Table 1.

After selecting the 10 mmol dm^{-3} acetate buffer system (pH 4.76), the sampling rate was varied from 0.4 to 1 l min^{-1} for a sampling period of 6 h. This study indicated that a maximum sampling rate of 0.7 l min^{-1} can be used without loss of sulphur dioxide (Table 2).

Experiments were also performed to establish the optimum sampling period by sampling air at 0.5 l min^{-1} for different sampling periods ranging from 4 to 8 h (Table 3). This study indicated that the buffer system permits a sampling period of 7 h. Based on the above study it is clear that the modified trapping solution can be employed successfully for sampling sulphur dioxide at a sampling rate of 0.5–0.7 l min^{-1} for 6 h.

The stability of the collected sulphur dioxide samples was studied by preparing a standard sodium sulphite solution in the buffered formaldehyde solution containing 7 mmol dm^{-3} formaldehyde–10 mmol dm^{-3} sodium acetate buffer (pH 4.76), and establishing the concentration of sulphur dioxide by taking samples after different periods of time. This sulphite solution was found to be stable for 25 d in the buffered formaldehyde solution without any deterioration (Fig. 3).

Effect of Interfering Species

The effect of common air pollutants on the determination of 15 μg of sulphur dioxide was studied by introducing the gas under examination into the trapping solution in the form of anions, together with the sulphur dioxide. Nitrogen dioxide, when present in excess of 5 μg, caused a low recovery of sulphur dioxide. The negative interference of up to 500 μg of nitrogen dioxide was overcome by the incorporation of 1 ml of a 2.5% solution of sulphamic acid together with potassium iodate and other reagent solutions. Hydrogen sulphide interfered seriously at all levels causing positive errors. The interference of up to 5 μg of hydrogen sulphide was overcome by the addition of 1 ml of a 0.03% solution of mercury(II) chloride to the trapping solution after sampling and developing the colour by following the recommended procedure. No interference was observed in the presence of bromate (1000 μg), chromate (1000 μg), nitrate (2000 μg) and Hg^{II} (250 μg) in the determination of 15 μg of sulphur dioxide.

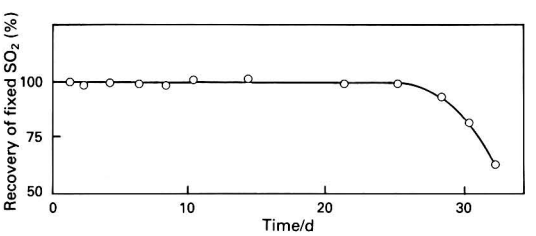

Fig. 3 Stability curve for fixed SO_2. Trapping solution, 7 mmol dm^{-3} HCHO–10 mmol dm^{-3} NaOAc–10 mmol dm^{-3} HOAc (pH 4.76)

Application of the Method

The proposed method was used for the determination of low concentrations of sulphur dioxide generated from two permeation devices (type H and type M) developed by Balasubramanian *et al.*[15] The simple permeation devices (H and M), made with PTFE as the permeation mediums for sulphur dioxide, generate 214 ± 5 and 125 ± 4 ppb of sulphur dioxide, respectively, when dry air is passed through the system at a flow-rate of 0.26 ± 0.01 l min^{-1}. The sulphur dioxide concentrations were established using a Seres Model SF 30 pulsed UV fluorescence monitor capable of measuring 1–10000 ppb of sulphur dioxide with an accuracy of ±1%.

Air samples from the permeation devices (H and M), after mixing with air, were collected in 15 ml of the buffered formaldehyde trapping solution at a flow-rate of 0.5 l min^{-1}. The final volume of the trapping solution after sampling was made up to 50 ml with the buffered formaldehyde solution. A 15 ml aliquot of this solution was analysed using the proposed procedure and the standard pararosaniline procedure.[2] Although the sampling rate was maintained at 0.5 l min^{-1}, the concentration of sulphur dioxide in ppb was calculated by taking the volume of air passing through the permeation devices (0.26 l min^{-1}). The calculated molar absorption coefficients for the pararosaniline method and the proposed method are 3.2×10^4 and 4.3×10^3 dm^3 mol^{-1} cm^{-1}, respectively. The value for the proposed method is less by one order of magnitude because it is calculated by taking into account the use of 5 ml of solvent mixture for the extraction of the compound from 50 ml of aqueous solution. The results obtained are shown in Table 4 from which it is clear that the concentrations of sulphur dioxide obtained by both methods are comparable.

Conclusion

Sulphur dioxide can be precisely determined down to a level of 2 μg using the proposed procedure. The calibration graph is rectilinear in the range 0–40 μg of sulphur dioxide. The

Table 4 Determination of sulphur dioxide generated from the permeation device. Sampling rate, 0.5 l min^{-1}; and sampling time, 6 h. The volume of solution taken for analysis was 15 ml in all instances*

	Concentration of sulphur dioxide						
	Pararosaniline method			2′,7′-Dichlorofluorescein method			
Permeation device	Sulphur dioxide/μg in 15 ml	Sulphur dioxide/μg in 50 ml	Sulphur dioxide (ppb)	Sulphur dioxide/μg in 15 ml	Sulphur dioxide/μg in 50 ml	Sulphur dioxide (ppb)	Estimated concentration of sulphur dioxide (ppb)†
H	15.11	50.36	205.52	15.25	59.83	206.7	—
	16.0	53.33	216.98	16.00	53.33	216.98	214 ± 5
	15.85	52.83	215.45	16.0	53.33	216.98	—
M	9.20	30.67	125.3	9.0	30.0	122.24	—
	9.5	31.67	128.7	9.0	30.0	122.24	125 ± 4
	9.3	31.0	126.44	9.4	31.33	127.97	—

* Sampling solution was made up to 50 ml with buffered formaldehyde before analysis.
† Determined by using a Seres SF 30 pulsed ultraviolet fluorescence monitor.

relative standard deviation is 3.5% for ten determinations of 15 μg of sulphur dioxide. By using the modified trapping solution, air can be sampled for periods of up to 7 h at a sampling rate of 0.5 l min^{-1} without a decrease in the recovery of sulphur dioxide. In addition, the fixed sulphur dioxide is stable for 25 d. The application of the proposed method to the determination of trace amounts of sulphur dioxide generated from two permeation devices has been used to demonstrate the usefulness of the method.

References

1 Robinson, E., and Robins, R. A., *Sources, Abundance and Fate of Gaseous Atmospheric Pollutants*, Final Report, SRI Project Sec. 8501, Stanford Research Institute, Menlo Park, CA, 1968.
2 West, P. W., and Gaeke, G. C., *Anal. Chem.*, 1956, **28**, 1816.
3 Scarringelli, F. P., Saltzmann, B. E., and Frey, S. A., *Anal. Chem.*, 1967, **39**, 1709.
4 Pate, J. B., Lodge, J. P., and Wartburg, A. F., *Anal. Chem.*, 1962, **34**, 1660.
5 Dasgupta, P. K., DeCesare, K., and Ulrey, J. C., *Anal. Chem.*, 1980, **52**, 1912.
6 Selvapathy, P., Ramakrishna, T. V., Balasubramanian, N., and Pitchai, R., *Analyst*, 1987, **112**, 1139.
7 *Vogel's Text-book of Quantitative Inorganic Analysis, Including Elementary Instrumental Analysis*, English Language Book Society, Longman, London, 1978, p. 384.
8 *Vogel's Text-book of Quantitative Inorganic Analysis, Including Elementary Instrumental Analysis*, English Language Book Society, Longman, London, 1978, p. 386.
9 March, J., *Organic Chemistry Reaction Mechanism and Structure*, Wiley, New Delhi, 3rd edn., 1986, p. 478.
10 Bhatt, A., and Gupta, V. K., *Analyst*, 1983, **108**, 374.
11 Chaube, A., Baveja, A. K., and Gupta, V. K., *Analyst*, 1984, **109**, 391.
12 Humphrey, R. E., Ward, M. N., and Hinze, W., *Anal. Chem.*, 1970, **42**, 698.
13 Raman, V., Rai, J., Singh, M., and Parashar, D. C., *Analyst*, 1986, **111**, 189.
14 Dasgupta, P. K., *Anal. Chem.*, 1981, **53**, 2084.
15 Balasubramanian, N., Selvapathy, P., and Pitchai, R., *Indian J. Environ. Health*, 1988, **30**, 360.

Paper 0/02121K
Received May 14th, 1990
Accepted September 28th, 1990

Studies on the Co-colour Reaction of Platinum(IV) and Palladium(II) With 4,4′-Bis(dimethylamino)thiobenzophenone

Zhao-Lan Liu, Wen-Bao Chang, Jian Hong and Yun-Xiang Ci*
Department of Chemistry, Peking University, Beijing 100871, People's Republic of China

The sensitive co-colour reaction of Pt^{IV} and Pd^{II} with 4,4′-bis(dimethylamino)thiobenzophenone (TMK) in the presence of ascorbic acid and Triton X-100 was investigated. The effect of pH on the absorbance of the complex was studied using an acetic acid–sodium acetate buffer, the optimum pH range being between 2.8 and 4.5, in the presence of ascorbic acid and Triton X-100. The orange–red complex exhibits an absorption maximum at 530 nm with a molar absorptivity of 1.96×10^5 dm^3 mol^{-1} cm^{-1} for Pd^{II} (in the presence of 10 μg of Pt^{IV}) and 2.98×10^5 dm^3 mol^{-1} cm^{-1} for Pt^{IV} (in the presence of 10 μg of Pd^{II}). The Pt : Pd : TMK ratio in the complex was found to be 1 : 2 : 12. Beer's law is obeyed over the concentration range 0–0.8 ppm of Pd^{II} and 0–0.48 ppm of Pt^{IV} in the presence of 10 μg of Pt^{IV} and 10 μg of Pd^{II}, respectively. The optimum conditions for the co-colour reaction of Pt^{IV} and Pd^{II} with TMK and the interferences of foreign ions are reported. The proposed method has been used successfully for the spectrophotometric determination of platinum and palladium in synthetic samples. Based on the experiments, the structure of the complex and the mechanism of the co-colour reaction are proposed and discussed.

Keywords: *Platinum; palladium; 4,4′-bis(dimethylamino)thiobenzophenone; co-colour reaction; spectrophotometry*

The reagent 4,4′-bis(dimethylamino)thiobenzophenone (Thio-Michler's ketone) (TMK) has been used for the spectrophotometric determination of mercury,[1] gold,[2–4] silver,[5,6] platinum,[7] palladium[8] and iridium.[9] The colour reaction of platinum with TMK in the presence of ascorbic acid (vitamin C) (VC) occurs only in a boiling water-bath for 15–20 min. Neither platinum nor palladium alone gives a colour reaction with TMK in the presence of VC and Triton X-100 (TX-100) at room temperature. However, an orange–red complex formed immediately when TMK was added to a solution containing Pt^{IV} and Pd^{II} in the presence of both VC and TX-100 at room temperature. This co-colour reaction[10] has been exploited for the development of a spectrophotometric method for the determination of platinum and palladium with high sensitivity and reasonably high selectivity.

Experimental

Reagents

All reagents were of analytical-reagent grade.

Palladium(II) standard solution. A stock standard solution containing 1 mg ml^{-1} of palladium was prepared by dissolving 100.0 mg of palladium metal (99.9%) in 3–5 ml of hot *aqua regia* and evaporating the solution almost to dryness. The residue was treated with 5 ml of concentrated hydrochloric acid and evaporated to a small volume (1 ml or less). This treatment was repeated three times to destroy any nitroso complexes formed. The resulting residue, after the final evaporation, was dissolved in and diluted to 100 ml with 1 mol dm^{-3} hydrochloric acid. Appropriate dilutions of the stock solution were made as required.

Platinum(IV) standard solution. A stock standard solution containing 1 mg ml^{-1} of platinum was prepared in the same way as for the palladium(II) solution.

4,4′-Bis(dimethylamino)thiobenzophenone solution. A 0.02% m/v solution of TMK was prepared in ethanol and stored in an amber-coloured bottle under refrigeration.

Ascorbic acid solution. A 2% m/v solution of ascorbic acid was prepared in de-ionized water, stored in an amber-coloured bottle under refrigeration, and replaced every 3 d.

Triton X-100 solution. A 5% m/v solution of TX-100 was prepared in de-ionized water.

Buffer solutions. Buffer solutions in the pH range 2.5–6.5 were prepared using 5 mol dm^{-3} sodium acetate solution and 5 mol dm^{-3} acetic acid.

Apparatus

Model UV-300 (Shimadzu) and Model 722 (Shanghai Analytical Instruments Factory No. 3, China) spectrophotometers were used for all absorbance measurements. A Model S-3 pH meter (Shanghai Analytical Instruments Factory No. 2, China) was used for pH measurements.

General Procedure

Add 1.5 ml of 2% VC solution to a 25 ml calibrated flask containing 10 μg of Pt^{IV} and 10 μg of Pd^{II} and mix thoroughly. After 1 min, add 5.0 ml of buffer solution (pH 3.3) and mix thoroughly, and after a further 3 min, add 2.0 ml of 0.02% TMK solution and 3.0 ml of 5% TX-100 solution. Dilute the

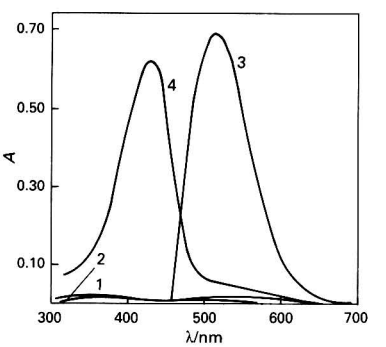

Fig. 1 Absorption spectra. 1, Pd^{II} + TMK + VC + TX-100 against reagent blank; 2, Pt^{IV} + TMK + VC + TX-100 against reagent blank; 3, Pt^{IV} + Pd^{II} + TMK + VC + TX-100 against reagent blank; and 4, reagent blank (VC + TMK + TX-100) against water. Pt, 10 μg; Pd, 10 μg; VC, 4.5×10^{-3} mol dm^{-3}; TMK, 2.1×10^{-5} mol dm^{-3}; TX-100, 3.3×10^{-3} mol dm^{-3}; and pH, 3.3

* To whom correspondence should be addressed.

mixture to the mark with de-ionized water, mix thoroughly and measure the absorbance at 530 nm against a reagent blank.

Results

Spectral Characteristics

The absorbance spectra of the Pd^{II}–TMK–VC–TX-100, Pt^{IV}–TMK–VC–TX-100 and Pt^{IV}–Pd^{II}–TMK–VC–TX-100 systems and the reagent blank (TMK–VC–TX-100) are shown in Fig. 1. The complex resulting from the Pt^{IV}–Pd^{II}–TMK–VC–TX-100 system exhibits maximum absorbance at 530 nm. Under similar conditions, the other systems do not absorb appreciably at this wavelength. All subsequent studies were therefore made at 530 nm.

Effect of Acidity

The effect of pH on the absorbance of the complex was studied using acetic acid–sodium acetate buffer solution. Fig. 2 shows the optimum pH range to be between 2.8 and 4.5. A 5.0 ml volume of buffer solution of pH 3.3 was used for subsequent studies.

Effect of Ascorbic Acid Solution

A total of 1.0–2.0 ml of 2% ascorbic acid solution in a final volume of 25 ml sufficed for a solution containing less than 10 μg of Pt^{IV} and 10 μg of Pd^{II} (Fig. 3). A 1.5 ml volume of 2% VC solution was selected for subsequent studies.

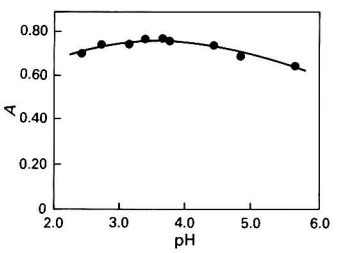

Fig. 2 Effect of pH. Pt, 10 μg; Pd, 10 μg; VC, 4.5×10^{-3} mol dm^{-3}; TMK, 7.03×10^{-4} mol dm^{-3}; and TX-100, 3.3×10^{-3} mol dm^{-3}

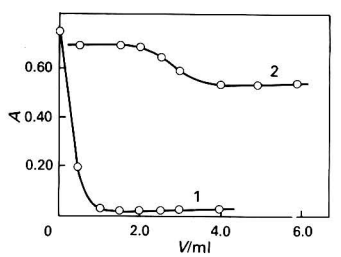

Fig. 3 Effect of VC on 1, the colour reaction of Pd^{II} with TMK; and 2, the colour reaction of Pt^{IV} with TMK

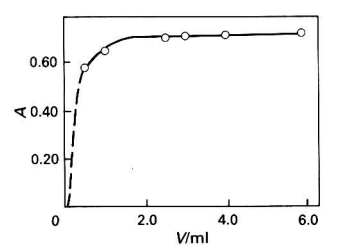

Fig. 4 Effect of TMK concentration. Pt, 10 μg; Pd, 10 μg; VC, 4.5×10^{-3} mol dm^{-3}; TX-100, 3.3×10^{-3} mol dm^{-3}; and pH, 3.3

Effect of TMK Concentration

The effect of TMK concentration was investigated by measuring the absorbance at 530 nm of solutions containing 10 μg of Pt^{IV} and 10 μg of Pd^{II} with various amounts of the reagent in a solution of pH 3.3 (Fig. 4). A total of more than 1.5 ml of the 0.02% m/v reagent solution in a final volume of 25 ml is sufficient for solutions containing less than 10 μg of Pt^{IV} and 10 μg of Pd^{II}. A 2.0 ml volume of 0.02% m/v TMK solution was used for subsequent studies.

Effect of TX-100

In the absence of TX-100 the solution is turbid, which makes the determination of the absorbance of the complex very difficult. Triton X-100 is able to increase the solubility, sensitivity and stability of the complex. A total of 3.0 ml of 5% TX-100 solution was chosen for subsequent investigations.

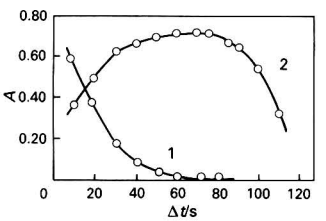

Fig. 5 Effect of VC stop-time on 1, the colour reaction of Pd^{II} with TMK; and 2, the co-colour reaction of Pt^{IV} and Pd^{II} with TMK

Table 1 Effect of foreign ions on the determination of platinum (10 μg) and palladium (10 μg)

Ion added	Tolerance limit/μg	Ion added	Tolerance limit/μg
Ag^{I}	10	Mn^{II}	100, 2000*
Al^{III}	100, 500*	Mo^{VI}	175
As^{V}	20	Ni^{II}	100, 250*
Au^{III}	0.5	Os^{VIII}	15
Ba^{II}	500	Rh^{III}	27
Bi^{III}	25	Ru^{III}	30
Ca^{II}	1200	Tb^{III}	15
Cd^{II}	100, 250*	Zn^{II}	4000
Ce^{IV}	500	Zr^{IV}	4000
Co^{II}	300, 2950*	Cl^{-}	80000
Cr^{III}	20	I^{-}	80000
Cu^{II}	5, 300*	F^{-}	80000
Fe^{III}	50, 100*	Br^{-}	80000
La^{III}	60	SO_3^{2-}	80000
Mg^{II}	1000, 1500*		

* In the presence of 6.0 ml of 1.0×10^{-2} mol dm^{-3} EDTA.

Table 2 Determination of Pd^{II} and Pt^{IV} in a synthetic sample of composition Mg^{II} 2000, Zn^{II} 800, Al^{III} 100, Ni^{II} 100, Co^{II} 50, Fe^{III} 50 and Rh^{III} 5.0 μg per 25 ml

Determination of palladium—*

Pt^{IV}/ μg per 25 ml	Pd^{II} added/ μg per 25 ml	Average Pd^{II} recovery† μg per 25 ml	%
10.0	5.0	5.0	100
10.0	10.0	10.0	100

Determination of platinum—*

Pd^{II}/ μg per 25 ml	Pt^{IV} added/ μg per 25 ml	Average Pt^{IV} recovery† μg per ml	%
10.0	5.0	5.2	104
10.0	10.0	9.6	96

* In the presence of 6.0 ml of 1.0×10^{-2} mol dm^{-3} EDTA.
† Average of six experiments.

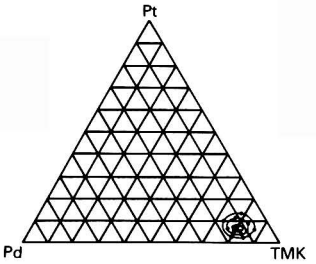

Fig. 6 Three-component phase diagram

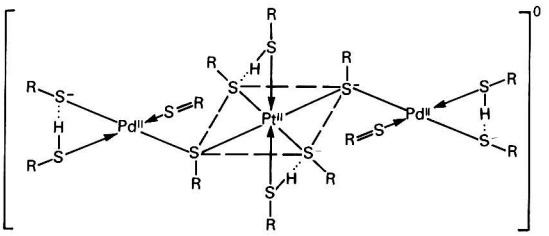

Fig. 7 Structure of the complex

Effect of Order of Addition of Reagents

Reagents should be added to the Pt^{IV} and Pd^{II} solution in the following order: 2% VC, buffer solution, 0.02% TMK solution and 5% TX-100. A change in this order had an adverse effect on the development of the colour of the Pt^{IV}–Pd^{II}–TMK complex.

Effect of VC Stop-time

The stop-time is defined as the period between the addition of VC and the addition of buffer solution.

For the colour reaction of Pd^{II} with TMK, the absorbance decreased as the VC stop-time increased [Fig. 5(1)]. If the stop-time is more than 50 s, the absorbance decreases to a negligible level.

For the co-colour reaction of the Pt^{IV}–Pd^{II}–TMK–VC–TX-100 system, after subtracting the absorbance of the colour reaction of Pd^{II} with TMK, the graph shown in Fig. 5(2) was obtained, indicating that the optimum VC stop-time was 55–75 s. A VC stop-time of 60 s was chosen for subsequent studies.

Effect of Foreign Ions

Interferences caused by foreign ions in the system were studied using solutions containing 10 μg of Pt^{IV}, 10 μg of Pd^{II} and the foreign ion. The tolerance limit was taken as the concentration that caused an error of not more than ±5% in the determination of platinum and palladium. The results are given in Table 1. It is interesting to note that EDTA does not interfere in the co-colour reaction of Pt^{IV} and Pd^{II} with TMK, hence it can be used as a complexing agent to mask the interfering metals.

Calibration Graph and Limit of Determination

Under the optimum conditions described above, Beer's law was obeyed in the ranges 0–0.8 ppm of Pd^{II} in the presence of 10 μg of Pt^{IV} and 0–0.48 ppm of Pt^{IV} in the presence of 10 μg of Pd^{II}. The molar absorptivities for Pd^{II} (in the presence of 10 μg of Pt^{IV}) and for Pt^{IV} (in the presence of 10 μg of Pd^{II}) are 1.96×10^5 and 2.98×10^5 dm^3 mol^{-1} cm^{-1}, respectively. A straight-line calibration graph passing through the origin was obtained using the recommended procedure. The correlation coefficients were 0.9999 for Pd^{II} and 0.9994 for Pt^{IV}.

Applications

The proposed method was used for the determination of platinum and palladium in a synthetic sample. The composition of the sample and the results are given in Table 2.

Discussion

The TMK reacted with neither palladium nor platinum alone, hence the reaction between TMK and noble metal ions probably occurs through bonding to sulphur rather than bonding to nitrogen. These noble metals are known to be the sulphide group metals.

The reaction between metal ions and TMK has been described,[6] and the molar ratio of metals in the complex with TMK was determined by experiments for palladium [atomic radius (r) = 1.28 Å] and platinum (r = 1.30 Å), which have similar atomic radii owing to the lanthanide contraction in the Periodic Table. It is probable that Pt^{IV} is first reduced to Pt^{II} in the presence of ascorbic acid, then platinum and palladium react with TMK proportionally to form a heteropolynuclear complex; this may be the essence of the co-colour reaction.

In order to establish the composition of the complex, the continuous variation, the molar ratio and the three-component phase diagram (Fig. 6) methods were applied. The Pt : Pd : TMK molar ratio was found to be 1 : 2 : 12.

It was also found that TX-100 was able to increase the solubility, sensitivity and stability of the complex; this indicates that the complex is electroneutral.

According to the properties of the complex and the molar ratio of metals and reagent in the complex, the structure shown in Fig. 7 for the complex formed by the co-colour reaction is proposed.

References

1 Cheng, K. L. *Mircochem. J.*, 1966, **10**, 158.
2 Tsukahara, I., *Talanta*, 1977, **24**, 633.
3 Liu, Q.-Z., Li, H.-R., and Chen, S.-Q., *Anal. Chem. (China)*, 1979, **7**, 43.
4 Wei, D.-X., *Metall. Anal.*, 1982, **4**, 34.
5 Li, L.-Y., Yu, S.-K., Li, N.-X., and Qu, Y.-L., *Chem. Reagents (China)*, 1984, **6**, 357.
6 K. L. Cheng, *Microchim. Acta*, 1967, **5**, 820.
7 Chang, W.-B., Li, X.-P., Kang, R.-Y., and Ci, Y.-X., *Rare Metal*, 1986, **5**, 122.
8 Li, L.-Y., Sun, Y.-M., and Jin, G., *Anal. Chem. (China)*, 1985, **4**, 285.
9 Yao, F.-J., Xu, S.-J., and Ci, Y.-X., *Rare Metal*, 1987, **6**, 145.
10 Chang, W.-B., and Ci, Y.-X., *Microchem. J.*, 1989, **39**, 149.

Paper 0/01649G
Received April 12th, 1990
Accepted August 13th, 1990

BOOK REVIEWS

Pharmaceutical Thermal Analysis. Techniques and Applications

J. L. Ford and P. Timmins. *Ellis Horwood Series in Pharmaceutical Technology.* Pp. 313. Ellis Horwood. 1989. Price £55.00. ISBN 0 7458 0346 6 (Ellis Horwood); 0 470 21219 5 (Halsted Press).

'Thermal analysis has long been the Cinderella of the instrumental techniques available to the pharmaceutical researcher'. So begins the author's preface and it might turn out that by their efforts this situation changes.

This is a highly readable account of the theory and practice of thermal analysis for pharmaceutical applications. The 14 chapters cover: (*i*) instrumentation, theory and practice, and information content of data (ch. 1–3); (*ii*) thermogravimetry and kinetics (ch. 4); (*iii*) purity of materials (ch. 5); (*iv*) applications to solids, solid dispersions, polymeric drug delivery systems and solid dosage forms (ch. 6–9); (*v*) compatibility studies (ch. 10); and (*vi*) applications to semi-solid systems, liposomes, freeze drying and other applications (ch. 11–14).

The work is thoroughly referenced and will appeal both to the pharmaceutical development worker and to the student, as a valuable work of reference.

C. Burgess

Selective Sample Handling and Detection in High-performance Liquid Chromatography. Part B

Edited by K. Zech and R. W. Frei. Elsevier. 1989. *Journal of Chromatography Library. Volume 39B.* Pp. xi + 394. Price $129.95; Dfl265.00. ISBN 0 444 88327 4.

This book is the second of a two-volume series, published in the *Journal of Chromatography Library* series, on selective sample handling and detection in high-performance liquid chromatography (HPLC). The book consists of seven chapters written as reviews by experts in their fields, with the late Professor Roland Frei contributing, not only as an editor, but also as an author of two of the chapters.

In Chapter I the authors review the applications of chelating silica as solid phases for pre-concentration, metal-ion chromatography and enantiomer separation. By highlighting this single but important area of chemically modified silicas, a fitting illustration is provided of the potential of solid-phase chemistries in sample handling and detection, an important theme in the book. Sample handling techniques for ion chromatography are described in Chapter II, covering sample collection and dissolution, contamination effects and the use of pre-concentration columns. Whole-blood sample clean-up for chromatographic analysis is detailed in Chapter III with the determination of cyclosporine chosen as an illustrative example. The following three chapters are concerned with selective detection methods. Chapter IV deals with radiocolumn liquid chromatography with sections on the use of radioisotopes in chemical analysis and on off-line and flow-through liquid-scintillation counting. The uses of immobilized enzymes and solid-phase chemistries for post-column reaction detection are described in Chapter V, including examples of their use with miniaturized HPLC systems. New selective luminescence detection techniques based on immobilized fluorophores, liquid-phase phosphorescence and alternative phosphorophores/luminophores are covered in Chapter VI. The book concludes with a review of the use of continuous separation techniques in flow-injection analysis, of particular relevance and potential in clinical, food and environmental analysis.

The book is very well produced, is full of detailed examples and instrumental configurations and is aimed at investigators specializing in the areas outlined. There is a strong emphasis on the chemical principles involved in the analysis of complex samples, an approach which adds further to the quality and value of the production.

J. D. Glennon

ASTM Standards on Chromatography. Second Edition

American Society for Testing and Materials. Pp. xvii + 805. American Technical Publishers. 1989. Price £60.00. ISBN 0 8031 1219 X.

This book is a compendium of all of the ASTM chromatographic methods, and as such must be a heterogeneous collection of applications. Most analysts using chromatography in any of its forms will find something of use and interest in its covers; very few will find all of it useful.

Some of the standards included have little to do with chromatography in real terms, such as the first in the book. This deals with the sampling and analysis of alkaline detergents, and although a very valuable collection of methods is given, most of them refer to volumetric and gravimetric procedures for the normal detergent constituents. Chromatography is used in an ion-exchange method for separating and measuring the different phosphates, or with an alternative paper-chromatographic method. These two methods between them account for 6 pages out of a total of 25.

There are standards relating to 115 matrices, ranging from acetate esters through atmospheres, detergents, oils, polymers, waxes, petroleum products, rubbers, solvents, *etc.* There are 128 components or properties measured in this range of sample matrices, and it is apparent that the number of combinations and permutations is fairly high. All told, there are 141 standards including four proposed standards.

The quality of the methodology presented and the clarity of presentation are uniformly high as one would expect; equally predictable is the absence of any use of recently introduced procedures such as solid-phase extraction or chiral columns. Any publication of this type will always suffer from both the time taken in its preparation and its origin as a committee generated document in this respect, but at least any method found in this book can be taken and used in the certain knowledge that it should work!

Overall, I think it a very useful work; it is a pity that the binding does not match the quality of the contents. The book is a large paperback, and in my copy the first two leaves are already coming adrift. I believe that a book, such as this one, intended for use on the bench, should be presented in a form that allows it to lie flat and not to lose pages too readily. My ideal format would be a three-ring binder, which would even allow ready updating.

R. C. Rooney

ERRATUM

Determination of Trace Amounts of Fluorine, Boron and Chlorine From a Single Sodium Carbonate Fusion of Small Geological Sample Masses

Alfons Hofstetter, Georg Troll and Dietmar Matthies

Analyst, 1991, **116**, 65

Page 66, **Reagents** *Standard sodium chloride solution: for* 'Sodium chloride (0.8242 g) (dry) is dissolved in 1 l of doubly distilled water'. *Read* 'Sodium chloride (0.8242 g) (dry) is dissolved in 0.5 l of doubly distilled water'.

CUMULATIVE AUTHOR INDEX

JANUARY–FEBRUARY 1991

The XXVII Colloquium Spectroscopicum Internationale

XXVII CSI

1991
NORWAY

will be held in

Grieg Hall, Bergen, Norway
June 9–14 1991

IUPAC

This traditional biennial conference in analytical spectroscopy will once again provide a forum for atomic, nuclear and molecular spectroscopists worldwide to encourage personal contact and the exchange of experience.

Participants are invited to submit papers for presentation at the XXVII CSI, dealing with the following topics:

Basic theory and instrumentation of—

- Atomic spectroscopy (emission, absorption, fluorescence)
- Molecular spectroscopy (UV, VIS and IR)
- X-ray spectroscopy
- Gamma spectroscopy
- Mass spectrometry (inorganic and organic)
- Electron spectroscopy
- Raman spectroscopy
- Mössbauer spectroscopy
- Nuclear magnetic resonance spectrometry
- Methods of surface analysis and depth profiling
- Photoacoustic spectroscopy

Application of spectroscopy in the analysis of—

- Metals and alloys
- Geological materials
- Industrial products
- Biological samples
- Food and agricultural products

Special emphasis will be given to trace analysis, environmental pollutants and standard reference materials.
The scientific programme will consist of both plenary lectures and parallel sessions of oral presentation. Specific times will be reserved for poster sessions.

PRE- AND POST-SYMPOSIA

In connection with the XXVII CSI the following symposia will be organised:

Pre-symposia—

I. GRAPHITE ATOMISER TECHNIQUES IN ANALYTICAL SPECTROSCOPY
June 6–8, 1991, Hotel Ullensvang, Lofthus, Norway.

II. CHARACTERISATION OF OIL COMPONENTS USING SPECTROSCOPIC METHODS
June 6–8, 1991, Hotel Hardangerfjord, Øystese, Norway.

III. MEASUREMENT OF RADIO-NUCLIDES AFTER THE CHERNOBYL ACCIDENT
June 6–8, 1991, Hotel Solstrand, Bergen, Norway.

Post-symposium—

IV. SPECIATION OF ELEMENTS IN ENVIRONMENTAL AND BIOLOGICAL SCIENCES
June 17–19, 1991, Hotel Alexandra, Loen, Norway.

For further information contact:

THE SECRETARIAT
XXVII CSI
HSD Congress-Conference
P.O. Box 1721 Nordnes
N-5024 Bergen, Norway.
Tel. 47-5-318414, Telex 42607 hsd n, Telefax 47-5-324555

FIRST FOLD HERE

THE ANALYST READER ENQUIRY SERVICE
For further information about any of the products featured in the advertisements in this issue, write the appropriate number on the postcard, detach and post.

FOLD HERE

THE ANALYST READER ENQUIRY SERVICE

FEB'91

For further information about any of the products featured in the advertisements in this issue, please write the appropriate number in one of the boxes below.
Postage paid if posted in the British Isles but overseas readers must affix a stamp.

PLEASE USE BLOCK CAPITALS LEAVING A SPACE BETWEEN WORDS *Valid 12 months*

NAME

2 COMPANY

PLEASE GIVE YOUR BUSINESS ADDRESS IF POSSIBLE. IF NOT, PLEASE TICK HERE ☐

3 STREET

4 TOWN

5 COUNTY
POST CODE

6 COUNTRY

7 DEPARTMENT
DIVISION

8 YOUR JOB TITLE
POSITION

9 TELEPHONE NO

OFFICE USE ONLY RECD PROCD

FOLD HERE

Postage will be paid by Licensee

Do not affix Postage Stamps if posted in Gt. Britain, Channel Islands, N. Ireland or the Isle of Man

BUSINESS REPLY SERVICE
Licence No. WD 106

Reader Enquiry Service
The Analyst
The Royal Society of Chemistry
Burlington House, Piccadilly
LONDON
W1E 6WF
England

ANALAO 116(2) 117–220 (1991) February 1991

The Analyst

The Analytical Journal of The Royal Society of Chemistry

CONTENTS